UNIVERSITY OF SOUTHAMPTON

FACULTY OF ENGINEERING, SCIENCE & MATHEMATICS

School of Engineering Sciences

Three dimensional geometrical and material nonlinear finite element analysis of adhesively bonded joints for marine structures

by

Narasimhan Sampathkumar

Thesis for the degree of Doctor of Philosophy

June 2005

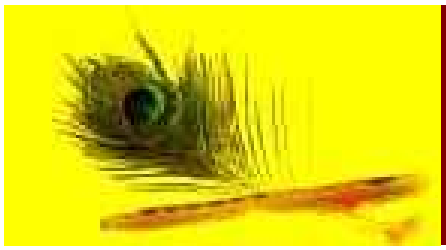

Sarvam SriKrishna-arpaNam asthu ||

(all my deeds dedicated to Sri Krishna..)

Acknowledgements

I sincerely express my gratitude to Professor Ajit Shenoi who offered me this research work and for his invaluable guidance as my supervisor. It was a great privilege to work with him and his continued support throughout the work period and particularly at critical stages of my research are highly regarded.

I also express my thanks to Prof. W.G. Price, the head of Fluid Structure Interactions Research Group and to Prof. P.A. Wilson for providing the computational facilities and their kind support throughout the research programme. Special thanks to Dr. James Blake, Dr. A.K.Nayak and my colleagues E. Jarry and S.W. Boyd for the useful discussions I had at times. Also my thanks are to Dr. Ming-Yi Tan for his technical support and to all other colleagues in Fluid Structure Interactions Research Group.

This work would not have been possible without the support from my Parents, Brothers and from my sister Pavithra. Their care towards my wellbeing, their patience and forbearance are acknowledged gratefully. I am extremely thankful to my friends Neeraj, Vinu, Arindam, Darun, Krishnan and many other friends in the university campus for their encouragement and for providing homely comfort.

Abstract

The use of adhesive bonding as a structural joining method has been gaining recognition in marine industry in recent years, though it has been widely adopted in other fields such as aerospace, automobiles, trains and in civil constructions. The type of materials used and design practices followed in marine structures are different from what is applied in other disciplines. Therefore new research approaches are required and recent novel ideas are explored in the context of application of bonded joint configurations in marine environment.

The research is directed at developing analysis tools for predicting the displacement, stress and strain fields in adhesively bonded joints between dissimilar adherends. In the finite element formulation, the adherends may be isotropic or orthotropic layered materials, which are assumed to behave linear elastically. The adhesive material is assumed to behave as elasto-plastic continuum, where the nonlinear behaviour is modelled as either a rigid or a semi-rigid adhesive solid that can be represented by the Ramberg-Osgood material model. The yield behaviour of the polymeric adhesive is modelled using a modified von Mises criterion, which accounts for the fact that plastic yielding of polymer materials may occur under the action of hydrostatic as well as deviatoric stresses. The geometric nonlinearity is based on the assumption of large displacement, large rotation but small strain, and it is implemented in the code using the total Lagrangian approach.

The scheme is applied on three case studies *viz.*: a study of adherend imbalances in a single lap joint, stress analysis of a butt-strap joint system and a hybrid joint are undertaken. The influence of geometric and material nonlinearity on joint deformations and

adhesive stresses, are studied for a single lap joint with dissimilar adherends, aluminium and a Fibre Reinforced plastic composite material, with varying adhrend thickness ratios. The adhesive stress-strain data obtained from the model are compared with the experimental stress-strain curve and the numerical results are validated with the analytical solution. Three dimensional effects like *'anticlastic'* and *bending-twisting'* are shown in the joint with a dissimilar adherends. Key results are obtained that explains the state of nonlinear adhesive stress state in the joint.

Analysis of butt-strap joint focussed on nonlinear modelling of a semi-rigid adhesive material that is used to bond two dissimilar adherends, steel and aluminium. The analysis demonstrate that the influence of geometric and material nonlinearity on the joint deformations as well as the adhesive stresses is significant. Nonlinear adhesive stresses are compared with the actual strength of the highly flexible adhesive, highlighting the need for the consideration of material nonlinearity in the bonded joints. Failure modes for the joint are inferred from the observations made on the adhesive stress state in the butt-strap joint.

Last study, deals with three dimensional analysis of a GRP-Steel hybrid joint carried out to model the initiation and propagation of crack under a set of static loading cases. Earlier studies were restricted only to two dimensional analysis. This three dimensional analysis showed that the adhesive normal stress is not constant across the width of the joint. Critical locations of stress concentrations are identified and the failure mechanisms are compared with the experimental specimens.

The observations made from this research study using a three dimensional finite element program, compliments the present knowledge in the field of adhesively bonded joints.

List of Publications produced from this thesis

1. Narasimhan S., Shenoi R.A. and Jeong H.K. (2004) Three-dimensional stresses in adhesively bonded lap joints with non-identical adherends, *IMechE proceedings, Part-L: Journal of Materials: Design and Applications*, Vol.218, No.L4, pp. 283-298.

2. Narasimhan S. and Shenoi R.A. (2005) Analysis of bonded butt-strap joints for marine structural applications, *Marine Structures*, Review in Progress.

3. Narasimhan S., Shenoi R.A., Blake J.I.R. and Boyd S.W. (2005) Stress concentrations in three dimensional hybrid composite-steel joint model, *Proceedings of Fifth Intl. Conference on Composite Science and Technology (ICCST/5)*, American University of Sharjah, Sharjah-UAE, pp. 143-148.

4. Narasimhan S. and Shenoi R.A. (2005) Numerical modelling of hybrid GRP-Steel joint subjected to in-plane and out-of-plane loadings, Communicated to *Composites-Part B*.

Contents

List of Figures

List of Tables

Nomenclature

u	displacement vector with components u,v and w in x,y,z directions
J	deformation gradient
$J_2^{'}, J_3{'}$	second and third invariants of the deviatoric stress tensor S_{ij}
J_1	first stress invariant
ϵ	Green's strain
ϵ_o	initial strain vector
$\varepsilon^e, \varepsilon^{vp}$	elastic and viscoplastic strain components
σ	vector of second Piola-Kirchoff stress
σ_m	mean stress
σ_y	effective yield stress
$\sigma_1, \sigma_2, \sigma_3$	principal stresses
S_{ij}	deviatoric stress tensor
τ_{oct}	octahedral stress
ρ	density in the deformed state
N	shape function
D	elasticity matrix
E	Young's modulus
ν	Poisson's ratio
μ	shear modulus
B	strain-displacement matrix
B_o	small strain displacement matrix
B_L	large strain displacement matrix

f vector of equivalent nodal forces

f_p vector of applied nodal forces

f_b force vector due to body forces

f_t force vector due to surface tractions

f_{ϵ^o} force vector due to initial strain

f_{σ^o} force vector due to initial stress

b body force

p surface traction

K_T total tangent stiffness matrix

K_o small displacement stiffness matrix

K_L initial or large displacement matrix

K_σ initial stress or geometric matrix

ξ, η, ζ curvilinear coordinates

δ_{ij} Kronecker delta

F yield function

γ fluidity parameter

Q plastic potential

$\phi(F)$ flow function

C_{ijkl} constitutive tensor for elastic materials

$I_1^{'}$ first invariant of the general strain tensor

$I_2^{'}$ second invariant of the general strain tensor

α time stepping parameter

ψ vector of residual force

λ ratio of compressive to tensile yield stress

Δt_{CR} critical time step length

L adherend length

C overlap length

H adherend thickness

h adhesive thickness

LE	Linear Elastic solution
GE	Geometric non-linear Elastic solution
VP	Viscoplastic solution
VPG	Geometric non-linear viscoplastic solution

Chapter 1

Introduction

Adhesive bonding technology has expanded greatly in recent years as more and more advanced fibre reinforced composite materials are being utilized in structural applications. Research and development of adhesive bonding technology has developed over the past fifty years and has been mainly directed towards the requirements of the aerospace industry. Today, progress is such that modern adhesives offer a joining technique of interest to engineers in a far wider range of industries than just that of aircraft applications. These include constructions in automobiles, trains, ship and marine structures, civil construction, rehabilitation of infrastructures etc. The civil and marine engineering sector are becoming increasingly aware of adhesives as a method of joining. The use of adhesive bonding as a joining method is an accepted means of attaining high structural efficiency and improved fatigue life. One of the major advantages of adhesive bonding is that it enables dissimilar materials to be joined without the need for modifications in the adherend material as required when the joint is bolted/riveted. Adhesive bonding is attractive since it allows for a more gradual diffused load transfer in to the structure, thus reducing the localized stresses encountered in the use of bolts and rivets.

1.1 Adhesively Bonded Joints

Structural adhesives are used in different types of joints. Commonly used adhesively bonded joints are shown in fig 1.1. They are:

1. Single lap joint,
2. Double lap joint,
3. Step lap joint,
4. Scarf joint,
5. Butt strap joint and
6. Tubular lap joint.

Among these, single lap joint is often preferred and adopted due to its simplicity and ease of fabrication. The single lap joint consists of two adherends and an adhesive layer joining them together. The adherend may be either metallic or fiber reinforced composite.

1.1.1 Function and Failure of Adhesively Bonded Joints

Adhesives, being viscous, flow over the surface of a solid and because of their intimate contact, interact with solid's molecular forces. Then, as a result of the adhesive curing process, they become strong solids which, retaining intimate contact with the surfaces, hold them together. In general, the adhesives are not as strong as metal/composite adherends and hence the adhesive interlayer will always tend to be the weakest link in a bonded structure. Care is therefore needed to ensure that service stresses are well within adhesive's capabilities. This is normally achieved by providing a relatively large area in bonding.

The failure of adhesively bonded joints can occur for any of the following reasons or combination of them:

1. Cohesive failure within the adhesive,

2. Adhesive failure which occurs at interface of adhesive and adherend, and

3. Failure of adherends which also includes delamination in composite structures.

The other type of failure is progressive separation of adherends occuring by failure of the adhesive under cyclic loading. The main cause of failure in adhesively bonded joints is due to the brittle nature of adhesives. The adhesive is more prone to damage when the structure is shock loaded and momentary distortion of adherend generates large peel and cleavage forces that the adhesive may not be able to resist. Hence, an accurate analysis of bonded joints is needed in order to determine the failure mode that could occur in a joint for the worst anticipated combination of load.

1.1.2 Advantages and disadvantages of adhesive connections

The guide to the structural use of adhesives (1999) outlines the following advantages and disadvantages in adhesive connections *viz-a-viz* other fastening techniques like bolts and welding connections.

Advantages

- no damage to parent material (cf. drilling for bolts, etc.,)
- no damage to exposed surfaces (cf. spot-welding)
- fewer pieces required to form connections (cf. bolts, washers etc.,)
- smaller additional pieces, e.g. gusset plates, required to form connection (cf. bolted connections where minimum edge distances may determine plate dimensions)
- high effective stiffness of joint (cf. bolted connections which may slip)
- improved fatigue performance, because of reduction in stress concentrations
- high, uniform strength and stiffness along joint

- tolerance to dimensional inaccuracies
- dissimilar materials can be joined readily
- elimination of bimetallic corrosion
- good noise and vibration damping
- efficient method of joining thin materials
- potential for simpler, faster fabrication

Disadvantages

- lack of experience of use when compared with traditional materials and methods
- properties will vary between different suppliers, and are constantly being 'improved'
- surface treatment required
- requires a high level of supervision by experienced staff
- generally requires a carefully controlled environment during assembly and curing of a joint which is often difficult to achieve (particularly important for site assembly)
- possible Health and Safety implications
- time taken for connection to achieve full load carrying capacity (cf. bolting or welding)
- completed connection not easily inspected
- strength limited under certain directions of loading; joints must be suitably designed
- connection can not be disassembled (cf. bolts)
- adhesive properties affected by temperature and humidity (cf. bolts)
- possible complete loss of performance in fire

- creep effects may be significant, particularly at elevated temperatures
- lack of agreed design guidance (applies to some materials only)

1.2 Sources of Nonlinearity

In many practical engineering problems, linear elastic analysis is not adequate. For an accurate analysis one should consider the actual nonlinear behaviour. Nonlinearities in solid mechanics arise from two distinct sources. One is due to the kinematics of deformation of the body and the other from the constitutive behaviour(i.e., stress-strain relations). The analysis in which the first type of nonlinearity is considered is called as geometric nonlinear analysis, and those in which the second type is considered is a materially nonlinear analysis.

1.2.1 Geometric Nonlinearity

If the load-displacement relationship is not linear for components made from materials of linear properties, then this represents a geometric nonlinearity. In some structural problems it will be assumed that both displacement and strains developed in the structure are small. In practical terms this means that the geometry of the elements is basically unchanged during the loading process and that the first order, infinitesimal, linear strain assumptions can be used. If the accurate determination of the displacements is needed, geometric nonlinearity have to be considered while analysing the structures. Here the strain displacement will not be linear but it will contain some quadratic terms. The geometrically nonlinear analysis may be further classified based on the types of nonlinearities considered. Two such cases are (i) large displacements, large rotations but small strains and (ii) large displacements, large rotations but large strains. In the first case it is assumed that the rotations of the elements are large but the extensions and changes of angle between the elements are small. In the second case the extension of a element and the angle changes between two elements are large, and the displacements and the rotations are also large. There are two methods of geometric nonlinear formulation such as total

Lagrangian formulation and Eulerian formulation. In the total Lagrangian formulation all the variables are with reference to the original configuration, whereas in the Eulerian formulation they are reffered to the current configuration.

1.2.2 Material nonlinearity

By far the most common sources of material nonlinearity in solid mechanics have been divided into two independent groups of phenomena, described respectively by 'plasticity' and 'creep'. For the first group, the classical theory of plasticity (Hill (1950), Perzyna (1963,66)) provides a theoretical description of the stress-strain relationship. The material performance is described by an irreversible straining which is not time dependent and which can only be sustained till a certain level of stress has been reached. The second group of phenomena includes all the time effects and results in the creep strains developed at finite rate. Indeed, many structural materials, especially under high operating temperatures, exhibits the phenomenon of creep; in which a redistribution of stress and/or strain with time occurs which may be elastic or plastic in nature.

The concept of elasticity and plasticity are best illustrated by means of simple uniaxial stress-strain models.The components which combine to form these models are shown in figures 1.2, 1.3 & 1.4 together with their corresponding stress-strain behaviour. Pure elasticity is represented by a Hookean spring which has a linear relationship between stress and strain. Pure plasticity is represented by a St.Venant's slider which has zero strain until the stress reaches the yield stress at which point we have what is known as perfect plasticity, and for an elasto-plastic material the model consists of a Hookean spring and a slider in series. For the uniaxial model shown in figure 1.4 the behaviour is purely elastic until the stress level reaches the yield stress σ_y. When the slider yields and there is a continuing deformation at constant stress, then it is impossible for the stress to exceed the yield stress. If unloading takes place from the yielded state the strain path followed is different from the loading path. Elasto-plastic behaviour is loading path dependant since it has been shown by experiments that if two loading paths reach the same point

on the yield surface by different routes then the plastic strains are different. This necessitates the use of an incremental form of plasticity in which the increments of plastic strain throughout the loading history are determined and the total strain is obtained by summation.

1.3 Selection of structural adhesives

Adhesives are versatile and their selection does not usually depend upon a single property, but rather on a balance of several properties, which could be met by more than one adhesive. Hence, the proper selection of adhesive becomes crucial from a performance point of view. The basic chemical type of adhesive is very important, the choice being from epoxide, acrylic, phenolic and polymeric materials. On strength requirements, one should consider shear, cleavage and peel, impact strength, deformation and creep as the main criteria for selection.

Guide to the structural use of adhesives (1999) gives guidelines of structural adhesives and their application and design. Adhesive connections may be divided, very broadly, into three categories, namely structural, semi-structural and non-structural. They may be considered as follows:

- structural: the bonded joint carries all the load in a particular direction, at service load or at both service and ultimate loads; failure in the bond line leads to a significant change in the behaviour of the structure or in its load carrying capacity.
- semi-structural: the bonded joint is required chiefly to distribute the loads, the main load carrying being by some other mechanism; failure in the bond line may result in some change of behaviour under service loads but the ultimate strength will not be affected.
- non-structural: the bonded joint is subjected to a nominal stress; the consequences of failure in the bond line are structurally insignificant (though failure can still lead to a risk of serious injury).

A number of different aspects must be taken into account when considering the use of an adhesive to form a structural connection. These include:

- design of the geometry of the joint
- selection of the adhesive itself, taking into account the materials to be joined, the stresses to be carried and the environmental conditions both during application, curing and in service
- preparation of the surfaces to be joined
- workmanship
- Health and Safety and environmental considerations, both during assembly and throughout the life of the structure

1.4 Aim and Scope of the Research

The aim of this study is to understand the nonlinear behaviour of different types of adhesives that are increasingly being used for bonding marine structural components. It is also aimed to study the influence of geometric and material nonlinearities on joint deformations and adhesive stresses. Specific attention is devoted towards behaviour of bonded joints with dissimilar adherends, joints with thick adhesive layers and hybrid joints consisting of more than two different adherend materials. It is envisaged here that nonlinear stress analyses could provide an enhanced understanding of the problem pertaining to selection of suitable types of adhesives and dimensioning of joints.

1.4.1 Motivation

The focus of this study is related to the application of bonded joints in marine structural components. The use of adhesive bonding in marine industry was initially restricted to special applications, such as window panes and seat rails in passenger ships. But the

adoption of adhesive materials in structural components that transfer load, as an alternative to mechanical fasteners, in the ship industry, has been slow compared to the progress seen in other industries such as aerospace and automobile industries. The type of materials used and the structural design practiced in the marine industry are different from other fields and therefore, bonding technologies, say from aerospace field, cannot be used directly in ship building or repair. Significant research has been directed therefore towards the exploration of FRP composites in a maritime environment (Mouritz *et al.*, 2001). The prime objective of adhesive bonding in ship structures is to use of light weight composite materials wherever feasible; reduced superstructure and hull weight can result in various advantages such as payload increase, speed range, stability and reduced maintenance. Light weight structures are predominantly used in super-structure, advanced mast systems, bulkheads, decks, propellers, propulsion shafts and rudders in different types of marine structures *viz.* patrol boats, hovercraft, corvettes, fishing boats and fast boats. The major advantage of using adhesive bonding is joining different kind of materials, metal-to-metal, metal-to-FRP, in the above mentioned vessels. Accordingly, current research on joining dissimilar materials is reviewed and the scope for further study is explained in the next chapter. Two case studies of bonded dissimilar joints that are directly employed in marine industry are considered here; the analyses and the details are provided in the following section.

As it will be discussed in the critical review of literature, current research trends in numerically modelling the above mentioned case studies lack comprehensive approach when the purpose is to study the load transfer mechanism among the structural components. This warrants an improved set of methodology that could address all the issues concerning the behaviour of bonded structural joint systems. Though there are good number of commercial Finite Element Analysis (FEA) software packages to simulate the realistic state of structural joint system, when it comes to characterisation of particular type of structural adhesives it is found that the available commercial FEA packages have few shortcomings. An user of such FEA packages is still need to develop his own interface algorithm to

account for certain type of material nonlinear formulation in this case, a modified von Mises equation and the Ramberg-Osgood equation to characterise a semi-rigid adhesive material. Considering this fact and also in order to account for geometric and material nonlinearities that exist in a bonded structures it has been decided to develop a finite element code in a three dimensional domain. Development and utilisation of a in-built FE code also provides better study of the numerical modelling at any stage of the analysis while the user of any commercial package will not have access to its source code to monitor the numerical process.

1.5 Areas of investigation

A three dimensional finite element analysis of two types of structural components is proposed here. The first type of component relates to the numerical modelling of a butt-strap joint system that is derived from the deck-to-superstructure connection, in a 34m long Vosper Thornycroft (VT) Patrol craft that is shown in figure 1.5. An experimental investigation on the load carrying capacity of the deck-to-superstructure connection is carried out by Jarry & Shenoi (2005) with the box joint and a single butt-strap joint specimen. The numerical modelling that relates to experimental study on the strength of the butt-strap joint is undertaken here. This joint consists of two dissimilar adherends, aluminium and steel bonded by a semi-rigid adhesive material Plexus MA550.

The second study deals with stress analysis of a typical hybrid steel-GRP joint based on the design for hangar to weather deck connections on the *La Fayette* class frigates, currently in service in the French navy (figure 1.6). This hybrid joint consists of three different materials, steel/GRP/Core bonded by an adhesive material. The geometry and the loading conditions are shown in figure 1.7. As it will be revealed in the literature review, the need for identifying the stress concentration locations that initiates failure in the joint forms the main objective for this study.

Prior to these two studies, it is decided to look at the three dimensional behaviour of

a typical single lap joint consisting of non-identical adherends. This is for the reason that the above mentioned case studies deal with dissimilar materials that are increasingly explored in marine structures. Therefore, an idealised joint is chosen for the parametric study. Actual joints will contain a spew fillet (see figure 1.8) of adhesive at the edges that will influence the behaviour of the joint (Adams *et al.*,1997 and Frostig *et al.*,1999). For computational efficiency and ease of building the 3-D models the effect of the spew fillet is not considered in this work. The objectives and the methodology adopted for all three types of problem are described in chapter 3.

1.6 Layout of thesis

For the ease of understanding, the lay-out of thesis is explained here.

- Chapter-1: **Introduction** - Presenting the basic information on adhesively bonded joints, their advantages and disadvantages against the conventional mechanical fastening methods. Aim and the scope of the research is outlined.
- Chapter-2: **Critical Literature Review** - Collection of review on bonded joints covering lap joint theories, adhesive modelling, experimental/numerical modelling followed by discussion.
- Chapter-3: **Proposed Methodology** - This chapter gives the background to the problems considered and the methodology is proposed.
- Chapter-4: **Solution procedures and FE formulation** - This chapter presents numerical implementation of geometric and material nonlinear equations in to a finite element program code.
- Chapter-5: **Study on adherend imbalances in single lap joint** - This chapter covers a study on adherend imbalances in a lap joint, addressing three dimensional stresses based on a parametric study. Three dimensional effects and failure modes seen in a typical lap joint are described.

- Chapter-6: **Analysis of Butt-strap joint structures** - This chapter deals with performance of a butt-strap joint system bonded by semi-rigid adhesive that forms a structural component in the superstructure of a Patrol craft.

- Chapter-7: **Stress analysis of GRP-Steel hybrid joints** - This chapter attempts to identify the critical stress locations that occur in a GRP-Steel hybrid that transfers significant load in a weather-to-deck-superstructure of an helicopter hangar in a French navy *Lafayette* class frigate.

- Chapter-8: **Discussion** - Provides over all discussion on the formulation of the FE code and the key results obtained from the analyses.

- Chapter-9: **Conclusion** - Concludes with the overview of this thesis, followed by discussions on results, future works and concluding remarks.

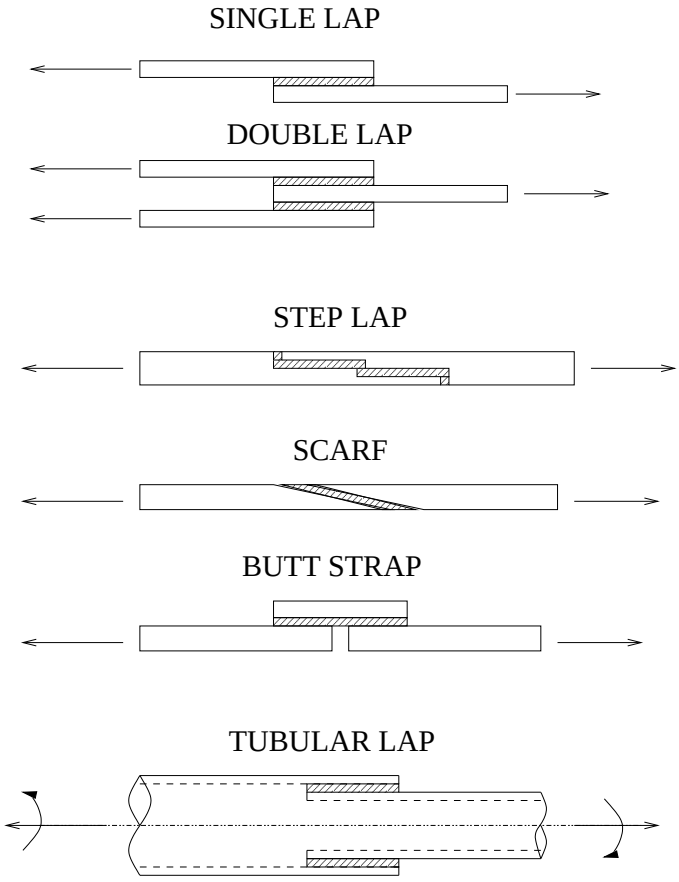

Figure 1.1: Types of Lap Joints

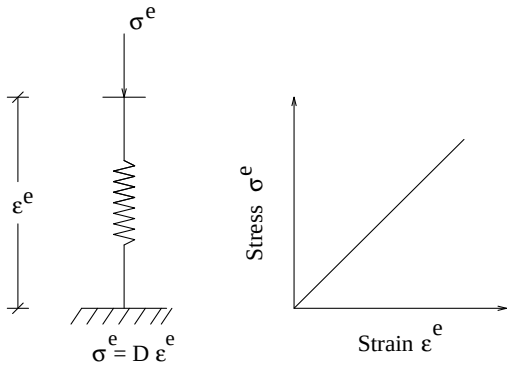

Figure 1.2: Uniaxial stress-strain model showing Elastic behaviour

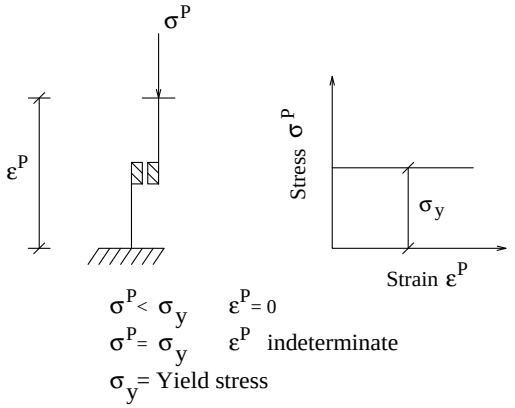

Figure 1.3: Uniaxial stress-strain model showing Plastic behaviour

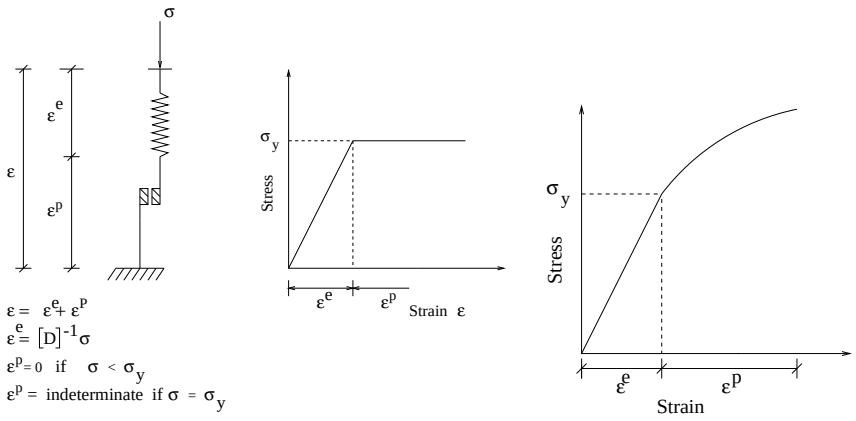

Figure 1.4: Uniaxial stress-strain model showing Perfectly-plastic and Elasto-plastic behaviour

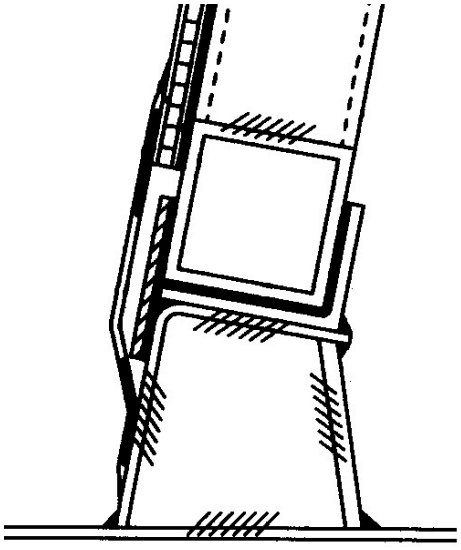

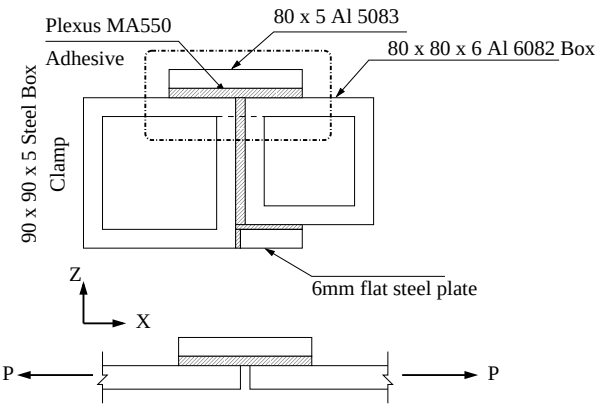

Figure 1.5: 34m VT Customs & Excise Cutter and sketch of Deck to superstructure joint unit under a tensile load

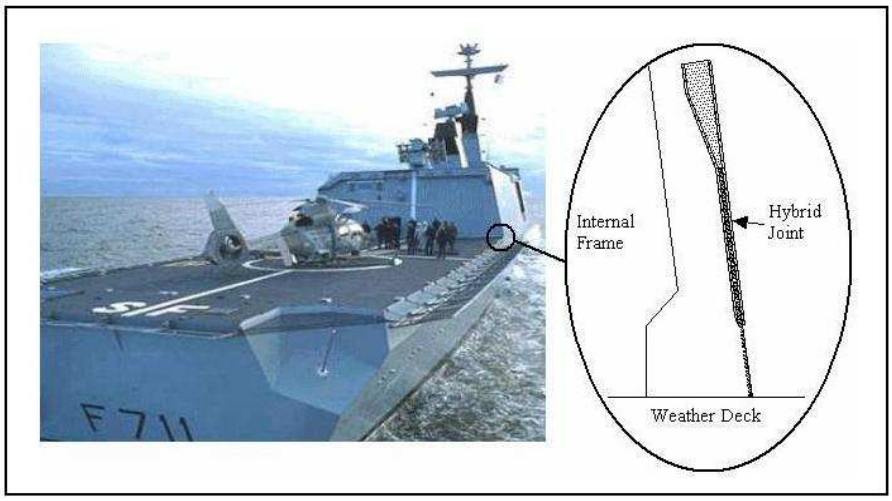

Figure 1.6: Helicopter hanger on the French La Fayette class frigate (Courtesy of DCN)

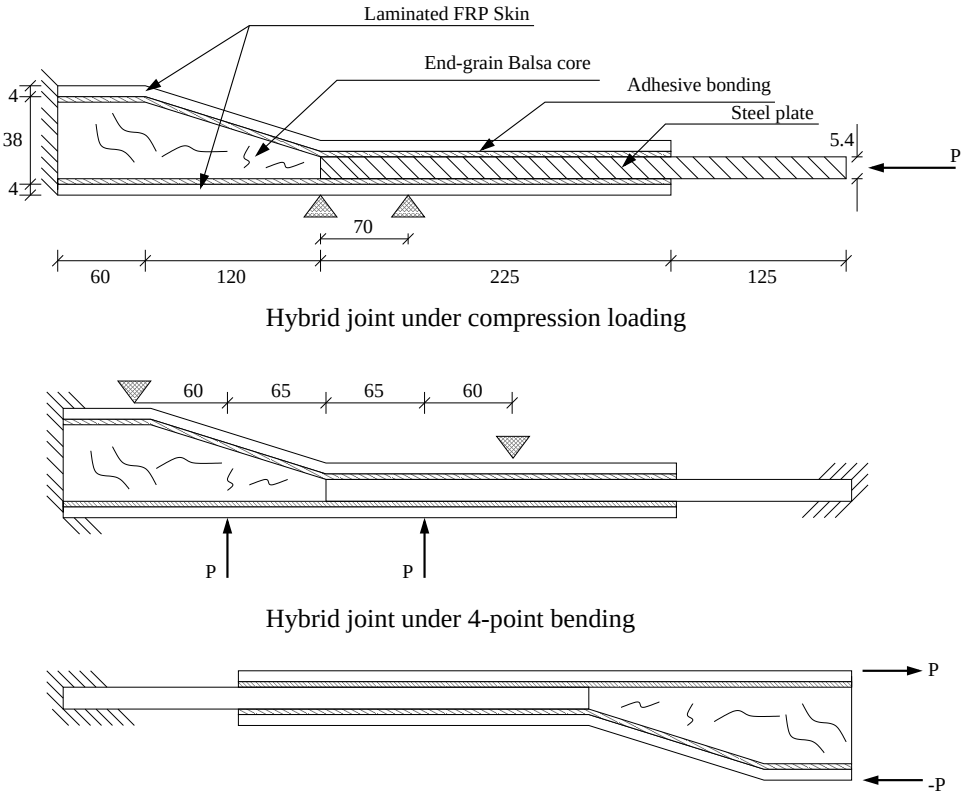

Figure 1.7: Boundary condition and loading combinations in hybrid joint

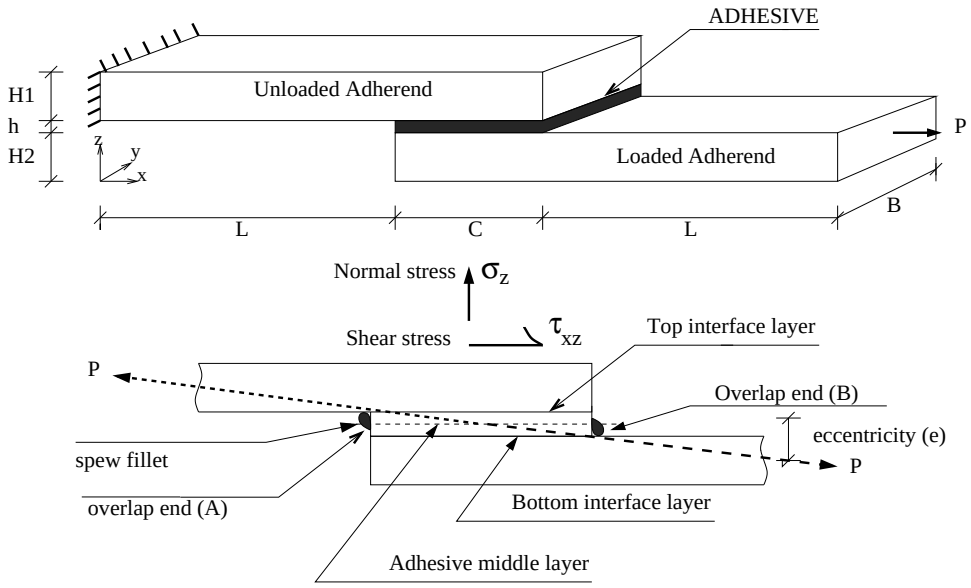

Figure 1.8: Notation for the single lap joint

Chapter 2

Critical Literature Review

2.1 Introduction

This chapter reviews the research work on bonded joints under the categories of lap joint theories, adhesive modelling, experimental work and numerical approach/modelling, followed by discussion for each section. The final section outlines the contribution of the reviewed papers in the context of the current research and identifies the weaknesses with respect to modelling of adhesives and to analyses of bonded connections. This offers scope for the definition of new research for further development which is presented in the next chapter.

2.2 Lap joint theories

2.2.1 Review

The earliest work on adhesive bonded joints, and in particular lap joints, has been attributed to Volkerson (1938), although in reality the analysis was for riveted plates. His work addressed 'Differential shear' and centered on a 'shear lag' model that neglected the effects of joint eccentricity, and considered only adhesive shear deformation and adherend deforms in tension, for homogeneous and isotropic material. The main limitation of this model is that it does not take into account the bending due to eccentricity of the load

direction. The analysis found that the thicker the adhesive layer, the higher the strength. However, one has to be reminded that adhesive thickness cannot be increased indefinitely and that beyond a certain thickness, it cannot be counted as an adhesive layer, but as a third material in the structure in which case an anisotropic plate analysis should be applied. Further, this result is not supported by experimental evidence which shows that thicker bond lines give lower strengths (Adams and Grant, 1993).

As mentioned above the theory developed by Volkerson (1938) takes no account of the fact that First, the directions of two forces are not collinear which leads to a bending moment being applied to the joint in addition to the in-plane tension, causing the adherends bend, allowing the joint to rotate. Goland and Reissner (1944) used a beam-on-elastic foundation that took rotation into account by using a bending moment factor k, which relates to the resultant moment. In this paper, the approach was in three parts. In the first, it was shown that the bending moment is not transmitted integrally and, therefore, a bending coefficient k is derived. In the second part, the assumption was made that the adhesive is relatively rigid, and in the third part, it was assumed that the adhesive is relatively flexible, where it is known as Goland and Reissner's second theory. The second theoretical approximation is applicable to metal-to-metal adhesively bonded joints, whereas the first approximation assumes the joint to be monolithic. The second theory also has a limitation in the sense that it neglects the shear deformation and peel stresses across the adherend thickness. Furthermore, it does not take into account the fact that shear should be zero at the joint edge. The proposed methods are valid only for material with elastic behaviour, whereas most adhesives present elasto-plastic behaviour (Hart-Smith, 1973). The Goland-Reissner analysis is limited to situations in which the adherends are identical, the joint-edge loads are not in equilibrium, and the stresses across the adhesive layer are constant.

Cornell (1953) presented a variation and extension of Goland and Reissner's approach by assuming that the two lap-joint plates act like simple beams and the more elastic

cement layer is an infinite number of shear and tension springs. He used Euler's beam theory to describe the adhrends. Good agreement was found with photoelastic experimental results when applying bending, axial and shear loading, and also highlights the importance of fillet radius. It should be stressed that this method is more suitable to assess fatigue stress rather than static stress because of the assumption that the adhesive layer is modelled as an infinite number of springs. The only limitation of the method is found in the assumption that adhesive stiffness is negligible.

Lubkin (1957) suggested a theory for scarf joints having a negligibly thin adhesive layer. Hence it was developed on the assumption of uniform stress/strain across its thickness. Based on the semi-inverse method, he showed that the stresses were constant along the joint for all scarf angles, provided the adherends have the same elastic properties for the tensile load. For non-identical adherends, he showed that a scarf angle can be determined which provides homogeneous elongation of the adhesive layer. Hart-Smith (1974) described the scarf joint as mathematically the most difficult to solve, due to the governing differential equations not having standard closed form integrals. Scarf joints of dissimilar adherends have been analysed by Wah (1976a,1976b) who highlighted a marked effect of longitudinal stress and observed that the maximum stress occurs near the stiffer adherend. He also suggested an approach using Eigen solutions for determining shear and tensile stresses developed under pure bending.

Allman (1977) has derived a solution that satisfies the stress free boundary condition for a symmetric lap joint. His elastic stress analysis is based on the strain energy density of a particular joint. The adherends were modelled to account for bending, shear and normal stresses. Like Goland and Reissner (1944), Allman also set the adhesive shear stress at the overlap ends to zero. He allowed for a linear variation of the peel stress across the adhesive thickness, although the adhesive shear stress was treated as constant through the thickness. In spite of this limitation, this is an improvement on earlier theories. He noted that for non-identical adherends the solution gets unnecessarily complicated and

therefore preferred approximate numerical techniques, should this situation arise.

Further extension of Goland and Reissner's model, through use of a more complete shear-strain/displacement equation for the adhesive layer, is illustrated by Ojalvo and Eidinoff (1978). Ojalvo and Eidinoff's theory predicts the variation of shear stress through the bond thickness, even for thin layers. This through-the-bond-thickness variation of shear stress identifies two anti-symmetrical adherend-bond interface points at which the shear stresses are highest. The results also highlight the differences in stresses obtained by theories which include and those which neglect the effect of bond thickness.

On transverse stresses in bonded joints, Adams and Peppiatt (1973) have shown the existence of significant stress across the width of an adhesive joint. They considered the existence of shear stresses in the adhesive layer and direct stresses in the adherends acting at right angles to the direction of the applied load, these stresses being caused by Poisson's ratio strains in the adherends. Edge effects in the joints can be complicated by the presence of spew fillets that occur when excessive resin is squeezed from the joint. Adams and Peppiatt (1974) have observed that their presence is actually beneficial, reducing adhesive stress by up to 30%.

With the limitations in the various classical theories mentioned above, Hart-Smith (1973) extended the Goland and Reissner model to treat joints with elastic-plastic adhesives and to determine the critical bending moments in adherends at the end of the overlap. He also addressed the stiffness imbalance between adherends and the influence of laminated composite adherends (as distinct from isotropic metal adherends). The elastic-plastic theory used by Hart-Smith predicts an increase in joint strength and was shown to be capable of explaining premature failure predictions found when using linear elastic analyses. The quantitative effects of stiffness imbalance were also accounted for. Three distinct and characteristic failure modes are predicted. The first is that of failure of adherend just outside the joint, due to in-plane stresses that arise from the combination of direct load

stresses and bonding stresses resulting from eccentricity in the load paths. The second mode is the failure of the adhesive layer in shear, though the inclusion of plasticity in the analysis has demonstrated that this potential failure mode is extremely rare in structural practice. The third failure mode may be manifest in either of two forms and is associated with the adhesive peel stresses. With the FRP composite adherends, the interlaminar tension strength is so much less than the peel strength of good structural adhesives that the failure occurs within the continuous laminate at the ends of the joint.

A comparison of different lap joint theories mentioned above were studied by Carpenter (1991). He took into account the earlier assumptions from Goland and Reissner's model. The effect of a given assumption on predicted adhesive stress is difficult to determine with a differential equation approach. A set of control parameters prescribing the kind of assumptions for various cases and their influence on prediction of stresses are discussed. In the case of membrane shear-bending study, the maximum adhesive peel stress was affected very little by most assumptions. But factors like shear deformation of adherends, plane stress/strain option and whether a consistent shear stress-strain equation is employed, have a bearing on the maximum adhesive peel stress. Finite element modelling of joints is also considered and the author says that using one row of isotropic adhesive elements gives results comparable to that of lap joint theories. More rows of adhesive element in the model results in a further increase in maximum adhesive peel and shear stresses. This highlights the refinement of the mesh grid in the model, which enhances idealization of the joint. In the same vein, it also shows a deviation from predicted results from lap joint theories. Carpenter concludes that the maximum adhesive stress derived from these theories are artificial stresses, which in no way correspond to those obtained from a solution of the linearized equations of elasticity, which predict a singular stress state at the corners of adhesive-adherend interfaces.

Improved theoretical solutions for adhesively bonded single and double-lap joints are proposed by Tsai (1998). The adherend shear deformations have been included in the

theoretical analyses by assuming a linear shear stress (strain) through the thickness of the adherends, which earlier theories had not accounted for. This assumption is quite appropriate for laminated composite adherends in particular, and the experimental and numerical results have been reported to be more closely correlated.

2.2.2 Discussion

The above review has illustrated that the development of theoretical models of the adhesive joint has taken over five decades. Volkersen (1938) first proposed a simple shear deformation in the adhesive layer which neglected the eccentricity in the load-path. Later Goland and Reissner (1944) postulated a beam-on-elastic foundation, simulating the joint as consisting of two beams bonded with a negligible adhesive layer (i.e. ignoring the presence of the adhesive layer). They also assumed the non-existence of axial stress and that other stresses would not vary through the thickness of the adhesive layer. Most importantly they took account of rotation due to eccentricity in load-direction which Volkersen (1938) had not considered.

Cornell *et al.*(1953) modelled the adherends as two Euler beams and the adhesive as an infinite number of springs. The results may perhaps be suitable for fatigue stress, given that the adhesive layer is modelled as springs. Allman (1977) presented an elastic stress analysis based on the strain energy density of a particular joint. The effects of bending, stretching and shearing of the adherends were included, and the shearing and tearing action accounted for. He found that the shear stress concentration is 11% higher than that of Goland and Reissner's first analysis while the the average peel stress at the joint edge is 67% lower. All these lap joint theories have assumed zero adhesive shear stress. Ojalvo and Eidinoff (1978) upgraded the theory by considering linear variation of longitudinal and transverse deflections through the adhesive between the adherends.

Phenomenological considerations were discussed at length by Hart-Smith (1973) which

improves our understanding of the sources of non-uniform load transfer, adherend sensitivity, stiffness imbalance and thermal mismatch. He extended the Goland and Reissner model to treat joints with elastic-plastic adhesives. He determined also the critical bending moment in adherends at the end of overlap and discussed the possible three failure modes in the bonded joint. On the other hand, the significance of transverse stresses and the existence of stress gradients through the thickness of the adhesive layer, close to the joint edges were observed by Adams and Peppiatt (1973,1974).

Lap joint theories proposed earlier were compared by Carpenter (1991). His own finite element model suggested that a refined mesh of adhesive layer leads to enhanced maximum adhesive peel and shear stresses and deviated substantially from those predicted by the above theories. The common feature of these theories is that simplifying assumptions are made concerning the behaviour of the adherends and adhesive. These assumptions remove the stress singularities which occur at the edges of the interfaces of the adhesive and adherends and yield differential equations which can be solved to yield the stresses in the adhesive. Maximum adhesive stresses from these solutions can then be used in joint design.

Further, it can be said that various pioneer authors have compromised on important characteristics of the bonded joint factors such as load eccentricity, bending moment factor, variation of stresses through the thickness of the adhesive layer, adherend-adhesive shear stresses. These authors also modelled adherends as beams/plates, ignoring transverse normal/shear stress gradient in an attempt to arrive at the solution for the differential equation. But a review of the literature right from Volkersen (1938) shows that there is a significant development in the theories proposed over the period.

2.3 Modelling of Adhesives

2.3.1 Review

This section briefly outlines the different modelling techniques adopted for adhesive materials in bonded joints. Based on the nature and properties of adhesives, there are various constitutive relations and different types of failure criteria accounted for in numerical studies. Elastic and inelastic behaviour of adhesives in joints are also considered by some researchers. In this section, the focus is on the type of modelling used and the failure criteria, followed in predicting the strength of adhesives. To begin with, Ojalvo and Eidinoff (1978) have defined an adhesive model by a set of shear-strain/displacement equations and accounted for variation of through thickness stress in the adhesive layer while formulating differential equations based on Goland and Reissner's theory. The theory of Goland and Reissner is extended here by a more complete relation between shear strain and displacement corresponding to linearly varying displacements through the adhesive thickness. Based on Ojalvo and Eidinoff's work, an FE model for single lap joint was developed by Lin and Lin (1993), which includes linear variation of longitudinal and transverse deflection in adhesive material. The adherend is modelled as a Timoshenko beam and hence, the realistic behaviour of the joint is restricted by beam theory. The results showed that maximum shear and normal stress increase as adhesive thickness is reduced which is supported by three dimensional FE analysis by Pandey and Narasimhan (2001).

Mortensen and Thomsen (1997,2002a,b) have considered adhesive material as linear elastic, inelastic tension/compression springs, and adopted plate theory for adherends that care considered as beams or wide plates in cylindrical bending. Nonlinear adhesive properties are included by using a tangent modulus approach. In their latter paper, they have suggested the use of adhesive with relatively low values of elastic shear and tensile moduli, i.e. flexible adhesive. These authors have also used modified von Mises criterion as suggested by Gali *et al.* (1981). Gali *et al.* predicted that the yield behaviour of polymeric

structural adhesive is dependent on both deviatoric and hydrostatic stress components. A consequence of this phenomenon there is a difference between the yield stress in uniaxial tension and compression. This ratio is incorporated in the von Mises equation. For most structural adhesive, this criterion is appropriate.

Crocombe and Bigwood (1992) also attempted the modelling of nonlinear behaviour of adhesive by considering a coupled set of shear and tension springs, with adherends as wide cylindrically bent plates. The Finite Difference method was used and they employed full elasto-plastic analysis for the full joint. While the adherend was accounted by the von Mises equation, the adhesive was modelled by a modified Prager model. This model however, was validated for one-dimensional problems only.

While the above papers treat the adhesive as a set of linear/nonlinear shear and tension/compression springs, other researchers have modelled them as proper linear/nonlinear plane/solid elements. This approach is more appropriate than the spring analogy, which accounts for one-dimensionality. Adams and Peppiatt (1974) adopted linear behaviour for plane strain adhesive elements in their single/double lap joints. Mori and Sugibayashi (1992) adopted linear behaviour for their stepped-lap joint plane strain analysis and used von Mises criterion for both adhesive and adherends. The stress-strain behaviour of adhesive FM-73 shows nonlinearity but it is not included in their analysis.

Roy and Reddy (1988a) analysed the single lap joint by considering geometric nonlinearity and by representing the adhesive as a linear plane strain element. In their other paper (1988b), the viscoelasticity of adhesive FM-73 is studied together, with diffusion in bonded joints. The suggested FE model incorporates Schapery's nonlinear viscoelastic constitutive relation and the nonlinear diffusion model of Lefebvre. This nonlinear viscoelastic behaviour is typified by an accelerated and stress-enhanced creep. Earlier, Delale and Erdogon (1981) assumed the adhesive to be a viscoelastic material and showed that the peak value of the normal stress in the adhesive is not only consistently higher

than the corresponding shear stress but also decays more slowly.

Li *et al.* (1999) have carried out nonlinear FE analysis to study stress and strain distributions across the adhesive thickness in composite single lap joints. Two types of epoxy adhesives, flexible and rigid were considered; both were assumed to have linear stress-strain behaviour. Failure in the joint was attributed to crack initiation in the interface layer and the results suggests that more rigid adhesive would lead to considerably lower strains within the adhesive layer. The same authors, while comparing the strength of flexible and rigid adhesives in their most recent paper (Li and Lee, 2001), have observed that the peel and shear stresses was influenced by the modulus of the bonding adhesive: the stiffer the adhesive, the higher the stresses .

Three dimensional modelling of adhesive material as a solid brick element is attempted by Andruet *et al.* (2001) and by Pandey and Narasimhan (2001). While the former accounts for only the linear behaviour of the adhesive, the latter have developed a viscoplastic constitutive relation and considered the modified von Mises yield function. The stress-strain relation of the adhesive is represented by Ramberg-Osgood relation as described by Ramamurthy and Rao (1978). Tong *et al.* (1995) have attempted to establish the relationship between surface displacement and adhesive peel stress in bonded double lap joints. For this, they have done elastic/plastic material nonlinear analysis and have used the von Mises yield criterion. But they have considered only linear elasticity in adhesive/adherend to validate their theoretical relation of peel stress with surface displacement, obtained from holographic interferometry. Further work by Sheppard *et al.* (1998), has developed strain based von Mises equation as a 'cohesive' failure criterion in assessing the damage zone for the bonded joints.

Wang *et al.* (2004) have tried modelling rubber-like flexible adhesive (PU) using the theory of hyperelastic continua. The strain energy based hypothesis of Beltrami and the von Mises yield condition were taken as failure criteria. Given that elastic response is

leading up to large strains, geometric nonlinearity was also included in the analysis. Miao *et al.* (2000) have reported on the modeling of the flexible adhesive *Sikaflex360HC*, in a single lap joint. Highly nonlinear material property was included in the analysis and the rubber-like behaviour is modelled using the HYPER56 element in ANSYS. HYPER56 element is based on large elastic strain deformations as proposed by the Rivlin model. The prediction of shear deformation of the elastomer *Sikaflex360HC*, layer by using HYPER56 element did not correlate well with test data, which invites further analysis using different types of elements.

A paper by Yu *et al.* (2001) presented a complete range of experimental data for a typical adhesive system which is rate-dependent. They have given an extensive set of constitutive data which included constant strain rate, creep, relaxation and recovery for a two-part cold-cure epoxy supplied by Permabond, E27. The study showed that the constant strain rate and creep data were linked through a unique stress-strain relationship and that the rate dependent elasto-plastic model was better than power-law creep model. Chiu and Jones (1995) discussed the use of unified constitutive models for the adhesive FM73. This model is different from other theories which require a definition of yield surface. Here it is not required and the material is always inelastic. When the state of stress is elastic, the inelastic strain is negligibly small but non-zero. The authors have showed that this overstress theory is capable of reproducing the stress relaxation and creep of the adhesive.

2.3.2 Discussion

The review of adhesive modelling in the previous section highlights a few of the common aspects followed in research. The three main features are:

- choice of element for adhesive material
- adhesive stress-strain behaviour
- failure criterion to predict adhesive's strength/failure

Many authors have preferred modelling adhesive as a coupled set of shear and tension/compression springs. This spring analogy is quite convenient in incorporating linear/nonlinear behaviour, but it is constrained to one-dimensional direction. This restriction is overcome by going for plane strain elements in a 2D model and solid brick elements in 3D model. Also it is preferable to use elements with mid-side nodes since displacement continuity is desired at adhesive-adherend interface. Quadratic interpolation in longitudinal and transverse directions increases the accuracy of results even in coarser mesh. In this sense, 8-noded plane strain or 20-noded solid element is highly desirable. The down side of using this approach is a much greater computational effort and may be the reason why many researchers have avoided using a full 3-D analysis.

An overview of the current research work on adhesive modelling and its implementation in bonded structures is given in fig. 2.1. The majority of researchers have worked on the rigid adhesive (Epoxy series) and, largely, they are 2D plane stress/strain analysis, mostly of elastic formulation. The von Mises equation is widely used as a failure criterion to describe adhesive behaviour. It is well established however, that structural adhesives are pressure-dependent and hence von Mises does not represent the system adequately. Hence Gali *et al.* (1981) have derived a modified von Mises equation, taking into account the pressure-dependent nature of adhesives. But as the table suggests, very few authors have adopted this scheme in their modelling. Very little work is available on flexible adhesives (Polyurethane series) and this area in bonded systems remains to be explored. Authors like Wang *et al.* (2004) and Miao *et al.* (2000) have used hyper-elastic equations for modelling highly nonlinear elastic adhesive. While the former used the von Mises equation, the latter has modelled with hyper-elastic elements HYPER56 in ANSYS with Mooney-Rivlin form.

		1-D tension/comp. shear spring	2-D plane stress/ strain	3-D solid elements
Adhesive material	Rigid (Epoxy)	[35][71][72]	[3][9]36][60][64] [70][81][91][95][100]	[9][82]
	Flexible (PU)		[60][68]	[110]
Adhesive formulation	Elastic	[38][71][72]	[9][60][64][77]	[9][101]
	Hyper-elastic		[68]	[110]
	Visco-elastic		[36][92]	
	Elasto-plastic	[35]	[70][81][95]	[82]
	Visco-plastic		[81]	[82]
Failure criteria	Von Mises		[70][95][100]	[110]
	modified von Mises	[71][72]	[81]	[82]
	modified Prager model	[35]		

Figure 2.1: Comprehensive review of adhesive modelling

On adhesive stress-strain behaviour, it is again appropriate to have a nonlinear model as the experimental results for various adhesives have shown nonlinear behaviour beyond their yield limit. Rigid adhesives yield in plastic region while flexible adhesives are highly nonlinear in elastic region. This calls for proper constitutive relations in the model. Implementation of constitutive equations related to Elasto-plastic, visco-elastic and visco-plastic formulation can result in realistic behaviour of the adhesive. With hardening as a parameter, there are algorithms to model bi-linear, multi-linear stress-strain besides the nonlinear curve represented by the Ramberg-Osgood relationship which is based on empirical formulae. However, in the literature, very few papers are found to take into account the rate dependency for adhesive modelling. Delale and Erdogan (1981) have performed visco-elastic analysis using Laplace transforms. Roy and Reddy (1988b) have used Schapery's integral form of nonlinear viscoelasticity. This model provided good rate dependency, allowed full recovery and gave the correct form for the nonlinear volumetric deformation but did not model accurately the varying elastic modulus, hydrostatic stress sensitivity and non-recoverable deformation. To analyse the yielding of adhesive in plastic region with time, a visco-plastic model was developed by Bingham (1922) and later improved by Brinson. Pandey *et al.* (1999,2001) have performed 2D and 3D nonlinear analysis of bonded joints considering viscoplasticity and its effect on adhesive stress distributions were highlighted.

On prediction of cohesive failure in bonded joints, most of the researchers have used the von Mises function. However, the von Mises yield criterion, which was developed for metals and includes no hydrostatic stress sensitivity, is often used for polymers. Gali *et al.* (1981) demonstrated that the yielding of polymeric structural adhesives is dependent on both deviotoric and hydrostatic stress components. Prior to their work, Raghava *et al.* (1973) introduced the ratio of yield stress in uni-axial tension and compression in the von Mises equation, and noted as modified (pressure dependent) von Mises yield criterion. Crocombe and Bigwood (1992)have used the Drucker-Prager yield function to mark failure.

2.4 Experimental modelling of adhesive joints

2.4.1 Review

This section reviews the experimental aspects in bonded joints. Although a wide literature is available, only selected papers relevant to static testing and strength prediction are discussed here.

Roy *et al.* (1997) have reported that a unidirectional laminate has more ultimate strength than cross–ply laminates in their examination of double lap shear joint. The effect of laminate stacking sequence on crack initiation was studied by employing a strain gauge on the specimen. The failure was within the laminate itself, well before the adhesive showed any sign of cohesive or interfacial failure; very few specimens were tested for this strength prediction.

Shin *et al.* (1997) tested statically and dynamically adhesively bonded composite-steel lap joint for high-speed train structures. Rubber toughened adhesive $IPCO9923$ was used for bonding the carbon epoxy with the steel structure. By attempting different sets of stacking layers, the performance of the single lap joint was evaluated. Three different failures, interlaminar delamination, interfacial and in-plane failure, were observed in tests. Shin et al. used the Tsai-Wu failure criterion for in-plane failure of composite, Ye-delamination criterion for interlaminar delamination in composite and von Mises yield criterion for the adhesive. Stress-strain behaviour of rubber toughened adhesive $IPCO9923$ was modelled multi-linearly.

Tsai and Morton (1994) and Tsai, Morton and Matthews (1995) have used Moire interferometry as a means for measuring the displacement profile for their single lap joint. The Moire fringe patterns represent horizontal and vertical displacement contours and the strains were determined by differentiating the displacement field. This was helpful in comparing the adhesive/adherend interlaminar strain distributions with the values

obtained from numerical analysis. Variations in strain distribution due to the stacking sequence in the laminate formed the major part of their study, but it has to be borne in mind that these fringe patterns represent surface deformations only and not any interior displacements.

Deformation and strength of stepped-lap joints bonded with adhesive resin under static tensile loading were investigated by Mori and Sugibayashi (1992). They studied the effect of overlap length and the number of steps in a joint for maximum static strength before failure. Strain gauge measurements were used for strength prediction in experiments and compared with von Mises strains from the analysis. The work showed that strength values in butt are smaller than at the overlap regions. This is clear from the fact that cracks initiate in the butt region. The strength of the joint seems to increase with longer overlap and a greater number of steps, but optimum length and steps were to be decided by further studies.

Cossich (1998) in his MPhil thesis, studied mechanical behaviour of in-plane joints in sandwich structures under static flexural loads. He did experimental, analytical and numerical investigation on a scarf jointed sandwich structure. When strain measurement technique was employed on the specimen by using the strain gauges, tip stresses at the interface of adherend, core and adhesive layer were observed to arrive at the optimum in-plane scarf joint configurations. It was mentioned that a scarf angle of 60^o is the optimum from the analysis while realistic scarf joints at lesser angles were found to have maximum shear area along the bondline. Ahn and Springer (1998a,1998b) have presented their test results and models on repair of composite laminates. Their aim was to evaluate the effectiveness of techniques used for repairing damaged fibre reinforced laminated composites by assessing the tensile strength of the repaired laminate and the failure load of laminates repaired by scarf, uniform lap or the stepped lap technique. Subsequent to the test results, numerical models were also proposed. Special attention was paid to obtain a systematic set of data which indicate how the type of repair material, the geometry

of the repair, the moisture content of the repaired area, the preparation of the surface prior to repair and the processing conditions used during repair, affect the strength of the repaired part. The model takes into account anisotropy of each ply in the laminate, and non-elastic behaviour for the adhesive layer between the laminate and the repair patch. The proposed model considers the structures as one dimensional in nature and no other transverse behaviour is taken into account.

Hashim (1999) tested bonded joints of thick steel adherends for marine structures. The main aspects included the understanding of adhesive properties and their limitations, design and behaviour of structural joints and the use of stress analysis. The bending behaviour of bonded panels was tested under four-point bending and the results showed that the elastic central deflection was higher than the theoretical value. However Hashim used beam theory which assumes the panel/beam section is continuous, to validate the experimental results, and did not take into account material discontinuity in bonded joints. This shows that beam theory cannot be satisfactorily used for validating bending test results and calls for three dimensional finite element analysis, which might give more accurate matchings.

Earlier, Hashim *et al.* (1998) proposed design guidelines for the structural integrity of composite pipe-work systems. They tested adhesively bonded taper/taper connections (GRE) and a double lap shear joint (steel) under a monotonic loading of 0.5mm/min in an Instron universal testing machine. Two failures, adhesive layer and failure in composite adherend just outside the edge of the joint, were reported. von Mises criterion was used for numerical validation. However, the assumption made here is that the behaviour of double-lap shear joints might realistically simulate pipe joints of larger diameters.

On the effect of fibre orientation over the load carrying capacity of prepreg bonded joints, Li *et al.* (2001), found that 0^o fibres perform better than $+45^o$ or -45^o fibres for single lap joints. Displacement controlled testing was done by Sheppard *et al.* (1998) to assess

the critical size of damage zone in metal and Gr/Ep composite lap joints. Cohesive failure was observed in metal lap joints while adherend failure was reported in composites due to their brittle nature. Also the critical size of composite joints was less than that observed in aluminium joints. Strain based von Mises criterion was used for validating experimental results.

Hildebrand and Hentinen (1998) have developed joint elements for joining large FRP sandwich panels to ships. Usually, it is very difficult, even impossible to perform adhesive bonding in a metal shipyard environment, where the conditions in terms of cleanliness, temperature and humidity form a severe obstacle for achieving adhesively bonded joints with high and even quality. But these authors have suggested the concept of prefabricated joint elements which are adhesively bonded to the sandwich panel by the FRP manufacturer and then welded to the ship structure. This allows the adhesive joint to be manufactured in a suitable environment and, the shipyard to weld the FRP parts to the ship, in a similar manner as corresponding metal parts. Hiledbrand and Hentinen have analysed and tested three different joint concepts, *viz.* Overlaminated, Flexible and Clevis, based on their functions and usage. They reported crack and shear failure in experimental studies under static tensile and three-point bending tests. The adhesive used in flexible joint with steel profile was a one-component polyurethane with a break elongation of 300%. To model such a rubber type adhesive, the Mooney-Rivlin model was used for its stress-strain behaviour. Such types of joints, with metals on one side and FRP on the other, are to be analysed effectively and tested for better design.

Experimental determination of residual strength and stiffness of metal-composite joints under cyclic loading of hybrid joints similar to those considered by Hildebrand and Hentinen (1998) was studied by Boyd *et al.* (2004) They studied fatigue life and the effect of cyclic loading on the residual strength of metal-composite joints under in-plane compression, and subjected to the out-of-plane 4-point bending test.

Wright *et al.* (2000) have studied the feasibility of using large FRP double skinned composite sandwich panels as major bulkheads in an 83m Vosper Thornycroft corvette designed to replace their steel counterparts. Two types of steel-composite joints, symmetric and asymmetric in geometry were subjected to static and fatigue testing: the symmetric joints were found to be superior for connection designs. Flexural testing of GRP-steel hybrid joint with Balsa core was carried out by Clifford *et al.* (2002). The results showed sudden loss in stiffness and the authors suggested that simple modifications to the design and materials can yield significant improvements in performace.

2.4.2 Discussion

As described in previous section, various researchers have carried out considerable experimental work to verify the various theories relating to bonded lap joints. In practice, it often proves difficult to implement the boundary conditions specified in theories exaclty. Adams and Peppiatt (1973) used rubber models in showing the importance of the end-shape of the adhesive layer. Similarly, Tsai *et al.* (1994,1995), have adopted Moire interferomentry as a means of measuring the displacement profile, from the fringe contours and patterns. Besides this, the majority of the authors have used strain gauge measurement which is commonly used in collecting experimental data.

Most workers highlight variation of joint strength with lap length and adherend thickness. In addition to this, the lay-up and stacking sequence of adherends are extremely important. Specimens of unidirectional cross-ply laminates have been examined by Roy *et al.* (1997) to study the effect of stacking sequence on crack initiation. Li *et al.* (2001) have also done a similar investigation on fibre orientation. Matthews *et al.* (1982) in their review say that double lap joints have more comparable experimental results with theoretical ones but not for single lap joints owing, to their nonlinear behaviour. In-plane testing and 4-point testing have been done by most of the researchers on patch repair work and in developing hybrid joint connections.

2.5 Numerical modelling of adhesive joints

2.5.1 Review

As lap joint theories are limited by their assumptions, later researchers attempted the modelling of bonded joints by numerical approaches using finite difference and finite element methods. The finite element method avoids the approximations of the closed-form theories, presented earlier, by neglecting the strain energy of certain stresses within the joint, and thus enabling more accurate answers to be found outside the bounds of Goland and Reissner's (1944) criterion. Carpenter (1991) found that more refining of adhesive elements leads to an increase in maximum adhesive peel and shear stress well above the values predicted by lap joint theories. With the advances achieved in computing, there were major contributions in numerical methods in the field of bonded joints.

Lap Joints:

Early finite element analysis by Wooley and Carver (1971) used a program based on linear displacement functions within triangular elements. They assumed the total length of adherends beyond the lap is long and a plane stress state exists. The constant strain quadrilateral element is obtained by combining four constant strain triangular elements. One end of the adherend was assumed to be hinged and the other end was allowed to move freely in the direction parallel to the original bond line. The study dealt with the influence of Young's moduli ratios and geometries on the peel and shear stress distributions. It gave excellent correlation with Goland and Reissner's work but as Adams *et al.* (1997) points out, made no allowance for adherend flexure.

Adams and Peppiatt (1974) used constant strain, two-dimensional, triangular elements which give the stress at the centroid of the element. The results are compared with lap joint theories but the adhesive is modelled for linear stress-strain behaviour while most of the structural adhesives are nonlinear. Roy and Reddy (1988a) have presented nonlinear

analysis of single lap joint to account for the large displacement and rotations in the geometry. They have proposed a two dimensional updated Lagrangian formulation for the model. But it is illustrated to ascertain the rotation and bending for a cantilever beam model only and not for the single lap joint.

Hart-Smith (1981) has detailed further developments in the design and analysis of adhesive-bonded structural joints. The effect of flaws and pores present in the adherends were also addressed by him. The author advocates that with metal adherends, the peel stresses would be limited by the adhesive strength, unless they were designed out. In fibrous composite joints however, any peel stresses must be restricted not to exceed the weaker interlaminar tension strength of the composite rather than the peel strength of the adhesive. To account for the non-uniform adhesive properties, Hart-Smith outlined equations for elasto-plastic analysis. He suggests that for nominally uniform thick adherends, it is better to design the peel stresses out of the joints by tapering the ends of the overlap, than to accept loss of strength imposed by premature peel failures. This is particularly so for fibrous composites which are even weaker in interlaminar tension than are adhesives under peel (normal stress) loading. The inclusion of peel stresses with the shear stresses, would complicate the analysis considerably, both in setting up the governing differential equations and in specifying the adhesive (or composite) failure criteria under combined loading. In the conclusions, it is mentioned that many important aspects of adhesive bonding cannot be handled adequately by an adhesive model that is uniform throughout. Some of these aspects are load redistribution around flaws and porosity, the effects of variation in thickness of the adhesive layer, and non-equilibrium absorption of moisture to change the adhesive properties.

Harris and Adams (1984) have presented the strength prediction of a single lap joint. They modelled the adherend and the adhesive as elasto-plastic. They have analysed the single lap joint with edge spew fillet and considered the geometric nonlinearity, but the type of geometric nonlinear formulation used is not given. They have found that the

maximum stress decreases with the increase in the applied load, when the geometric nonlinearity is considered, and results in higher strength of the joint. The finite element solutions were compared with the closed form solutions and discrepancies were found in predicting the maximum stresses based on closed form analysis.

Tsai and Morton (1994) analysed the three dimensional nature of a single lap joint specimen using the constant strain elements in which boundary conditions accounts for the geometrically nonlinear effects. It was been shown that a three dimensional region exists in the joint specimen, where adherend and adhesive stress distributions in the overlap length near (and especially on) the free surface, are quite different from those occurring in the interior. It was further observed that the adhesive peel stress was extremely sensitive to three dimensional effect. The maximum value of peel stress occured at the end of the overlap in the central two-dimensional core region, rather than at the corners where the three dimensional effects were found. But the authors say that the proposed model is applicable only to short joints.

Tsai *et al.*(1995) have done the experimental and numerical studies of a laminated polymeric composite single-lap adhesive joint. Full-field Moire interferometry is used to measure the surface deformation of the adherends and adhesive (including a spew fillet). It is observed that adhesive longitudinal strain in the spew fillet is insensitive to the three dimensional deformation effect, but not the adhesive shear strain in the spew fillet. The adhesive longitudinal strain is not small enough to be neglected in the stress analysis. Authors have paid much attention to looking at aspects of the laminate such as material non-homogeneity, residual stresses, low transverse strength and shear stiffness, and free-edge problems. Discussions on adherend strain distributions showed that neglecting the adherend shear deformation, usually assumed in the theoretical modelling, would result in inaccuracy in the analysis of composite laminated joint. Initial 2D finite element analysis results showed the need for 3D analysis of the joint to address the effect of bending-twisting coupling on the adhesive strain (or stress) distributions, free edge effect

and the anticlastic effect. It is mentioned that these effects could play a major role in failure initiation of the test specimen.

Stresses in bonded adherends for single lap joints have been compared between numerical and photo-elastic results by Bezine *et al.* (1996). The paper concentrates on a thick adherend which is applied mainly in ship building structures. Single lap joints were considered for analysis because of the complications it throws up by the presence of bending moments which lead to rotation of the overlap. But they have not attempted or suggested the need for geometric nonlinear analysis to account for bending and rotation. Also, instead of applying load on the model, the authors preferred to apply initial prescribed displacements, which is not appropriate and poses many difficulties in modelling. They have showed that stress concentrations appear in the adherends and can lead to failure by delamination, in particular for composite/composite joints. They have concluded that overlap length does not have a very significant influence on stress concentrations in adherends while later studies shows that overlap has a significant influence in adhesive stresses.

Whitney (1997) has presented a stress analysis of a composite double-lap joint using higher order plate theory in which normal strain is included in addition to classical shear deformation. In order to physically capture the proper free-edge effects, each adherend is considered as a separate plate with appropriate interface continuity conditions enforced. The adhesive layer is considered as of negligible thickness. In the end, despite the geometric symmetry of the joint, local bending due to free-edge effects is observed, i.e. the interlaminar stresses are not completely symmetric/anti-symmetric. Whitney concludes that the suggested theory is of sufficient order to satisfy free-edge boundary conditions and produce classic free-edge behaviour (vanishing shear and peak normal stress at the boundary). Also a large (over 30% of the applied axial stress), interlaminar normal stress is encountered at the right hand corner of the joint, suggesting this as a prime location for the initiation of joint failure. Neglecting the adhesive layer in this paper is similar to that

of the Goland and Reissner model. Although Whitney assures the continuity of interlaminar shear and normal stress through the thickness of adhesive, this formulation cannot be useful in predicting stresses in adhesive layer. Sheppard *et al.* (1998) has suggested a damage zone model for the failure analysis of adhesively bonded joints: failure load is predicted by von Mises strain and the model reveals cohesive failure in the adhesive. Also Sheppard has assessed the critical size of the damage zone for the adherends. The composite adherend has a smaller critical size as it is more brittle in nature than metal adherend.

A three dimensional finite element analysis of adhesively bonded plates was presented by Bogdanovich *et al.* (1997) using 3D 'full Lagrange' 27-noded finite element available in the *ABAQUS* package. The analysis is mainly done to address local 3-D regions in the bonded joints by doing a 'submodel' analysis. In this method, a number of local 3-D regions which are of special interest due to expected high stress gradients, are solved separately using displacement values calculated in the first step as the boundary conditions. This concept allows us to increase consistently the accuracy of stress predictions without increasing the total number of degrees of freedom in the computational model. The procedure is applied for the stress analysis of composite to metal double-lap joints. It is identified that this tool is efficient for improving both the displacement and stress calculations at the corner lines.

A finite element formulation based on Timoshenko beam theory and assuming variation of the transverse shear stress and transverse normal stress through the thickness of the adherends, was presented by Lin and Lin (1993). They have considered only linear variation of longitudinal and transverse deflection through the adhesive interface and the through thickness shear stress in the adhesive was held constant. This limitation arises largely because of beam modelling and calls for continuum analysis.

Crocombe and Bigwood (1992) attempted to model the elasto-plastic response of adherends. The adhesive is assumed to behave as a coupled set of nonlinear shear and tension springs, and the adherends as cylindrically bent plates which yield under the action of combined tension and bending. But they have used the finite difference method and the derivations for plastic response of adherend is obtained by bending of neutral axis in the beam, which is one dimensional. Hence this cannot address transverse adherend/adhesive shear stress distributions.

A similar approach, modelling of adherends as wide beams or plates in cylindrical bending and adhesives as linear shear and tension/compression springs, was adopted by Mortensen and Thomsen (2002). The analysis allowed the inclusion of nonlinear adhesive properties. The formulation is based on generally orthotropic laminates using classical lamination theory and the modified von Mises yield criterion is used for nonlinear adhesive. The authors suggest design guidelines, such as the use of symmetric laminates, adherends with high bending stiffness, and the use of zero degree plies adjacent to the face of the adhesive layer.

Pickett and Hollaway (1985) have presented the finite element analysis of single, double, and tubular lap joints. They have considered a linearly elastic behaviour for both the adhesive and the adherends. The single lap joint has been analysed by considering the geometric nonlinearity, where as the double and the tubular lap joints were analysed without considering the geometric nonlinearity. The authors used the program based on the total Lagrangian method developed by Zienkiewicz (1971). The linear finite element formulation, which does not account for the joint rotation during the load, is shown to overestimate the peak adhesive stresses, whereas a close agreement is reached for the peak values in the classical and geometric nonlinear finite element analysis of a single lap joint. However, for a double lap joint the classical and the finite element solutions differ by 25% in their prediction of the peak stress. The authors concluded that this is due to the assumption that the boundary stress resultants are simple tension forces only and that any bending effects which result from the eccentric loading, will be ignored in the classical

theory. In the tubular lap joint, the maximum peel stress differs by 40%, with the finite element results being consistently higher than the classical results. This was attributed to the error in the boundary conditions.

Altus (1985) has analysed the double lap joint three dimensionally to observe the singularities. He has pointed out that a 3-D singularity exists at the corner point of the double lap specimen for the multi-material cases which was not found in the 2-D case. The shear energy, which represents the tendency for yielding, is observed at the 3-D corner. Both the plain stress and plain strain solutions give higher bounds for the critical values, by which the need for 3-D analysis is emphasized.

Andruet *et al.* (2001) have reported the formulation of two and three dimensional geometric nonlinear finite elements for bonded joints. Bernoulli beam elements for adherends and CST element for adhesive is used for 2D while shell and brick elements were used for 3D analysis. The analysis is restricted to 3D effects only, ignoring the issues of edge-effect and material nonlinearity in adhesive.

Earlier work on lap joints with dissimilar adherends was undertaken by Barker *et al.* (1973). Linear FE analysis was carried out to find the stresses in adhesive joint bonded between composite and metallic substrates. The results report that debonding of the joint will probably occur at adhesive ends when the layer is thin, because of higher shear stress. Stress expressions are given by Wu *et al.* (1997) with an improvement on Goland and Reissner's (1944) solution. Belingardi *et al.* (2002) investigated the effect of spew and chamfer size on the stresses in hybrid joints bonded between steel and FRP. Their results have showed that spew and chamfer angles of 45^o are sufficient to obtain a considerable reduction of the stress peaks.

Hybrid joints and composite patch repair:

Erdogan and Ratwani (1971) developed a model for calculating stresses in a stepped lap

joint. One adherend was assumed to consist of an isotropic material while the other as orthotropic material: linear elastic conditions were assumed. The thickness variation of the stresses in both the adherends and in the adhesive was ignored. All normal or peel stresses were thus neglected. Mori and Sugibayashi (1992) have done analytical and experimental work on stepped-lap joint to predict the strength and deformation. Plane strain conditions were assumed and the von Mises criterion was applied both to adherend and the adhesive layer. Mori and Sugibayashi (1992) found that the strength values in the adhesion interface of the butt part are small especially near the edges of the adhesive layer. Overlap length and number of steps seems to influence the final fracture strength.

Johnson (1989) studied the effect of ply stacking sequence on stress in a scarf joint. The discontinuity between individual plies and the variation of laminate stacking sequence on the joint's stress distribution was investigated. Plane stress analysis for an unit tensile load, produced stresses that were significantly different from the smooth curves predicted by closed-form solution. The different load-carrying capacity of the oriented plies caused irregular stress distributions whose characteristics were related to the location of each ply within the stack. The stresses tend to vary within a limited band when the number of plies was increased but the average value of stress in the band is close to the results produced by an equivalent homogeneous laminate.

Mortenson and Thomsen (1997) have performed linear and nonlinear analysis of stepped and scarf joints for composite laminates. The adherends are modelled as beams or wide plates in cylindrical bending, and are considered as orthotropic. The analysis accounts for coupling effects induced by adherends made as asymmetric and unbalanced laminates. The governing equations are formulated in terms of first-order ordinary differential equations, which are solved numerically using the 'multi-segment method' of integration. Newly developed analysis gives robust results and is computationally efficient. Consideration of adhesive as a nonlinear material even for the low levels of external loading is recommended in the paper.

Scarf joint repairs to Gr/Ep honeycomb structure have been investigated by Baker *et al.* (1999). Their FE results predict that high stresses will occur at ply drop-offs and at the top of the scarf. Shear stress in the adhesive is not uniform over the length of scarf due to varying longitudinal compliances of the plies within Gr/Ep adherends. They have done 3D analysis to ensure that cross-compliance coupling between the plies is properly accounted for. On their experimental analysis, they have observed some creep deformation in the adhesive, which may be significant for the failure of the scarf joints under hot/wet conditions. Ikegami *et al.* (1990) investigated the strength of scarf joints between GRP and metals. Effect of scarf length and elastic imbalance on the deformation are examined, which showed that the stress concentration in the adhesive layer and the adherend is pronounced at the adhesive edge of the obtuse scarf angle of the GRP adherend. The greater the scarf length, the flatter is the stress distribution. They also found that elastic imbalance between adherends reduces the joint strength.

Lam Y.C. *et al.* (1995) have validated their stress intensity results from multi-layer theory by performing 3D FE analysis of plates bonded with unbalanced laminates. For one-sided repair cases, they have showed that the length of the unpatched portion in the length direction contributes to an important effect on stresses in the symmetric section of the patched plate. Soutis and Hu (1997) have examined the compressive behaviour of bonded patch repaired with composite laminates: a nonlinear stress analysis was performed on a double-lap joint in order to identify critical joint parameters and to design an efficient external patch repair. The authors found that oversized patches not only increase the structure's weight but also increase the stress concentrations in the repaired region, which can cause premature failure. It was observed that by reducing the patch thickness near the edges of the overlap and increasing the local adhesive thickness, the stress concentration in both shear and peel stresses are decreased. Also a three dimensional finite element analysis was performed to determine the stresses in the optimum repaired configuration and is used with a stress failure criterion to predict the ultimate

failure load. Finally, it has been observed that by using the optimum patch configuration, bonded repairs can recover 80% of the undamaged laminate strength.

Sun *et al.* (1996) has done analysis using Mindlin plate theory for a cracked aluminum plate repaired with bonded composite patches. The adhesive layer is modelled as effective springs connecting the patch and aluminium plate. A procedure for calculating the strain energy release rate along the debond front at the aluminium-adhesive interface is proposed. The stress intensity factor obtained for the double-sided patches is matching with the results of boundary element solutions and three dimensional solutions. For the single-sided patch, there were some discrepancies with three dimensional finite element model.

Ahn and Springer (1998a,1998b) have presented their test results and models on repair of composite laminates. Their aim is to evaluate the effectiveness of techniques used for repairing damaged fibre reinforced laminated composites, by assessing the tensile strength of the repaired laminate and the failure load of laminates repaired by scarf, uniform lap and stepped lap techniques. Subsequent to the test results, numerical models were also proposed. Special attention was paid to obtain a systematic set of data which indicates how the type of repair material, the geometry of the repair, the moisture content of the repaired area, the preparation of the surface prior to repair, and the processing conditions used during repair, affect the strength of the repaired part. The models take in to account anisotropy of each ply in the laminate, and in the repair and non-elastic behaviour of the adhesive or resin inter-layer, between the laminate and the repair patch.

2.5.2 Discussion

The literature covered in the previous section dealt with a wide range of numerical modelling aspects of bonded joints from simple stresses in bonded joints to nonlinearity in the system and numerical models for step-lap, scarf, double lap and patch repair structures. While most of researchers have taken Goland and Reissner's (1944) model as the basis for

their analysis, others have preferred plate analysis and a 3D continuum approach to account for natural behaviour of the bonding system. The accuracy comes in the idealization of the joint by proper selection of the finite element and meshing schemes adopted. The inability of classic theories to account for edge-effect, transverse normal/shear variation has lead to modelling by the finite element method. Also, while addressing nonlinearities in the joining system, both geometrical for bending/rotation, and material nonlinearity for the adhesive, has to be accounted. Crocombe and Bigwood (1992) even attempted to consider material nonlinearity in adherends. All this requires a technique like the finite element method to simulate the realistic behaviour. But one has to compromise on larger computing time required for any nonlinear analysis. While Hart-Smith (1981) prefers the continuum mechanics approach in analysis of bonded structures, Adams *et al.* (1997) sees FEM as being the only accurate solution for determination of adhesive and adherend stress distributions. This preference is particularly relevant since it is the only technique that can adequately account for adherend plasticity and the presence of spew fillets.

An overview of the current research work on numerical modelling and its implementation in bonded structures is given in figure 2.2, which indicates that most of the work has been done for metal and composite adherend material in the 2D domain. Very few papers have presented three dimensional analysis. With such detailed collection of review, much attention is paid here to the following aspects:

- modelling of bonded composite laminates
- dissimilar adherends
- scarf and step-lap joints
- ply orientation and stacking sequence
- through thickness and interlaminar stress/strain distributions
- three dimensional effects
- yield criteria for adhesive and failure mode

			2D Plane stress/strain		3D Analysis	
			Linear	Nonlinear	Linear	Nonlinear
Joint type	Lap Joints	Identical adherend	[3][9][19][38] [111][114]	[35][45][48] [72][95][102]	[8][9][101]	[76][82]
		Non-identical	[13][18][89][116]	[48][79]	[22]	
	Scarf/ Stepped-lap	Identical	[34][37][70]			
		Non-identical	[29][57][71]			
	Hybrid/ Patch repair		[25][32][34] [54][115]	[5][6]	[9][11] [59][99]	[98]
Failure criteria	Tensile Stress/strain				[101]	
	von Mises		[19][70]	[35][48][95]		
	modified von Mises			[72][81]		[76][82]
Failure Mode	Adherend failure			[48]		
	Adhesive failure		[3]	[48][95]	[22][101]	
	Interfacial failure		[111]	[48]		

Figure 2.2: Comprehensive review of numerical modelling

Tsai *et al.* (1995) have done two-dimensional analysis of composite laminates. Issues arising out of interlaminar stress/strains have led to the necessity for considering three dimensional analysis. Such 3D analysis can address edge-effect, anti-clastic effect and bending-rotation coupling in the laminates. Little literature is available pertaining bonded systems for these issues. Some authors like Johnson (1989) look at the effects of ply stacking sequence on the stresses developed within the adhesive and adherends. The results shows that the adhesive interface shear stresses oscillate about an average determined by Erdogan and Ratwani's solution (1971).

On scarf and step-lap joints, Hart-Smith (1974) describes the scarf joint as mathematically the most difficult to solve, due to the governing equations not possessing standard closed form integrals. This could lead to a model of various stepped-lap joints approximating for a smooth scarf joint. Distribution of stresses in a typical step-lap joint is addressed by Erdogan and Ratwani (1971), and recently by Mori and Sugibayashi (1992) also. The problem of non-identical adherends is handled by Erdogan and Ratwani (1971) by bonding isotropic and orthotropic materials together. As it is seen from figure 2.2, most of the work on scarf/stepped-lap joints has been done for linear case only and that too in plane stress/strain condition. Only Baker *et al.* (1999) have attempted to look at variation in stress across the plies in the scarf joint adherend. To accomplish this, they have adopted a 3D finite element method. On hybrid joints/patch repair models, Cossich (1998) has analysed sandwich structure with aluminium/composite skin, with the balsa core for the flexure case. While Cossich's numerical results shows the optimum scarf angle as 60^o, the experimental specimen were of small scarf angles.

On the choice of finite elements, Whitney (1997) has proposed a higher-order plate theory for the adherends but neglects the presence of adhesive similar to the Goland & Reissner's (1944) model. Authors like Lin & Lin (1993) and Mortensen and Thomsen (2002a,b), have opted for beam elements for adherends. Adhesives are modelled as linear tension/compression springs. On three dimensional anlysis, Andruet *et al.* (2001)

have attempted for three dimensional analysis but for isotropic material. Altus (1985) addressed stress singularities in three dimensional zone in the joints. Bagdonovich and Kizhakkethara (1997) attempted three dimensional modelling with the concept of a sub-modelling approach, which outlines stress singularities. On laminates, Mortensen and Thomsen (2002a) gave design guidelines for the use of symmetric laminates and ply orientation.

From the review, it can be summarised that the previous finite-element analyses of adhesive joints were either based on simplified theoretical models or the analyses themselves did not exploit the full potential of the finite element method. Further, several investigations involving finite element analyses of the same adhesive joint system have reported contradictory conclusions about the variations of stresses in the joint. This can be again attributed to their assumptions about lap theories and about modelling approaches. Thus, it is understood that there is a need for a realistic modelling of adhesive joints.

2.6 Summary

In earlier sections, a critical review of the literature is presented followed by discussions of various types of bonded structures and adhesive material with respect to modelling and its applications. The following main points can be emphasised as the highlights of the work in the current research field.

- Almost all the proposed theories are developed for the single lap joints with compromises on load eccentricity, bending moment factor, through thickness stress variation etc., in an attempt to arrive at an analytical solution. Only Lubkin (1957) proposed a theory for scarf joints.

- Most of the work on adhesive modelling considers 2D plane stress/strain with the elastic constitutive equation. Few authors have formulated adhesive nonlinearity based on bi-linear, multi-linear stress/strain relationship.

- On the choice of failure criteria for the adhesive material, the most used yield criterion is the von Mises criterion even though the modified von Mises equation which considers pressure-dependent nature of adhesive is appropriate.

- For flexible rubber-like adhesive material modelling, very little literature is available. Highly nonlinear elastic behaviour is modelled using a hyper-elastic concept of continuum.

- Yielding of rigid adhesives in plastic region is highlighted, by authors like Hart-Smith and Adams, and they are rate-dependent as well.

- As far as modelling of adhesive bonded joints are concerned, most of the work has resorted to a 2D analysis of single lap joint to validate their analytical/experimental results. However, joining of composite laminates and the effect of ply stacking sequence calls for appropriate orthotropic plate theory or three dimensional analysis.

- Investigation of joints with adherend imbalances (on their geometric and stiffness parameters) have been primarily done for the linear case without accounting for the geometric nonlinearity in single lap joints.

- However, hybrid joints and patch repair models have been realistically modelled, in accordance with the practice in industry, by considering stepped-lap, scarf and external patch with FRP or GRP materials. Again, the von Mises equation is taken as the the failure criteria for both metals and composites by the majority of the researchers.

- The literature review shows that only a few three dimensional analyses of laminates of different ply orientation in bonded joints have been used to study the through thickness and interlaminar stress/strains, while some have modelled composite adherend as a skin laminated with orthotropic properties.

- Work on scarf joints and sandwiches with scarf bonding looks for the optimum scarf angle which is reported as 60^o; in practice, scarf angles are very small in the range of 1:20 to 1:40, especially for marine structure applications.

From the comprehensive review outlined in earlier sections, it can be seen that modelling of bonded joints and structures can be enhanced by combining various formulations. Further research therefore, needs to be performed so as to remove current weaknesses and hence to contribute to further developments. Following issues can be mentioned provides scope for the research and some of them are selected in this research work.

- Given that adhesives are pressure-sensitive, it is more appropriate to consider modified von Mises equation as a failure criterion rather than the commonly adopted von Mises equation.

- The stress-strain relationship of the adhesive can be represented by the Ramberg-Osgood relation. This empirical equation is useful in modelling nonlinear relation, particularly for flexible adhesives, which are highly nonlinear in the elastic region.

- For rigid and semi-rigid adhesives, the stress/strain profile can be obtained by specifying their hardening parameter, which results in a bi-linear elasto-plastic hardening or in a elasto-perfectly plastic (non-work-hardening) condition. The Ramberg-Osgood curve can also be fitted for comparison.

- Results on single lap joints will be more realistic if the load eccentricity and load increments are accounted for. Hence, a program to include geometric nonlinearity is recommended.

- It is also envisaged that a three dimensional analysis will be useful for edge-effect, anti-clastic effect, through thickness variations and 3D zones, in the lap joint.

- A three dimensional analysis will be helpful in looking at inter-laminar stresses across the plies of different orientation in a bonded laminate structure also. While the review refers to some of the experimental work on bonded laminate structures, little is known on the numerical validation.

- Modelling and analysis of scarf joints with small scarf angles should be possible in 3D modelling. Outcome from the 3D analysis can offer good understanding of the repair works followed in marine structures.

- Investigation on the use of FRP components in larger ships of steel construction which could benefit from weight reduction. With the possible modelling of hybrid joints bonded comprising steel, FRP and Balsa core materials, useful guidelines can be framed for using FRP in large ship structures.

Chapter 3

Proposed Methodology

3.1 Introduction

The previous chapter reviewed the literature in some detail, on the basis of four categories *viz.*, theoretical approach/modelling, experimental work, numerical approach/modelling and adhesive modelling, in bonded joints. As a result of the critical study, a broad range of research proposals are identified and listed in the previous section. Some of these research proposals are now considered in relation to the application of bonded joints in marine structures. The problems chosen and the research methodology for studying them is proposed in following sections.

3.2 Study of lap joint with non-identical adherends

It is known that the stress pattern around adhesively bonded joints with non-identical adherends is characterized by a high stress gradient through the thickness. Hence the idealization of the structure as a 2D plane requires good engineering judgement. Even the simplest configuration, such as a single lap joint under the action of tensile forces, undergoes a combined action of bending and stretching and leads to complications in the stress flow in a three dimensional pattern. The solution procedure for stress analysis of single lap joints with imbalances in adherend thickness has to account for discontinuity

in geometry and material properties, anisotropy in adherends, nonlinear behaviour of adhesive material, etc. Load eccentricity in a typical single lap joint exhibits specific three dimensional effects such as (i) free-edge effect; (ii) anticlastic effect; and (iii) bending-twisting coupling effect. None of these can be assessed by two dimensional plane stress or plane strain analysis, especially in the presence of cracks. This study attempts to address the above mentioned three dimensional effects in a typical single lap joint with non-identical adherends.

It can be summarised from the literature review described out in chapter 2 that a wide range of issues have been accounted for in analysing bonded joints. The majority of the work has been done using a plane stress/strain assumption, thus ignoring typical three dimensional effects such as *anticlastic, twisting-bending*, that are common in a single lap joint. However high stress gradients at the overlap ends resulting from material discontinuity and differences in material properties and thickness, have not been adequately discussed. It is important that analyses should comprise both material and geometrical nonlinear formulations that can be applied in three dimensional domain, in order to reflect realistic behaviour. In the light of above, it is proposed to develop a three dimensional material and geometrical nonlinear finite element program for the analysis of bonded joints. This program comprises the following features: (a) the bending of adherends; (b) differential straining of adherends; (c) pressure dependent properties of adhesive material and (d) stress free boundary conditions at the edges. Material nonlinear formulation is coded based on the constitutive relations for the pressure-dependent adhesive using a modified von Mises yield criterion. Particular attention is paid here to the three dimensional behaviour of the lap joint with dissimilar adherends and the resulting stress variations in adhesive layer.

The proposed study focusses on the following four issues:

1. the influence of geometrical nonlinearity on joint deformation under a varying load and the influence of material nonlinearity on adhesive stresses,

2. the effect of geometry and material properties on the behaviour of a joint with dissimilar adherends,

3. adhesive stress distribution pattern arising from the variation of adherend thickness and

4. the identification of the above mentioned three dimensional effects arising from the eccentric load path in a single lap joint.

3.2.1 Study of a butt-strap joint system

This work concerns the numerical modelling of a single butt-strap joint system that is derived from the deck-to-superstructure connection of a 34m long Vosper Thornycroft (VT) Patrol craft as sketched in figure 1.5. This joint consists of two dissimilar adherends, aluminium and steel, bonded by a semi-rigid adhesive material Plexus MA550. The purpose of the analysis is to identify the possible failure modes in an adhesively bonded single butt-strap joint by obtaining the realistic stress state in the adhesive-adherend interface layers. By considering both material and geometric nonlinearities for a three dimensional finite element (FE) model of the bonded joint, the focus is fixed upon the three dimensional joint deformations and the adhesive stresses in particular, for the joints with thicker adhesive layers.

Three dimensional effects are likely to be dominant in the case of a single butt-strap joint bonded by a flexible adhesive material that has a high value of Poisson's ratio. Furthermore, the large difference in adherend and adhesive material properties often results in large out-of-plane deformations, stress reduction at three dimensional corners and lateral contraction. In general, three types of adhesives are used to bond the structural components. They are rigid, semi-rigid and flexible adhesive systems. Rigid adhesives have a distinct initial yield limit and yields further in a plastic region which are usually modelled by elasto-plastic bi-linear hardening condition (refer chapter 5). Flexible adhesives are highly nonlinear in elastic region and use theory of hyper-elastic continua for

modelling (Wang *et al.*, 2004). On the other hand, semi-rigid adhesives have lower value of yield stress and their transition from elastic region to plasticity is not distinct. Material properties for these types of adhesives are presented in table 3.1 for comparison. Of the three types, semi-rigid and flexible adhesive systems are found to be appropriate for many marine applications. In particular, semi-rigid adhesive material like Plexus MA550 is suitable since it has high gap filling capabilities with relatively high strength (Brede, 2001).

With regard to modelling the behaviour of these types of adhesives, a set of constitutive equations and a yield criterion equation are necessary to implement in a finite element program. Stress-strain behaviour for a semi-rigid adhesive material can be obtained by a nonlinear curve represented by Ramberg-Osgood relation (Ramberg and Osgood, 1943). They have described a simple stress-strain formula in terms of three parameters viz., Young's modulus and two secant yield strengths. Though Matthews *et al.* (1982) have mentioned in their review, the application of Ramberg-Osgood to describe stress-strain law for an adhesive material few researchers have attempted to model an adhesive material; in this current work however, the Ramberg & Osgood equation is proposed as an ideal choice for an adhesive material that is classified as semi-rigid in behaviour. This equation can adequately represent the adhesive material which does not show clear transition from elastic to plastic region as mentioned above.

Characterisation of the adhesive material by an appropriate choice of stress-strain relation is necessary which could reflect the realistic stress state in a joint system. This is because a simple linear formulation for the adhesive material normally results in huge stress values at critical locations that are well above the actual strength of the adhesive material. For the case of a double-butt strap joint, Mitra *et al.* (1995) have looked at the interfacial stresses and deformations and have reported increased stress values as a result of linear formulation. Such a scenario is more likely in the case of a single butt-strap joint configuration. This joint with an eccentric load path bonded by a flexible adhesive

materials warrants an ideal formulation which can address the realistic strength capacity of the adhesive and bending of adherends due to joint rotation.

Hence, in order to have a realistic assessment of displacements and stresses in a joint system, it is important to have a comprehensive analysis that could comprise the aspects mentioned above *viz.*: a) Geometric nonlinearity, b) Material nonlinearity, c) Three dimensional modelling. Guidelines framed by Germanischer Lloyd (2001) also outline the significance of nonlinear effects and recommend geometric nonlinearity for flexible structures with large deformations and material nonlinearity, wherever the plastification occurs in structural components. Therefore, a three dimensional finite element program incorporating the above aspects is developed for the analysis. The methodology included characterisation of semi-rigid adhesive material by which the resulting adhesive stresses are compared with the actual strength of the adhesive. Following this, observations related to on-set of nonlinearity are made to identify the possible failure modes in a three dimensional domain.

3.2.2 Study of GRP-Steel hybrid joint

The hybrid joint considered in the study is based on the design for hangar to weather deck connections on the *La Fayette* class frigates (figure 1.6). The objective of the work is to understand the failure mechanisms of the hybrid joint when it is subjected to various loading cases like in-plane, out-of-plane and flexural forces encountered in the superstructure. Particular attention is paid to the stress profile in a three dimensional domain and critical locations of stress concentration, that lead to failure of the joint.

The application of hybrid composite-metal joint structures has been gaining momentum over the past few years in various disciplines of aerospace, land transport and in marine industry (Mouritz et.al., 2001). Although the use of such hybrid joints in the aerospace industries was a common practice, the use of composite material as a reinforcement for

a ship superstructure was only recently pioneered by Grabovac et.al., (1993). They designed a carbon fibre composite doubler to reinforce the aluminium alloy deck of a Royal Australian Navy FFG-7 frigate superstructure. Further hybrid joint designs for joining large FRP-Sandwich to metal structures were developed by Hildebrand and Hentinen (1998). They have analysed and tested three different joint concepts *viz.* Overlaminated, Flexible and Clevis similar to the one shown in figure 1.7 based on their functions and usage. They reported crack and shear failure in experimental studies under static tensile and three-point bending tests. The adhesive used in flexible joint with steel profile was a one-component polyurethane with a break elongation of 300%. To model such a rubber type adhesive, the Mooney-Rivlin model was used for its stress-strain behaviour.

Wright et. al.. (2000) studied the feasibility of using large FRP double skinned composite sandwich panels as major bulkheads in an 83m Vosper Thornycroft corvette design, to replace their steel counterparts. Two types of steel-composite joint, symmetric and asymmetric in shape were subjected to static and fatigue testing; the authors preferred symmetric joints to asymmetric ones for connection designs. Flexural testing of GRP-steel interface with Balsa core was performed by Clifford et. al., (2002). Various designs of hybrid joint were proposed in order to reduce the stress concentration by varying the length of steel insert. Similar work was attempted by Cao and Grenestedt (2003) but they re-designed hybrid the joint by reducing the steel penetration in order both to remove the stress concentration in the critical areas and to achieve further reduction in weight. Recently Boyd et. al., (2004) performed the experimental and numerical investigation of a similar hybrid joint based on the design for the hangar-to-weather deck connections on the *La Fayette* class frigates. They characterised the fatigue life of the hybrid joint and assessed the residual strength of the joint under in-plane and out-of-plane loading. They developed a stress reduction model to account for the nonlinear behaviour of the joint after the initial failure.

The present study deals with three dimensional modelling of the hybrid joint that was

referred by Boyd et.al., (2004). Numerical modelling of hybrid joints have been either plane strain or plane stress with thickness problem in the research work described above. All of these authors have observed that the critical stress concentration occurs at the interface layer where the three materials *viz.* Core-GRP-Steel are bonded. But a three dimensional analysis of the hybrid joint has not been attempted for this particular type of geometry. It is felt that a three dimensional analysis of hybrid joint is necessary while considering the following aspects: (i) shape and asymmetric geometry of the joint, (ii) set of interface layers where materials of varying properties are bonded, (iii) eccentricity in the load path in case of in-plane loading (iv) moment induced used in case of out-of-plane and flexural loading situation and (v) stress variation across the lateral direction. Given the complications in the joint geometry and the different materials of which the joint is composed, three dimensional analysis of such a joint can provide a better understanding of the behaviour of the joint.

3.3 Proposed Methodology

Concerning the numerical modelling, a wide range of issues pertaining to bonded connections and structures have been discussed in the previous chapter. It can be observed from the review that attention has been paid to one particular area of interest in the model or structure while compromising on other aspects, for example, studying adhesive behaviour without accounting for geometric nonlinearity in single lap joints for load eccentricity, or doing geometric nonlinear analysis but ignoring the plasticity in adhesive materials. It will be more precise to consider the various aspects governing the behaviour of bonded structures before opting for the analyses. Therefore, the main objective of this research work is to arrive at such a comprehensive tool comprising various formulations in one place. Once that formulation is available, it will be applied for different kinds of bonded structures and the emerging results shall provide a useful insight for a better understanding of their behaviour.

As a result of the literature, it is proposed here to develop a programming tool which

can handle the issues of geometric and material nonlinearity in a three dimensional domain. Also it is been decided to use modified von Mises equation as a failure criterion, and stress-strain relation based on the Ramberg-Osgood curve. These two formulations are not currently available in standard finite element codes like $ANSYS$ and $ABAQUS$. To use such packages it is necessary to develop an interface algorithm (a macro program). Hence the approach here will be to develop own program code. Therefore a $FORTRAN$ code for a three dimensional finite element program, considering both the nonlinearity for bonded joints, is written and explained in detail in the following chapter. The program deals with the modelling of a 20-noded 3D iso-parametric finite element for both adherend and adhesive materials. The total Lagrangian method is implemented for large displacement, large rotation but small strain to account for geometrical nonlinearity and elasto-plastic constitutive equations are numerically implemented to include material nonlinearity. Besides this, the modified von Mises equation is formulated as a failure criteria for the adhesive material. The Ramberg-Osgood relation is adopted for characterising a semi-rigid adhesive material. Developed FE code can be used for models with more than three materials, the minimum number of materials used in dissimilar joints. The program also handles materials with orthotropic properties. As mentioned earlier, the available program has all the features one would like to use for the comprehensive analyses. The following points can be highlighted as the special feature of the program:

- The formulation is a three dimensional one which gives realistic displacement/stress result and is useful in identifying the three dimensional nature of the structure in a particular region where stress concentration are critical.

- Geometric nonlinear analysis is possible for joints where large displacements/rotations are occurring, as in single lap joints. Also, it will be useful in modelling of semi-rigid adhesives that show excessive deformation even at low levels of load magnitudes.

- As adhesives unlike metals, are pressure-dependent, it is more appropriate to use the modified von Mises equation as their failure criterion. This algorithm is included in the program and consideration of von Mises criteria is also possible. This gives a

choice for failure criteria for adhesive and adherend materials.

- Elasto-plastic analysis can be done by modelling bi-linear stress/strain curve. The Ramberg-Osgood equation can produce more realistic stress/strain behaviour, particularly for flexible adhesives which are highly nonlinear within the elastic region.

- The program has been coded to model materials with orthotropic properties paving the way for analysis of composites and sandwich core materials.

With the program tool available, issues related to bonded structures addressed in the previous section are now to be attempted.

Table 3.1: Material properties for different types of adhesives (Brede, 2001)

Adhesive Type	Young's modulus (MPa)	Poisson's ratio	Shear modulus (MPa)	Tensile strength (MPa)
Vantico Araldite420 (rigid)	1894.7	0.40	679.3	28.3
Plexus MA550 (semi-rigid)	361.0	0.47	119.0	12.0-14.0
Sikaflex 292 (flexible)	2.1	0.49	0.62	2.8

Chapter 4

Solution Procedures and FE formulation

4.1 Introduction

This chapter describes the formulation of an FE program which computes both geometric and material nonlinear algorithms. Geometric nonlinear aspects and their implementation in the program code for a three dimensional domain are described in some detail. Following this, a finite element formulation based on elasto-plastic constitutive equations is presented. Geometrical nonlinear Equations can be found in standard text books and they are presented here for the complete description of FE formulation in a three dimensional domain. Equations related to material nonlinearity and incremental equations of equilibrium forms the major contribution in this chapter. Computational procedure adopted in the FE program code is illustrated at the end of the chapter.

4.2 Geometric nonlinear aspects

The present formulation is only restricted to large displacement, large rotation but small strain problems. There are two formulations of geometrically nonlinear problems namely the total Lagrangian formulation based on the initial configuration of the body and the

Eulerian formulation based on the deformed configuration of the body. A critical review of both the methods can be found in references Bathe *et al.* (1975) and Gadala *et al.* (1984). Some applications of geometric nonlinearity can be found in references Hofmeister *et al.* (1971), Zienkiewicz and Nayak (1973), Bargan and Clough (1973), Bathe and Ozdemir (1976), Argyris and Kleiber (1977) and Bathe and Bolourchi (1979).

It is apparent that with two types of formulation available, in the development of a general purpose nonlinear program a decision needs to be made on the procedure to be adopted. Both the procedures (the total Lagrangian and the updated Lagrangian) are derived from the basic principle of virtual work and are valid for nonlinear material behaviour, large displacements and large strains (Bathe *et al.*, 1975). In theory there is no difference in the formulations. Therefore the question of which formulation is to be used depends on the numerical effectiveness of the methods. Bathe *et al.* (1975), Schrefler *et al.* (1983) and Wood *et al.* (1977) discussed the updated Lagrangian and the total Lagrangian formulations and pointed out that the total Lagrangian approach offers advantages since the initial configuration remains constant which simplifies the formulation and the computation. An advantage of the total Lagrangian formulation is that the derivatives of the interpolation functions are with respect to the initial configuration, and therefore need to be formed only once if they are stored on the back up storage for use in all the load steps. Further anisotropy presents no problem in the total Lagrangian formulation (Schreler *et al.*, 1983). Hence in the present work the total Lagrangian approach is used.

4.2.1 Definitions of strains and stresses

In the field of continuum mechanics, strain is a fundamental quantity in measuring the degree of deformation in a deformed body. Strain usually means the change in dimension per unit reference configuration. Many different definitions of strain can be obtained by different types of change of configuration or different types of unit reference configuration. When the deformations are small, all these definitions are nearly same, but when the deformation is finite these definitions will give quite diverse values of strains. The two

basic definitions of finite strains are the Lagrangian finite strain and the Eulerian finite strain. Different definitions of strains and the corresponding conjugate stresses can be found in Fung (1965), Bathe (1996) and Youzhi and Desai (1990). Before the total Lagrangian formulation is presented, the definitions of the stresses and the strains used in the formulation will be given.

Deformation and strain :

let

$X = [x, y, z]^T$

define the rectangular coordinates of a material point in a body shown in fig 4.1 before the deformation. If this point is displaced by

$U = [u, v, w]^T$

measured relative to the fixed frame of reference, its new coordinates will become

$$\overline{X} = [\overline{x}, \overline{y}, \overline{z}]^T = X + U \tag{4.1}$$

Let us consider two neighbouring particles P_o and Q_o on the undeformed body. They move to P and Q after deformation as shown in fig 4.1. If the distance between $P_o\&Q_o$ and $P\&Q$ are given by dX & $d\overline{X}$ respectively. The relation between dX and $d\overline{X}$ is given by

$$d\overline{X} = JdX \tag{4.2}$$

where

$$J = \left[\begin{array}{c} \overline{x},\overline{y},\overline{z} \\ \hline x,y,z \end{array} \right] = \begin{bmatrix} \frac{\partial \overline{x}}{\partial x} & \frac{\partial \overline{x}}{\partial y} & \frac{\partial \overline{x}}{\partial z} \\ \frac{\partial \overline{y}}{\partial x} & \frac{\partial \overline{y}}{\partial y} & \frac{\partial \overline{y}}{\partial z} \\ \frac{\partial \overline{z}}{\partial x} & \frac{\partial \overline{z}}{\partial y} & \frac{\partial \overline{z}}{\partial z} \end{bmatrix} \tag{4.3}$$

is a Jacobean matrix defining the deformed state. Similarly $\overline{J}$ from the definition (5.2) can be written as

$$\overline{J} = J^{-1} = \left[\begin{array}{c} \overline{x},\overline{y},\overline{z} \\ \hline x,y,z \end{array} \right]^{-1} \tag{4.4}$$

The change in length can be written as

$$\frac{1}{2}(d\overline{S}^2 - dS^2) = \frac{1}{2}(d\overline{X}^T d\overline{X} - dX^T dX) = dX^T \epsilon dX = d\overline{X}^T \overline{\epsilon} d\overline{X} \tag{4.5}$$

where

$$\epsilon = \frac{1}{2}(J^T J - I) \tag{4.6}$$

is the Lagrangian definition of the strain (Green's strain) and

$$\overline{\epsilon} = \frac{1}{2}(I - \overline{J}^T \overline{J}) \tag{4.7}$$

is the Eulerian definition of strain.

I is an identity unit matrix.

By substituting Eq. (4.1) into the Eqs. (4.6) and (4.7) the explicit engineering expressions for the strain components are obtained and they are given in the next section.

Definitions of stresses :

The natural definition of stresses is the Eulerian one referring in the usual way to the forces per unit deformed area. Thus,

$$\overline{\sigma} = \begin{bmatrix} \overline{\sigma}_x & \overline{\tau}_{xy} & \overline{\tau}_{xz} \\ \overline{\tau}_{yx} & \overline{\sigma}_y & \overline{\tau}_{yz} \\ \overline{\tau}_{zx} & \overline{\tau}_{zy} & \overline{\sigma}_z \end{bmatrix} \tag{4.8}$$

in the matrix notation.

The forces acting on the area $d\overline{A}$ are given in the vector form as

$$d\overline{F} = \overline{\sigma} d\overline{A} \tag{4.9}$$

Hill (1950) has defined particular conjugate pairs of stress and strain variables. Thus for the Green's strain the conjugate stress is the second Piola-Kirchoff stress σ.

The equivalent force vector acting on an original undeformed area dA is given by an

expression

$$dF = \sigma dA \tag{4.10}$$

and the actual force on the deformed area

$$d\overline{F} = JdF \tag{4.11}$$

But the relation between dA and $d\overline{A}$ is given by

$$d\overline{A} = |J|J^{T^{-1}}dA \tag{4.12}$$

or

$$dA = |J|^{-1}J^T d\overline{A} \tag{4.13}$$

From Eqs. (4.9) to (4.13), we have the stress transformation relation

$$\sigma = |J|J^{-1}\overline{\sigma}J^{T^{-1}} \tag{4.14}$$

which shows that the second Piola Kirchoff stress is also a symmetric one.

4.2.2 Explicit form of Lagrangian formulation

Before a finite element solution can be obtained, a more explicit presentation of various terms arising is necessary. This will be presented in the context of a three-dimensional solid.

Strain-displacement relationships:

The Green's strain in vector notation can be written using the engineering definitions as

$$\epsilon_x = \frac{\partial u}{\partial x} + \left[(\frac{\partial u}{\partial x})^2 + (\frac{\partial v}{\partial x})^2 + (\frac{\partial w}{\partial x})^2\right] \tag{4.15}$$

and

$$\gamma_{xy} = \frac{\partial u}{\partial x} + \frac{\partial v}{\partial x} + \left[\frac{\partial u}{\partial x}\frac{\partial u}{\partial y} + \frac{\partial v}{\partial x}\frac{\partial v}{\partial y} + \frac{\partial w}{\partial x}\frac{\partial w}{\partial y}\right] \tag{4.16}$$

and so on. The strain matrix is given as

$$\epsilon = [\epsilon_x, \epsilon_y, \epsilon_z, \gamma_{xy}, \gamma_{yz}, \gamma_{zx}] = \epsilon_o + \epsilon_l \tag{4.17}$$

where ϵ_o is the usual linear, infinitesimal strain vector (Zienkiewicz and Taylor, 2000) and ϵ_l is the nonlinear contribution. The nonlinear part is conveniently written as

$$\epsilon_l = \frac{1}{2}\begin{bmatrix} \theta_x^T & 0 & 0 \\ 0 & \theta_y^T & 0 \\ 0 & 0 & \theta_z^T \\ \theta_y^T & \theta_x^T & 0 \\ 0 & \theta_z^T & \theta_y^T \\ \theta_z^T & 0 & \theta_x^T \end{bmatrix} \begin{bmatrix} \theta_x \\ \theta_y \\ \theta_z \end{bmatrix} = \frac{1}{2}\underline{A}\theta \tag{4.18}$$

where

$$\theta_x = \left[\frac{\partial u}{\partial x}\frac{\partial v}{\partial x}\frac{\partial w}{\partial x}\right]^T \tag{4.19}$$

$$\theta_y = \left[\frac{\partial u}{\partial y}\frac{\partial v}{\partial y}\frac{\partial w}{\partial y}\right]^T \tag{4.20}$$

$$\theta_z = \left[\frac{\partial u}{\partial z}\frac{\partial v}{\partial z}\frac{\partial w}{\partial z}\right]^T \tag{4.21}$$

Equilibrium equations :

The governing nonlinear equilibrium equations will be established from the virtual work equation, in the Eulerian coordinate system. This is given by the integration over the deformed volume $\overline{V}$ and the deformed area $\overline{A}$ as, (Zienkiewicz and Nayak, 1973),

$$\int_{\overline{V}} \delta\overline{\epsilon}^T \overline{\sigma} d\overline{V} = \int_{\overline{V}} \overline{\rho}\delta u^T q d\overline{V} + \int_{\overline{A}} \delta u^T \overline{p} d\overline{A} \tag{4.22}$$

in which $\overline{\rho}$ is the density in the deformed state and $\overline{\sigma}$ and $\delta\overline{\epsilon}$ refer to the vector forms of the Eulerian stress and the deformation increment in the distorted coordinate $\overline{X}$.

Alternatively, the above equation can be written in terms of the variables referred to

the original, undistorted, coordinates as

$$\int_V \delta\epsilon^T \sigma dV = \int_V \rho\delta u^T q dV + \int_A \delta u^T p dA \tag{4.23}$$

where σ is the second Piola-Kirchoff stress and $\delta\overline{\epsilon}$ is the increment of Green's strain, both referred to the undeformed coordinates.

Then the relation between ρ and $\overline{\rho}$ is given by (Zienkiewicz and Nayak, 1973),

$$\rho = \frac{\overline{\rho}}{|J|} \tag{4.24}$$

The tractions p defined with respect to the undeformed body are given in terms of the tractions $\overline{p}$ acting over a deformed surface area as (Schrefler *et al.*, 1983),

$$p = \left(\frac{d\overline{A}}{dA}\right)\overline{p} \tag{4.25}$$

where $\overline{p} = p$, for the small strain case with $|J| = 1$ and $\left(\frac{d\overline{A}}{dA}\right) = 1$
Using the usual finite element approximation for the displacement, expressions for the displacement are written as

$$u = \sum N_i u_i \quad v = \sum N_i v_i \quad w = \sum N_i w_i \tag{4.26}$$

where N_i denotes the shape function of node i and u_i, v_i, w_i are the displacements of a node i in the x, y, z coordinate directions respectively.

The displacement u within the element is given as a function of the n nodal displacements as

$$u = N\delta \tag{4.27}$$

where $\delta = [\delta_1, \delta_2, ..., \delta_n]$ and N is a shape function matrix with $\delta_i = [u_i, v_i, w_i]$.

After substituting the above expressions for ϵ_o and differentiating,

$$d\epsilon_o = B_o d\delta; \delta_i = [u_i, v_i, w_i]^T; \delta = [\delta_1, \delta_2, ..., \delta_n]; \tag{4.28}$$

where B_o is the small displacement strain matrix and it is given by a typical component sub matrix for the node i as

$$B_o^i = \begin{bmatrix} \frac{\partial N_i}{\partial x} & 0 & 0 \\ 0 & \frac{\partial N_i}{\partial y} & 0 \\ 0 & 0 & \frac{\partial N_i}{\partial z} \\ \frac{\partial N_i}{\partial y} & \frac{\partial N_i}{\partial x} & 0 \\ 0 & \frac{\partial N_i}{\partial z} & \frac{\partial N_i}{\partial y} \\ \frac{\partial N_i}{\partial z} & 0 & \frac{\partial N_i}{\partial x} \end{bmatrix} \tag{4.29}$$

Differentiation of ϵ_l yields

$$d\epsilon_l = \frac{1}{2} d\underline{A}\theta + \frac{1}{2}\underline{A} d\theta \tag{4.30}$$

which due to the structure of the matrices involved becomes

$$d\epsilon_l = \underline{A} d\theta \tag{4.31}$$

Now, the (9 by 1) vector θ can be written as

$$\theta = Gd = [G1....Gi....] \begin{bmatrix} \delta_1 \\ . \\ \delta_i \\ . \end{bmatrix} \tag{4.32}$$

where

$$G_i = \begin{bmatrix} I_3 & \frac{\partial N_i}{\partial x} \\ I_3 & \frac{\partial N_i}{\partial y} \\ I_3 & \frac{\partial N_i}{\partial z} \end{bmatrix} \tag{4.33}$$

and I_3 is a 3 by 3 identity matrix.

substituting Eqn. (4.32) into Eqn. (4.30), we get

$$d\epsilon_l = B_l d\delta \tag{4.34}$$

with

$$B_l = \underline{A}G \tag{4.35}$$

Thus the strain displacement matrix becomes

$$B = B_o + B_l \tag{4.36}$$

The total strain matrix in Eq. (4.17) can be written, using Eqs. (4.18), (4.32) and (4.36) as

$$\epsilon = \left(B_o + \frac{1}{2}B_l\right)\delta \tag{4.37}$$

For computational purposes, it is convenient to obtain B_l explicitly by multiplying out the appropriate terms in Eq. (4.35). The expression for the three dimensional analysis is

as follows (Zienkiewicz and Nayak, 1973):

$$B_l^i = \begin{bmatrix} \frac{\partial u}{\partial x}\frac{\partial N_i}{\partial x} & \frac{\partial v}{\partial x}\frac{\partial N_i}{\partial x} & \frac{\partial w}{\partial x}\frac{\partial N_i}{\partial x} \\ \\ \frac{\partial u}{\partial y}\frac{\partial N_i}{\partial y} & \frac{\partial v}{\partial y}\frac{\partial N_i}{\partial y} & \frac{\partial w}{\partial y}\frac{\partial N_i}{\partial y} \\ \\ \frac{\partial u}{\partial z}\frac{\partial N_i}{\partial z} & \frac{\partial v}{\partial z}\frac{\partial N_i}{\partial z} & \frac{\partial w}{\partial z}\frac{\partial N_i}{\partial z} \\ \\ \frac{\partial u}{\partial y}\frac{\partial N_i}{\partial x} & \frac{\partial v}{\partial y}\frac{\partial N_i}{\partial x} & \frac{\partial w}{\partial y}\frac{\partial N_i}{\partial x} \\ + & + & + \\ \frac{\partial u}{\partial x}\frac{\partial N_i}{\partial y} & \frac{\partial v}{\partial x}\frac{\partial N_i}{\partial y} & \frac{\partial w}{\partial x}\frac{\partial N_i}{\partial y} \\ \\ \frac{\partial u}{\partial z}\frac{\partial N_i}{\partial y} & \frac{\partial v}{\partial z}\frac{\partial N_i}{\partial y} & \frac{\partial w}{\partial z}\frac{\partial N_i}{\partial y} \\ + & + & + \\ \frac{\partial u}{\partial y}\frac{\partial N_i}{\partial z} & \frac{\partial v}{\partial y}\frac{\partial N_i}{\partial z} & \frac{\partial w}{\partial y}\frac{\partial N_i}{\partial z} \\ \\ \frac{\partial u}{\partial x}\frac{\partial N_i}{\partial z} & \frac{\partial v}{\partial x}\frac{\partial N_i}{\partial z} & \frac{\partial w}{\partial x}\frac{\partial N_i}{\partial z} \\ + & + & + \\ \frac{\partial u}{\partial z}\frac{\partial N_i}{\partial x} & \frac{\partial v}{\partial z}\frac{\partial N_i}{\partial x} & \frac{\partial w}{\partial z}\frac{\partial N_i}{\partial x} \end{bmatrix} \tag{4.38}$$

From Eq. (4.27) the virtual displacement is,

$$du = Nd\delta \tag{4.39}$$

The virtual work Eq. (4.23) is now rewritten as

$$d\delta^T \int_V B^T \sigma dV = d\delta^T \int_V N^T \rho q dV + d\delta^T \int_A N^T p dA \tag{4.40}$$

Since the virtual displacements $d\delta$ are arbitrary, Eq. (4.40) gives the equilibrium equations in the discretised form as,

$$\int_V B^T \sigma dV + f = 0 \tag{4.41}$$

where the vector of equivalent nodal loads f is given by

$$f = \int_V N^T \rho q dV + \int_A N^T p dA \tag{4.42}$$

If the nodal point loads, initial strain and the initial stresses are considered, then the generalized expression for the equivalent load vector becomes,

$$f = f_p + f_b + f_t - f_{\epsilon_o} + f_{\sigma_o} \tag{4.43}$$

where f_p represents the vector of applied nodal loads, and

$$f_b = \int_V [N]^T b dV \tag{4.44}$$

$$f_t = \int_S [N]^T p dS \tag{4.45}$$

$$f_{\epsilon_o} = \int_V [B]^T D \epsilon_o dV \tag{4.46}$$

$$f_{\sigma_o} = \int_V [B]^T \sigma_o dV \tag{4.47}$$

are the vectors due to the body forces b, the applied tractions p on the surface S, the initial strain ϵ_o, and the initial stress σ_o respectively.

This is identical with that obtained in the infinitesimal displacement case with the crucial exception that B is a linear function of the nodal displacement δ. In order to find the total equilibrium path, f is applied as a series of incremental loads. Thus the incremental form of the above equation can be written as,

$$d(\int_V B^T \sigma dV) = df \tag{4.48}$$

where

$$d(\int_V B^T \sigma dV) = \int_V (dB^T \sigma + B^T d\sigma) dV = K_T d\delta \tag{4.49}$$

As B_o does not vary with δ, we have,

$$dB^T = dB_l{}^T = G dA^T \tag{4.50}$$

dσ can be written as

$$d\sigma = Dd\epsilon \tag{4.51}$$

and therefore, after some transformation utilizing the properties of θ matrices (Zienkiewicz and Nayak, 1973) K_T can be written as,

$$K_T = \int_V (B^T DB + G^T MG)dV = K + K_\sigma \tag{4.52}$$

where

$$K = \int_V B^T DBdV and K_\sigma = \int_V G^T MGdV \tag{4.53}$$

Further,

$$K = K_o + K_l \tag{4.54}$$

$$K_o = \int_V B_o^T DB_o dV \tag{4.55}$$

$$K_l = \int_V (B_o^T DB_l + B_l^T DB_l + B_l^T DB_o)dV \tag{4.56}$$

K_o represents the usual, small displacement stiffness matrix, K_l is known as the initial displacement matrix or the large displacement matrix andK_σ is known as the initial stress or the geometric stiffness matrix and the matrix M is given by

$$M = \begin{bmatrix} \sigma_x I_3 & \tau_{xy} I_3 & \tau_{xz} I_3 \\ \tau_{yx} I_3 & \sigma_y I_3 & \tau_{yz} I_3 \\ \tau_{zx} I_3 & \tau_{zy} I_3 & \sigma_z I_3 \end{bmatrix} \tag{4.57}$$

Thus equation (4.48) in the incremental form can be written as,

$$\int_V B^T DBdV + \int_V G^T MGdV + \delta f = 0 \tag{4.58}$$

In this derivation the constitutive law for the material relating directly the increments of the Piola-Kirchoff stresses with the increments of the Lagrangian strain is used (Zienkiewicz and Nayak, 1973). For small strain elasticity this definition is obviously

most convenient and indeed the D matrix is a familiar one of elastic constants referred to original coordinates. One word should be added concerning the interpretation of the stresses. While for all small strain problems, the second Piola-Kirchoff stresses correspond with the real stresses, in the case of large strain problems these require a transformation to the Eulerian stresses (Zienkiewicz and Nayak, 1973).

4.2.3 Isoparametric finite element formulation

The formulation and the numerical integration of the isoparametric element has been widely discussed and is given in detail in any text book on the finite element method. Rewriting the Eq. (4.26) as,

$$u = \sum N_i u_i \quad v = \sum N_i v_i \quad w = \sum N_i w_i \tag{4.59}$$

where u_i, v_i, w_i are the parameters associated with the nodes and N_i are the shape functions associated with the curvilinear system ξ, η, ζ.

$$N_i = N_i(\xi, \eta, \zeta) \tag{4.60}$$

The relationships of the curvilinear and Cartesian coordinates are given in an identical form with

$$\begin{gathered} \xi = \sum N_i \xi_i \quad \eta = \sum N_i \eta_i \quad \zeta = \sum N_i \zeta_i \\ X = \sum N_i x_i \quad Y = \sum N_i y_i \quad Z = \sum N_i z_i \end{gathered} \tag{4.61}$$

with x_i, y_i, z_i being the nodal coordinates in the global Cartesian system.

The derivative of N_i with respect to the two coordinate systems are related by

$$\begin{aligned} \left\{ \frac{\partial N_i}{\partial x} \right\}_i &= J_C^{-1} \left\{ \frac{\partial N_i}{\partial \xi} \right\}_i \\ &where \\ \left\{ \frac{\partial N_i}{\partial \xi} \right\}_i &= \left[\frac{\partial N_i}{\partial \xi}, \frac{\partial N_i}{\partial \eta}, \frac{\partial N_i}{\partial \zeta} \right]^T \end{aligned} \tag{4.62}$$

$$\left\{\frac{\partial N_i}{\partial x}\right\}_i = \left[\frac{\partial N_i}{\partial x}, \frac{\partial N_i}{\partial y}, \frac{\partial N_i}{\partial z}\right]^T \tag{4.63}$$

and

$$J_C = \left[\frac{\partial(x,y,z)}{\partial(\xi,\eta,\zeta)}\right] \tag{4.64}$$

is the 3 by 3 coordinate transformation matrix. This has to be evaluated at each integrating point and inverted to obtain the Cartesian derivatives.

On substitution of the relation (4.61), we can write

$$J_C = \begin{bmatrix} G_\xi^T X & G_\eta^T X & G_\zeta^T X \\ G_\xi^T Y & G_\eta^T Y & G_\zeta^T Y \\ G_\xi^T Z & G_\eta^T Z & G_\zeta^T Z \end{bmatrix} \tag{4.65}$$

with

$$G_\xi^T = \left[\frac{\partial N_1}{\partial \xi}, \frac{\partial N_2}{\partial \xi}, ..., \frac{\partial N_i}{\partial \xi}, ...\right]$$

$$X^T = [x_1, x_2, ..., x_i, ...] \tag{4.66}$$

etc

Adding Eqs. (4.29) and (4.38) and noting that $\overline{x} = x + u$, $\overline{y} = y + v$, $\overline{z} = z + w$, the total

B matrix can be written as,

$$B^i = \begin{bmatrix} \frac{\partial \overline{x}}{\partial x}\frac{\partial N_i}{\partial x} & \frac{\partial \overline{y}}{\partial x}\frac{\partial N_i}{\partial x} & \frac{\partial \overline{z}}{\partial x}\frac{\partial N_i}{\partial x} \\ \\ \frac{\partial \overline{x}}{\partial y}\frac{\partial N_i}{\partial y} & \frac{\partial \overline{y}}{\partial y}\frac{\partial N_i}{\partial y} & \frac{\partial \overline{z}}{\partial y}\frac{\partial N_i}{\partial y} \\ \\ \frac{\partial \overline{x}}{\partial z}\frac{\partial N_i}{\partial z} & \frac{\partial \overline{y}}{\partial z}\frac{\partial N_i}{\partial z} & \frac{\partial \overline{z}}{\partial z}\frac{\partial N_i}{\partial z} \\ \\ \frac{\partial \overline{x}}{\partial y}\frac{\partial N_i}{\partial x} & \frac{\partial \overline{y}}{\partial y}\frac{\partial N_i}{\partial x} & \frac{\partial \overline{z}}{\partial y}\frac{\partial N_i}{\partial x} \\ + & + & + \\ \frac{\partial \overline{x}}{\partial x}\frac{\partial N_i}{\partial y} & \frac{\partial \overline{y}}{\partial x}\frac{\partial N_i}{\partial y} & \frac{\partial \overline{z}}{\partial x}\frac{\partial N_i}{\partial y} \\ \\ \frac{\partial \overline{x}}{\partial z}\frac{\partial N_i}{\partial y} & \frac{\partial \overline{y}}{\partial z}\frac{\partial N_i}{\partial y} & \frac{\partial \overline{z}}{\partial z}\frac{\partial N_i}{\partial y} \\ + & + & + \\ \frac{\partial \overline{x}}{\partial y}\frac{\partial N_i}{\partial z} & \frac{\partial \overline{y}}{\partial y}\frac{\partial N_i}{\partial z} & \frac{\partial \overline{z}}{\partial y}\frac{\partial N_i}{\partial z} \\ \\ \frac{\partial \overline{x}}{\partial x}\frac{\partial N_i}{\partial z} & \frac{\partial \overline{y}}{\partial x}\frac{\partial N_i}{\partial z} & \frac{\partial \overline{z}}{\partial x}\frac{\partial N_i}{\partial z} \\ + & + & + \\ \frac{\partial \overline{x}}{\partial z}\frac{\partial N_i}{\partial x} & \frac{\partial \overline{y}}{\partial z}\frac{\partial N_i}{\partial x} & \frac{\partial \overline{z}}{\partial z}\frac{\partial N_i}{\partial x} \end{bmatrix} \tag{4.67}$$

The derivative $\frac{\partial \overline{x}}{\partial x}$, etc are again the components of a Jacobian matrix

$$J = \left[\frac{\partial(\overline{x}, \overline{y}, \overline{z})}{\partial(x, y, z)}\right] \tag{4.68}$$

which is called the deformation Jacobian matrix and which is given by a similar form to the coordinate Jacobian matrix already established as,

$$J = \begin{bmatrix} G_x^T\overline{X} & G_y^T\overline{X} & G_z^T\overline{X} \\ G_x^T\overline{Y} & G_y^T\overline{Y} & G_z^T\overline{Y} \\ G_x^T\overline{Z} & G_y^T\overline{Z} & G_z^T\overline{Z} \end{bmatrix} \tag{4.69}$$

where

$$G_x^T = \left[\frac{\partial N_1}{\partial x}, \frac{\partial N_2}{\partial x}, ..., \frac{\partial N_i}{\partial x}, ...\right]$$

and

$$\overline{X}^T = [\overline{x_1}, ..., \overline{x_2}, \overline{x_i}, ...], etc \tag{4.70}$$

in which $\overline{x_i} = x_i + u_i$ represents simply the updated nodal coordinates.

As the vector G_x etc given in the above equation have already been calculated, it is a simple matter to calculate the new coordinate and thus all the terms of the deformation Jacobian matrix.

With the value of B matrix known, the first part of the tangential matrix given in Eq. (4.52) can be evaluated. To evaluate the second part of the tangent stiffness matrix, we require to evaluate the gradient matrix G. The sub matrix of G can be given by,

$$G_i = \begin{bmatrix} \frac{\partial N_i}{\partial x} & 0 & \frac{\partial N_i}{\partial y} & 0 & \frac{\partial N_i}{\partial z} & 0 \\ 0 & \frac{\partial N_i}{\partial x} & 0 & \frac{\partial N_i}{\partial y} & 0 & \frac{\partial N_i}{\partial z} \end{bmatrix}^T \tag{4.71}$$

4.3 Material nonlinear formulation for adhesive material

The stress-strain behaviour of the adhesive material is nonlinear and rate sensitive and, becomes predominant after the elastic yield limit has been reached. Modern adhesives, particularly those such as the rubber-modified epoxies, have a large plastic strain to failure. The most extensive work is done by Hart-Smith (1981) who chose an elastic-plastic model to characterise the adhesive such that the total area under the stress-strain curve was equal to that under true stress-strain curve. If the maximum stress is less than yield, the true elastic curve may be used, while for a peak stress intermediate between yield and failure a different, and more accurate model is chosen. The bilinear model is closer to the true adhesive characteristic over its entire range of loads. In effect, Hart-Smith (1981) equates the yield stress and the failure stress, and says that failure occurs

when the adhesive reaches its limiting shear strain. He also modelled adhesive nonlinearity based on the idealized, elastic-perfectly plastic (non-work-hardening) stress-strain curve. Deformation theory of plasticity, based on a secant modulus, effective stress and by Ramberg-Osgood accounted in modelling. Adhesives are viscous due to their material properties, *viz.,* hydrostatic (mean) stress dependent yield criterion, different yield strengths in tension and compression, nonlinear time dependent stress-strain relationship and sensitivity to temperature and humidity. Following sections describes equations that govern the elasto-plastic constituive law and its numerical implementation in the finite element program.

4.4 Elasto-plastic analysis of solids

The nonlinear behavior of real materials originates from both plasticity and creep and it is difficult to distinguish between both the effects. One of the earliest material models in which both the effects were included was that of the Bingham (1922) solid. On this basis, Perzyna (1963,66) and Olszak and Perzyna (1970), proposed the rate dependent elasto-plastic model as a more realistic simulation of the inelastic behavior of a large spectrum of materials. The model has been widely adopted and successfully applied to finite element analysis of various continuum mechanics problems.
Generally, the theoretical constitutive relations which model an elasto-plastic behavior are characterized by :

1. A yield criterion - which defines the elastic limit.

2. A flow rule - which relates the incremental plastic strains to the incremental stresses.

3. A hardening rule - which specifies the conditions for subsequent yielding once a point has yielded.

In the following, the basic concept and elasto-plastic constitutive relations of the Perzyna's model are briefly summarized.
In this model the total strain tensor ε_{ij} and consequently $\dot{\varepsilon_{ij}}$, can be decomposed into the

elastic and the inelastic (plastic) parts as,

$$\varepsilon_{ij} = \varepsilon^e_{ij} + \varepsilon^p_{ij} \tag{4.72}$$

$$\dot{\varepsilon_{ij}} = \dot{\varepsilon}^e_{ij} + \dot{\varepsilon}^p_{ij} \tag{4.73}$$

in which ε^e_{ij}, ε^p_{ij} represent respectively the elastic, plastic components, while $\dot{\varepsilon}^e_{ij}$, $\dot{\varepsilon}^p_{ij}$ represent the corresponding strain rate components. In a uniaxial context such a material is shown in figure 1.3 where the elasto-plastic element remains inactive when $\sigma < \sigma_y$.
The elastic strain is related to the total stress according to the generalized Hook's law,

$$\varepsilon^e_{ij} = \frac{S_{ij}}{2\mu} + \frac{(1-2\nu)}{E}\sigma_m\delta_{ij} \tag{4.74}$$

in which $S_{ij} = \sigma_{ij} - \delta_{ij}\sigma_m$ is the deviatoric stress tensor. $\sigma_m = (1/3)\sigma_{ii}$ is the mean hydrostatic pressure and μ, E, ν are the shear modulus, elastic modulus and the Poisson's ratio respectively.
Consequently, the corresponding elastic strain tensor can be written as

$$\dot{\varepsilon}^e_{ij} = \frac{\dot{S_{ij}}}{2\mu} + \frac{(1-2\nu)}{E}\dot{\sigma_m}\delta_{ij} \tag{4.75}$$

Eqs. (4.74) and (4.75) completely describe the reversible part of the deformation. The elasto-plastic response of the material becomes manifest as soon as some specified combinations of the stress components at a point exceed a characteristic value. This behaviour is governed by the scalar yield function of the form

$$F = \overline{F}(\sigma_{ij}, \varepsilon^p_{ij}, k) - \sigma_y(k) = 0 \tag{4.76}$$

in which σ_y is the uniaxial or effective yield stress, ε^p_{ij} is the plastic strain, k is a history dependent hardening parameter and the value of $F < 0$ implies an elastic state.
The plastic strain rate is expressed in its general form as a function of the current stress according to

$$\dot{\varepsilon}^p_{ij} = f(\sigma_{ij}) \tag{4.77}$$

A specific form of the above which retains a wide generality for material description but at the same time defines the inelastic increment of strain in the same form as employed in the conventional plasticity theory, was proposed by Perzyna (1963,66), as

$$\dot{\varepsilon}_{ij}^{p} = \gamma \left\langle \phi(F) \right\rangle \frac{\partial Q(\sigma_{ij})}{\partial \sigma_{ij}} \tag{4.78}$$

in which γ is the fluidity parameter controlling the plastic rate, $\phi(F)$ is a positive monotonic increasing flow function, and the notation $<>$ implies that the elasto-plastic straining occurs only for values of $\phi(F) > 0$.The scalar quantity Q can be interpreted as a plastic potential and for associated elasto-plasticity $Q = F$, where F is the yield function introduced in Eq. (4.76).

Finally, the total rate of stress change in an elasto-plastic medium can be expressed as

$$\dot{\sigma}_{ij} = C_{ijkl}(\dot{\varepsilon}_{kl} - \dot{\varepsilon}_{kl}^{p}) \tag{4.79}$$

where C_{ijkl} is the usual constitutive tensor for elastic materials.

Various yield functions and plastic potentials can be introduced into the formulation depending upon the nature of the material modelled. In what follows, isotropic material material will only be considered for which both F and Q can be defined in terms of the invariants, so that

$$F(\sigma_{ij}) = F(\sigma_m, J_2^{'}, J_3^{'}) - \sigma_y(k) \tag{4.80}$$

and similarly Q, in which σ_m is the mean stress and $J_2^{'}$, $J_3^{'}$ are the second and third invariants of the deviatoric stresses, S_{ij}. In tensor notation, the stress invariants are:

$$\begin{aligned} \sigma_m &= \tfrac{1}{3} J_1 \quad = \tfrac{1}{3}\sigma_{ii} \\ S_{ij} &= \sigma_{ij} - \delta_{ij}\sigma_m \\ J_2^{'} &= \tfrac{1}{2} S_{ij} S_{ij} \\ J_3^{'} &= \tfrac{1}{3} S_{ij} S_{jk} S_{kl} \end{aligned} \tag{4.81}$$

For perfectly plastic materials the yield function in Eq. (4.80) remains fixed in the principal stress space. The hardening theories assume that the yield function changes during the inelastic deformation. However, in this work the isotropic hardening rule is considered. A full description and discussion of the general elasto-plastic model can be found in the references, Perzyna (1963,66) and Olszak and Perzyna (1970).

4.5 Finite element formulation of Quasi-static elasto-plastic problems

In this section the finite element formulation of the theoretical elasto-plastic model described in the previous section is summarized. Time integration schemes of equations which govern the elasto-plastic straining are discussed. The vector form of the elasto-plastic constitutive relation is presented initially.

4.5.1 Vector form of the elasto-plastic constitutive relations

The basic elasto-plastic constitutive relations of the Perzyna's (1963,66) model are converted to vector form as this is more suitable for the finite element analysis.
Attention is restricted to an isotropic plastic material, for which the state variables are simply the stresses σ. Thus with a yield function

$$F = \overline{F}(\sigma) - \sigma_y = 0 \tag{4.82}$$

and assuming an associated elasto-plasticity, so that $F = Q$, the plastic strain rate can be expressed in the form Eq. (4.78) as

$$\dot{\varepsilon}^p_{ij} = \gamma \left\langle \phi(F) \right\rangle \frac{\partial F}{\partial \sigma} = \gamma \left\langle \phi(F) \right\rangle a \tag{4.83}$$

in which the fluidity parameter γ can depend on time or a static dependent parameter such as strain. Different choices have been recommended for the function ϕ, but the two

most common forms are (Owen and Hinton, 1980):

$$\phi(F) = e^{M(\overline{F}-\sigma_y)/\sigma_y} - 1 \tag{4.84}$$

and

$$\phi(F) = \left[\frac{\overline{F}-\sigma_y}{\sigma_y}\right]^N \tag{4.85}$$

in which M and N are arbitrarily prescribed constants.

The fluidity parameter γ and the function $\phi(F)$ are determined from the dynamic properties of the material.

The vector $'a'$ is termed the flow vector, and in the case of an associated plasticity, represents the derivative of the yield function Eq. (4.82) with respect to the stress vector σ. By recalling the formulation in Eq. (4.80) the flow vector can be represented in terms of the stress invariants as

$$a^T = \frac{\partial F}{\partial \sigma} = \frac{\partial F}{\partial \sigma_m}\frac{\partial \sigma_m}{\partial \sigma} + \frac{\partial F}{\partial J_2'}\frac{\partial J_2'}{\partial \sigma} + \frac{\partial F}{\partial J_3'}\frac{\partial J_3'}{\partial \sigma} \tag{4.86}$$

The flow vector $'a'$ can be expressed in the suitable form for numerical computation as (Owen and Hinton, 1980):

$$a = C_1 a_1 + C_2 a_2 + C_3 a_3 \tag{4.87}$$

in which the constants C_i are yield criterion dependent, and are derived from the yield criterion which the adhesive material follows. Owen and Hinton (1980), have given the values of C_i for different yield criteria such as the Tresca, von Mises, Mohr-Coloumb and the Drucker-Prager equations. However, in order to account the pressure-dependent nature of structural adhesives, the modified von Mises is considered as yield criterion in this work and is described in the following section. Specific forms of the constants C_i and the vector a for the modified von Mises yield criterion are given in appendix 4.2.

4.5.2 Modified von Mises yield criterion

For a ductile material, plastic residual strains are large and therefore a plastic yield criterion can be applied by a function that is similar to that of von Mises. The yield behaviour of polymeric structural adhesives is dependent both on deviatoric and hydrostatic stress components. As a result, there is a difference between the value of yield stresses in uniaxial tension and compression. The ratio between the compressive and tensile yield stress value is termed as Raghava's equivalent (Raghava *et al.*, 1973). Such a pressure-sensitive nature of the adhesive conflicts with the basic assumption of the von Mises criterion, according to which the yield strength of the ductile material is unaffected by the mean stress component. Therefore, a modified von Mises criterion has been proposed by Gali *et al.* (1981). The modified von Mises equation is written as:

$$k_a \quad \tau_{oct} \quad +k_v\sigma_m = 1 \tag{4.88}$$

$$\tau_{oct} \quad = \quad \frac{1}{3}\left[(\sigma_1-\sigma_2)^2+(\sigma_2-\sigma_3)^2+(\sigma_3-\sigma_1)^2\right]^{1/2} \tag{4.89}$$

$$\sigma_m \quad = \quad \frac{1}{3}\left[\sigma_1+\sigma_2+\sigma_3\right] \tag{4.90}$$

k_a, k_v are the material constants responsible for yielding due to the distortional and isotropic stress components respectively.

Equation (4.88) can be written in terms of stress invariants as :

$$F = C_s(J_2)^{\frac{1}{2}} + C_v J_1 - \sigma_y \tag{4.91}$$

where : $C_s = \frac{\sqrt{3}(1+\lambda)}{2\lambda}$, $C_v = \frac{(\lambda-1)}{2\lambda}$, $\lambda = \frac{\sigma_c}{\sigma_t}$

J_1 is the first invariant of the general stress and λ is the ratio between compressive and tensile yield stresses.

The effective strain is given by

$$e = C_s\frac{1}{1+\upsilon}(r_2^{'})^{\frac{1}{2}} + C_v\frac{1}{1-2\upsilon}r_1^{'} \tag{4.92}$$

where υ is the Poisson's ratio, $r_2^{'}$ is the second invariant of the deviatoric strain tensor and $r_1^{'}$ is the first invariant of the general strain tensor. This accounts for the differential yield stresses in tension and compression in adhesive behaviour.

The yield surface for the modified von Mises equation is different from the cylindrical von Mises yield surface in a three dimensional principal stress space (Hinton & Owen, 1980). When the influence of both the deviatoric and the hydrostatic stresses are accounted, the adhesive material behaves similar to a soil and differently from a ductile metal. Hence the modified von Mises yield function, when viewed in three dimensional principal space will appear like a paraboloid as shown in figure 4.2. The space diagonal is a line defined by $\sigma_1 = \sigma_2 = \sigma_3$ where $\sigma_1, \sigma_2 \& \sigma_3$ are the principal stresses. Any plane perpendicular to the space diagonal is referred to as an octohedronal plane. The modified von Mises yield condition is a cone with the space diagonal as its axis. Adhesives, similar to soil samples yield differently under tensile and compressive loads, hence the parabolic form of the yield surfaces shown in figure 4.2.

4.5.3 Time discretization of elasto-plastic equations

Time dependent deformations of elasto-plastic solids are governed by the rate-type constitutive relations given in Eq. (4.77) as

$$\frac{\partial}{\partial t}\varepsilon^P(x,t) = \dot{\varepsilon^P} = f(\sigma) \tag{4.93}$$

The above flow rule holds for every time t, and plastic strain changes in the time interval dt is defined by

$$d\varepsilon^P = \int_t^{t+dt} \dot{\varepsilon}_n^P dt = g(\sigma, dt) \tag{4.94}$$

Assuming that the plastic strain rate defined by Eq. (4.93) is known only for discrete time stations, Δt_n, apart, the relation (4.94) can be approximated in the traditional manner

of initial value problems (Owen and Hinton, 1980):

$$\Delta\varepsilon_n^P = [(1-\alpha)\dot{\varepsilon}_n^P + \alpha\dot{\varepsilon}_{n+1}^P]\Delta t_n; \quad 0 \leq \alpha \leq 1 \tag{4.95}$$

Where $\Delta\varepsilon_n^P$ represents the vector of elasto-plastic strain increment occurring in a time interval $\Delta t_n = t_{n+1} - t_n$. The exact form of this relationship depends on the selection of the time stepping parameter α. For example, α=0 gives a Euler time integration scheme which is also referred as 'fully explicit' (or forward difference method) since the strain increment is completely determined from conditions existing at time, t_n. On the other hand α=1 gives a 'fully implicit' (or backward difference) scheme with the strain increment being determined from the strain rate corresponding to the end of the interval. The case α=1/2 results in the so called 'implicit trapezoidal' scheme which is also known generally as the Crank-Nicholson rule in the context of linear equations.

In Eq. (4.95) the strain rate at the instant of time $t_{n+1} = t_n + \Delta t_n$ is not explicitly known. To overcome this difficulty an iterative process can be employed at each time step, taking initially that $\dot{\varepsilon}_{n+1}^P = \dot{\varepsilon}_n^P$. This technique has been used by Zienkiewicz and Cormeau (1974) and found to improve accuracy. However, the computational time and storage requirements are considerably increased.
Here, the plastic strain rate $\dot{\varepsilon}_{n+1}^p$ is expressed in a limited Taylor series expansion as

$$\dot{\varepsilon}_{n+1}^P = \dot{\varepsilon}_n^P + H_n\Delta\sigma_n \tag{4.96}$$

where

$$H_n = \Big[\frac{\partial\dot{\varepsilon}^P}{\partial\sigma}\Big]_n = H_n(\sigma_n) \tag{4.97}$$

and $\Delta\sigma_n$, is the stress change occurring in the time interval $\Delta t_n = t_{n+1} - t_n$.

The plastic strain rate derivative matrix H_n, defined in Eq. (4.97) depends on the yield criterion employed and specific forms for von Mises condition of the H_n matrix can be

found in Owen and Hinton (1980). The evaluation of the H_n matrix for the Modified von Mises criterion and its constraints are given in Appendix 4.2 .

Finally, Substituting from Eq. (4.96) in Eq. (4.95) the elasto-plastic strain increment can be written as:

$$\Delta\varepsilon_n^P = \dot{\varepsilon}_n^P \Delta t_n + C_n \Delta\sigma_n \tag{4.98}$$

where

$$C_n = \alpha \Delta t_n H_n \tag{4.99}$$

The Explicit time integration scheme is based on a relatively simple numerical algorithm (Zienkiewicz and Taylor, 2000) but the process is only conditionally stable. Implicit schemes on the other hand require more computational effort per time step but larger time step lengths can be employed in the solution (Owen and Hinton, 1980). For the majority of solutions an explicit scheme provides the most economical results for a given solution accuracy. However in selected circumstances the use of an implicit time integration scheme is either advantageous or unavoidable. For example, if creep behaviour (Zienkiewicz and Taylor, 2000) is to be modelled by reducing the yield stress of the material to zero, then the theoretical value of the limiting time step length for time integration by an explicit algorithm tends to become zero.

4.5.4 Stress-Strain Constitutive Relations

The stress-strain relations completes the finite element formulation. From Eq. (4.79) the incremental stress change occurring in time interval $\Delta t_n = t_{n+1} - t_n$ is given by

$$\Delta\sigma_n = D\Delta\varepsilon_n^e = D(\Delta\varepsilon_n - \Delta\varepsilon_n^P) \tag{4.100}$$

in which D is the elasticity matrix. The total strain increment is evaluated in terms of the displacement as

$$\Delta\varepsilon_n = B_n \Delta d_n \tag{4.101}$$

Finally, using Eqs. (4.101) and (4.98), the stress increment defined in Eq. (4.100) can be expressed as

$$\Delta\sigma_n = \hat{D}_n\Big(B_n\Delta d_n - \dot{\varepsilon}_n^p\Delta t_n\Big) \tag{4.102}$$

where

$$\hat{D}_n = (I + DC_n)^{-1}D = \Big(D^{-1} + C_n\Big)^{-1} \tag{4.103}$$

The matrix $\hat{D}_n$ is a symmetric matrix when the plastic law is associative (Owen and Hinton, 1980), while for non-associated plasticity, the matrix C_n is unsymmetric. In Eqs. (4.101) and (4.102) the notation B_n is employed to denote the strain displacement matrix. It is constant for small displacement, however, it is displacement for the large displacement. The explicit form of the matrix B_n is given in Eqs. (4.29) and (4.38).
For a good performance of explicit schemes the matrix inversions implied in Eq. (4.103) must be undertaken to a precision, noting that for α=0 and linear elastic problems the expression Eq. (4.103) becomes $\hat{D}_n = D$.
The initial stress and strain can be simply introduced into Eq. (4.102) and the stress increment is now given as

$$\Delta\sigma_n = \hat{D}_n\Big(B_n\Delta d_n - \dot{\varepsilon}_n^P\Delta t_n - \Delta\varepsilon_n^O\Big) + \Delta\sigma_n^O \tag{4.104}$$

where $\Delta\varepsilon_n^O$ and $\Delta\sigma_n^O$ are respectively the initial strain and stress present at the start of the problem or time interval Δt_n considered.

4.6 Incremental equations of equilibrium

In general a nonlinear static and dynamic finite element analysis is performed most effectively by the incremental formulation in which the static and transient values are updated incrementally corresponding to the successive time steps (or load steps) in order to trace out the complete solution path. In this solution it is important that the governing finite element equations are satisfied at each time step to sufficient accuracy, because otherwise

the solution errors can be significantly accumulated that can lead to the solution instabilities.

The incremental time stepping algorithm for the elasto-plastic problem is briefly reviewed here.

The governing equations of equilibrium which have to be satisfied at any instant of time t_n are given in the form of equation (4.41) as

$$\int_V B_n^T \sigma dV + f_n = 0 \tag{4.105}$$

During a time increment $\Delta t = t_{n+1} - t_n$, the equilibrium equations which must be satisfied are given by the incremental form of the equation (4.105) as (Owen and Hinton, 1980)

$$\int_V B_n^T \Delta\sigma dV + \int_V dB_n^T \sigma dV + \Delta f_n = 0$$

or

$$\int_V B_n^T \Delta\sigma dV + K_{\sigma n} \Delta d_n + \Delta f_n = 0 \tag{4.106}$$

where Δf_n represents the change in loading occurring during the time interval Δt_n. In majority of the problems encountered in engineering, the load increments are applied in discrete steps and thus $\Delta f_n = 0$ for all the time steps except the first one within an increment. This load increment includes the effect of all the initial strains, body forces and the external boundary load.

The incremental stress change vector occurring in time interval Δt_n is given by:

$$\Delta\sigma_n = D\Delta\varepsilon_n^e = D\left(\Delta\varepsilon_n - \Delta\varepsilon_n^p\right) \tag{4.107}$$

where D is the elasticity matrix. The total strain increment is evaluated in terms of the displacement increment as

$$\Delta\varepsilon_n = B_n \Delta d_n \tag{4.108}$$

from Eq. (4.98) we have

$$\Delta\varepsilon_n^p = \dot{\varepsilon}_n^p \Delta t_n + C_n \Delta\sigma_n$$

in the case of an implicit integration scheme. In an explicit scheme the second term on the right hand side of the above equation will vanish. Using the above two expressions the incremental stress change vector can be now written after some modifications as

$$\Delta\sigma_n = D\left(B_n\Delta d_n - \dot{\varepsilon}_n^p\Delta t_n\right) \tag{4.109}$$

The initial stress and strain terms can be included into the above equation for the incremental stress change and it can be re-written as

$$\Delta\sigma_n = D\left(B_n\Delta d_n - \dot{\varepsilon}_n^p\Delta t_n - \Delta\varepsilon_n^o\right) + \Delta\sigma_n^o \tag{4.110}$$

where $\Delta\varepsilon_n^o$ and $\Delta\sigma_n^o$ are respectively the initial strain and the stress present at the start of the problem or the time interval Δt_n considered.
Substitution of $\Delta\sigma$ from Eq. (4.102) for implicit scheme, in to Eq. (4.106) gives the displacement increment occurring during the time step to be

$$\Delta d_n = \left[K_n^T\right]^{-1}\Delta V_n \tag{4.111}$$

where the tangential stiffness matrix K_n^T is given by

$$\left[K_n^T\right] = K_n + K_{\sigma n} \tag{4.112}$$

with

$$\begin{aligned} K_n &= \int_V B_n^T\hat{D}_n B_n dV \\ &and \\ K_{\sigma n} &= \int_V G^T M G dV \end{aligned} \tag{4.113}$$

The explicit form of M in the above equation is given in eq. (4.57). The incremental pseudo loads are given by

$$\Delta V_n = \int_V B_n^T \hat{D}_n \dot{\varepsilon}_n^p \Delta t_n dV + \delta f_n + \psi_n \tag{4.114}$$

in which ψ_n represents the vector of residual or out of balance forces given by

$$\psi_n = \int_V B_n^T \sigma_n dV + f_n \tag{4.115}$$

Thus for each time step a series of equilibrium iteration cycles should be performed, with the residual forces being applied until they become negligible small. A computationally economic alternative is to avoid the equilibrium iteration process but to add the residual forces to the pseudo loads to be applied for the next time step.

4.7 Convergence criteria

The elasto-plastic solution approaches a steady state solution asymptotically, so it is evident that some procedure is required where by the solution is terminated when the steady state is approached. It is generally termed as convergence requirement. Various convergence criteria will be discussed in this chapter. In the previous chapter it was seen that both the explicit and implicit time stepping algorithms can be employed for the integration of the rate sensitive constitutive equations and the selection of the various possible schemes depends upon the problem under consideration, requirement of accuracy and the computational cost.

The problem associated with the iterative processes is to determine as to whether the current iterate is sufficiently close to the root without knowing the true solution itself. The convergence criteria used for nonlinear structural problems can be broadly classified into three groups.

1. Force criteria

2. Displacement criteria

3. Energy criteria

The first two are mostly used in nonlinear structural problems. In the following sections these two types will be discussed.

4.7.1 Force criteria

The force criteria assumes a load step to be converged when the ratio of the Euclidean norm of the residual force vector to the Euclidean norm of the incremental force vector is less than the specified tolerance. This is given by

$$\frac{||\psi^i||}{||f^i||} \leq TOL \tag{4.116}$$

where ψ^i is the residual force vector of the i^{th} iteration, f_i is the load vector of the i^{th} iteration, TOL is the specified tolerance and $||.||$ denotes the Euclidean vector norm.
This comparison doesn't always make sense because the force quantities to be compared may be of completely different order or even of different dimensions.

4.7.2 Displacement criteria

In the displacement criteria the solution is assumed to be converged if the ratio of the Euclidean norm of the incremental displacement vector to the Euclidean norm of the total displacement vector is less than a specified tolerance. This can be expressed as

$$\frac{||\Delta\delta^i||}{||\delta^i||} \leq TOL \tag{4.117}$$

where $\Delta\delta^i$ is the incremental displacement in the i^{th} iteration, δ^i is the total displacement in the i^{th} iteration and TOL is the specified displacement tolerance.
The tolerance limit can be specified in the range of 10^{-2} to 10^{-6}, depending upon the desired accuracy.
In the elasto-plastic algorithm, convergence of the numerical process to the steady state

must be monitored by comparing, in some way, the values of the elasto-plastic strain rate determined during each time step. The steady state conditions are deemed to be achieved at the end of time step n, if

$$\left[\frac{\Delta t_{n+1} \sum_{\frac{All}{G.P}} \dot{\bar{\varepsilon}}^{p}_{n+1}}{\Delta t_1 \sum_{\frac{All}{G.P}} \bar{\varepsilon}^{p}_{1}}\right] \leq TOLER \tag{4.118}$$

where $\dot{\bar{\varepsilon}}^{p}_{n+1}$ is the effective strain rate at the end of the n_{th} iteration.
TOLER is the specified tolerance.
Above one is the global measure of convergence and it is used in the program. For all practical purposes it is sufficient.

4.8 Computational Procedure

The essential steps in the solution process can be summarized as follows. Solution to the problem must begin from known initial conditions at time t=0, which are of course the solution of the static elastic situation. At this stage $\delta_o, \varepsilon_o, \sigma_o, f_o$ are known and $\varepsilon^p = 0$. The time marching scheme can then be employed to advance the solution by one step at a time. The solution sequence is as follows:

1. Suppose that at time $t = t_n$ we have the equilibrium situation and $\delta_n, \varepsilon_n, \varepsilon^p_n, \sigma_n, f_n$ are known. The following quantities are assembled.

   - $B_n = B_o + B_L(\delta_n)$ where B_o and B_L are the strain displacement matrices due to the linear and nonlinear terms.
   - $C_n = C_n\left(\sigma_n, \Delta t_n\right)$
   - $\hat{D}_n = \left(D^{-1} + C_n\right)^{-1}$
   - $K^T_n = K_n + K_{\sigma n}$
   - $\dot{\varepsilon}^p_n = \gamma \left\langle \phi \right\rangle a^n$

   Once all the above terms are computed then we proceed to the next step.

2. The incremental values are calculated in this step.

   - Compute the displacement increment $\Delta\delta_n$ as

   $$\Delta\delta_n = \left[K_n^T\right]^{-1} \Delta V_n$$

   where

   $$\Delta V_n = \int_V B_n^T \hat{D}_n \dot{\varepsilon}_n^p \Delta t_n dV + \Delta f_n$$

   - Compute the stress increment $\Delta\sigma_n$ as

   $$\Delta\sigma_n = \hat{D}_n \left(B_n \Delta\delta_n - \dot{\varepsilon}_n^p \Delta t_n\right)$$

3. Compute the total displacement and the stresses for the next step.

$$\delta_{n+1} = \delta_n + \Delta\delta_n$$
$$\sigma_{n+1} = \sigma_n + \Delta\sigma_n$$

4. Update the elasto-plastic strain rate

$$\dot{\varepsilon}_{n+1}^p = \gamma \left\langle \phi \right\rangle a^{n+1}$$

5. Apply the equilibrium correction. First calculate B_{n+1} using the displacements δ_{n+1}. Substitute the updated stresses σ_{n+1} into the equilibrium equations and evaluate the residual forces as

   $$\psi_{n+1} = \int_V B_{n+1}^T \sigma_{n+1} dV + f_{n+1}$$

   add these to the vector of incremental pseudo loads for use in the next time step.

$$\Delta V_{n+1} = \int_V B_{n+1}^T \hat{D_{n+1}} \dot{\varepsilon}_{n+1}^p \Delta t_{n+1} dV + \Delta f_{n+1} + \psi_{n+1}$$

6. Check for the convergence of the numerical process to the steady state by comparing

in some way the values of the elasto-plastic strain rate determined during each time step. This can be done in two ways. In first case, steady state is achieved if the elasto-plastic strain rate, $\dot{\varepsilon}^p_{n+1}$, is acceptably close to zero at each Gaussian integration point throughout the structure (i.e., to within a specified limit of tolerance). This is called as local convergence check and it requires more time to achieve. An alternative is the global convergence check and it is given in the next section. If the steady state condition is not achieved then the solution is repeated from the first step.

The above algorithm can be employed with either a constant or a variable time step length.

The complete structure of the finite element program code is shown as a flow chart in fig. 4.3. Input data defining the elements, nodes, boundary conditions and material properties are assigned in the required arrays and dimensions. For each load increment, converged values of stress and strain are obtained on the incremental basis of a specified number of iterations. In every load increment, the stiffness of the element is calculated and a frontal solver method is used to the solve the simultaneous equations. Nonlinear behaviour of the adhesive material is computed by the algorithms that have effective stress-strain equations and the modified von Mises criteria.

4.9 Conclusions

This chapter described equations related to geometric and material nonlinear continuum mechanics problems and their numerical implementation. The elasto-plastic constitutive model as realistic representation of general nonlinear material behavior, was considered. The incremental time-stepping algorithm for the solution of quasi-static elasto-plastic problem was presented. Computational procedure which considers both geometric and elasto-plastic nonlinearity is given.

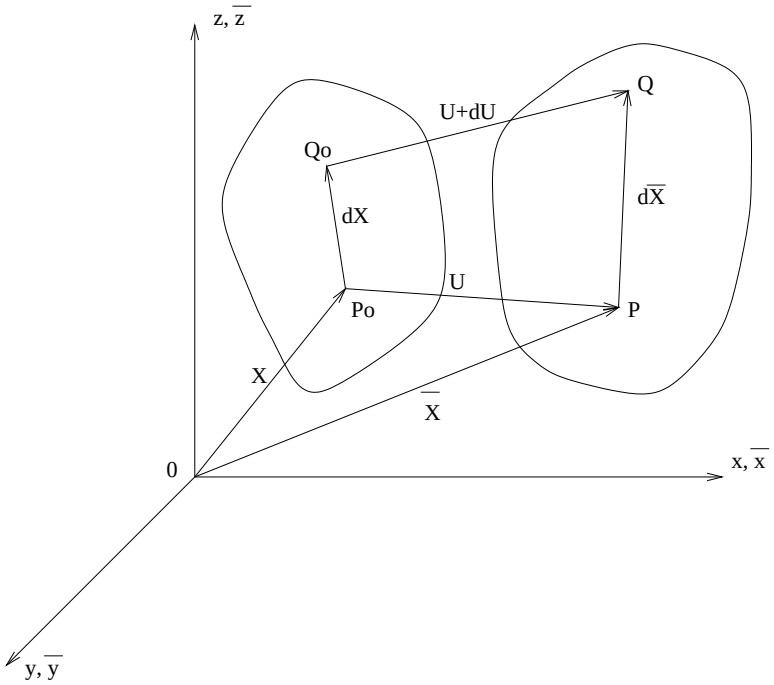

Figure 4.1: Motion of a body in Cartesian co-ordinate system

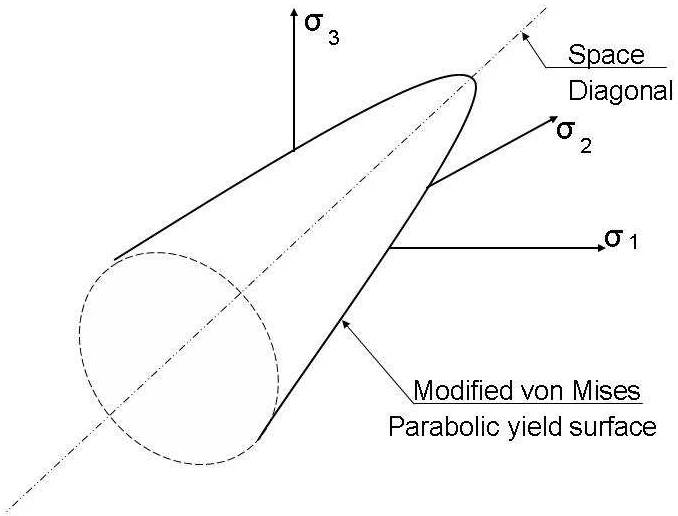

Figure 4.2: Modified von Mises yield surface in principal stress space

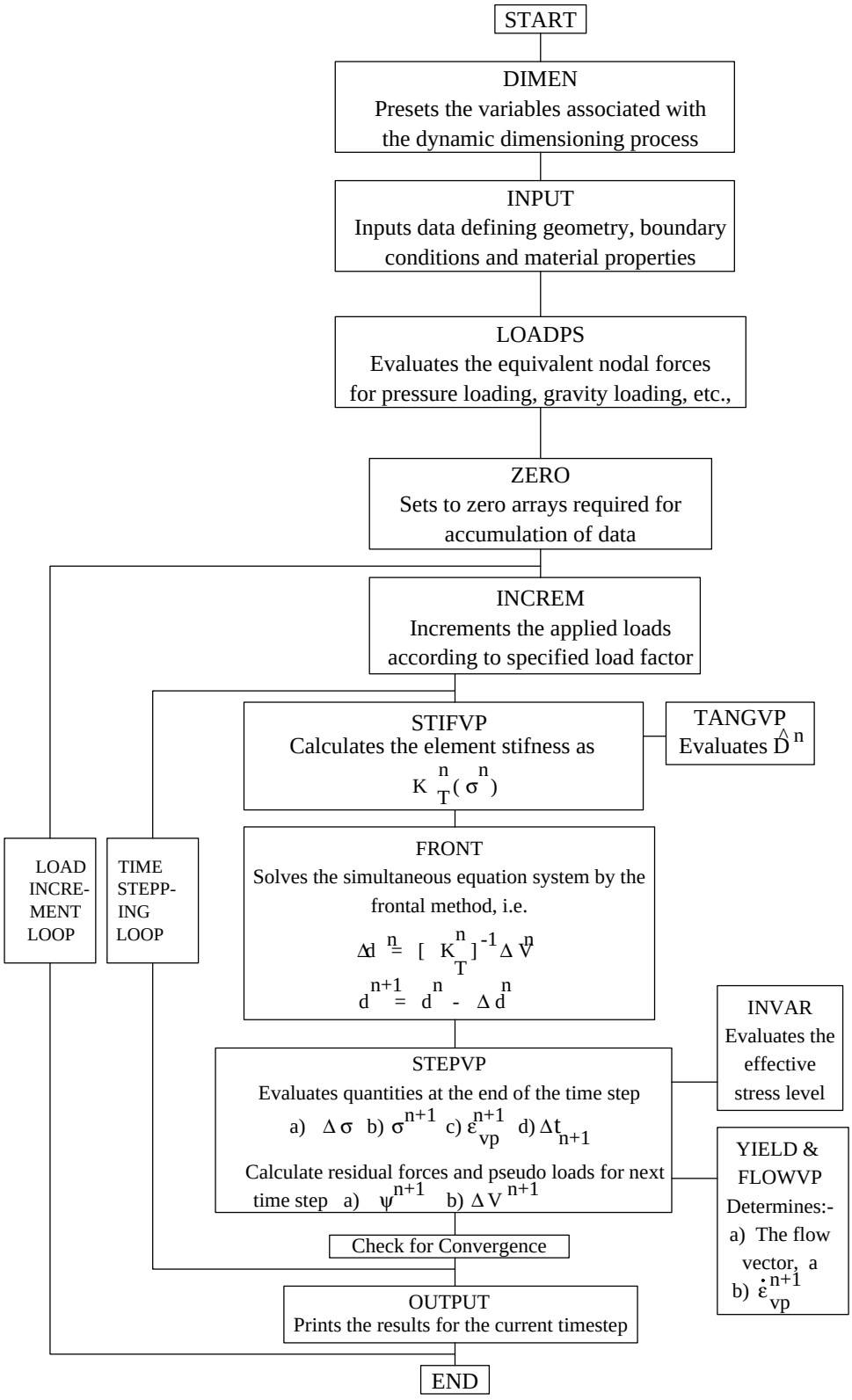

Figure 4.3: Flow Chart for three dimensional elasto-plastic program

Chapter 5

Study on adherend imbalances in single lap joint

5.1 Introduction

Motivation for this study on ahderend imbalances has been discussed in the literature and methodology chapters 2 & 3. As outlined in chapter 3, this chapter focusses on the following four issues:

1. Influence of geometrical nonlinearity on joint deformation under a varying load and the influence of material nonlinearity on adhesive stresses
2. Effect of geometry and material properties on the behaviour of a joint with dissimilar adherends
3. Adhesive stress distribution pattern arising from the variation of adherend thickness
4. Identification of three dimensional effects arising from the eccentric load path in a single lap joint.

5.2 Problem definition

Three dimensional finite element analysis is performed first for a single lap joint with identical isotropic aluminum adherends and later for joints with dissimilar adherends comprising aluminium and orthotropic composite parts. The composite part is a laminate made of E-glass woven roving mat (E-Lt 600) infused with Epoxy(PRIME20). Material properties are deduced from a tensile test method as per BS 2782: Part 3: Method 320E. Material properties of the adherends and adhesive are listed in table 5.1. Characterisation of adhesive material Araldite420 was performed and compared with experimental stress-strain curve. A single lap joint of adhesive thickness 0.5mm was modelled using three dimensional 20-noded isoparametric element with 3x3x3 Gaussian integration scheme. Maximum load under which the adhesive Araldite 420 fails by complete plasticity for a single lap joint with overlap length of 25mm is shown to be around 11kN (Bour and Joannic, 2001). Hence an in-plane tensile load with the magnitude of 10kN is applied at the end of the bottom adherend while the top adherend is held rigid: this load value is one that approaches the failure value reported in the previous work (Bour and Joannic, 2001). It is to be mentioned here that the lap joint considered here is without spew fillet in the FE model. This is for the reason that the main objective is to look at three dimensional effects critically in an idealized 'square edge' joint. The following analyses are performed for a single lap joint model:

1. Similar adherends: A single lap joint of aluminium with thickness 5.0mm bonded by adhesive layer thickness of 0.5mm is subjected to a tensile load of 10kN which is applied in 28 load increments. The behaviour of the joint is studied for elastic linear analysis (LE), geometric nonlinear analysis (GNL), perfectly-plastic analysis (PP) and perfectly-plastic with geometric nonlinearity (PPG) conditions.

2. Dissimilar adherends of varying thickness: Single lap joint model with aluminium and composite adherends bonded by Araldite420 is subjected to a tensile load of 10kN which is applied in 28 load increments on the composite part. The thickness of aluminium is kept constant at H1=5.0mm while that of the composite part is varied

from H2=5.0,7.5,10.0,12.5 and 15.0mm with the ratio of $H2/H1$, 1.0,1.5,2.0,2.5 and 3.0 respectively.

5.3 Material nonlinearity in the adhesive material

As observed from the literature, linear elasticity is not adequate to represent the stress-strain relation of an adhesive material that is non-linear, pressure-dependent and has differential yield strengths in tension and compression. Some structural adhesives exhibit inelastic behaviour since the plastic strains are induced even at low levels of loading. Hence the modelling of the adhesive as a nonlinear material by formulating an effective stress-strain relationship will be more appropriate than a linear model. Formulation of an elasto-plastic constitutive law and an appropriate definition of yield criterion is essential to describe the realistic stress-strain relation for the adhesive material. Equations related to elasto-plastic formulation and its implementation are described in section 4.4. There are various methods of representing the non-linear stress-strain curve such as a) Elastic-linear hardening model, b) Elastic-exponential hardening model and c) Ramberg-Osgood model. In this work, a bi-linear hardening model is adopted for the adhesive material.

In bi-linear hardening, the behaviour is initially elastic described by a given elastic modulus E of the material until yielding starts at the uni-axial yield stress σ_y. Thereafter, the response of the material is elasto-plastic with the slope of the stress-strain curve changing continually. The hardening parameter H' can be determined experimentally from a simple uniaxial yield test. It is expressed in terms of initial Young's modulus E and the elasto-plastic tangent Young's modulus E_T as (Owen and Hinton, 1980),

$$H' = \frac{E_T}{1 - \frac{E_T}{E}} \tag{5.1}$$

5.3.1 Characterisation of the adhesive material

The adhesive material considered in this work is a two component epoxy system, Ciba Araldite420, which is characterised by Bour and Joannic (2001). The behaviour in tension has been measured on bulk adhesive samples and material parameters are deduced from mean traction-displacement curves. Figure 5.1 shows a typical test measurement from a tensile test; the maximum stress is found to be 32.45MPa with Young's modulus being 1733MPa. It is also evident from the curve that after the initial yielding, the adhesive reaches an almost perfectly-plastic state. In this respect, a characterisation of the adhesive material is attempted by keeping the value of the hardening parameter H' equal to 0 intentionally to obtain a perfectly-plastic condition. This results in the stress-strain curve beyond the initial yield limit to become almost a flat line. Theoretically the effective strain will be infinite beyond any value of the initial yield stress. However when it comes to numerical implementation, because of computational constraints, a post-yield value obtained at the end of each increment need not be a converged result. Rather it could be restricted by a specified number of iterations in the increment. The effective stress-strain relationship for the Ciba Araldite 420 is obtained by specifying the Young's modulus E and the initial yield stress σ_y as 1733MPa and 32.45MPa respectively (as deduced from test results of Bour and Joannic, 2001). The resulting stress-strain curve is found to be similar to the test measurement as shown in figure 5.1.

5.3.2 Yield criterion for the rigid adhesive material

Modified von Mises equation is considered here as yield criterion for the rigid adhesive material, Ciba Araldite420. Bour and Joannic (2001) have reported from bulk adhesive tests that the compressive and tensile yield stress values for the Ciba Araldite420 are not the same. The ratio between the compressive and tensile yield stress value, termed as Raghava's equivalent (Raghava *et al.*, 1973) is found to be 2.086 (λ) from their tests. This has been incorporated into the analysis by a modified von Mises equation as suggested by Gali *et al.* (1981). The modified von Mises equation and its numerical form are presented in section 4.5.2.

5.4 Results and Discussions

5.4.1 Generation of FE mesh

Three dimensional FE mesh for the single lap joint with the geometry and boundary conditions shown in figure 5.2 is generated using the pre-processor PATRAN software. The nodal co-ordinates and the element connectivity information are extracted from the PATRAN model as required for the developed FE code through a set of interface programs. The details related to preparation of the input file are described in the appendix D. Two sets of single lap joint models are created, one with an unit width idealizing a two dimensional joint and the other with the wider width of 25mm similar to the joint specimen of Bour and Joannic (2001). The former model is created to check the adequacy of mesh density at the overlap ends where the sharp stress gradients are expected. The purpose of this 2D equivalent model is to observe the stress gradients at free edges on either side of the overlap ends and extend the similar mesh pattern for the actual joint model. A simple linear elastic (LE) is performed with the tensile load magnitude of 100N for the joint model. The pattern of FE mesh shown in figure 5.3 has 480 20-noded iso-parametric elements with 2981 nodes thus having 8943 degrees of freedom. Though further refinement is possible in the region of interest, elements near the overlap ends has aspect ratio closer to one. With the aim of achieving accurate results to the possible extent within a reasonable computational time, this particular FE model is chosen. Normal and shear stresses along the overlap length in the middle adhesive layer are presented in figure 5.4. The shear stress profile clearly shows that the maximum shear stress occurs a little inside of the overlap ends and a very steep gradient dropping towards zero at the overlap ends. Thus the requirement of 'zero shear stress' at free edge for an idealised lap joint is satisfied by this FE mesh pattern. This model has four rows of elements in adhesive and adherend in the through the thickness direction and refined along the length direction towards the overlap ends, thus ensuring the aspect ratio for adhesive elements is close to one. A similar mesh pattern is adopted for the wider joint as shown in figure 5.5. This model also has 480 elements with 2981 nodes and hence 8943 degrees of freedom.

5.4.2 Validation of FE results

Normal and shear stresses in the middle adhesive layer obtained by the developed FE program are compared with the analytical solution formulated by Bigwood and Crocombe (1989). Dimensions of the lap joint and acting forces for all the H2/H1 ratios are fed into a EXCEL spread sheet program which computes the analytical solution. Figures 5.6 and 5.7 show comparison of numerical and analytical results for the joint with identical adherend and with non-identical adherends. For identical adherends, e.g. aluminium-aluminium ($Al - Al$), FE results match the analytical solution reasonably well for both normal and shear stress as shown in figures 5.6 & 5.7. There is a difference between analytical estimations of maximum values of normal and shear stresses at the overlap ends. This is possibly because of the assumption in the analytical model that normal stresses do not vary through the thickness of either the adhesive or the adherends (Bigwood and Crocombe, 1989), while variations are accounted for in the three dimensional FE analysis. It is also to be noted that the analytical procedure does not capture the 'stress drop' at free edges even for the identical case Al-Al joint.

In the case of non-identical adherends, e.g. aluminium-composite ($Al - Cp$), normal and shear stress values for various $H2/H1$ ratios at the mid-plane of the adhesive layer, are broadly similar to analytical solutions with regard to shear stress distribution in the adhesive. There is however a slight difference in the peak values of compressive through-thickness stresses between the numerical and the analytical results. This is due to the limitations of the analytical expressions in predicting the stresses for the case of mismatch in the adherends (Bigwood and Crocombe, 1989). Thus, overall, it can be said that results generated from the developed three dimensional program are in acceptable agreement with the ones seen in a typical lap joint structures (Adams and Peppiatt (1974), Pandey and Narasimhan (2001), Tsai *et al.* (1995)).

Normal and shear stress plots for a 2D equivalent and for the actual 3D lap joint are provided in figures 5.4 & 5.10. While the shear stress in the former figure shows the stress

dip closer to zero, it is not so in the latter figure for the 3D lap joint. This highlights the limitation of creating adequate mesh density in the 3D domain. As mentioned in the previous section, both the models has same number of elements and nodes. Therefore, the aspect ratio of elements get distorted for the 3D model. However, the present 3D model shows the stress dip towards the overlap ends. Considering that nonlinear analyses are performed for the 3D model, the computational time required for solving the problem with large number of degrees of freedom is extremely high and this factor is a main constraint in capturing the stress dip closer to zero. For this specific lap joint configuration, total number of degrees of freedom is 17,886 and the computational time required for a geometric with material nonlinear analysis is close to 1100mins.

5.4.3 Nonlinear deformations

Figure 5.8 shows U_{xx}, U_{zz} displacements in a lap joint for the case of identical adherends and for the non-identical adherends for $H2/H1 = 2.0$ obtained from linear (LE) and geometrical nonlinear elastic (GNL) analyses. Maximum axial displacement occurs typically at the end of the bottom adherend and the maximum vertical displacement occurs just after the overlap end in the bottom adherend. The axial displacement variation along the length of the top metal adherend is relatively small in comparison to a steep variation seen in the bottom composite adherend. This is because of the large difference in the Young's modulus of these two dissimilar adherends. However in the case of similar adherends, the axial displacement variation along the length of the top and lower adherends is within the same range as shown in figure 5.8.

The linear and nonlinear displacement profiles shown in figure 5.8 suggest that the influence of the geometric nonlinearity is more pronounced for the vertical displacement (U_{zz}) than for the axial displacement (U_{xx}). To have an understanding of this phenomenon, maximum values of axial and vertical displacement obtained from LE and GNL analyses are plotted in figure 5.9 as a function of the applied load. Linear and nonlinear

displacements are compared for identical ($Al - Al$) and for non-identical ($Al - Cp$) adherends with different adherend thickness ratios. It should be noted that the nonlinear displacements in the $Al - Cp$ joint with $H2/H1$ ratio of 1.0 deviates at the very lower magnitude of the applied load and hence not presented here for the comparison. For the case of $Al - Cp$ joint with $H2/H1$ ratio of 1.5 also, the maximum nonlinear displacement value begins to diminish under the increasing load from 8.5kN onwards. Geometrical nonlinear analysis results in significant reduction of axial and vertical displacement from the linear displacement values for the joint with identical adherends than for the case of non-identical adherends. For $Al - Cp$ joints, the influence of geometrical nonlinearity decreases as the thickness of composite adherend is increased from 5.00mm to 15.00mm. It can be concluded from these results that geometrical nonlinearity has to be accounted for the structural components that are not symmetric in geometry and with varying material properties.

5.4.4 Nonlinear stresses

(i) Comparison of various analysis results: In order to observe the influence of geometric and material nonlinearity, adhesive normal and shear stress are plotted for the identical ($Al - Al$) and non-identical ($Al - Cp$) adherends with $H2/H1$ ratios of 2.0,2.5 & 3.0 corresponding to the applied load of 10kN. Figure 5.10 shows the comparison of stress distributions obtained from linear elastic (LE), geometrically nonlinear (GNL), perfectly plastic (PP) and perfectly plastic with geometrical nonlinearity (PPG) analyses for $Al-Al$ and $Al - Cp$ joints. Maximum normal and shear values obtained from different analyses for all the joint cases are listed in table 5.2 & 5.3. Maximum normal stress occurs little away from the end of the overlap length for all the joint cases. But the shear stress profiles for the case of the PP and the PPG are slightly different from the stress curves for the LE and GNL cases. For PP/PPG solution, the maximum stress occurs well inside of the overlap ends (at $X = 55mm$ & $70mm$ where X is defined in figure 5.2a), i.e. about 20% of overlap length from either end. As the magnitude of the load is increased, the occurrence of the maximum shear stress starts shifting from the end of the overlap towards the inner

adhesive region. This indicates the initiation of plasticity once the adhesive reaches its initial yield strength and subsequent spread of the the plastic zone under the increasing load. A similar behaviour has also been reported by Pandey and Narasimhan (2001).

One can observe from the tables and plots that there is some difference in the maximum normal and shear stress values at the overlap ends for different analyses in the order of LE, GNL, PP and PPG solutions for both identical and non-identical joints. A similar pattern of reduction in peak normal stress has also been reported in earlier studies in Pandey and Narasimhan, 2001. Normal stress values for PP and PPG solution are approximately 50% and 67 % of the LE solution for $Al-Al$ and $Al-Cp$ ($H2/H1 = 2.0$) joints respectively. Similarly, nonlinear shear stress values are 64% and 33% of the LE solution. Importantly, it has to be noted that the highest reduction of shear stress 33% occurs at the overlap end adjacent to the more flexible, composite adherend. Magnitude of PP/PPG shear stress values at either edges of the overlap are within a close range (table 5.3) for all types of joints. This shows that shear stress distribution in the adhesive layer is independent of the material composition in a lap joint. This discrepancy in adhesive stress values demonstrates that the linear formulation predicts stress values in the adhesive layer that are normally high compared to the adhesive yield stress of 32.45MPa.

On the other hand, PP/PPG solution predicts maximum normal stress as 38MPa for the $Al-Al$ joint at overlap ends and in the range of 53-61MPa and 23-29MPa at the beginning and at end of the overlap length ($X = 50.0mm \& X = 75.0mm$) respectively. To understand the perfectly-plastic behaviour of the adhesive in a lap joint, normal stress values (PP) at either end of the overlap length are plotted as a function of the applied load and compared with corresponding linear (LE) stress values as shown in figure 5.11. The plots (a) and (b) for $Al-Al$ and $Al-Cp$ joints in figure 5.11 clearly exhibit the perfectly-plastic behaviour of the adhesive material in a lap joint once it reaches the initial yield limit. After reaching this limit, the normal stress tends to remain constant under the increasing load. This clear departure from the linear stress values occurs from a load

magnitude of 3.75kN. This kind of perfectly-plastic behaviour of adhesive in a lap joint is quite comparable to the trend seen in the experimental stress-strain curve of the bulk adhesive shown in figure 5.1, thus validating the formulation of material nonlinearity in FE program. These plots also indicate the initiation of yielding for different joint cases. Normal stress attains initial yield stress value at both the ends of the overlap length only for $Al - Al$ joint and yields further uniformly up to 40.0MPa. However for the $Al - Cp$ joints, the normal stress exceeds the initial yield stress value only at the beginning of the overlap length ($X = 50.0mm$) from where the metallic adherend extends and stress values are well under the yield limit at the other end of the overlap from where the composite adherend extends. The adhesive material in these joints reaches the yield limit at different load steps depending on joint type and geometry. Joints with identical adherends ($Al - Al$) attain plasticity at a load magnitude of 5kN but the joints with non-identical adherends ($Al - Cp$) approach plasticity at load magnitudes of 4.375, 3.75 & 3.4kN for $H2/H1$ ratios 2.0,2.5 & 3.0 respectively. So, the thicker the bottom composite adherend, the sooner the adhesive reaches plasticity state. One reason for this is the thickness of the adhesive layer. It should be noted that while thickness of adherend is varied, the thickness of adhesive layer is kept constant at 0.5mm. The implication for practical cases is that in sizing or dimensioning a joint, both adherend type/thickness and adhesive thickness need to be considered in conjunction with each other in order to ensure a certain desired load transfer capacity.

Figure 5.12 shows adhesive normal and shear stress profiles in top, middle and bottom adhesive layer for the PPG analysis. Among the stress components, normal stress values are dominant than the shear stress values. The normal stress profile is relatively symmetrical than the shear stress profile along the overlap length for all the joint cases. The maximum normal and shear stress values are seen along the top and bottom adherend-adhesive interface layer than along the adhesive middle layer. This shows that the joint may have a *'adhesive'* failure mode before the stress state in the adhesive middle layer becomes critical. Among the three possible failure modes that could occur in a singe lap

joint as described in chapter 2, *'adhesive'* is the most common failure mode to occur in a lap joint which is evidently supported by the majority of experimental results. Among them, the conclusion drawn from this numerical analysis compares well with the experimental results of lap joint specimen that showed by *'adhesive'* failure mode carried out by Bour and Joannic (2001).

(ii) Three dimensional effects: Three dimensional normal and shear stress distributions in the adhesive material at the top and bottom interface layers and at the middle layer across the width of the joint are shown in figure 5.13 for $Al - Cp$ joint with adherend thickness ratio of $H2/H1 = 2.0$. It can be seen from the plots that normal stresses are not uniform across the width of the joint. Normal stresses decrease sharply from the middle portion of the width towards the corners, from 72MPa to 60MPa over 20% of the width on either ends in the middle adhesive layer and also considerably in the bottom interface layer. This indicates a typical three dimensional behaviour and an *'anticlastic effect'* as illustrated in figure 5.14. Section A-A in the sketch shows that the anticlastic effects were due to bending in one direction, the upper and lower adherends deform in convex (concave) manner in one direction and concave (convex) in perpendicular direction (Tsai *et al.*, 1995). This arises due to different elongation between the adherends and when this anticlastic deformation is resisted by the non-loaded adherend through the adhesive bond, three dimensional stresses develop in adhesive-adherend bonded corners. This results in anticlastic deformation which reduces the development of tensile normal stresses at the corners in the adhesive layer. With normal stresses being uniform over the central width of the joint and non-uniform towards the corners, such normal stresses can result in failure initiation in single lap joints with non-identical adherends.

5.5 Critical assessment of results

The purpose of this section, is to discuss the obtained results *viz-a-viz* other research works concerning the numerical modelling of lap joints with dissimilar adherends, thereby bringing out the knowledge gained from the current work. It can be seen from figure 2.2

and the relevant review in section 2.5.2 on numerical modelling that seven researchers have analysed single lap joint with dissimilar adherends. Among them, only Bogdonovich *et al.,* (1999) have attempted to analyse a composite-to-metal lap joint in a three dimensional domain however, this work is limited to a linear case. The research undertaken in this thesis differs from previous research works since it presents the results obtained from comprehensive analyses that accounted for geometric and material nonlinearities in a three dimensional domain.

Three dimensional analysis of single lap joint has provided interesting observations regarding the adhesive stress profiles. Though the numerical results are compared with the analytical results, this analysis also highlighted the limitations in using analytical solution for the reason that they always predict a finite stress value at the free edges while a FE analysis for a refined model can show the stress gradient and satisfy 'zero shear stress' at free edges. Authors like Frostig *et al.,* (1999) and Pandey *et. al.,*(1999) have shown this 'zero shear stress' at free edge phenomenon in their 2D analysis of single lap joint for identical adherends. However, this feature has not been captured in three dimensional domain so far. Here it is demonstrated that a 3D model can indeed capture this trend if the mesh is generated appropriately. But it is to be kept in mind that the higher the number of degrees of freedom, the longer will be the computational time especially for the nonlinear analysis.

The main novelty of these results is three dimensional effects seen in a single lap joint. Previous researchers like Tsai (1994), Pandey and Narasimhan (2001) and Andruet *et al.*, (2001) have showed three dimensional behaviour such as *'anticlastic'* and *'bending-twisting'* effects in a single lap joint however, these works only considered identical adherends. These effects arise mainly due to the differential elongation between the adherends and eccentricity in the load path. Obviously, three dimensional effects are expected to be more pronounced in the case of dissimilar joints due to the imbalances in adherend stiffness. Non-identical thickness and different material properties between the

adhrends results in suppression of tensile normal stress at the free edges. This phenomenon for the considered case of Aluminium-Composite lap joint is demonstrated in figures 5.13 & 5.14. Thus three dimensional behaviour for joints with adherend imbalances is brought out and highlighted in this study.

Another novel idea gained from the results is understanding of the state of nonlinear adhesive stresses in a dissimilar lap joint. A comparison of normal and shear stresses between various analyses presented in tables 5.2 & 5.3 highlights the fact that linear stress values are far higher than the actual strength of the adhesive, 32.45MPa for Ciba Araldite420, in this study. On the other hand, nonlinear stress values are closer to the strength of the adhesive material. The stress profiles seen in figure 5.11 demonstrate the presence of a perfectly-plastic condition in the lap joint and this reflects the experimental stress-strain profile of the Ciba Araldite420 shown in figure 5.1. The maximum normal stress normally occurs closer to either end of the overlap length for a lap joint with similar adherends (figure 5.6). However, for the case of dissimilar adherends, the maximum normal stress is more at the beginning of the overlap length (at $X = 50.0mm$) than at the end of the overlap length (at $X = 75.0mm$) from where the adherend of lesser stiffness extends. This trend is clearly shown in figure 5.11 for all the dissimilar joint cases considered. This implies that the stresses are concentrated near the interface layer between the adhesive layer and the weaker adherend and remains primary source of failure initiation. Assessment of such failure initiation from this numerical analysis can be helpful to frame guidelines on the site inspection of a joint structure. Though Hart-Smith (1985) observed such stress variation for dissimilar joints, he considered only the varying thickness ratio for similar adherends. For the case of lap joints with two different adherend materials, this observation on the adhesive stresses is made for the first time here.

5.6 Conclusions

This chapter presented a comprehensive three dimensional finite element analysis of adhesively bonded single lap joint considering material and geometrical nonlinearity. The

stress-strain relationship of the adhesive material is modelled by an elasto-plastic constitutive equation. A modified von Mises criterion was employed for the adhesive material. Displacement profiles in the joint and stress distributions in the adhesive layer have been obtained for different sets of analyses. They highlighted the three dimensional effects such as *'anticlastic'* and *'bending-twisting'* in the lap joint. Particular attention importance has been given to non-identical adherends with varying thickness and material properties under the action of tensile forces. The following conclusions can be drawn:

- Stress results obtained from the developed finite element program agree well with analytical solutions.

- The influence of geometrical nonlinearity on the joint deformation and the adhesive stresses have been demonstrated. It has been found that nonlinearity played significant role, especially in the case of dissimilar adherends of similar thicknesses, even at very low levels of the applied load.

- The elasto-plastic analyses have shown that the adhesive stress state is considerably different from the linear stress values and the normal stress versus load profile reflects a perfectly-plastic nature of the adhesive material.

- Normal stress values are found to be more dominant than the shear stress values. A possible failure mode could be *'adhesive'* since stress values along the top and bottom adhesive-adherend interface layer are found to reach the initial yield limit earlier than at the adhesive middle layer.

- The three dimensional effect and reduction of normal stress at the free edges due to *'anticlastic'* effect has been demonstrated from the stress plots.

Table 5.1: Material Properties of adhesive and adherends

	Aluminium	E glass E-Lt600	Ciba Araldite 420
E_{xx}	70.00 GPa	6.60 GPa	1.733 GPa
E_{yy}	70.00 GPa	6.49 GPa	1.733 GPa
E_{zz}	70.00 GPa	4.20 GPa	1.733 GPa
G_{xy}	26.31 GPa	3.00 GPa	0.5 GPa
G_{yz}	26.31 GPa	2.95 GPa	0.5 GPa
G_{zx}	26.31 GPa	1.91 GPa	0.5 GPa
ν_{xy}	0.33	0.097	0.45
ν_{yx}	0.33	0.097	0.45

Table 5.2: Maximum normal stress values (MPa) obtained from various analyses along the overlap length (mm) for different joint cases (X is as defined in figure 3a)

Normal stress values (MPa)								
Joint Type:	LE		GNL		PP		PPG	
H2/H1	X=50.0	X=75.0	X=50.0	X=75.0	X=50.0	X=75.0	X=50.0	X=75.0
Al-Al:1.0	67.41	74.18	65.33	68.86	37.95	40.26	38.91	40.05
Al-Cp:2.0	79.34	60.00	74.23	44.21	53.38	29.04	57.66	73.66
Al-Cp:2.5	89.55	53.65	83.70	49.88	57.79	26.53	60.82	47.10
Al-Cp:3.0	100.81	48.22	92.20	48.95	60.82	23.52	63.84	30.67

Table 5.3: Maximum shear stress values (MPa) obtained from various analyses along the overlap length (mm) for different joint cases (X is as defined in figure 3a)

Shear stress values (MPa)								
Joint Type:	LE		GNL		PP		PPG	
H2/H1	X=50.0	X=75.0	X=50.0	X=75.0	X=50.0	X=75.0	X=50.0	X=75.0
Al-Al:1.0	35.44	37.93	33.26	34.45	22.88	22.86	21.38	21.41
Al-Cp:2.0	29.99	82.97	26.94	70.19	22.41	27.97	21.96	30.61
Al-Cp:2.5	32.34	74.23	28.62	67.41	23.65	28.32	22.31	31.03
Al-Cp:3.0	35.27	67.02	30.47	63.57	23.52	28.25	22.71	28.41

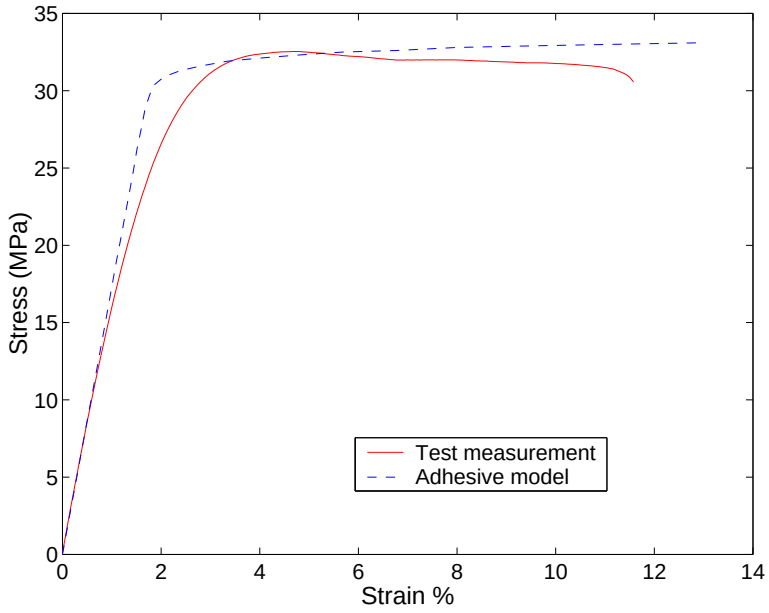

Figure 5.1: Comparison of experimental stress-strain behaviour of Ciba Araldite420 in tension with elastic-perfectly plastic modelling

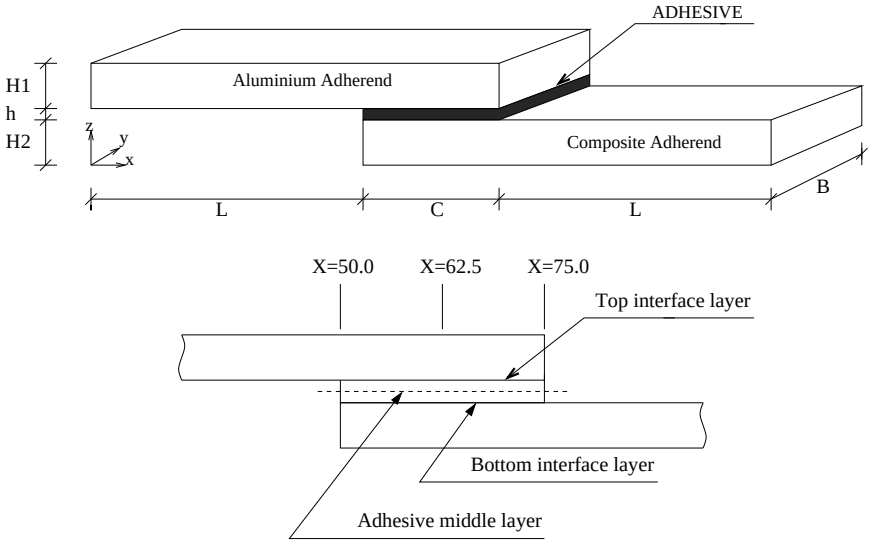

(a) The joint model with dimesnions: L=50.0mm, C=25.0mm, H1=5.0mm, H2=5.0,7.5,10.0,12.5,15.0mm, h=0.5mm, B=25.0mm

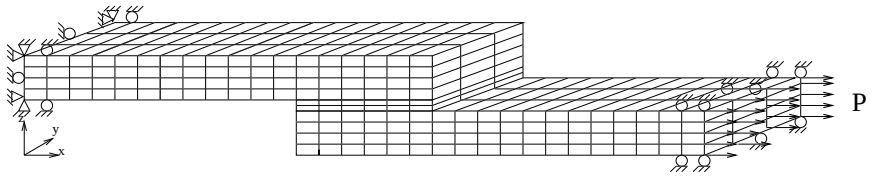

(b) Typical FE mesh with boundary conditions (Load P = 10.0kN)

Figure 5.2: Single lap joint geometry and boundary conditions

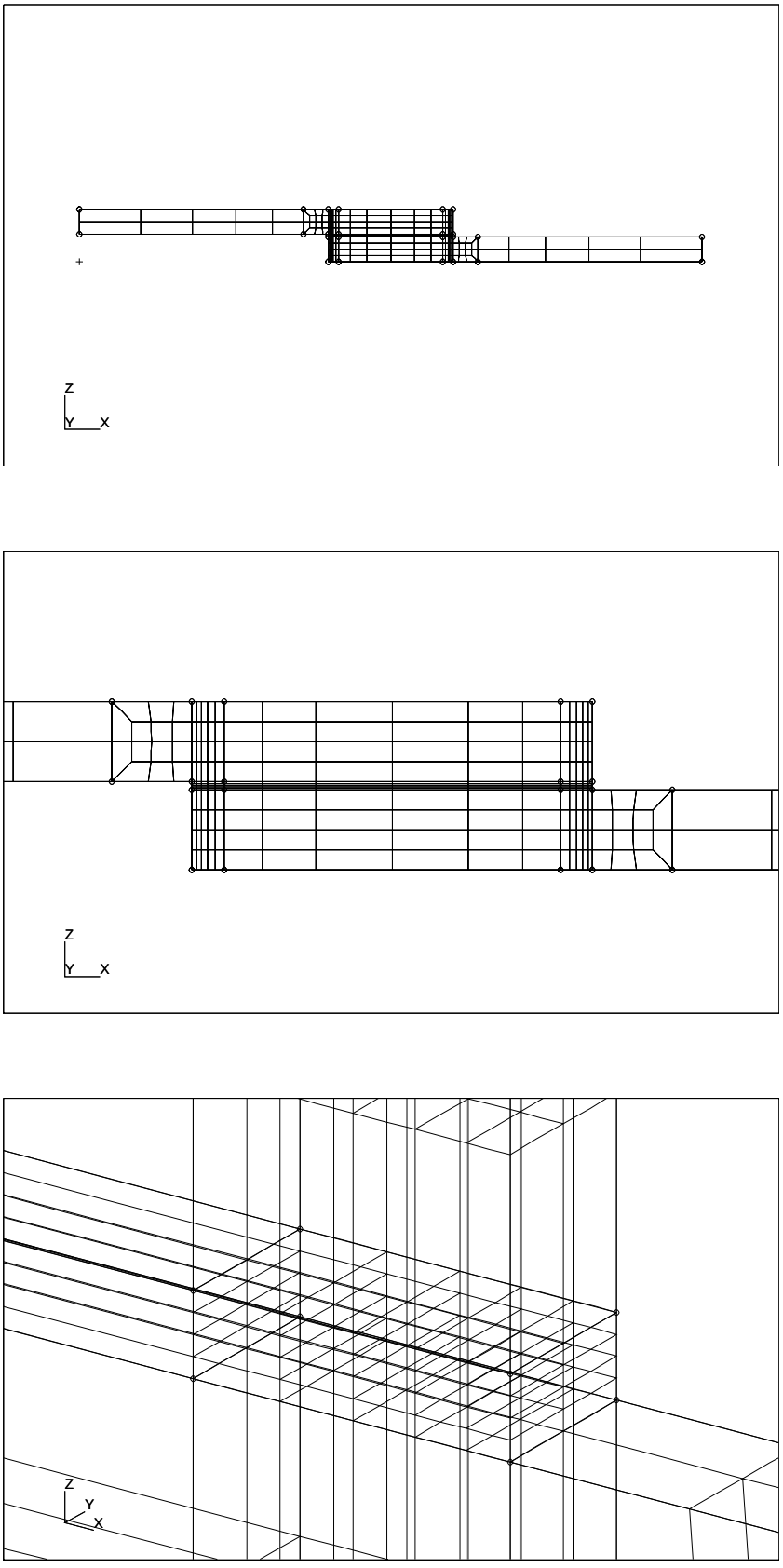

Figure 5.3: Finite element mesh of a single lap joint for H2/H1=1.0 and width b=1.0mm

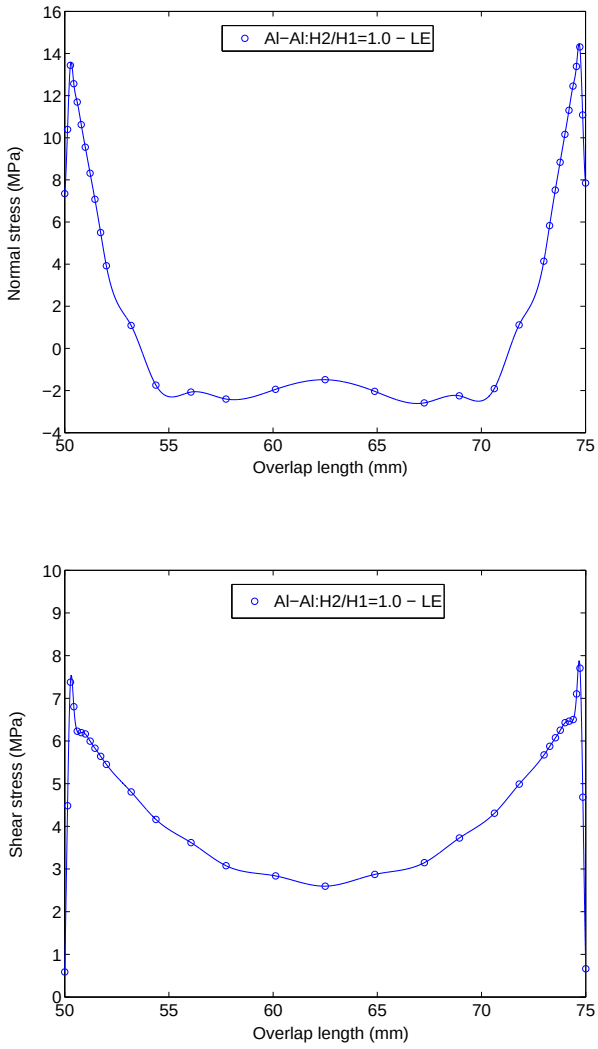

Figure 5.4: Normal and Shear stresses along the overlap length for Al/Al lap joint along the middle adhesive layer (applied load = 100N)

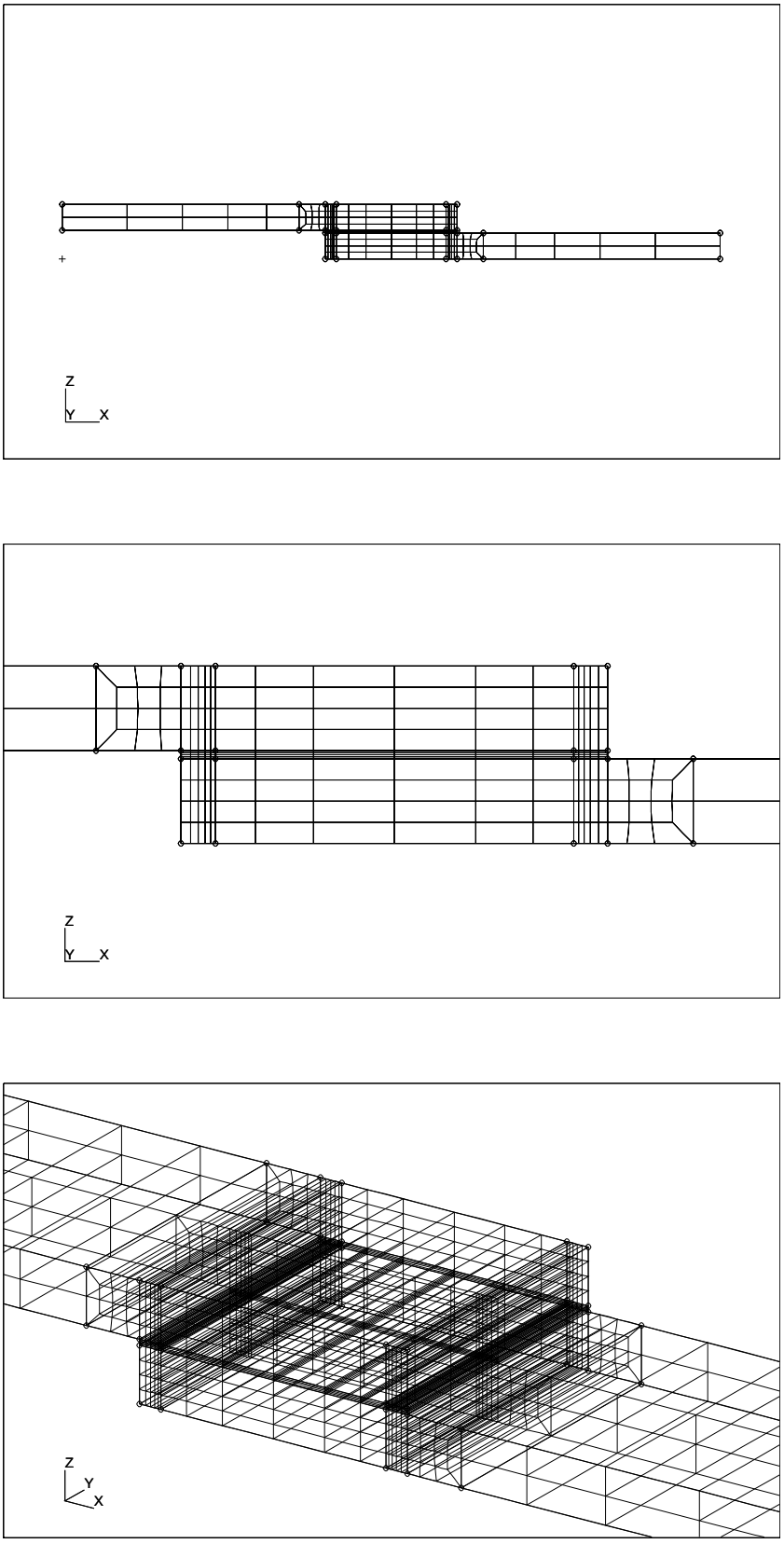

Figure 5.5: Finite element mesh of a single lap joint for H2/H1=1.0 and width b=25.0mm

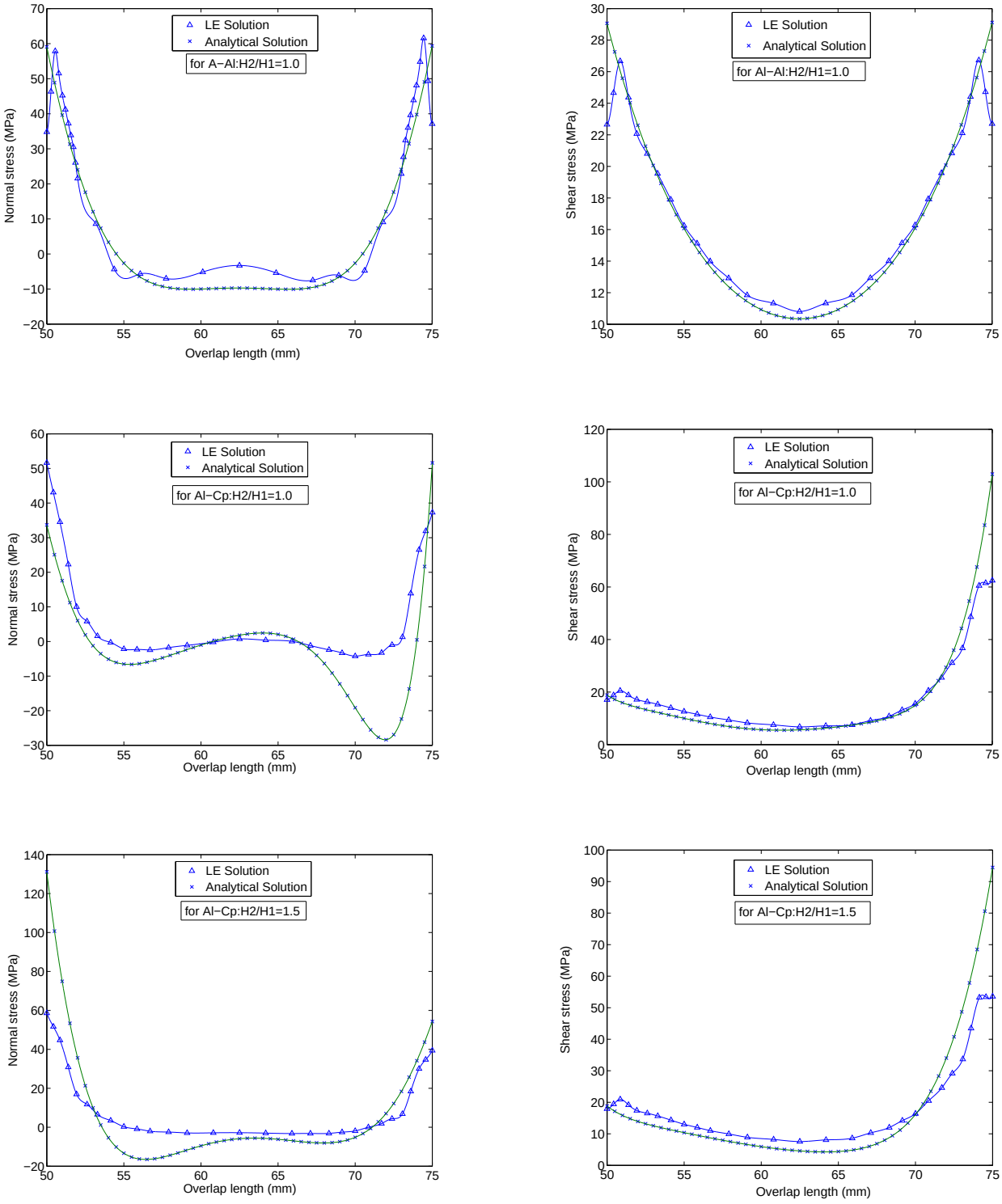

Figure 5.6: Comparison of numerical and analytical solution for normal and shear stress distributions for various H2/H1 ratios at the centre of adhesive layer for an applied load of 10kN

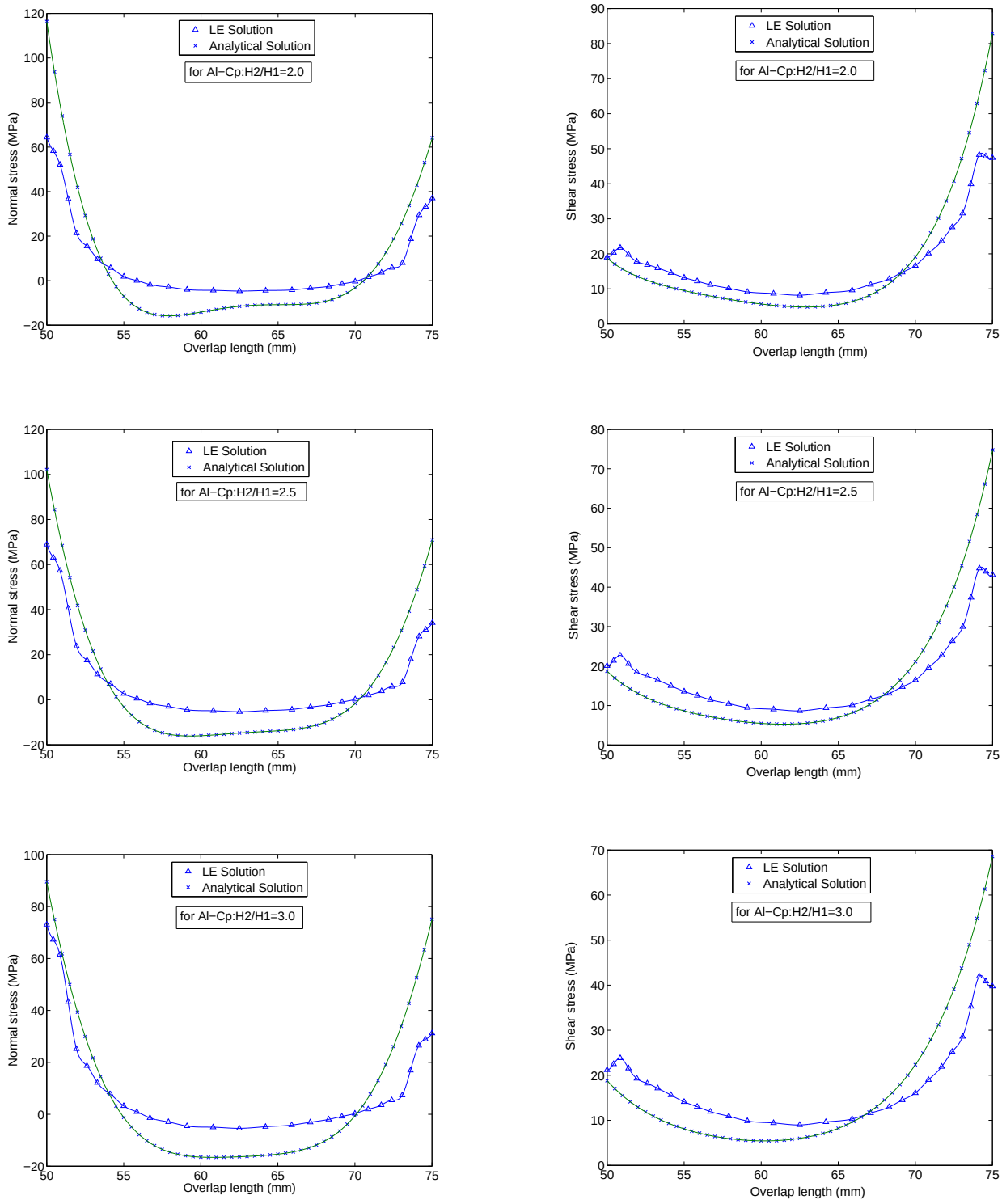

Figure 5.7: Comparison of numerical and analytical solution for normal and shear stress distributions for various H2/H1 ratios at the centre of adhesive layer for an applied load of 10kN

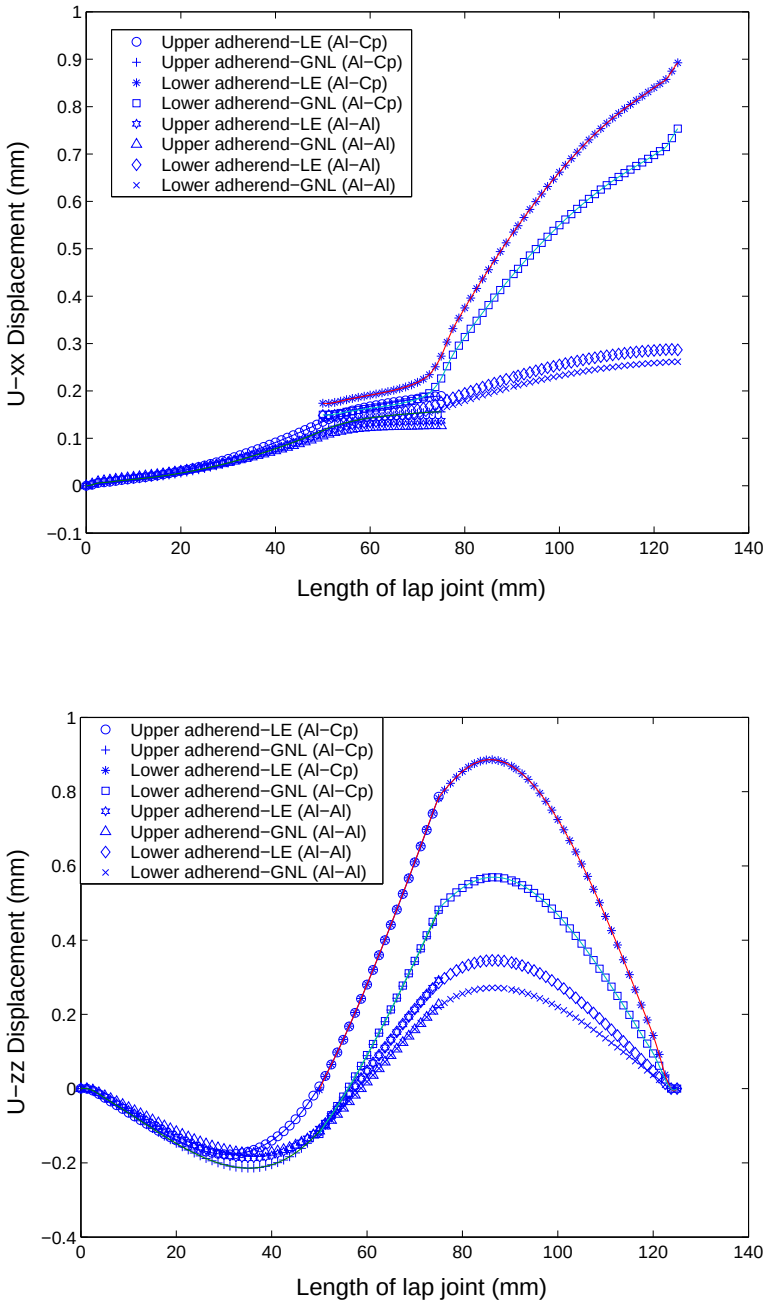

Figure 5.8: Comparison of deformation profiles for axial and vertical displacement in identical and non-identical adherends for linear and geometrical nonlinear solution (Applied load = 10kN)

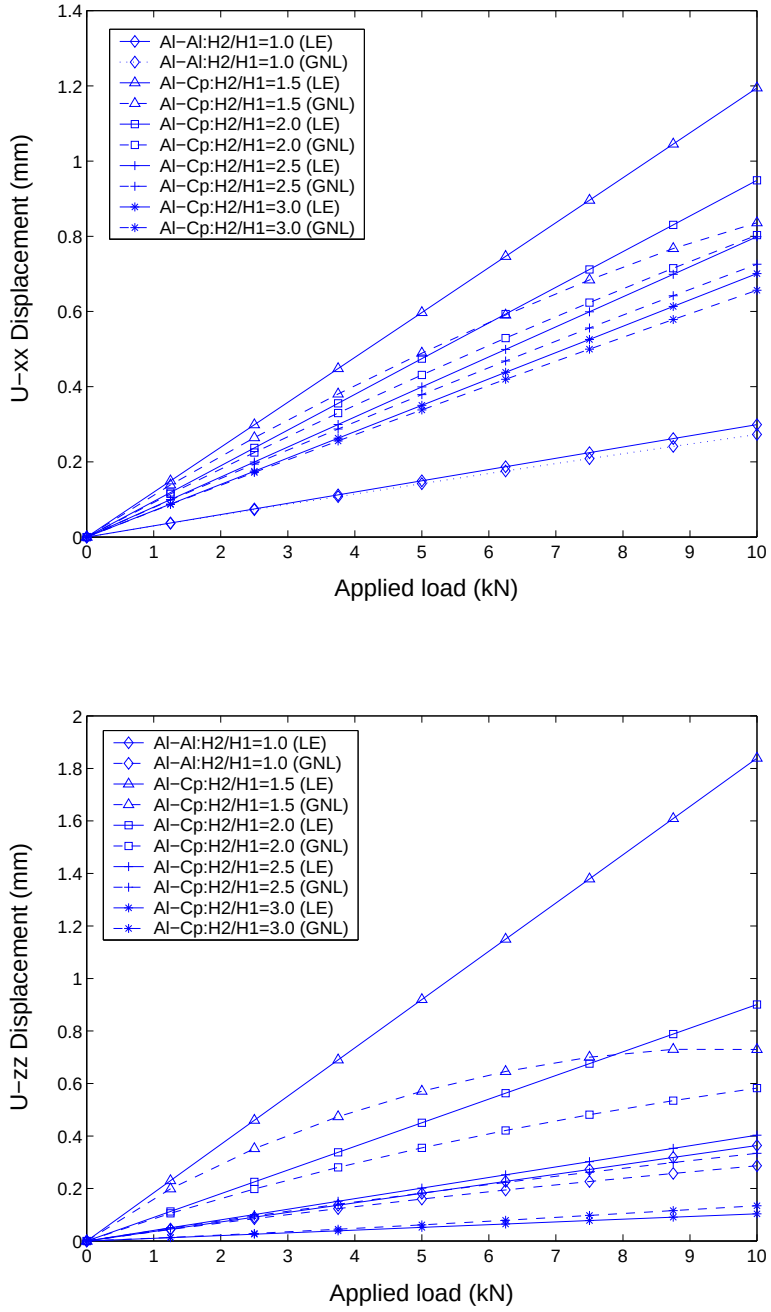

Figure 5.9: Linear and geometrical nonlinear axial and vertical displacement values for various $H2/H1$ ratios as a function of the applied load

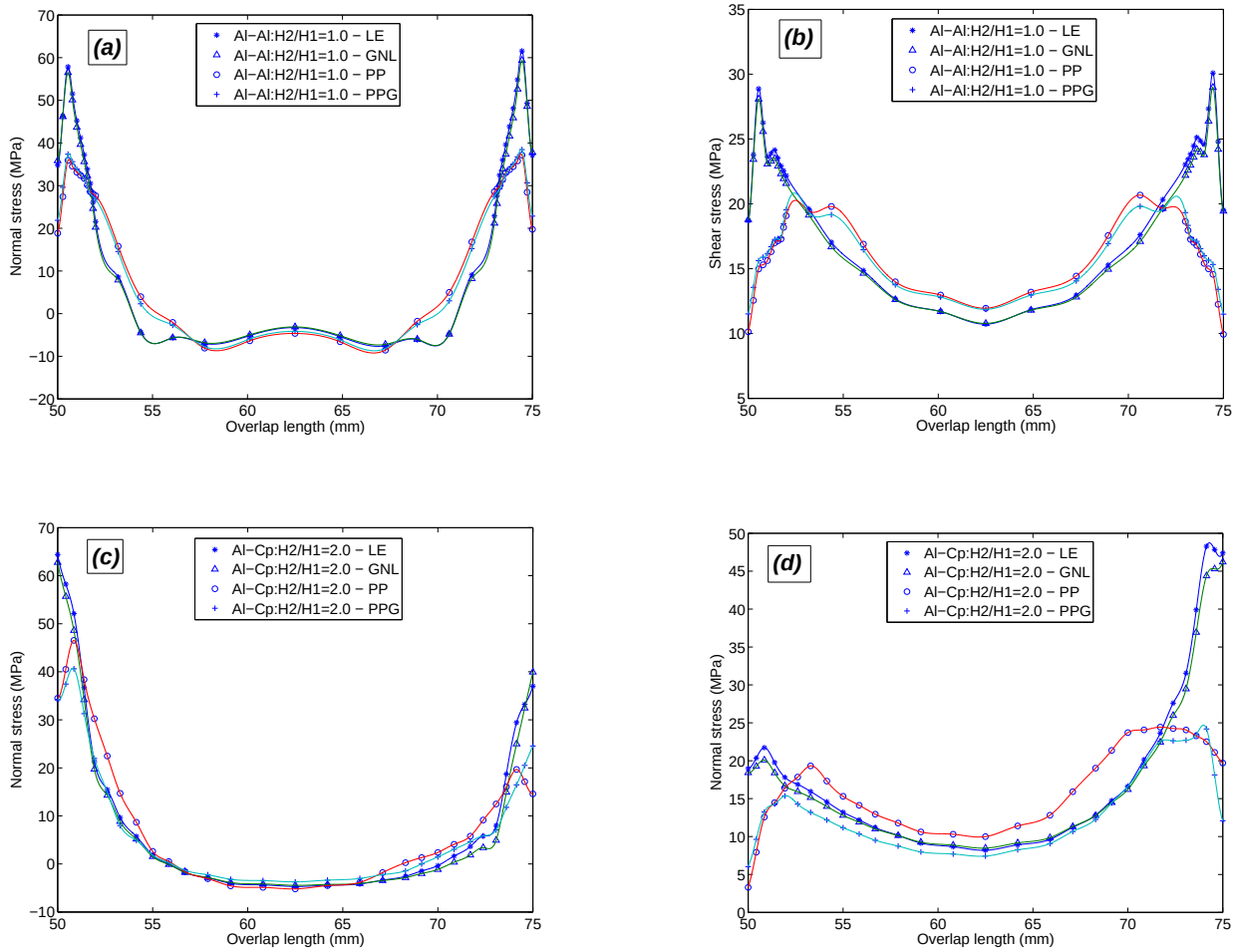

Figure 5.10: Comparison of Normal and shear stress distribution for different analyses with identical and non-identical adherends along the middle adhesive layer: (a) $Al - Al : H2/H1 = 1.0$, (b) $Al - Al : H2/H1 = 1.0$, (c) $Al - Cp : H2/H1 = 2.0$ and (d) $Al - Cp : H2/H1 = 2.0$ (Applied load = 10.0kN)

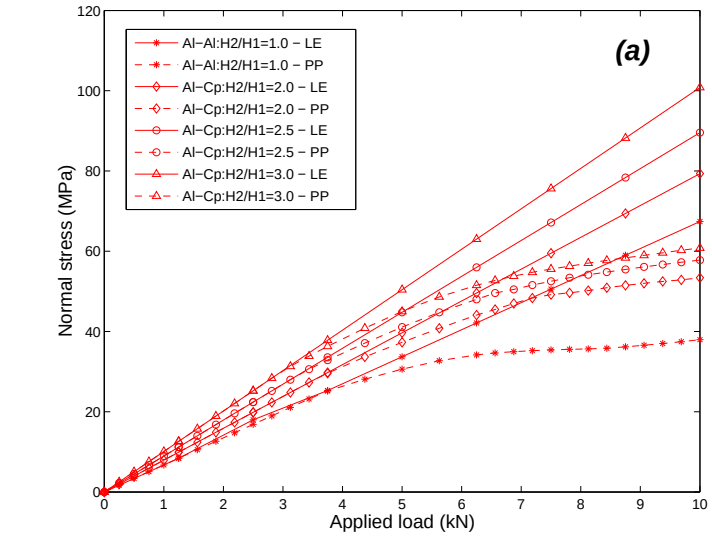

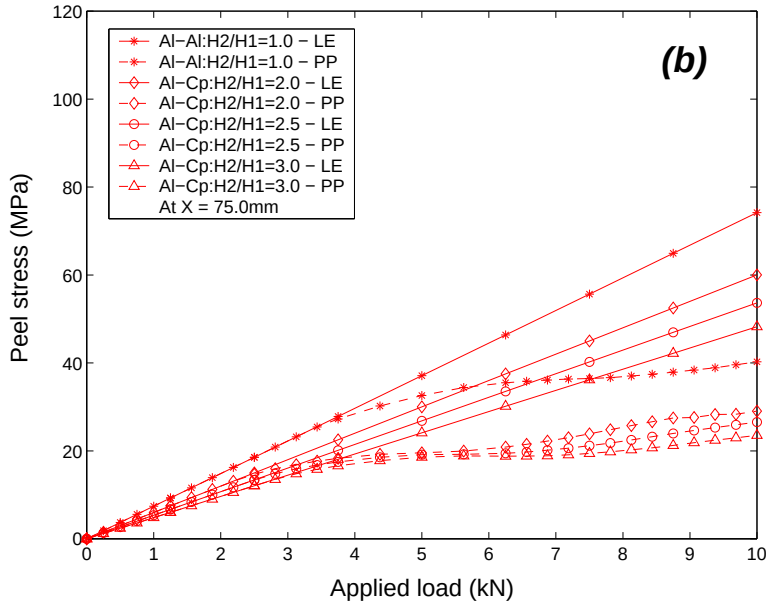

Figure 5.11: Variation of normal stresses at the overlap ends for the linear (LE) and for the perfectly plastic (PP) analyses as a function of the applied load for different adherend thickness ratios: (a) $atX = 50.0mm$ and (b) $atX = 75.0mm$

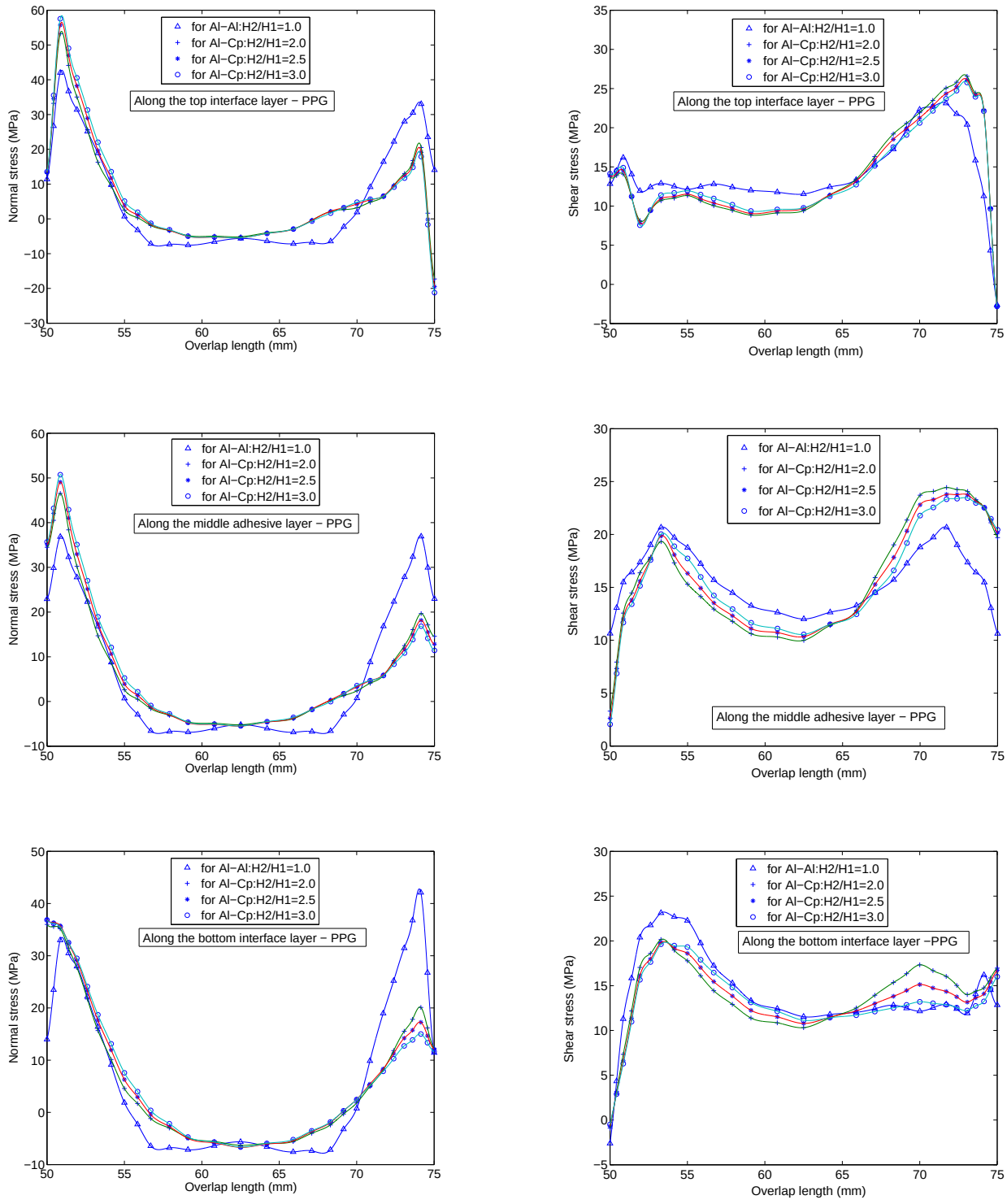

Figure 5.12: Normal and Shear stress distributions at top, middle and bottom adhesive layer for various $H2/H1$ ratios for an applied load of 10.0kN (PPG Solution)

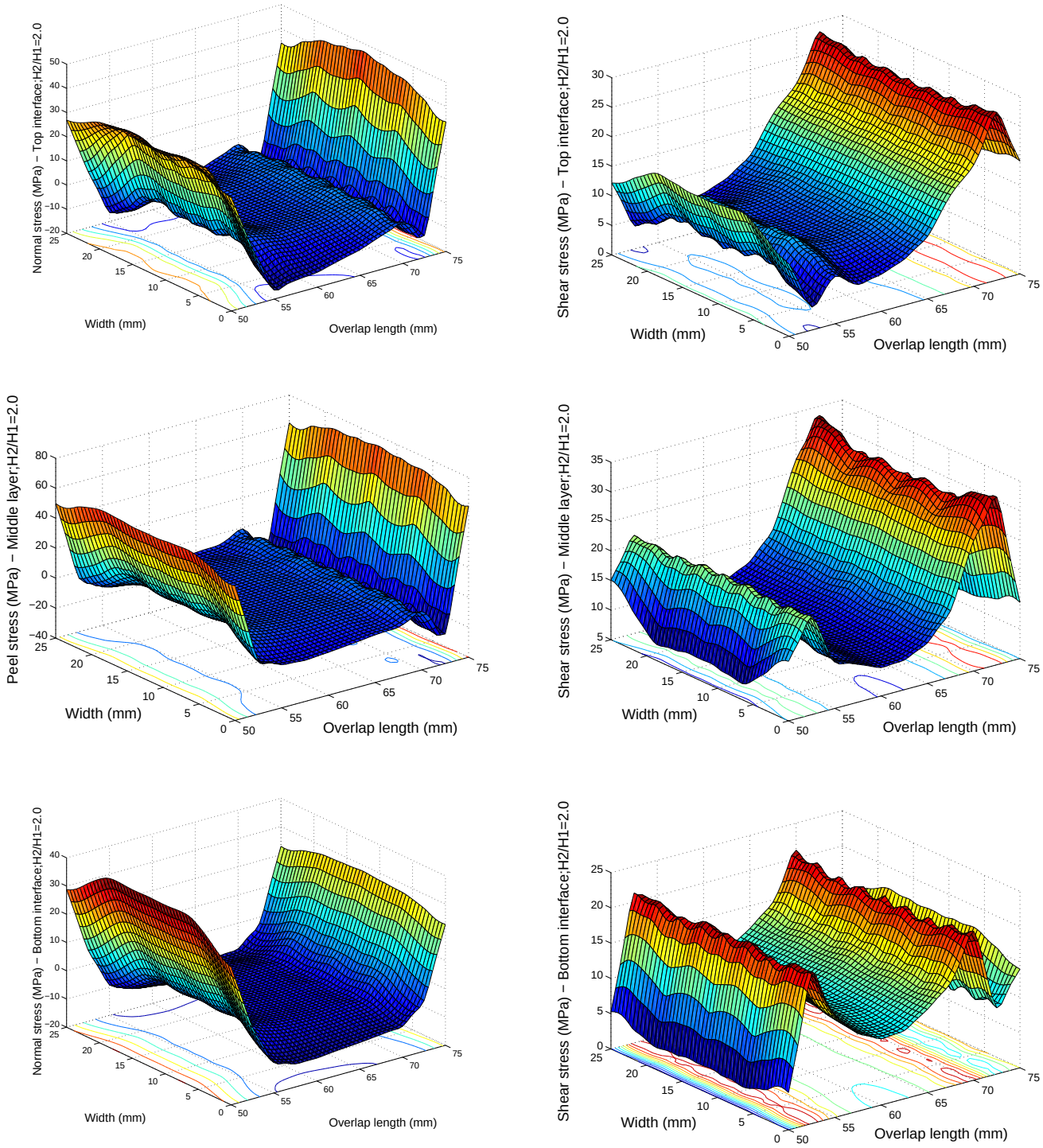

Figure 5.13: Three dimensional normal and shear stress distributions at top, middle and bottom adhesive layer for the joint with the thickness ration $H2/H1 = 2.0$ for an applied load of 10.0kN (PPG Solution)

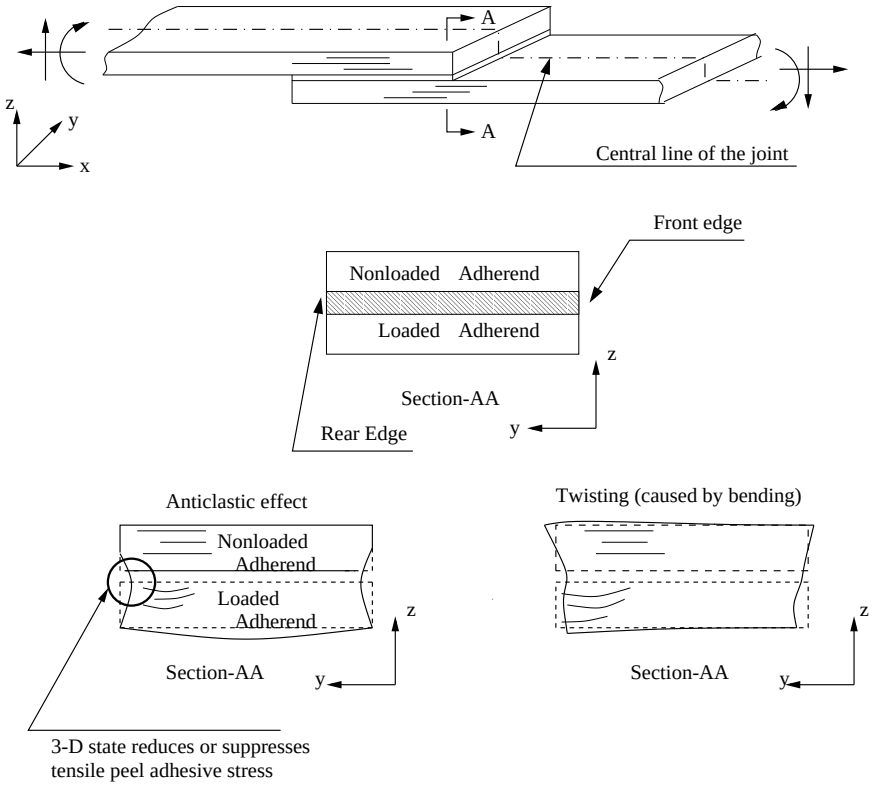

Figure 5.14: Anticlastic and Bending-Twisting effect on adherends and adhesive in single lap joint

Chapter 6

Analysis of Butt-strap joint structures

6.1 Introduction

This chapter concerns the numerical modelling of a single butt-strap joint system that is derived from the deck-to-superstructure connection of the Patrol craft as sketched in figure 1.5. The joint consists of two dissimilar adherends, aluminium and steel, bonded by a semi-rigid adhesive material Plexus MA550. Methodology for this analysis is outlined in chapter 3 after the relevant literature discussion in chapter 2.

6.2 Problem definition

The geometry of the single butt-strap joint is shown in figure 6.1. An experimental programme was conducted for butt-strap joints with adhesive thicknesses 1,3,5 & 10mm (Jarry and Shenoi, 2005). The bottom steel and Al 6082 adherends are strapped with the top Al 5083 adherend and bonded with a semi-rigid adhesive material Plexus MA550. The joint specimens were subjected to in-plane tensile loads at the rate of 1mm/min and the load-displacement curve were obtained until the joints failed. The maximum load carrying capacities of the joints were found to be 10kN for the joints with adhesive

thicknesses 1,3 & 5mm and 6.5kN for 10mm adhesive thickness (Jarry and Shenoi, 2005). A three dimensional finite element (FE) model for a single butt-strap joint was generated as per the dimensions shown in figure 6.1(a). The butt-strap joint was meshed using three dimensional 20-noded isoparametric element with 3x3x3 Gaussian integration scheme. The FE model had 412 3D elements with 2679 nodes, thus having 8037 degrees of freedom. The geometry, FE mesh and the boundary conditions are described in figures 6.1 and 6.2. An uniform tensile load of 10kN which is found to be the maximum load carrying capacity from the experiments was applied in 25 load increments for all the joints. As discussed in the literature review, the main focus of the work is on following issues:

- How realistic are the stresses in comparison to the strength of the adhesive material?
- Significance of performing of three dimensional analysis
- Identification of possible failure modes in butt-strap joint specimen

Three types of analyses were performed for all the joint cases *viz.* linear elastic (LE), geometric nonlinear (GNL) and geometrical-material nonlinear (GMNL) formulations. Normally, linear FE analysis results in adhesive stress values that are very high in magnitude in comparison to the actual strength of the adhesive material (Mitra and Ghosh, 1995) . This calls for an ideal material nonlinear model for the description of a semi-rigid adhesive in a bonded joint configuration. Characterisation of such adhesive by Ramberg-Osgood relation is found to be the appropriate choice as demonstrated here in the earlier section. Now the actual adhesive stress state in a single butt-strap joint for this material nonlinear model will be compared in relation to the actual strength of the adhesive material. Three dimensional deformation and stresses obtained from the nonlinear analyses will be helpful in understanding the behaviour of joints with thicker adhesive layer and in identifying the possible failure modes that could occur in a structural joint.

Material properties of the joint:

Al5083: E = 71.0GPa; Al6082: E = 69.5GPa; Steel: E = 200.0GPa and Plexus MA550: E = 361MPa, $\nu = 0.47$

6.3 Implementation of material nonlinearity

Structural adhesives like Plexus MA550 exhibit inelastic behaviour since plastic strains are induced even at low levels of loading. Hence modelling of the adhesive as a nonlinear material by formulating effective stress-strain relationship will be more appropriate instead of a linear model. The elasto-plastic constitutive relations for the adhesive material can be referred in section 4.4. There are various methods of representing the non-linear stress-strain curve like a) Elastic-linear hardening model, b) Elastic-exponential hardening model and c) Ramberg-Osgood model.

6.3.1 Characterisation of the adhesive material

Plexus MA550 is a two-part methacrylate adhesive designed for structural bonding of thermo-plastic, metal and composite assemblies (Brede, 2001). True stress-strain relations in the form of bulk adhesive tests for Plexus MA550 are available from the work of Brede (2001). This adhesive is highly flexible with a Poisson's ratio of 0.47. The stress-strain relationship is nonlinear and has no clear definition of a yield point. Further, the slope decreases monotonically as the stress increases. Hence of the three models mentioned above, a semi-rigid adhesive like Plexus MA550 can ideally be modelled by a three-parameter, Ramberg-Osgood model (1943):

$$\frac{\epsilon}{\epsilon_{ch}} = \frac{\sigma}{\sigma_{ch}} \left[1 + \left[\frac{\sigma}{\sigma_{ch}} \right]^{r-1} \right] \tag{6.1}$$

where σ_{ch} is the characteristic stress, ϵ_{ch} is the characteristic strain and they are related as $\sigma_{ch} = E\epsilon_{ch}$. The unknown parameters σ_{ch} and r can be obtained by the least squares technique. The procedure to determine these two parameters are explained in appendix B. The initial slope of the curve takes the value of the Young's modulus E. The effective stress-strain relationship for the adhesive Plexus MA550 is obtained by specifying initial yield stress σ as 13.0MPa (as deduced from test results of Brede, 2001), σ_{ch} is obtained as 9.0MPa and the value of r as 12.0 from the least squares computations (see appendix B). Figure 6.3 shows that the stress-strain relation using the Ramberg-Osgood equation (R-O

curve) for a perfectly-plastic condition agrees with the experimental data.

6.3.2 Yield criterion for the semi-rigid adhesive material

Brede (2001) determined the yield stress values for the Plexus MA550 from bulk tests under compression and tensile loading. Since this adhesive is pressure-dependent, the ratio between the compressive and tensile yield stress value is found to be 2.095 (λ) which is termed as Raghava's equivalent (Raghava *et al.* 1973). To reflect this behaviour, the modified von Mises criterion is proposed here as yield criterion. Equations concerning the yield criterion can be referred in section 4.5.2.

6.4 Results and Discussions

6.4.1 Validation of FE results

In order to validate the results obtained from the developed FE program, adhesive stresses in the butt joint are compared with the analytical solution formulated by Bigwood and Crocombe (1989). This is only for the general elastic analysis with the assumption that out-of-plane adherend strains are negligibly small compared to adhesive strains. The full elastic analysis is produced by considering the elemental length of a general adherend-adhesive overlap with adherend subjected to general tensile, shearing and moment loading. Equations adopted by Bigwood and Crocombe (1989) were implemented in the form of a spread-sheet program for the comparison of adhesive peel and shear stresses. As shown in figure 6.1(b) a single butt-strap joint can be considered as a combination of two single lap joint system. Material properties and load, moment and shear values for two single lap joints, one consisting of adherends Steel/Al5083 and an another with adherends Al5083/Al6082 are given as input for the analytical calculation. The resultant peel and shear stresses are compared with the numerical results obtained for the linear elastic (LE) case corresponding the applied load of 10kN. Stress plots in figures 6.4 and 6.5 show that the numerical results are in good agreement with the analytical results. The peel and shear stresses varies significantly towards the end of the overlap from the analytical ones,

obviously because of the butt-gap of 1mm in the butt-strap joint where the stresses are expected to peak because of geometry and material discontinuity. It can also be said that the analytical formulation predicts closer value for smaller adhesive thickness and as the adhesive thickness increases, stress value deviates, particularly for the shear stress component. In summary, the results generated from the developed three dimensional FE program are similar to the stress pattern seen in a typical lap joint structure.

6.4.2 Load-Displacement relation

Figure 6.6 shows a comparison of the experimental load-displacement curve with results obtained from the three dimensional finite element nonlinear program for butt-strap joint for different adhesive thicknesses. The results from the present analysis are compared with experimental results (Jarry and Shenoi, 2005). Linear (LE) and geometrical nonlinear (GNL) results are given for comparison to highlight the nonlinear nature of the adhesive (experimental one) and the robustness of the FE program to achieve a close result obtained from the geometrical-material nonlinear (GMNL) formulation.

From the plots in figure 6.6, it can be seen that the GMNL case show the closest agreement with the experiment results, in particular for the adhesive thicknesses 1, 3 & 5mm and deviates for 10mm thickness. A more refined FE mesh may be expected to give better result for the large thickness of 10mm but it is observed that even for this case, the computational time is high. The butt-strap joint considered here is non-symmetric in geometry and the load is eccentric. This results in rotation and bending of the adherends as observed in a single lap joint (refer chapter 5). It can be noted from the plots that influence of GNL is evident as the GNL curve starts deviating from LE curve right from the lower load magnitude of 4kN. Hence it is reasonable to account for geometric nonlinearity in the joint.

With nonlinear load-displacement curves giving reasonable correlation with the experimental curve, it is reasonable to expect that the stress state in the adhesive layer and

in the interfaces of the butt-strap joint from the nonlinear analyses will be predicted adequately.

6.4.3 Nonlinear deformations

Plots 6.7*a* and 6.7*b* show the typical profile of the axial (U_{xx}) and the vertical (U_{zz}) displacements corresponding to the maximum applied load of 10kN along the bottom interface layer for the joint with adhesive thickness 1mm. A similar deformation profile is observed for joints with other thicknesses and the comparison of maximum displacement values for different set of analyses are presented in tables 6.1 & 6.2. The displacement profiles are similar to the displacement curves shown by Mitra and Ghosh (1995), the one difference being axial displacements are symmetrical as the joint is of a double butt-strap configuration unlike the single butt-strap considered in our analysis.

- The influence of geometric nonlinearity is seen in figure 6.7 for both axial and vertical displacements since the load path is not symmetric. This causes bending of the joint similar to the one observed in the case of a single lap joint in the previous chapter. Maximum displacement values for GNL are also significantly less than the corresponding LE displacement values (tables 6.1& 6.2).

- The highly flexible nature of the adhesive can be understood from figure 6.7*a* and from table 6.1 where the maximum axial displacement values for GMNL case at the end of the butt-strap joint are more than twice the corresponding values obtained for linear or even for the geometrical nonlinear case.

- A very steep increase in the axial displacement profile (figure 6.7*a*) is observed at the centre of the joint where there is a 1mm gap between the bottom adherends. This occurs over the small length of the 'butt-gap' between the bottom adherends which is unfilled by the adhesive material and deforms more freely as the material is highly flexible. Displacement curves from the material nonlinear case (GMNL) capture this more realistically than other analyses. For the case of butt-strap joint

with adhesive filled in the gap, axial displacements vary gradually along the bond line (Mitra and Ghosh, 1995).

- The vertical displacement profile (U_{zz}) for the material nonlinear (GMNL) shows excessive elongation as in the case of axial displacement (figure 6.7*b*). It can be said from the profile that bottom adherends bend downwards at the centre of the joint while subjected to in-plane tensile loading. It is interesting to see that there is a sudden decrease in displacement value at the mid-node in the 1mm butt-gap. Displacements in this central butt-gap for all the adhesive thicknesses are shown in figure 6.7*c*. As the thickness of adhesive layer increases, U_{zz} decreases at the centre by 0.2mm for the 1mm joint to almost 1.3mm for the 10mm joint. This behaviour is pictorially shown in figure 6.8 and it indicates that as the adhesive thickness and the bulkiness of the material increases *(shaded area)*, the adhesive tends to hold the mid-node *(marked 'b')* while the end nodes *(marked 'a')* on either side undergoes maximum deformation due to bending of the bottom adherends. Infact, these end nodes deform in all the three directions significantly in lateral and vertical directions ($U_{yy} = 1.4mm$ & $U_{zz} = 1.3mm$) for the 10mm joint. The free surface in 1mm gap resists further downward deformation but the bending of the bottom adhrends results in peeling leading to joint failure. This has a direct influence on the peel stress which is discussed in following section.

- Three dimensional modelling of the butt-strap joint has provided an opportunity to look at the deformations in lateral direction whereas in a plane stress/strain analysis cannot present such scenario. From figure 6.9, one can see the extent of lateral contraction at the bottom adhesive layer for the joints of thickness 5 & 10mm . Lateral deformation is sketched in figure 6.8 for better understanding. This lateral contraction is almost nil at the top interface layer and increases sharply from the middle layer towards the free surface by 1.4mm. The presence of gap between the bottom adherends and high Poisson's ratio (0.47) of the adhesive material results in combined deformation of the flexible adhesive in both vertical and lateral directions.

6.4.4 Nonlinear stresses

Peel and shear stress profiles for the butt-joint with 1mm adhesive thickness along the top, middle and bottom adhesive layer are presented in figure 6.10. A comparison of maximum stress values obtained for the different set of analyses are given in tables 6.3 & 6.4.

Stress values under GMNL case are lower than those in the corresponding LE case, in particular for the joint thicknesses 1,3 & 5mm by 33.5%, 31.7% and 44.7% respectively. Figure 6.11 shows the variation of the maximum peel and shear stress with the load increment for all the joint thicknesses. These plots are useful in obtaining the onset of material nonlinearity in the adhesive as the load is increased. For all the joints, once the peel stress values reaches 14MPa, the adhesive strength (Brede, 2001), the material tends to yield further but constantly as the load is increased further. This shows the actual perfectly-plastic yielding of the adhesive in the joint system and relates well with the stress-strain profile of the bulk adhesive (figure 6.3). The stress variation, in particular for the joint with 3mm thickness, demonstrates this significantly. The adhesive reaches its strength at a relatively low level load of around 3-4kN for all the joints, but the semi-rigid nature of the adhesive enables the reduced rate of stress increment as the load is increased up to 10kN. Thus the adopted material nonlinear model predicts realistic stress values in the joint system in comparison to the linear elastic analysis. Maximum peel stress occurs at the central butt-gap for all the adhesive thicknesses where there is a geometric and material discontinuity. So, yielding of the adhesive under the increasing plastic strains may well begin at this butt-gap of 1mm prior to other regions, thus leading to adhesive peel failure (Hart-Smith, 1981).

With regard to the shear stress profile(figure 6.10), there is a sharp increase along the butt gap of 1mm for linear and geometric nonlinear elastic analyses. But the inclusion of material nonlinearity results in smoothening of the stress gradient over the central region of 20mm, mainly along the middle adhesive layer. Maximum shear stress values for the

GMNL case are about 20-33% of the corresponding LE values as seen in the case of peel stress. Maximum values are in the range of 12-15MPa for all the joint thicknesses; this is close to the adhesive strength. The variation of maximum shear stress values with the load increments can be seen in figure 6.11. Maximum shear stress occurs slightly away from the butt-gap unlike the peel stress which is seen exactly in the butt-gap where there is no shear stress.

Typical three dimensional peel and shear stress distributions for the 1mm joint along the bottom interface layer are presented in figure 6.12. Peel stress is maximum at the middle of the joint and reduces towards the edges. The peel stress reduces significantly from 33MPa at the middle to 21MPa towards the edges. This indicates the presence of a *'3D corner'* that results in *'anti-clastic'* effect as peelly seen in a typical single lap joint (Tsai *et al.*, 1995 and chapter 5). This behaviour is expected in a single butt-strap joint as it is equivalent to the single lap joint configuration considering the geometry and the load path. The three dimensional contour for shear stress, on the other hand does not show any significant change across the width of the joint.

In short, for the appropriate design of the butt-strap joints, considering linear stress values for semi-rigid adhesives can lead to overestimation: it is thus necessary to account for the material nonlinearity for the analysis. Failure initiation can be identified from the onset of nonlinearity in the stress variation. Results obtained from three dimensional analysis provide a better understanding while a plane stress/strain analysis may not capture the peel and shear stress adequately for a single butt-strap joint specimen.

6.4.5 Identification of failure modes

Peel and shear stresses from the geometrical-material nonlinear solution (GMNL) for all the adhesive thickness are separately shown in figure 6.13. The maximum peel stress value along the top interface layer decreases with increase in the adhesive thickness occurring at the centre of the butt gap. However the peel stress decreases sharply at the end of the

overlap towards the compressive direction. The joint with the 10mm adhesive thickness has a maximum compressive stress of 21MPa at the ends. This differential direction of peel stress along the top interface layer is due to the bending of the top Al 5083 adherend. Shear stress along the top interface layer also has a gradient from -10 to 10MPa on either side of the overlap length.

Peel and shear stresses along the middle adhesive layer show little variation for different adhesive thicknesses. However the peel stress range (-10 to 26MPa) is more than the shear stress range (-13 to 13MPa). A sudden drop in the peel stress at the central butt-gap is observed along the bottom interface layer for the adhesive thicknesses 3,5 & 10mm. This can be attributed to vertical deformation of the adhesive in the butt gap as seen in figure 6.7*c*. As the thickness of adhesive increases, displacements (U_{yy}, U_{zz}) and the peel stress show significant variation. From an examination of the enlarged detail in figure 6.8, it can be said that bulkiness of the adhesive in shaded area with no interface beneath resists further elongation. Hence there is a steep reduction in peel stress towards the butt-gap. Given that the stress magnitudes vary greatly within a butt gap of 1mm, it is more likely that rubber-like adhesive may tear apart between the stress extreme ranges. This results in initiation of crack which are difficult to detect and in such a situation, *'cohesive failure'* can be expected (Hart-Smith, 1985). Experimental samples shown in figure 6.14 seem to suggest this mode of failure for the case of 10mm thickness.

Shear stresses along the bottom interface layer are in the range of -15 to 15MPa higher than the stresses in middle adhesive layer. In addition to this, the stress gradient is steep over the butt gap of 1mm whereas the gradient is gradual along the middle layer. High peel stress values at the butt-gap indicates that joint failure is more likely to be *'adhesive'* in nature due to the peel stress component; a similar observation is made by Mitra and Ghosh (1995) in the case of butt-strap joints.

The above discussion presented a qualitative description of the possible failure modes

in a butt-strap joint specimen due to the nonlinear behaviour of the adhesive material. It is also possible to make a quantitative prediction the failure stresses based on the comparison of adhesive strength vis-a-vis modified von Mises stress values that is adopted for the adhesive material model. Failure prediction based on the stress values are not presented here for the reason that the considered butt-strap joint is an idealized one with the gap between the bottom adherends, which is different from the actual experimental joints as it does not take account of the spew fillet. However, the developed 3D nonlinear code could be used to predict the failure stress values and this could form an extension of the work to include the effect of the spew fillet.

6.5 Critical assessment of results

This section outlines the knowledge gained from the three dimensional nonlinear analysis of a butt-strap joint system. The analysis carried out here is significant for the reasons that the bonding adhesive material type is semi-rigid and that the relative thickness of the adhesive layer to the adherend is very large. Observations made from the results present an improved understanding on the influence of geometric and material nonlinearities over the joint deformation and the adhesive stresses.

The analyses performed in this work clearly demonstrate that the influence of geometric and material nonlinearity on the deformations experienced by a butt-strap joint are more pronounced due to the highly flexible nature of the adhesive material and the relative thickness of the bond layer. Plots in figure 6.7 reveal excessive axial and vertical deformations occurring in the butt-strap joint when geometric and material nonlinearities are considered. Additionally, Flexible adhesives like Plexus MA550 has high Poisson's ration of 0.47 and hence deforms considerably in the lateral direction. This phenomenon is captured by this three dimensional nonlinear analysis adequately and shown in figure 6.9 for the thick bond lines of 5 & 10mm. Figure 6.8 illustrates the combined deformation pattern seen in a butt strap joint. Thus three dimensional deformation pattern in a butt-strap joint bonded with a semi-rigid adhesive is brought out and highlighted in this work.

Mitra and Ghosh (1995) presented peel and shear stress values in the range of 100-450MPa in their linear analysis of a butt-strap joint which far exceeds the strength of the adhesive material. However, a comparison of peel and shear stresses obtained from various formulations in this study (see tables 6.3 & 6.4) show that the nonlinear stress values are far lower than the corresponding linear stress values. Additionally, nonlinear peel stress values are closer to the actual strength of the adhesive Plexus MA550. It is inferred from this that the adhesive stress values obtained from the conventional linear analysis are not realistic. Hence, it is concluded that one should account for geometric and material nonlinearities when the adhesive material is flexible and the joint is of butt-strap configuration.

In summary, the analyses of a butt-strap joint system with a semi-rigid adhesive has lead to an improved understanding of the joint behaviour. The analyses have provided new ideas related to the influence of nonlinearities on joint deformation and the adhesive stresses. Finally, nonlinear stresses have to be accounted while evolving a design formulae since it is highlighted that linear stresses can result in over estimation of the joint design.

6.6 Conclusions

This chapter attempted to examine local stresses that occur in a deck-to-superstructure bonded component in a 34m long Customs & Excise cutter. The load transfer mechanisms over a single butt-strap joint system are investigated for different adhesive thicknesses. Following are the main conclusions from these set of analyses.

- Characterisation of a typical semi-rigid adhesive like Plexus MA550 by Ramberg-Osgood relation found to be the appropriate choice for the modelling since it correlates well with the experimental results of the bulk adhesive material (Brede, 2001).
- Load-displacement curves obtained from the geoemtrical-material nonlinear (GMNL)

analysis are close to the curves of the experimental specimen thus showing the robustness of the developed FE program.

- Significant reduction of joint displacements and adhesive stresses are seen for geometrical-material nonlinear (GMNL) analysis in comparison to linear (LE) and geometric nonlinear (GNL) elastic analysis. The resultant nonlinear stress magnitudes are closer to the actual strength of the adhesive material once the material attains nonlinearity and remains perfectly-plastic under the increasing load.

- The three dimensional FE formulation has demonstrated the existence of *'3D corner'* in butt-strap joint and the extent of lateral contraction due to the highly flexible nature of the adhesive material.

- Prediction of failure modes from the numerical results are similar to the ones seen in the experimental specimens.

Table 6.1: Maximum values for axial displacement (U_{xx}) obtained from different set of analyses (Applied load 10kN)

Adhesive Thickness (mm)	LE (mm)	GNL (mm)	GMNL (mm)
1.0	0.544	0.469	0.916
3.0	0.735	0.609	1.680
5.0	0.945	0.710	2.378
10.0	0.833	0.661	3.334

Table 6.2: Maximum values for vertical displacement (U_{zz}) obtained from different set of analyses (Applied load 10kN)

Adhesive Thickness (mm)	LE (mm)	GNL (mm)	GMNL (mm)
1.0	-1.538	-1.053	-2.306
3.0	-1.594	-1.036	-3.163
5.0	-1.770	-1.044	-3.865
10.0	-1.352	-0.887	-4.607

Table 6.3: Maximum values for peel stress obtained from different set of analyses (Applied load 10kN)

Adhesive Thickness (mm)	LE (MPa)	GNL (MPa)	GMNL (MPa)
1.0	101.81(b)	101.06(b)	34.13(b)
3.0	68.36(m)	61.70(m)	21.76(t)
5.0	51.34(m)	45.84(m)	22.95(t)
10.0	27.30(b)	23.10(b)	21.90(m)

Table 6.4: Maximum values for shear stress obtained from different set of analyses (Applied load 10kN)

Adhesive Thickness (mm)	LE (MPa)	GNL (MPa)	GMNL (MPa)
1.0	42.43(b)	52.69(b)	13.35(b)
3.0	62.15(b)	66.91(b)	12.43(b)
5.0	68.75(b)	77.90(b)	12.57(b)
10.0	76.15(b)	77.01(b)	15.13(b)

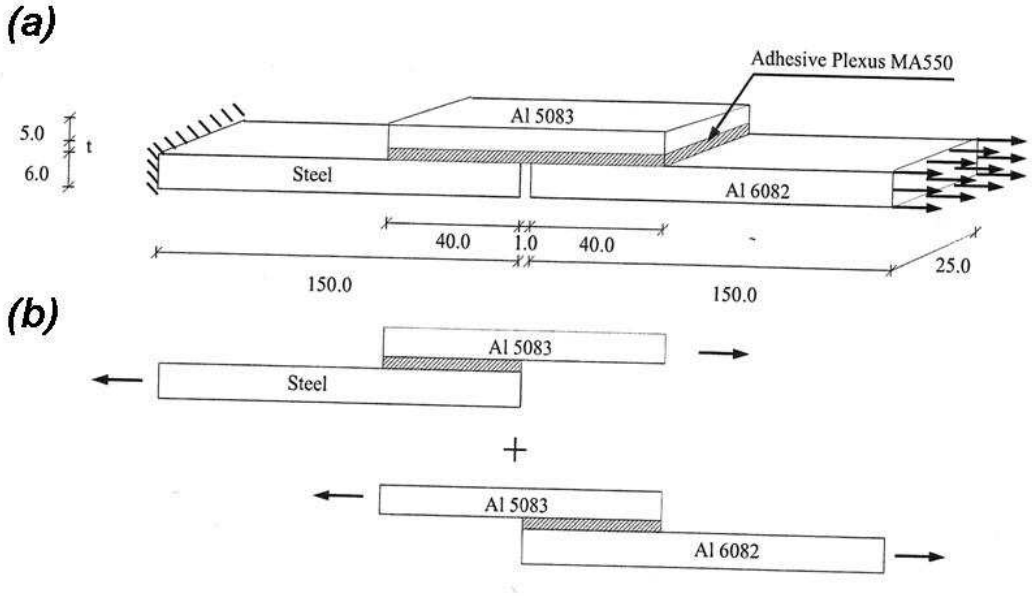

Figure 6.1: (a) Dimensions of the butt-strap joint model butt-strap joint model with adhesive thickness t = 1.0,3.0,5.0 and 10.0mm and (b) Superposition procedure

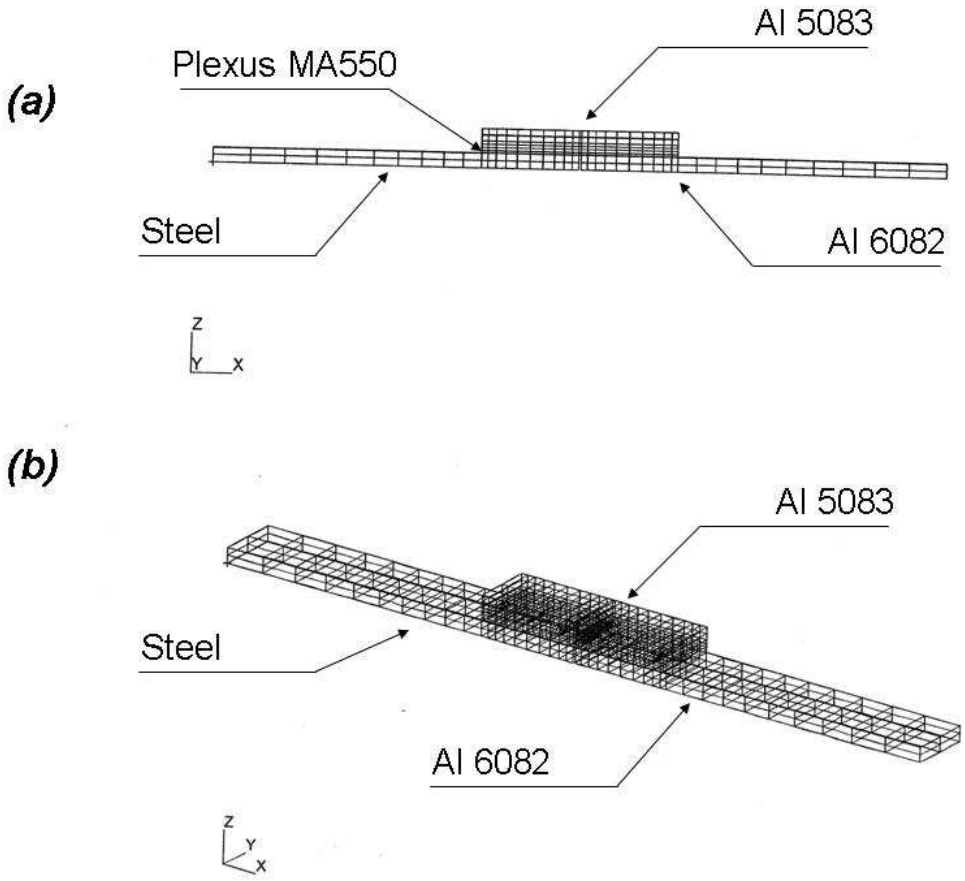

Figure 6.2: (a) 2-D view of the FE model and (b) 3-D view of the FE model

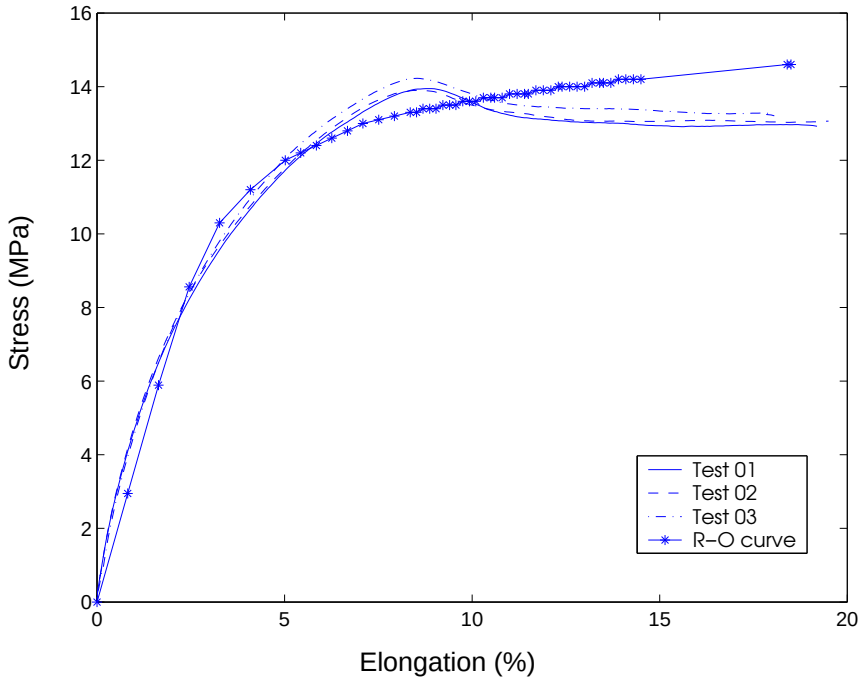

Figure 6.3: Comparison of experimental stress-strain behaviour of Plexus MA550 in tension with Ramberg-Osgood modelling

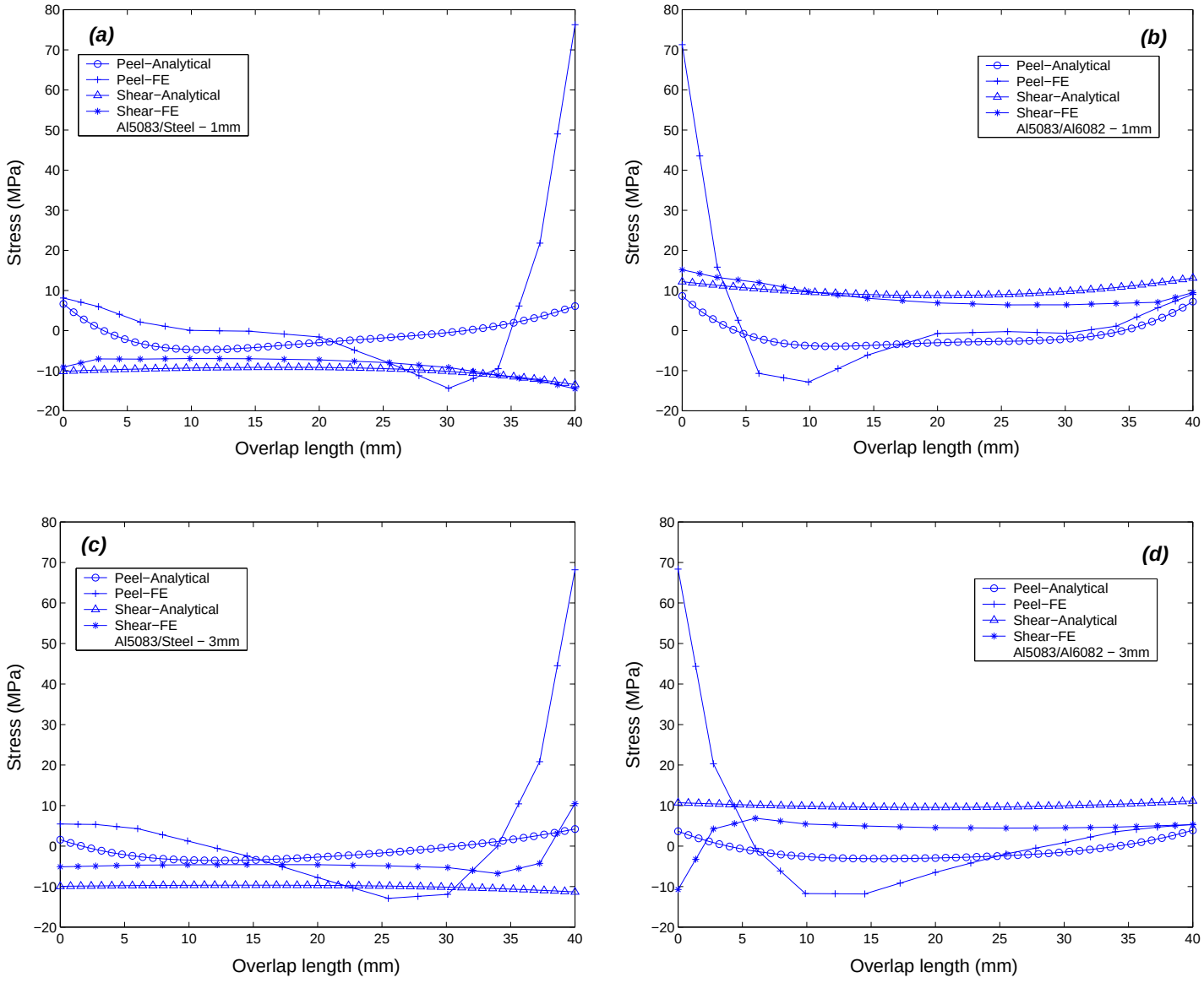

Figure 6.4: Validation of FE results with analytical solution for peel and shear stress along the overlap of the butt-strap joint (a,b) $t = 1mm$, (c,d) $t = 3mm$ (Applied load = 10kN)

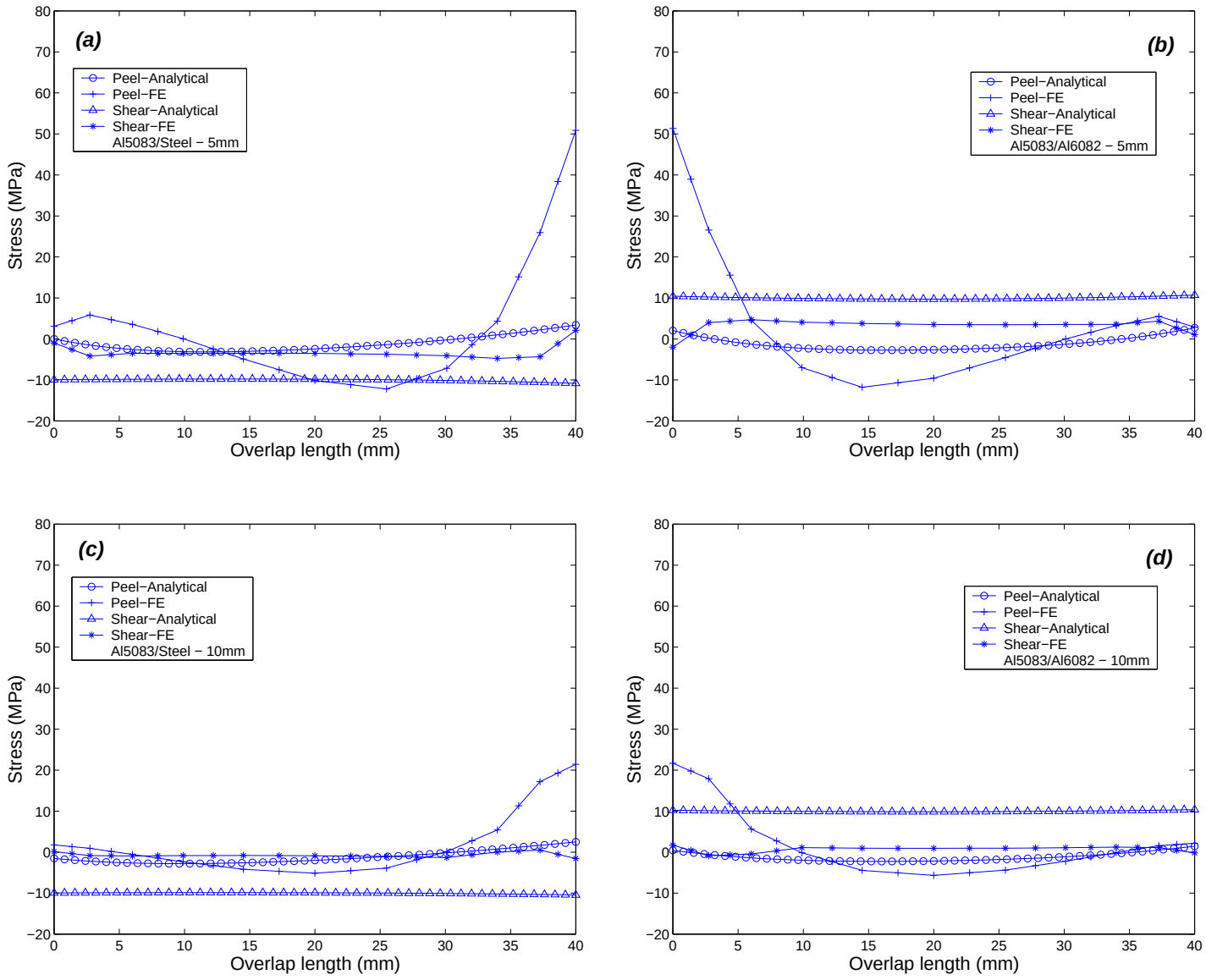

Figure 6.5: Validation of FE results with analytical solution for peel and shear stress along the overlap of the butt-strap joint (a,b) $t = 5mm$ and (c,d) $t = 10mm$ (Applied load = 10kN)

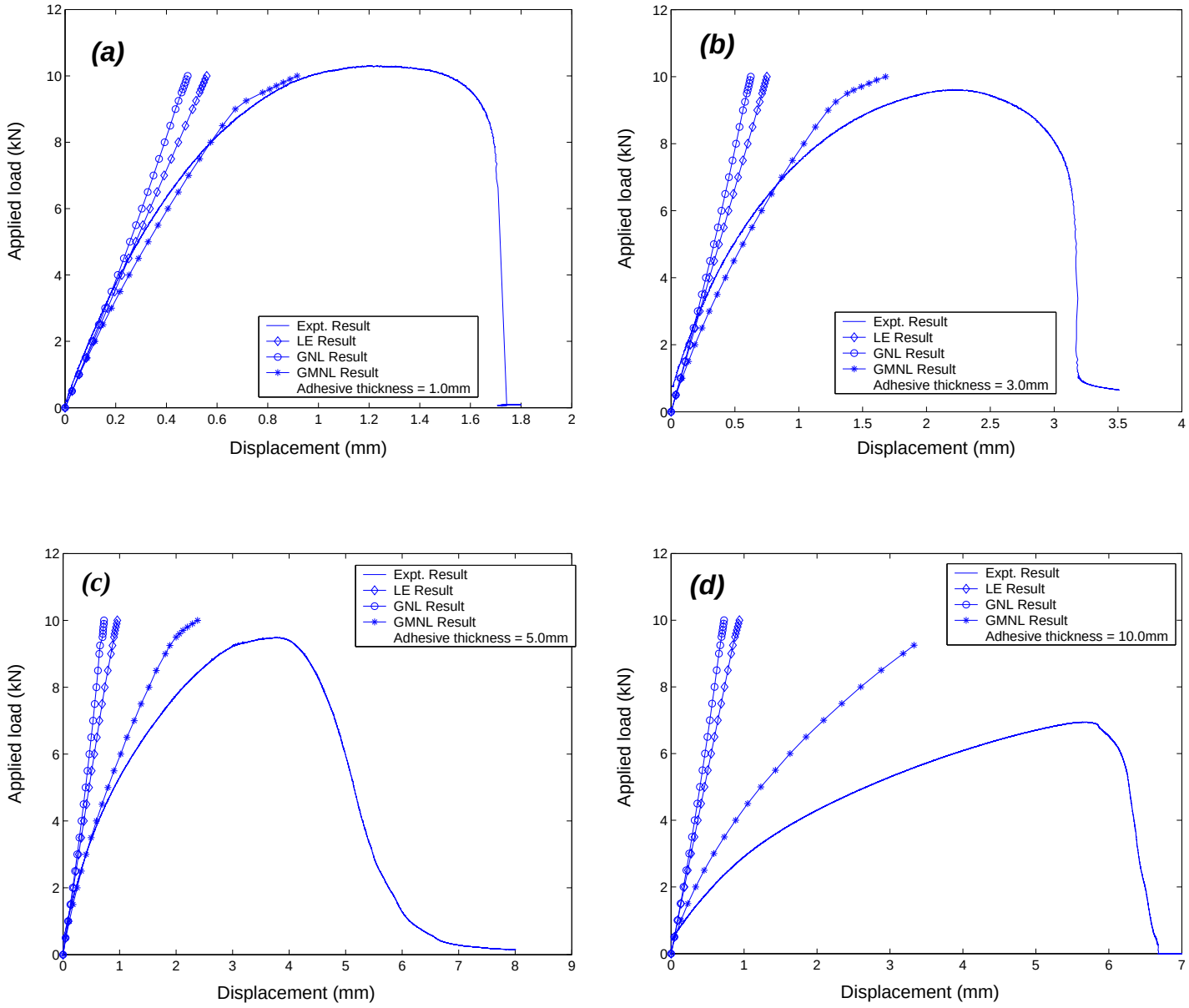

Figure 6.6: Comparison of experimental load-displacement curve with linear and nonlinear analysis for butt-strap joint with adhesive thickness: (a) $t = 1mm$, (b) $t = 3mm$, (c) $t = 5mm$ and (d) $t = 10mm$ (Applied load = 10kN)

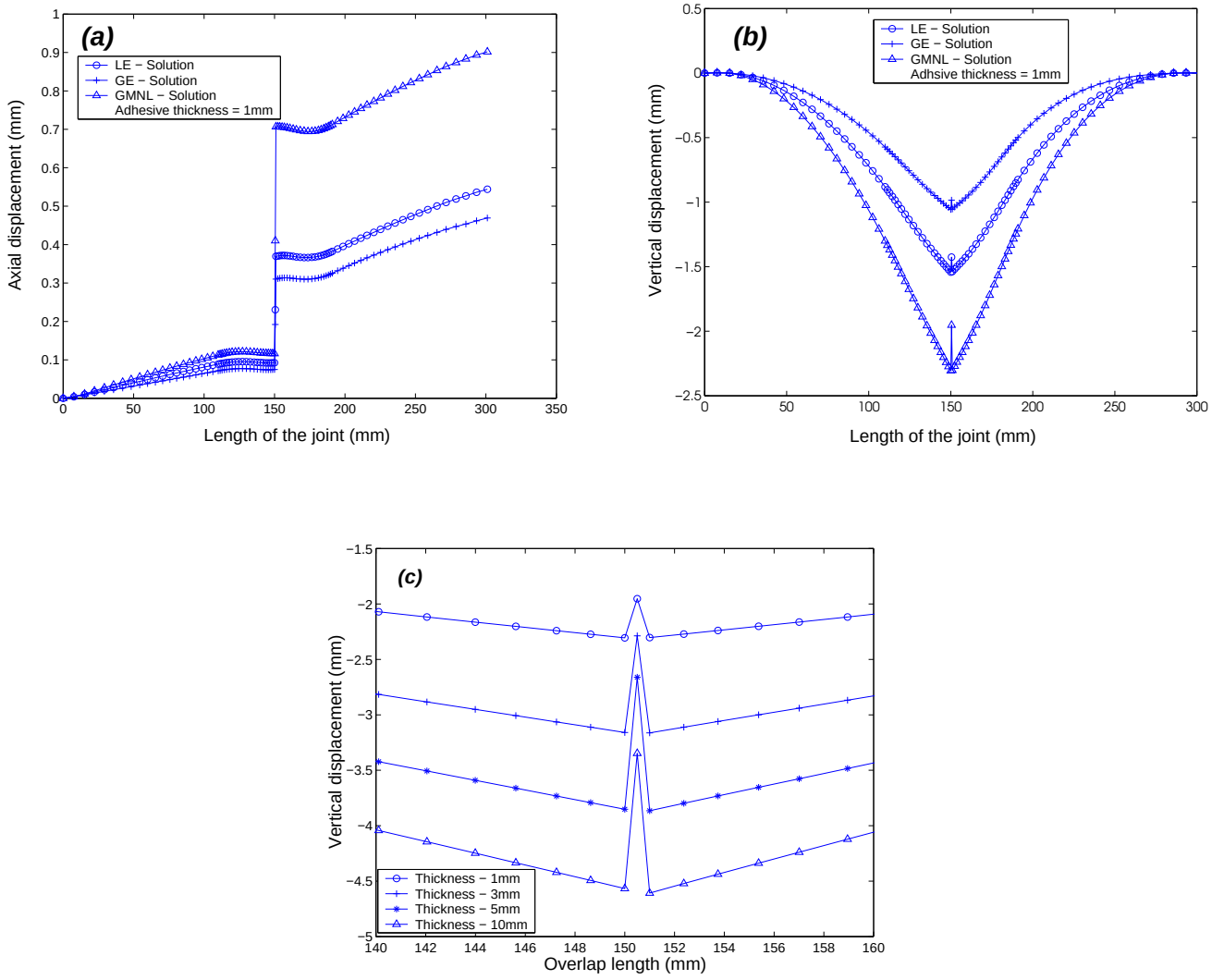

Figure 6.7: Deformation profile along the length of the butt-strap joint at the bottom adhesive layer (a): Axial displacement for the adhesive thickness of 1mm, (b): Vertical displacement for the adhesive thickness of 1mm and (c): Vertical displacement in the central butt-joint gap for the different adhesive thicknesses (Applied load = 10kN; GMNL Solution)

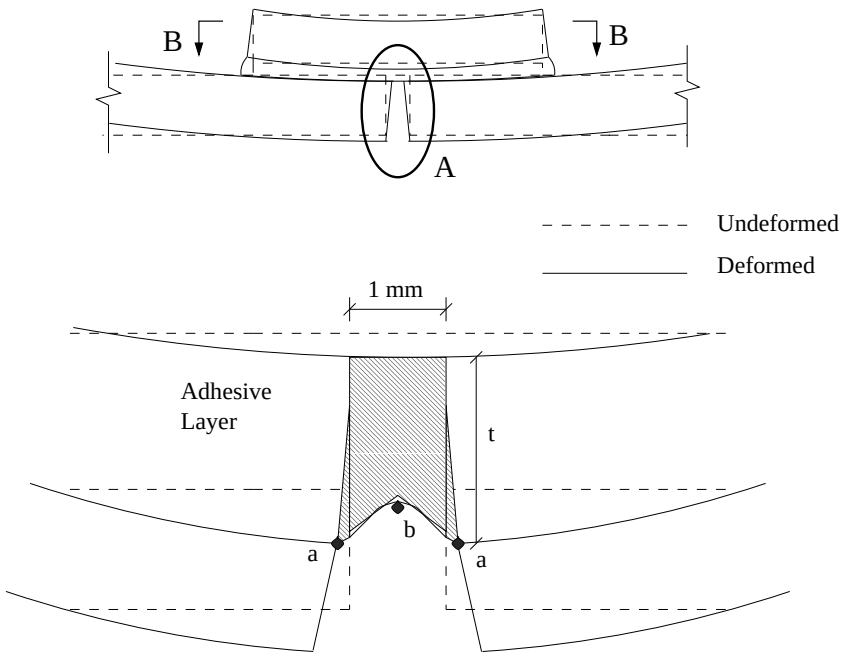

Enlarged detail - A: Deformation in 1mm butt-gap region

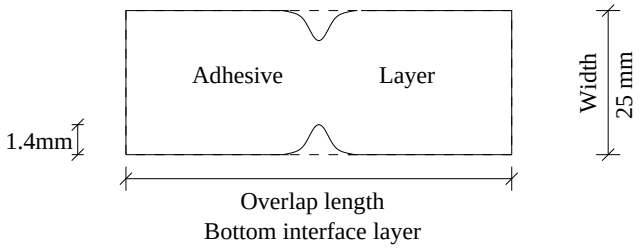

Section B-B: Lateral Contraction in adhesive layer

Figure 6.8: Detail of the deformed shape in the butt-strap joint and lateral contraction in adhesive layer (drawing not to scale)

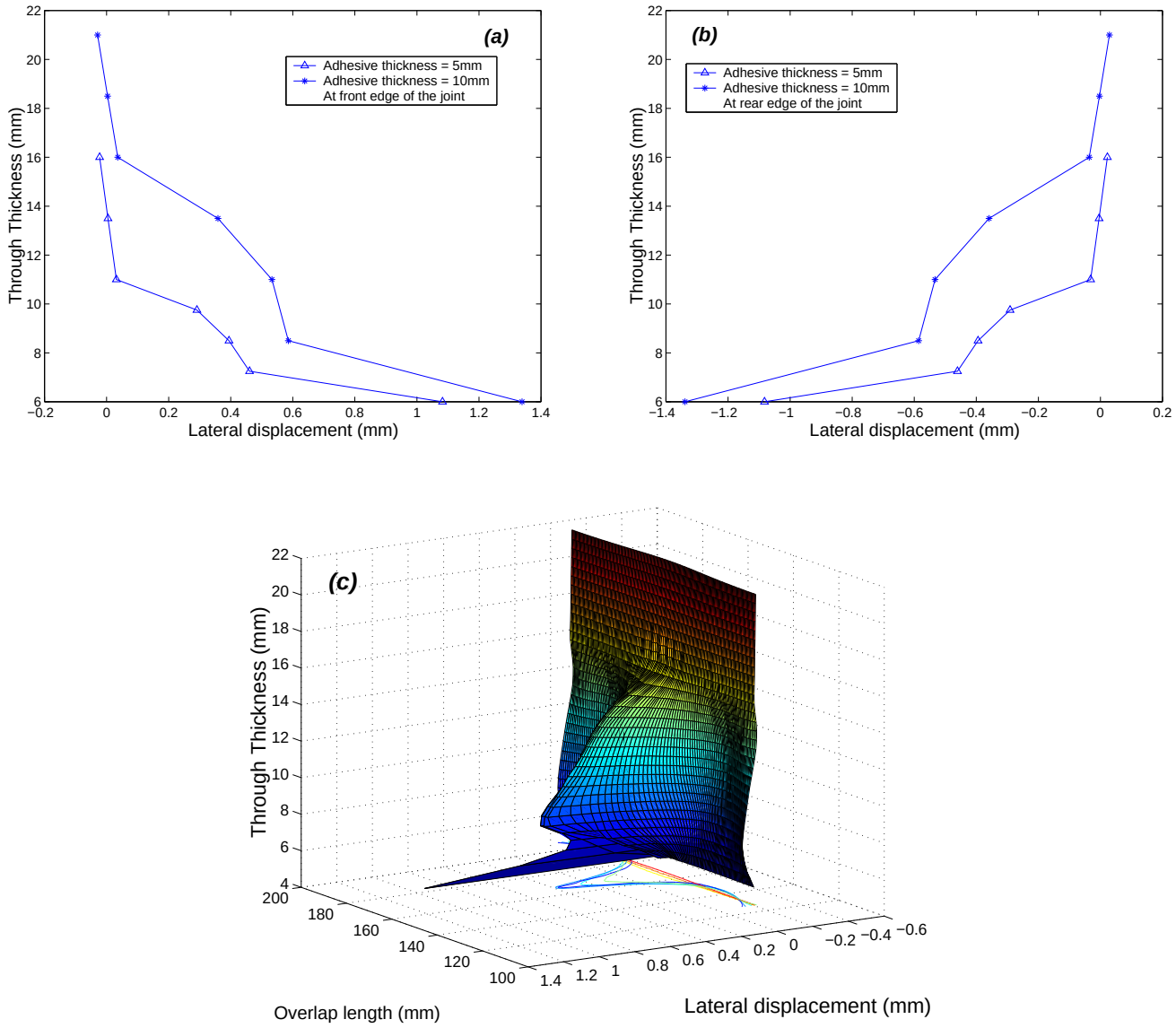

Figure 6.9: Lateral displacement (U_{yy}) variation through the thickness of the butt-joint for the adhesive thicknesses 5 & 10mm: (a) At front edge ($y = 0.0mm$), (b) At rear edge ($y = 25.0mm$) and (c) Three dimensional contour of U_{yy} through the thickness of adhesive layer along the front edge of the joint ($t = 10mm$) (Applied load = 10kN)

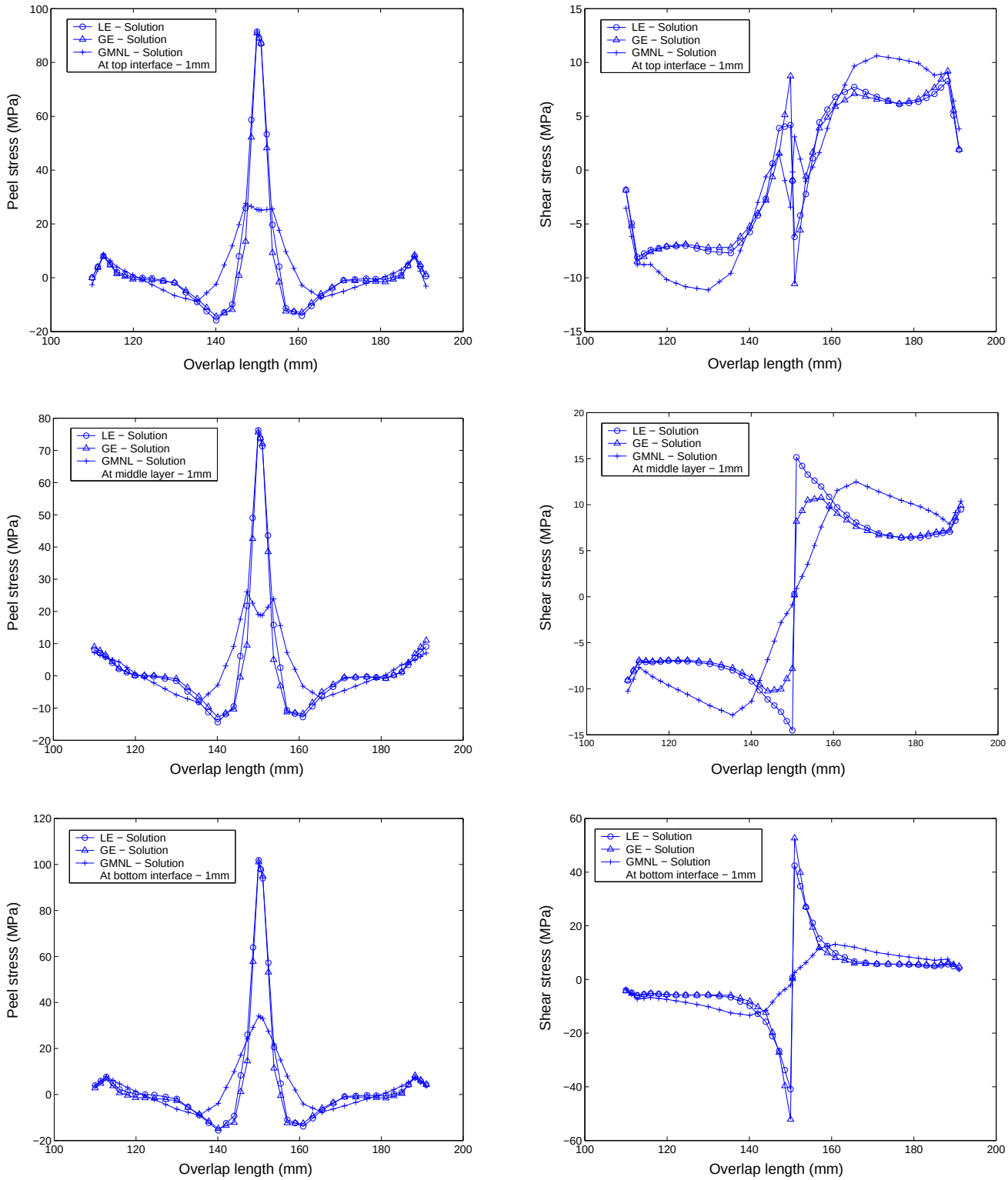

Figure 6.10: Peel and Shear stress distributions at top, middle and bottom adhesive layer for butt-strap joint with adhesive thicknesses 1mm for different set of analyses (Applied load = 10kN)

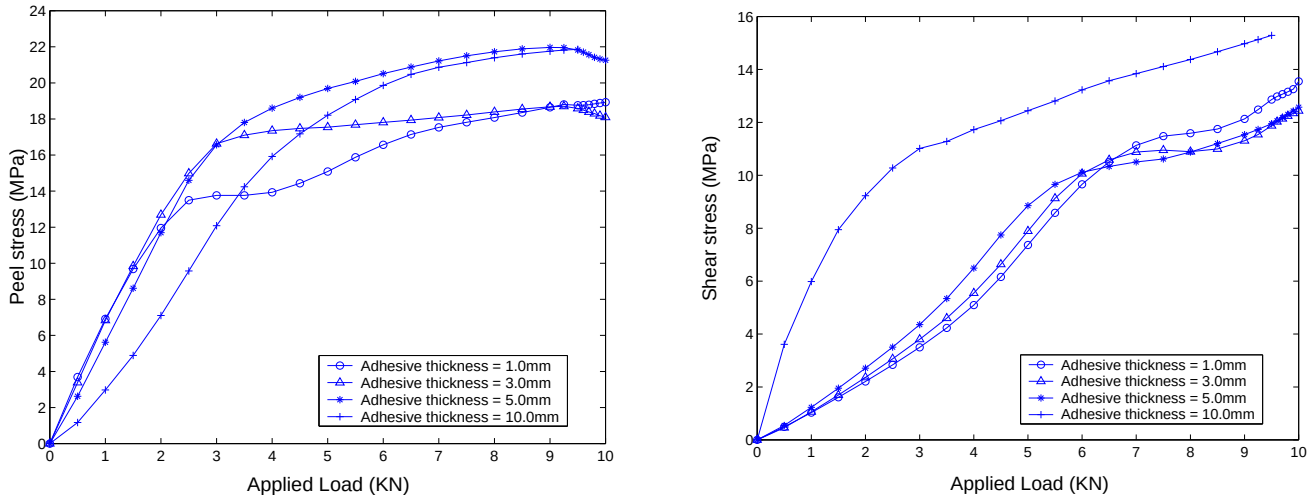

Figure 6.11: Maximum peel and shear stress Vs Applied load for butt-strap joint with different adhesive thicknesses 1,3,5 and 10mm for the geometrical-material nonlinear (GMNL) analysis

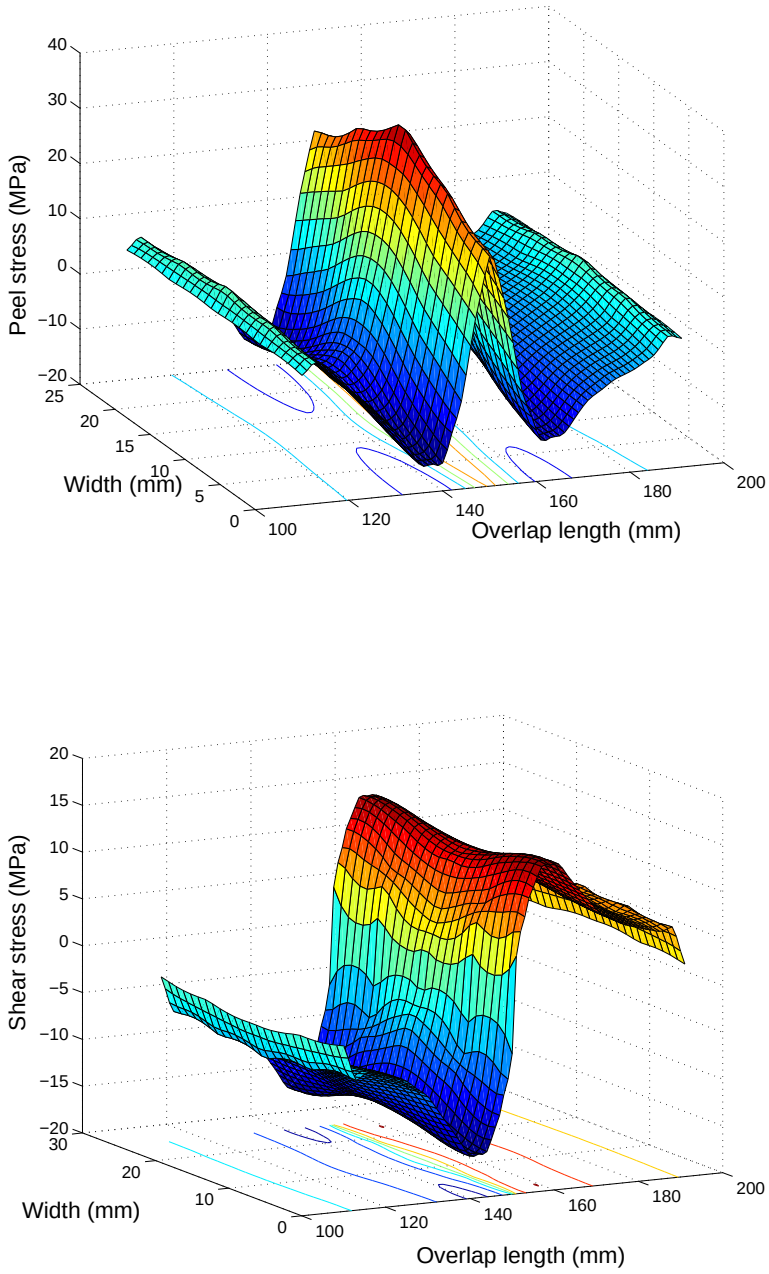

Figure 6.12: Three dimensional peel and shear stress distribution in the bottom interface adhesive layer for butt-strap joint with adhesive thickness of 1mm (Applied load = 10kN)

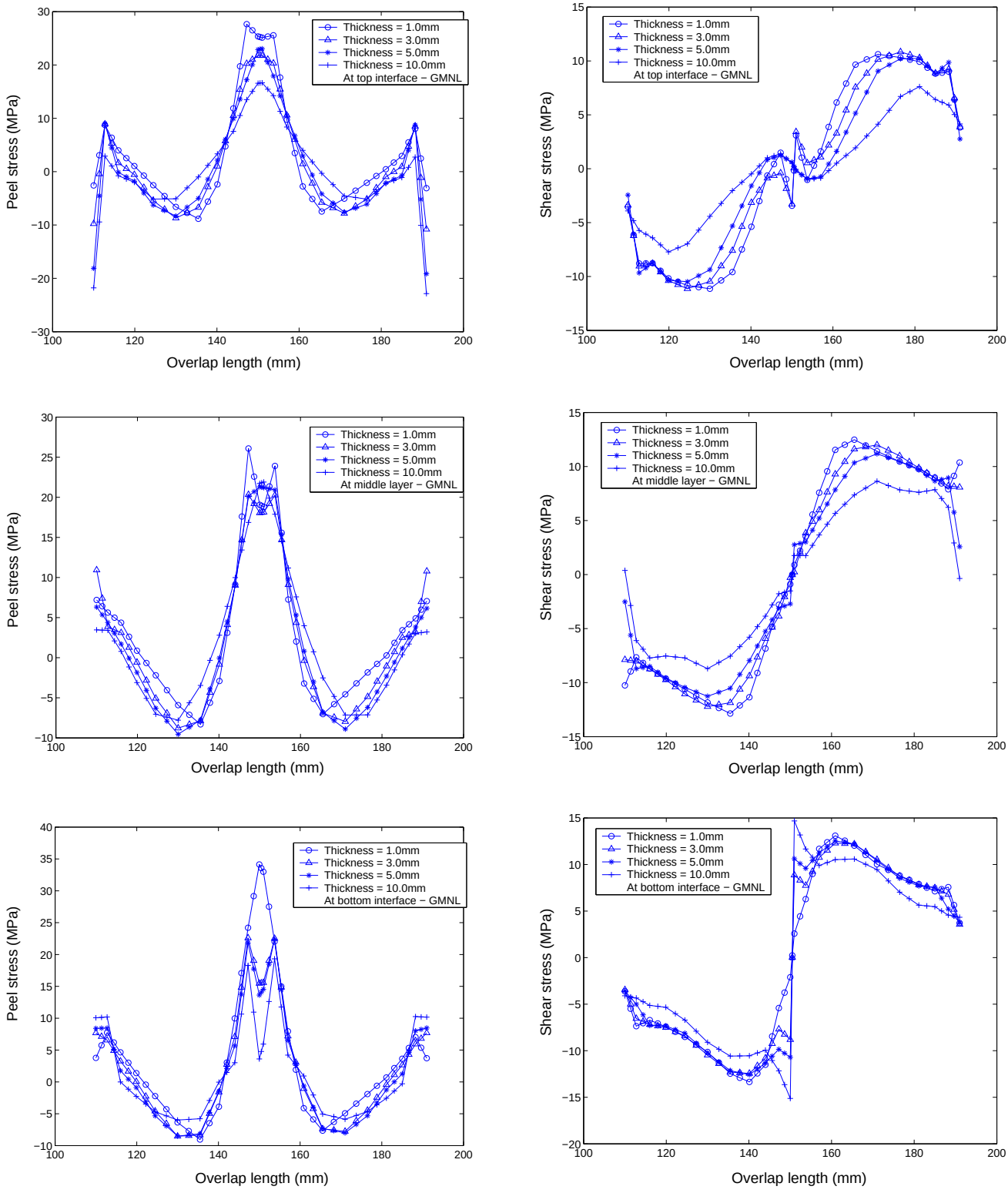

Figure 6.13: Peel and Shear stress distributions at top, middle and bottom adhesive layer for butt-strap joint with adhesive thicknesses 1,3,5 and 10mm for the geometrical-material nonlinear (GMNL) analysis (Applied load = 10kN)

Sample-A: Front edge

Sample-A: Rear edge

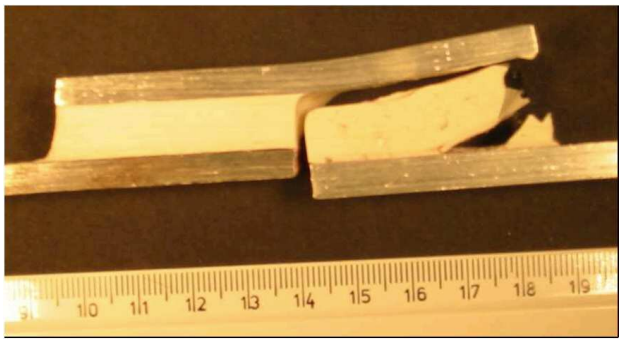

Sample-B: Front edge

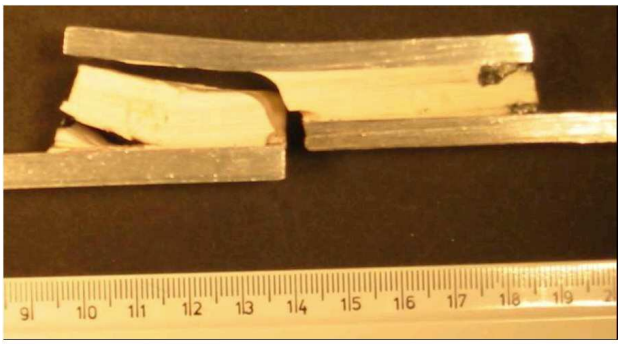

Sample-B: Rear edge

Figure 6.14: Failure modes seen in butt-strap joint with adhesive thickness 10mm [28]

Chapter 7

Stress analysis of GRP-Steel hybrid joints

7.1 Introduction

In this chapter, three dimensional modelling of hybrid GRP-Steel composite joint is attempted. Motivation and objectives are described in section 3.2.2. A set of linear FE analyses are performed for the hybrid joint for three load cases; in-plane compression loading, 4-point bending and for the flexural loading. Main attention is paid to stress concentration locations in the hybrid joint and identification of failure modes in the hybrid joint.

7.2 Problem Definition

The hybrid joint considered here is based on a possible connection between a GRP superstructure and steel hull and deck structure in a ship as shown in figure 1.6 (Boyd et.al., 2004). The joint is manufactured from a 3x1 twill weave $780g/m^2$ E-glass woven roving (Chomarat 800S4), vinylester resin (Dow Derakane 411-C50), $150kg/m^3$ Balsa wood core (Baltek AL600-10 Contourcore) and 6mm thick mild steel (D55). The properties of these materials are displayed in table 7.1. The joint specimen was prepared by vacuum resin

infusion moulding process where eight plies of glass reinforcement were laid over the top and bottom side of steel and balsa wood. This joint is asymmetric in geometry with the balsa core tapering on one side and flat on other side, as the requirement for a flush outer surface in superstructure to deck connections. Hybrid joints of this configuration form a component in mounting a helicopter hangar made of lightweight GRP superstructure, to a steel deck, as shown in figure 1.6. Considering that the length of the hangar will be smaller than the overall length of the hull, it can be assumed that the hangar structure would not be significant to the global bending strength of the hull girder. Hence the hybrid joint would be subjected only to the hangar's own weight, apart from accelerations due to motion. The joint would experience only a compressive force in relation to the weight of the hangar and any additional equipment mounted on it. Out-of-plane bending and rotation of the joint due to the joint under flexure could be the additional loading cases, should any external force be applied normal to the superstructure. Hence the hybrid joint model is analysed for these three types of loading scenario that are encountered in the full-scale structure. Dimensions and boundary conditions for different analyses are shown in figure 1.7. An FE model of the hybrid joint is generated using a 20-noded three dimensional isoparameteric element similar to the hybrid joint specimen. The FE model contains 548 elements with 3x3x3 Gaussian integration scheme and 3347 nodes thus having 10041 number of degrees of freedom (figure 7.1). FE analysis of this model may show high stress gradients across the areas where the mesh density is not adequate. Attaining adequate FE mesh for such complicated geometry and shape will result in consumption of large computational time. One has to balance both the mesh density of the model and computational efficiency as addressed in section 5.4.1. FE model produced here is a preliminary model for analysing such complex geometries and hybrid joints in 3-D domain.

7.3 Results and Discussions

7.3.1 Analysis of hybrid joint under in-plane compressive loading

A linear FE analysis is conducted similar to that of a static compression test performed by Boyd et.al. (2004) in a three dimensional domain. It is important that the numerical model adequately represent the hybrid joint specimen as seen in the full-scale structure accounting for the lateral dimension, width. Due to the asymmetric geometry of the joint (figure 1.7) any in-plane compressive load would produce a lateral deflection due to load eccentricity. In a real environment, the joint would be prevented from such lateral deflection and a similar boundary condition has to be imposed in the FE model. Therefore, a system of anti-bending guides were positioned at the flat side of the hybrid joint (figrue 1.7). The ultimate compressive strength of the joint under static compressive testing is found to be 108kN (Boyd et.al. 2004) and a relatively higher magnitude 120kN is applied uniformly at the steel end of the hybrid joint FE model. This load was applied in 12 increments of 10kN each. Numerical result of load Vs deflection curve (figure 7.2) shows a good correlation between experimental and numerical stiffness within the linear region, thus validating the FE program. It is envisaged therefore that the stress results from three dimensional linear model are reliable and may provide a better understanding of the failure mechanisms of the hybrid joint.

Considering the asymmetrical geometry and the presence of three different materials in the hybrid joint, there are prominent interface layers where the stress distributions could be observed. Accordingly, stress values are plotted along the horizontal and vertical planes through the hybrid joint, as shown in the figure 7.3 and the relevant notations are used in the discussion. Normal stress variations along different planes in the joint are plotted in figure 7.4. Normal stress is concentrated more along the vertical plane V43-V43 (at X=180.3mm) than along the planes on the flatter side. This location is *'critical'* where all the three materials *viz.* steel, balsa core and GRP are bonded and is likely

to play significant role in initiating the failure of the joint. Earlier numerical analyses have highlighted this *'crictical zone'* (Wright et. al., 2000 & Boyd et.al., 2004) as that where maximum normal and shear stress occurs. However, three dimensional plots a,c, &e in figure 7.4, show also that the stress value across the width is not uniform. Such variation of normal stress in the lateral direction have not been observed earlier in hybrid joints. The normal stress values along the mid-line of the width is maximum along the planes C-C/E-E and recedes steeply towards the free edges on either side. This reduction of normal (peel) stress at the edges, termed as *'anticlastic'* effect (see 'three dimensional effects' in section 5.4.4), indicates a possible three dimensional behaviour that is seen in typical single lap joint. Considering that geometry of the hybrid joint can be regarded in two parts, one with the balsa core in taper region and the other as a lap joint of steel bonded to GRP at top and bottom, it is expected that peel and shear stress would peak at the lap ends and be constant along the adhesive overlap. Accordingly, the stresses remain neutral and constant along the steel-GRP bondline, as seen in plots in figure 7.4. A similar pattern is observed by Wright et.al., (2000) for this particular type of hybrid joint. Shear stress plots in figure 7.5 suggest that they are higher than normal stress values and the variation is constant across the width, unlike the normal stress plots. It is interesting to note that the maximum shear stress is along the *'critical zone'* at X=180.3mm and in opposite directions along the planes E-E and F-F. This is due to the twisting caused due to load eccentricity; the shear stress is quite sensitive to twisting at the adhesive-steel interface.

Stress values plotted through the thickness at V43-V43 (figure 7.6) provide a useful insight to the debonding that occurs at the steel-adhesive interface. Normal stress is more concentrated towards the mid-line of the joint (plot a) while shear stress in plot(c) is constant across the width. Plot b shows a significant stress gradient along the steel-adhesive interface, from thickness 4.3 to 9.7mm. While the stress is constant at the top portion, a stress concentration develops as one moves further down towards to flat side. This suggests that failure initiation is bound to occur at this location of adhesive-steel interface

on the flat side instead at the adhesive-core interface layer. Besides, shear stress varies between ±70MPa between the top and bottom steel-GRP interface (plot c) and variation of this magnitude could propagate the crack further between steel and the GRP. So it is reasonable to expect that the hybrid joint of this asymmetric shape fails at the 'critical zone' and the damage propagates further along the steel-GRP interface. The damage pattern seen in the failed specimen of the hybrid joint in the static compression test exhibits similar failure mechanism(figure 7.7). This phenomenon adequately substantiates that the stress concentration locations identified from the three dimensional hybrid joint model are realistic.

7.3.2 Analysis of hybrid joint under 4-point bending

Three dimensional analysis of the hybrid joint subjected to 4-point bending is done to assess the lateral bending strength. Boundary conditions for this analysis are taken to represent the experimental set-up adopted by Boyd et.al.,(2004) (figure 7.12). The fully encastered end conditions for steel and the composite represent the actual conditions in the full-scale structure. The composite sandwich end is likely to be attached to a longitudinal stiffener while the steel end would be welded to the weather deck. Accordingly, boundary conditions at the ends and the points of hinge and loads are replicated in the joint model (figure 1.7). While the nodes at $X = 60.0mm$ & $X = 305.5mm$ on the taper side are restrained to represent the hinge, vertical loads are applied along the nodes at $X = 116.3mm$ & $X = 244.4mm$ on the flat side. A conservative load magnitude of 15kN is chosen since Boyd et.al. (2004) have reported that the initial failure load of various hybrid joint specimen under 4-point bending test is in the range of 11-13kN. As in the previous loading case, here also the objective of the three dimensional analysis is to identify the locations of high stress concentrations in the joint and thereby to predict the failure pattern. Normal stress (σ_{zz}) variation along the interface E-E and through the thickness at the section V43-V43 are plotted in figure 7.8. The stress magnitudes are significantly small in the range of -8 to 8MPa. The FEA results show that the largest stresses are in the axial direction. These cannot be responsible for the debonding failure mode shown

in the experimental work. However, the through thickness tensile stresses predicted by the FEA and shown in figure 7.8 are too small to be responsible for this debonding, but at the same time it should be noted that the FE meshing is too coarse at the interfaces to predict the local stresses accurately. Furhtermore, there are large discontinuities in the axial stress at the interfaces shown in figure 7.11 where the stiffer material carries the stress. A strain compatibility issue exists in reality as the adhesive cannot deform as much as the adherends and failure occurs; as the model is linear elastic the relative ductility of the steel, FRP and adhesive is not considered.

Figure 7.9 shows that the maximum value of bending stress is in the range of 100-140MPa in compressive and tensile directions (plots a & b) at the GRP/Steel interface on both sides. Stress plots show that the hybrid joint is subjected to alternate compressive and tensile bending between the two hinges (at V2-V2/V7-V7) because of the load points at V3-V3/V6-V6. Under the 4-point bending conditions, axial stress is almost non-existent from the encastred sandwich end to the steel/core interface at V41-V41 (figure 7.10). This indicates that there is no debonding along the core-adhesive interface in the taper region and the failure seems to initiate from the *'critical zone'*, as remarked in earlier analysis. Stresses increase rapidly at this junction up to 100MPa on the taper side (F-F) and up to -140 MPa on the flat side (E-E). Further there is a reversal of bending stress from this peak and higher stress concentration is seen close to the hinge location at V7-V7, albeit in the opposite direction. Axial stress profile seen through the thickness of the joint in plots 7.11a,b further reveals that failure is more likely to occur on adhesive-steel interface (V43-v43) than at the core-adhesive interface (V41-V41) layer, where the stress in mid-portion is neutral. Moving along the overlap, the GRP material is subjected to heavy bending given its proximity to the hinge and load points. This bending stress increases further at steel-adhesive-GRP interface on both sides to $\pm$100MPa at sections V6-V6 and V7-V7 (plots c & d). Due to the fact that the joint is fully constrained at both ends, the steel near the end clamp would yield to a higher level of bending stress. Higher stress concentration at the steel-adhesive-GRP interface layer causes the GRP portion on the

flat side to debond from the steel surface. This observation is confirmed by the failed hybrid joint specimen under 4-point bending as seen in figure 7.12.

Additionally, figure 7.10a shows the extent of bending stress variation along the tapered plane J-J from -60MPa at V2-V2 to 20MPa to V41-V41. There is a sudden drop in between as well. A similar variation is seen in stress values along the adhesive-core interface plane H-H on the taper side. Both these stress trends validate the complete debonding seen in the failed specimen as marked at the beginning of the taper between the core and GRP. Then the crack propagates inside the core material further. Overall, it can be concluded that the failure under the out-of-plane loading seems to initiate at two places separately, one at the *'critical zone'* and other at the beginning of the taper side between the core and GRP. GRP material detaches from the steel surface on the flat side because of increasing bending stress from the *'critical zone'* and also of the stress yielding at steel-adhesive interface towards to the far end.

7.3.3 Analysis of hybrid joint under flexural load

A hybrid joint structure is subjected to a flexural load on balsa-GRP end while clamping tightly on the steel end similar to a cantilever structure. The failure load for a similar hybrid joint under flexural testing is found to be in the range of 1.2-1.5kN, as observed by Clifford et.al., (2002). Hence an equal load of 1.5kN but in opposite direction is applied over 15 increments on top and bottom GRP skin on the balsa end as shown in figure 1.7.

Given that flexural load is being applied in the opposite direction, causing a clockwise rotation, the dominant stress component will be the axial bending stress σ_{xx}. The following observations are made from the stress plots.

- GRP material at the top and bottom experiences tensile and compressive bending respectively and the stresses are at maximum value of ±35MPa at Core/Steel junction (figure 7.13a,b). Further on, the stress remains constant at ±15MPa through out and remains neutral at the end along the top and bottom side.

- Axial stress values seem to increase further inside the joint and the adhesive stresses along the planes D-D/G-G and E-E/F-F (plots c-f). Stress profiles indicate heavy stress concentration of ±60MPa inside the adhesive and ±120MPa along the adhesive/steel interface layers. The tensile stress on the bottom side in particular can result in adhesive peeling between the GRP material and the steel.

- Nevertheless, initiation of failure could be occurring in the *'critical zone'* where all the materials GRP, steel and the sandwich core are bonded. Variation of axial stress through the thickness at different vertical planes are plotted in figure 7.14. This provides useful information on failure of the joint under flexural loading. Stress plots a & b at planes V2-V2 and V3-V3 suggest that the sandwich core material is quite intact under bending. This is because its Young's modulus is the strongest in the through-thickness direction.

- Stress plots c & d along the planes V41-V41 and V43-V43 in the *'critical zone'* reveal that debonding of steel from the adhesive is bound to occur because of the bending stress variation. While bending stress is neutral on the Core-Adhesive side, the Adhesive-Steel interface shows variation at ±10MPa and increases rapidly to ±35MPa in the vicinity of the plane V5-V5, later, it reaches towards the end at V8-V8 to the maximum value of ±100MP (plots e & f). It is to be noted that, even though the steel is capable of withstanding these stress magnitudes, it is likely that the adhesive will peel off because of heavy stresses on either side of the steel. This could result in detachment of the steel from the adhesive along the plane V43-V43 and further peeling off along the steel-adhesive overlap on the flat side. The failure mode obtained by Clifford et.al., (2002) reflects similar behaviour.

- From the above analysis of stress plots, it can be concluded that the failure initiates in the *'critical zone'* and likely to propagate towards GRP/Steel interface on the flat side which experiences bending in tensile direction.

7.4 Conclusions

Earlier works cited in the literature review in chapter 2 and in section 3.2.2 concerning the numerical modelling of hybrid joints are restricted to two dimensional analysis. This is the first time that a three dimensional analysis of a hybrid joint is attempted taking into account of the complicated shape & geometry of the joint, bonding of dissimilar materials, eccentricity in the load path and the interfacial stresses. Therefore, a three dimensional FE model of a hybrid composite-steel joint is generated and analysed for different set of loading cases: in-plane compression loading, 4-point loading and the flexural load. Numerical and experimental stiffness were to be found in good correlation up to linear region for the static compression analysis. Linear elastic analysis of the joint under the in-plane loading has shown that the normal stress is not uniform across the width of the joint. Researchers like Wright *et. al.,* (2000) and Boyd *et. al.,* (2004) have reported that normal and shear stresses are concentrated in the interface layer where GRP-Steel-Balsa core are bonded for the case of in-plane compression loading. Additionally, this three dimensional analysis has resulted in further understanding that the normal stress is more concentrated along the middle of the joint and decreases towards the free edge. It can be said that this reduction of stresses towards the free surface is a similar phenomenon of *'anticlastic'* effect normally seen in a single lap joint. It is observed that the critical stress values are invariably concentrated around the *'critical zone'* and remains the main source of failure initiation for all the loading scenario. However, it is to be noted that the normal and shear stress components are dominant for the in-plane compression loading case while the axial bending stress component initiates failure when the joint is subjected to out-of-plane loading. Predicted failure mechanisms deduced from the numerical model reflect the damage seen in the hybrid joint specimen.

This 3-D analysis has resulted in enhanced understanding on the behaviour of the complicated joint structures like hybrid joint. However, it is acknowledged here that the FE model with more refined mesh density would have resulted in locating the critical stresses that cause failure.

Table 7.1: Material properties of adhesive and adherends considered in the hybrid joint

	GRP skin	Balsa core	Steel	Vinylester
E_{xx}	20.6 GPa	56.951 MPa	209.0 GPa	2.75 GPa
E_{yy}	20.6 GPa	56.951 MPa	209.0 GPa	2.75 GPa
E_{zz}	6.77 GPa	2965.0 MPa	209.0 GPa	2.75 GPa
G_{xy}	3.03 GPa	147.0 MPa	80.3 GPa	1.323 Gpa
G_{yz}	3.03 GPa	147.0 MPa	80.3 GPa	1.323 Gpa
G_{zx}	3.03 GPa	147.0 GPa	80.3 GPa	1.323 Gpa
ν_{xy}	0.171	0.01	0.3	0.36
ν_{yz}	0.231	0.01	0.3	0.36
ν_{zx}	0.231	0.01	0.3	0.36

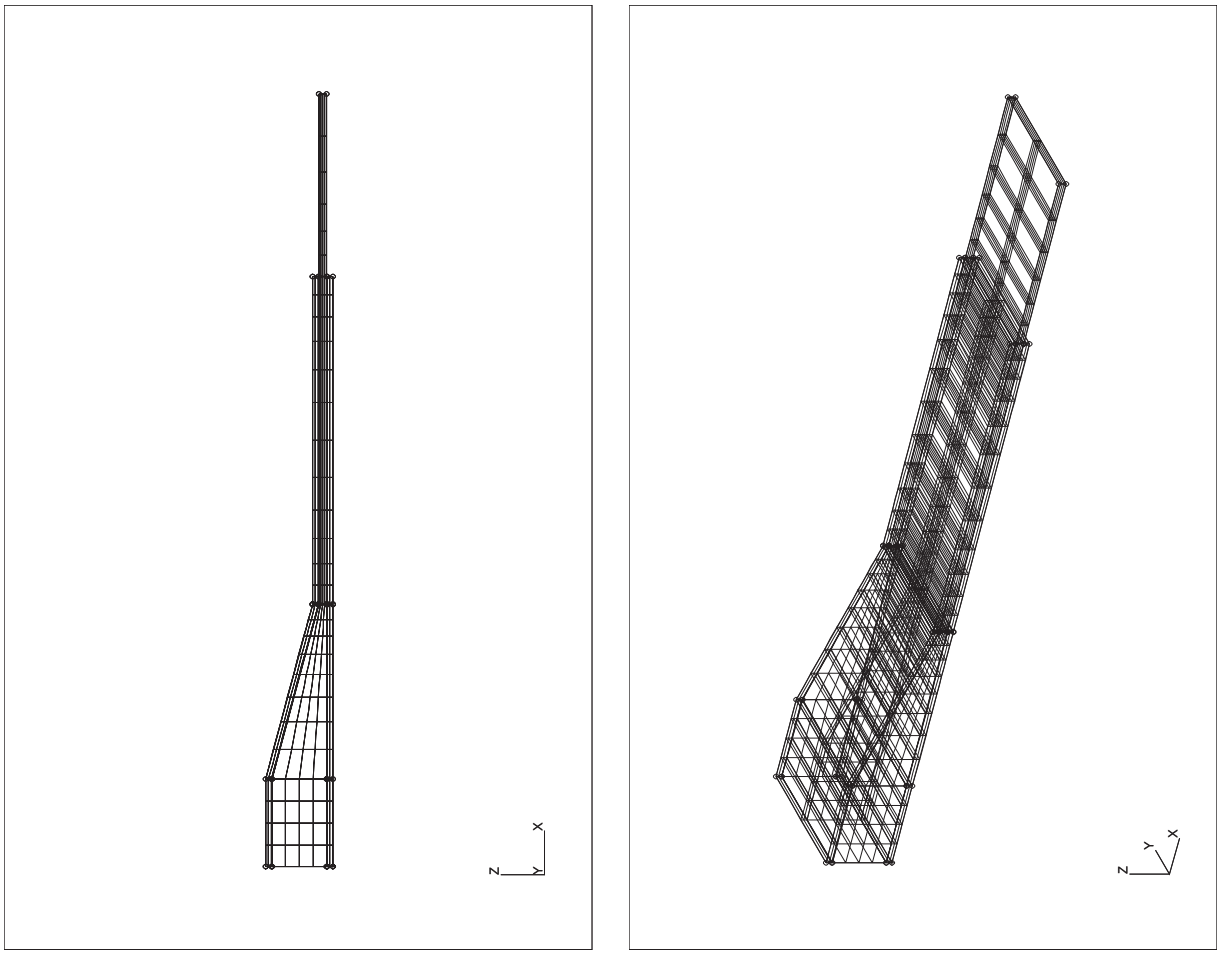

Figure 7.1: Finite element mesh of the hybrid joint structure

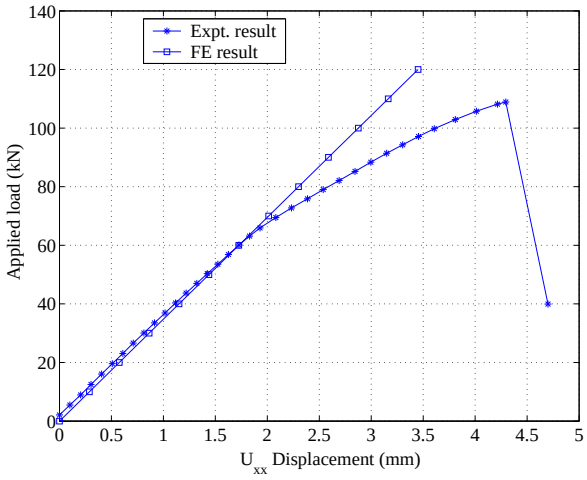

Figure 7.2: Load Vs Deflection curve for the hybrid joint under static compression load

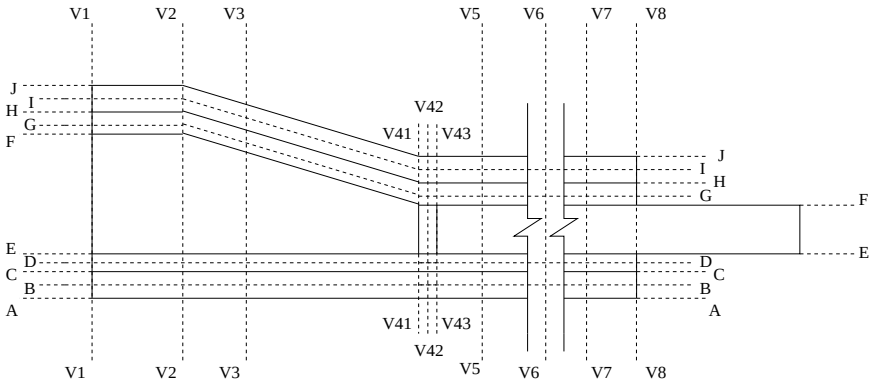

Figure 7.3: Notation for interface layers in hybrid joint where stress values are taken

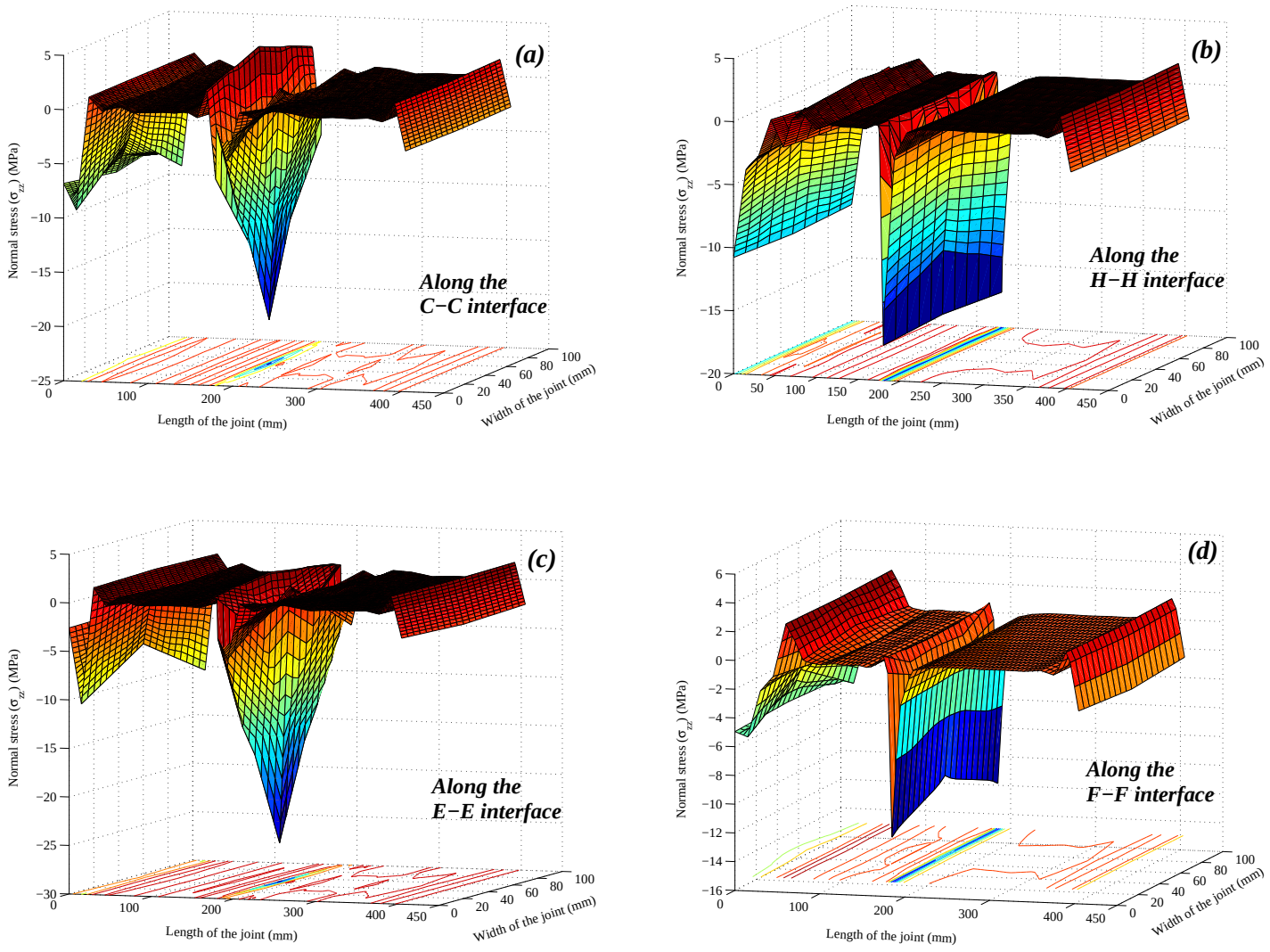

Figure 7.4: Normal stress (σ_{zz}) along the length of the hybrid joint at different planes under in-plane compressive loading (Load = -120kN)

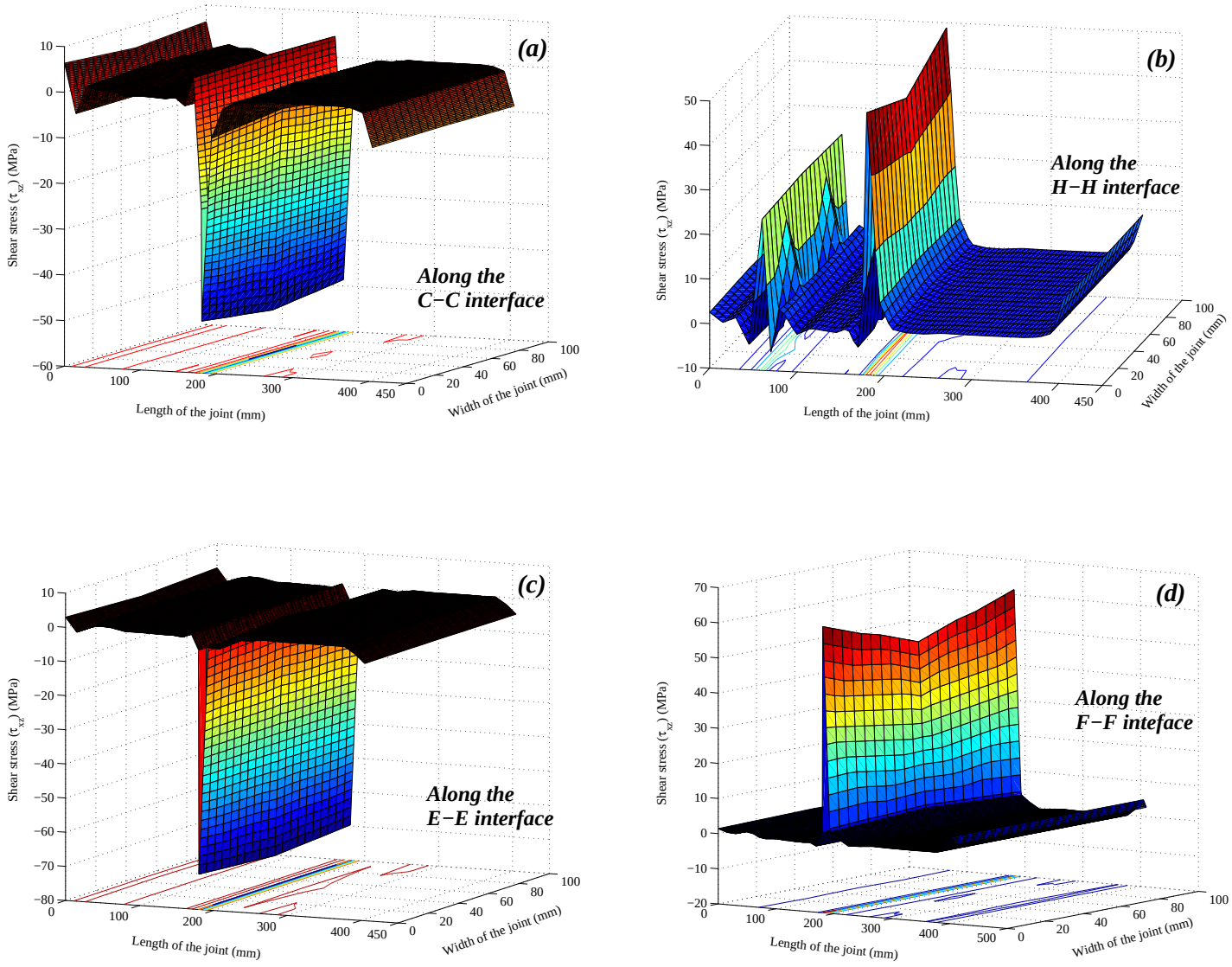

Figure 7.5: Shear stress (τ_{xz}) along the length of the hybrid joint at different planes under in-plane compressive loading (Load = -120kN)

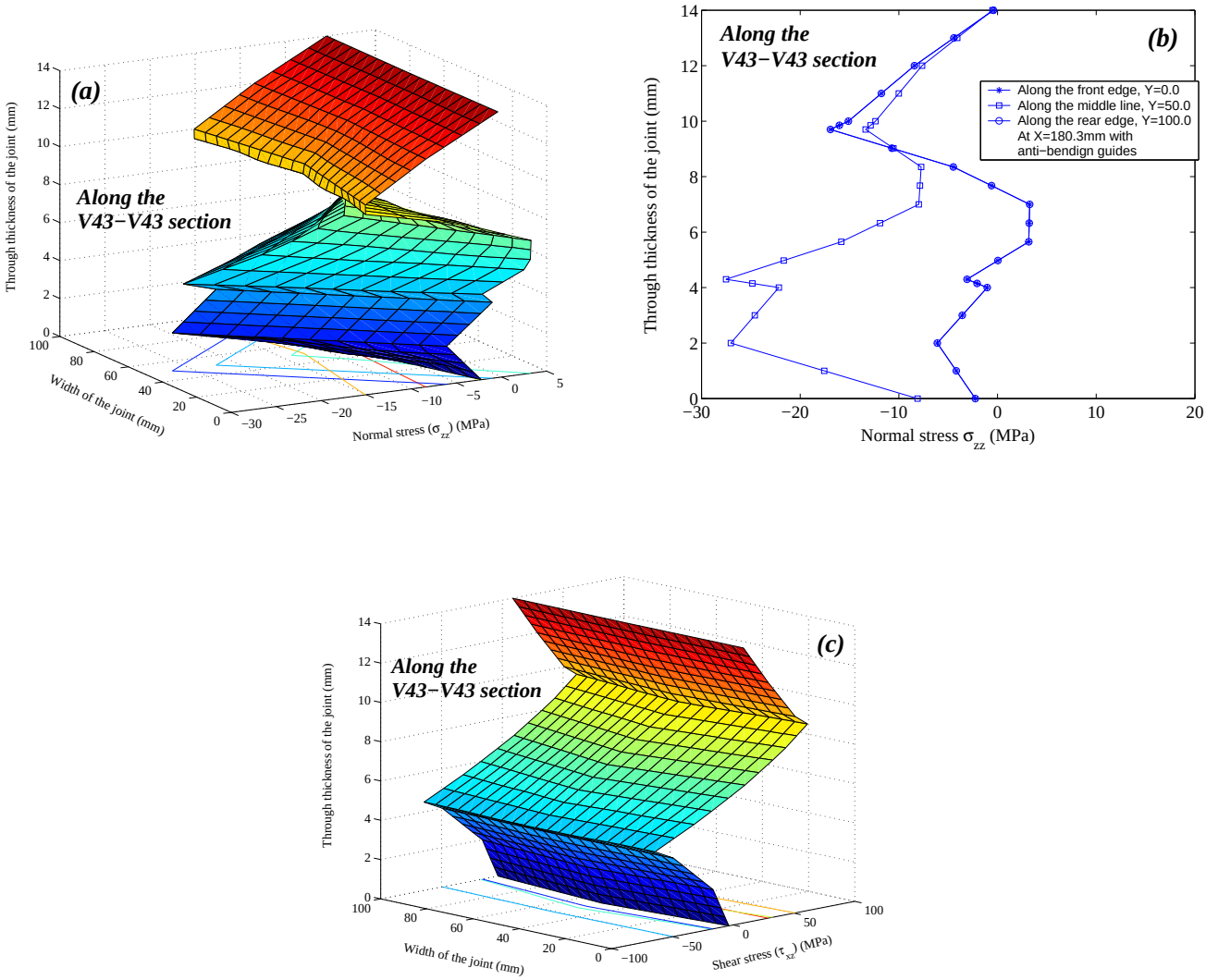

Figure 7.6: Through thickness variation of normal and shear stress along the plane V43-V43 in the hybrid joint (Load = -120kN)

Figure 7.7: Hybrid joint specimen under static compression test (Boyd et.al., 2004)

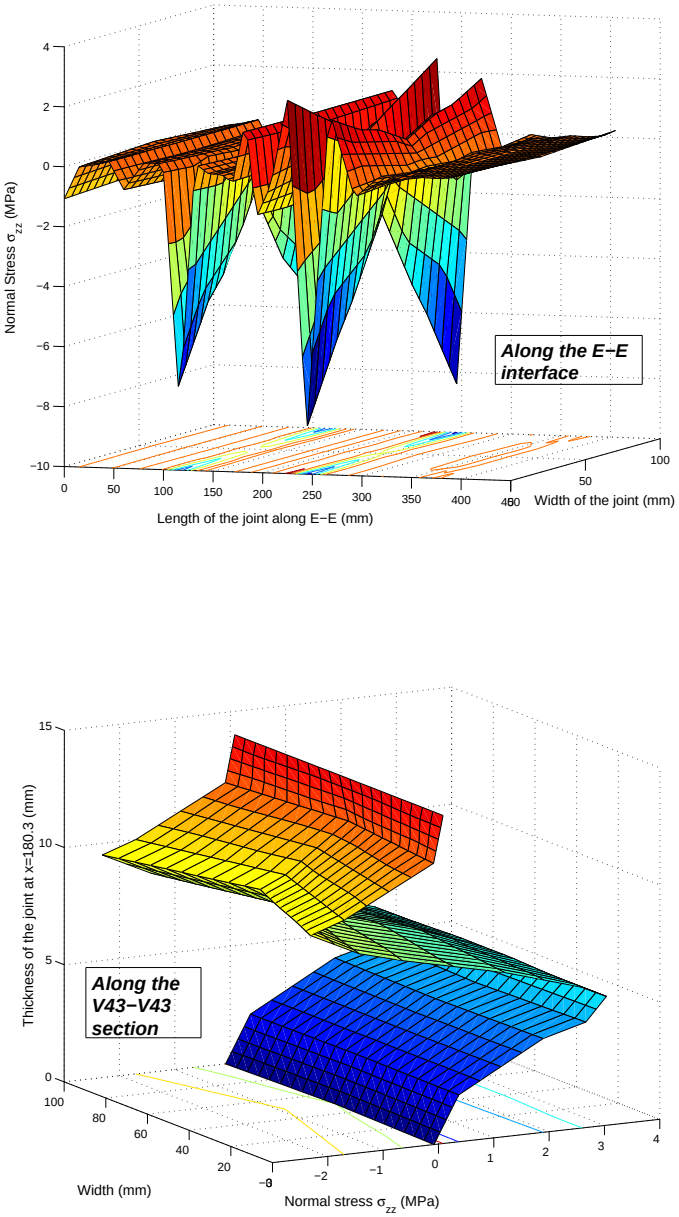

Figure 7.8: Normal stress (σ_{zz}) along the interface plane E-E and through the thickness at the section V43-V43 in the hybrid joint under 4-point bending test (Load = 15kN)

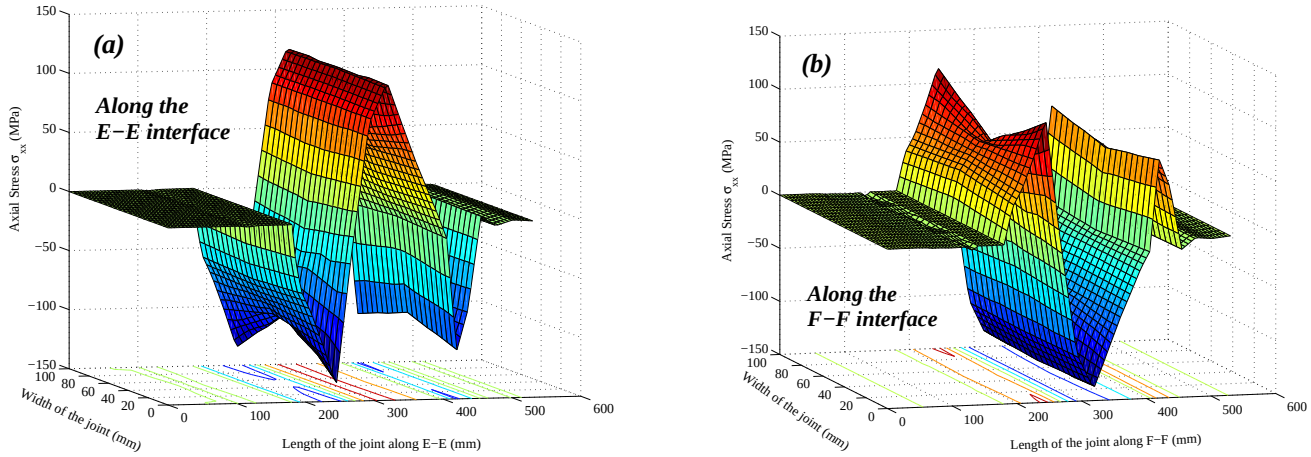

Figure 7.9: Axial stress (σ_{xx}) along the length of the joint at different planes subjected to 4-point bending test (Load = 15 kN)

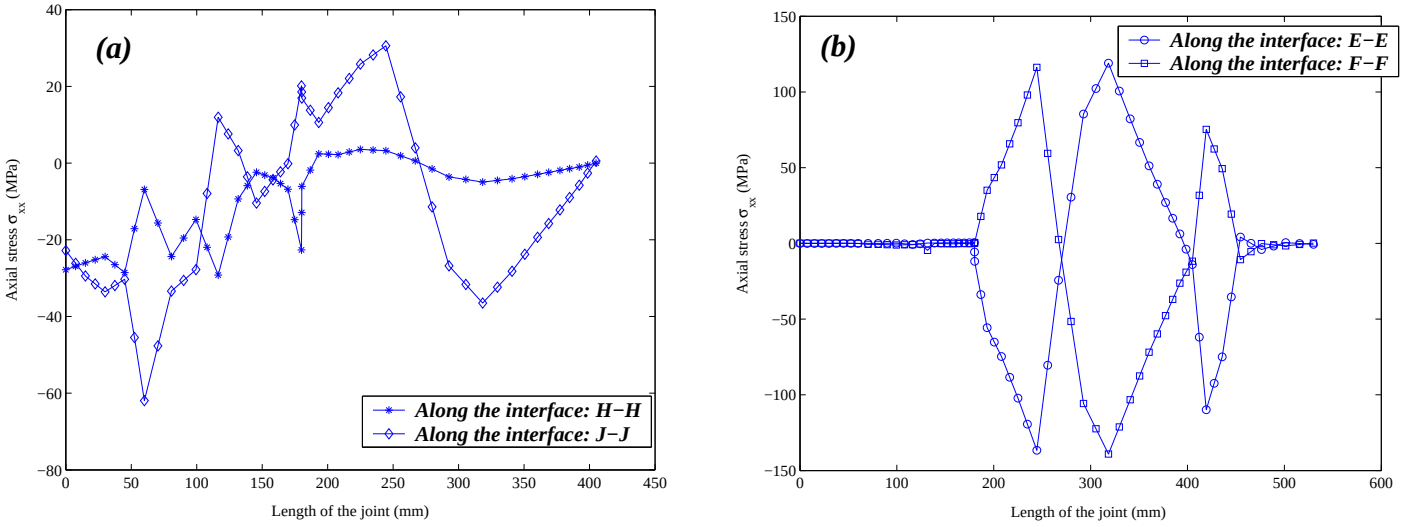

Figure 7.10: Variation of axial stress (σ_{xx}) along the length of the joint at different planes subjected to 4-point bending test (Load = 15 kN)

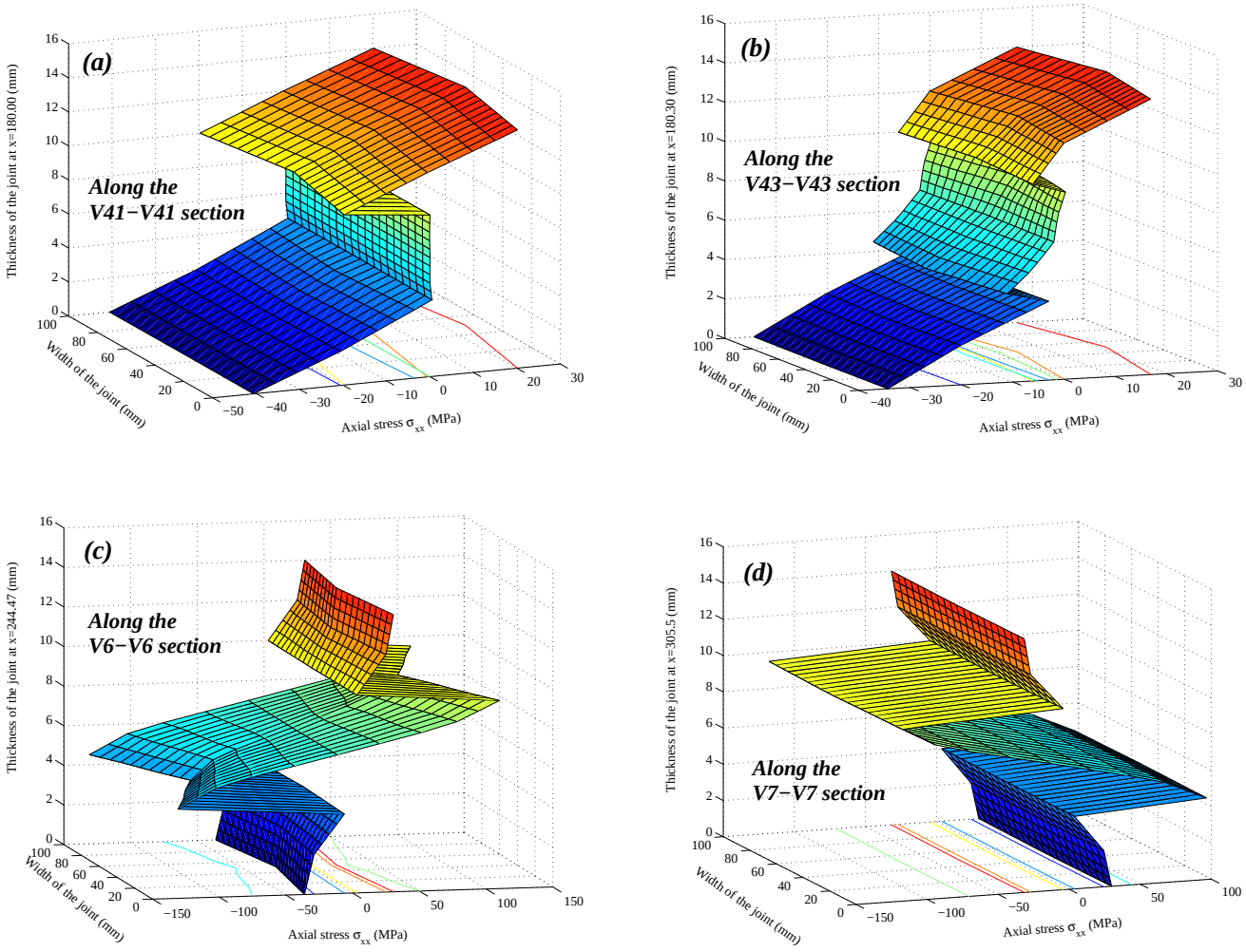

Figure 7.11: Axial stress (σ_{xx}) along the different vertical planes subjected to 4-point bending test (Load = 15 kN)

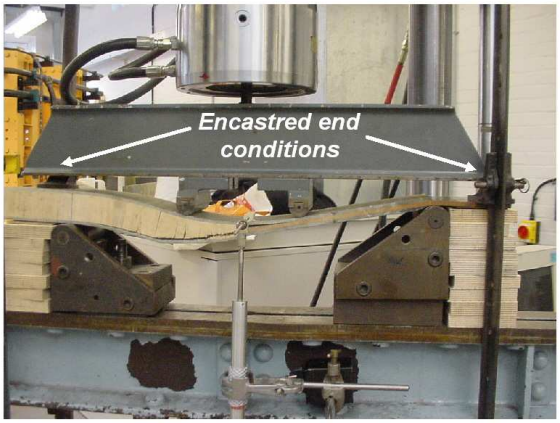

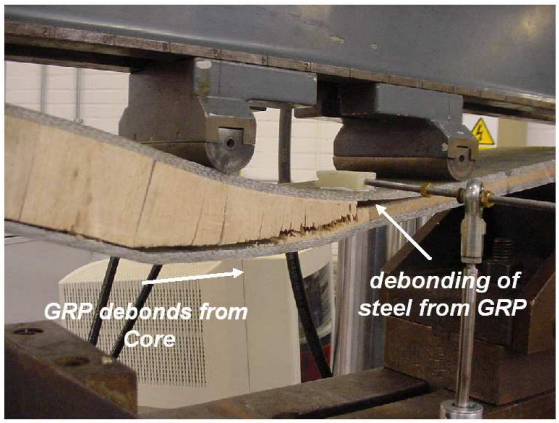

Figure 7.12: Hybrid joint specimen under 4-pt bending test (Boyd et.al., 2004)

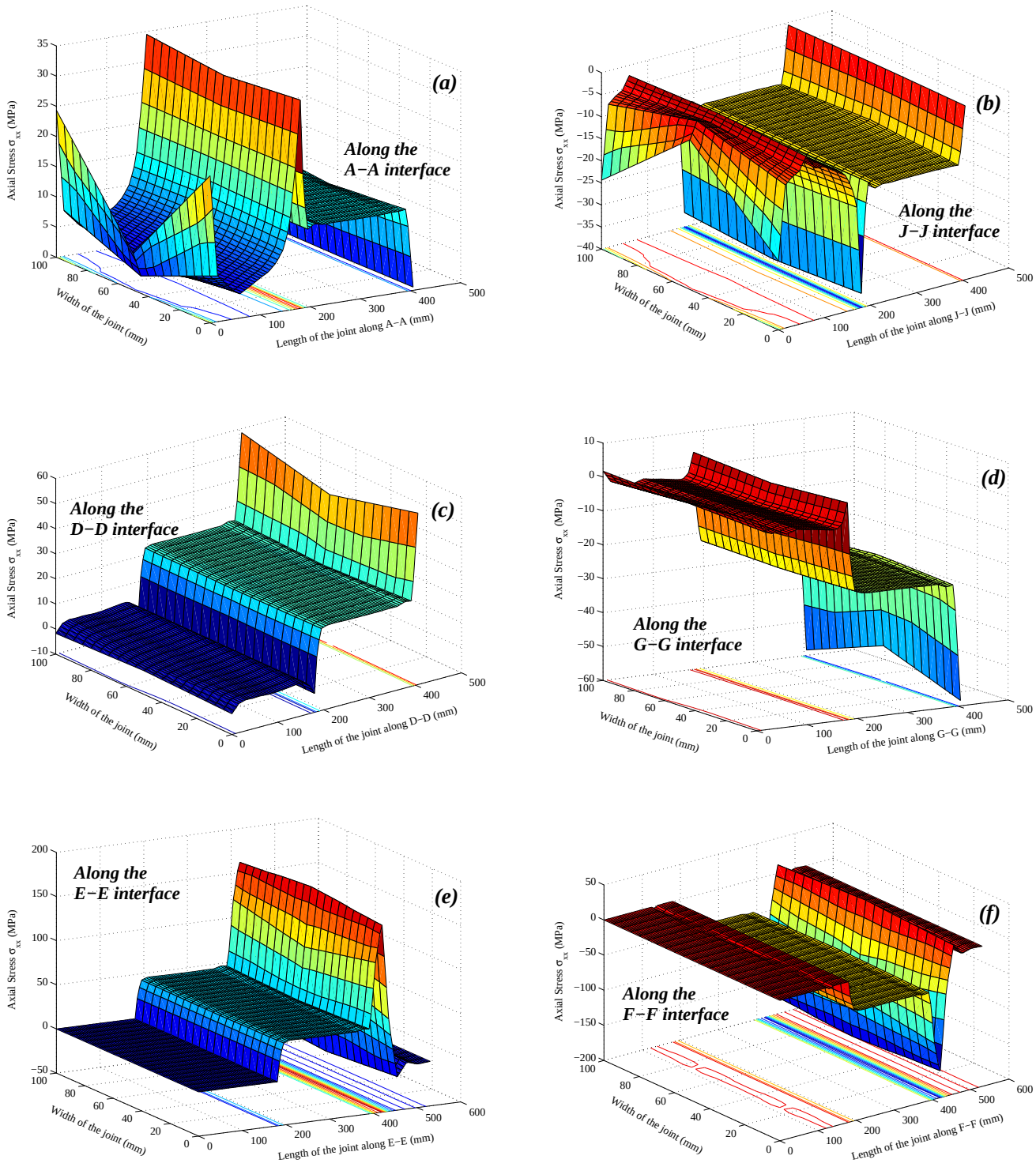

Figure 7.13: Axial stress (σ_{xx}) along the length of the joint at different planes subjected to flexural loading (Load = 1.5 kN)

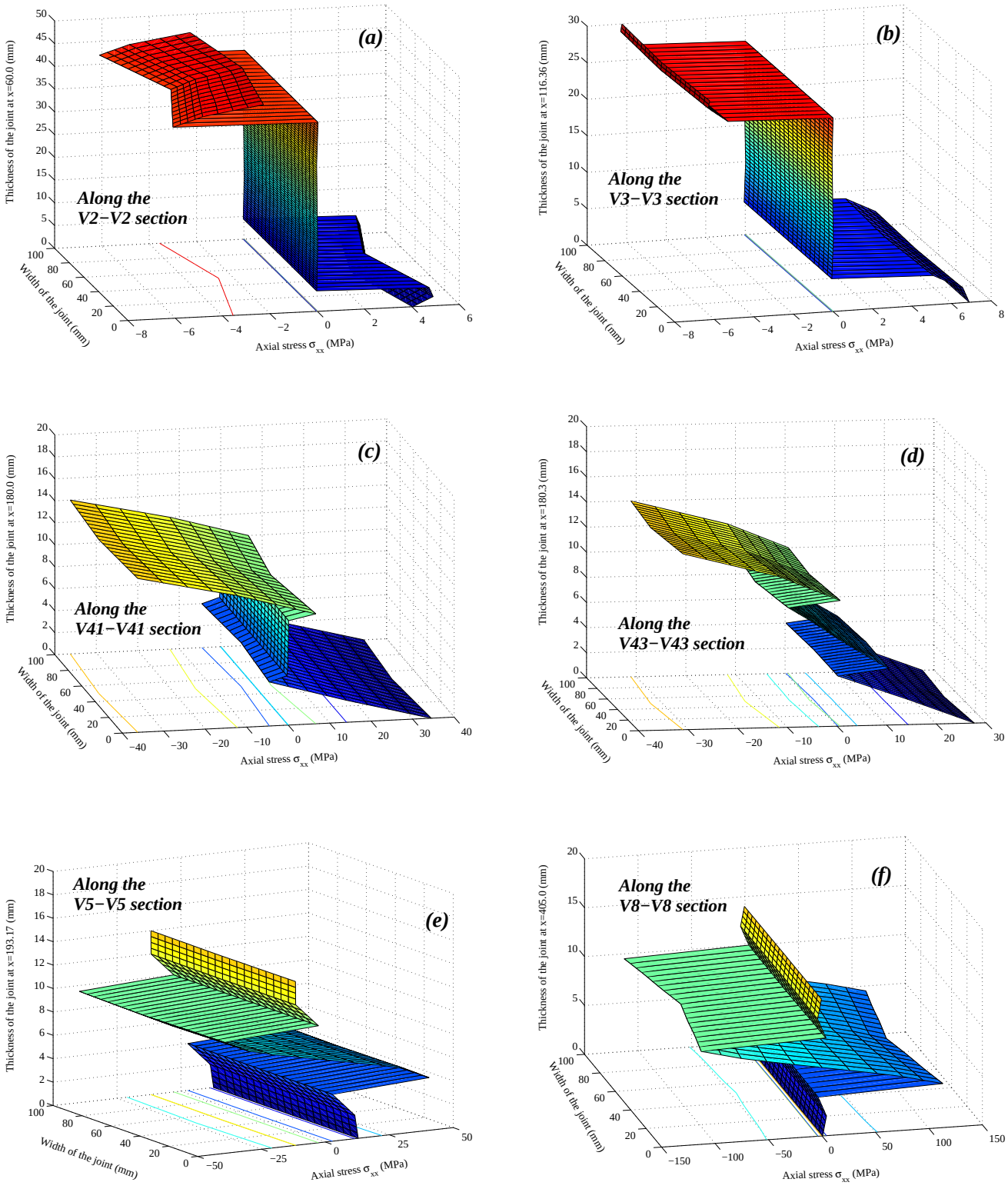

Figure 7.14: Axial stress (σ_{xx}) along the vertical planes subjected to flexural loading (Load = 1.5 kN)

Chapter 8

Discussion

8.1 Present work - An overview

In the present work, three dimensional analyses of adhesively bonded joints that are applicable to marine structures are undertaken. A brief introduction to adhesively bonded joints, their advantages/disadvantages *viz-a-viz* other fastening techniques is presented in the first chapter. In the second chapter, a detailed review of the literature on adhesively bonded joints is described, under different categories such as theoretical, experimental, numerical and adhesive modelling formulations and implementations. Following the critical review, a set of problems is identified as potential areas of research that can result in new knowledge and ideas in the field of the application of bonded joints, in the marine industry. Accordingly in, chapter 3, areas of investigation are outlined with critical discussion in the light of use of bonded joints in marine structural components. The motivation for choosing those particular case studies and the research methodology to analyse them is presented. The next chapter provides information related to numerical formulation of the geometrical and material nonlinear equations for a three dimensional domain. A schematic flowchart diagram showing the implementation of numerical equations as subroutines in *FORTRAN* computer language is given at the end of the chapter. Three dimensional stress analyses for a single lap, butt-strap and a hybrid joint are undertaken, in chapters 5, 6 & 7 respectively.

8.2 Discussion

8.2.1 Development of FE program

A detailed study presented in the literature review and the summary section 2.6 in particular, showed that there are merits in the current research as well as further scope for our understanding concerning the behaviour of adhesively bonded structural joints. It is felt that there is a need for a program in one package that could comprehensively account for all the modelling related issues, so that one could approach the problem in its totality; it is felt that such an approach would provide more realistic outcome. In light of this, it is proposed in chapter 3 to develop a single master FE program code that could comprehensively address the following issues:

- the geometric nonlinear behaviour of asymmetric joints,
- the three dimensional effects seen in joints arising out of the asymmetry and the eccentricity in the load-path,
- the nonlinear modelling of adhesive material: elasto-plastic behaviour of rigid-adhesive type in a bi-linear fashion, modelling of semi-rigid/flexible type of adhesives that change continuously in a nonlinear profile from low level of loads which require formulations like Ramberg-Osgood equation
- consideration of appropriate failure criterion for adhesive materials which are pressure-dependent

Based on the above facts and, importantly because commercial package users still need to write their own code for the implementation of the Ramberg-Osgood equation and for the modified von Mises criterion, it was decided to develop a three dimensional FE program code in *FORTRAN* language that is suitable for a 20-noded isoparametric element. The main features of this FE program are:

1. large displacements and rotations (but small strains) are accounted for by the total Lagrangian formulation of motion for both adhesive and adherend materials,

2. the Euler integration method is used to integrate the elasto-plastic constitutive equations,

3. the Frontal solver has been used to solve the resulting equilibrium equations,

4. displacement based convergence criteria has been used,

5. offers the choice of Gaussian points either as 2x2x2 or 3x3x3 for a 20-noded isoparametric element,

6. a three dimensional stress smoothing technique is employed to obtain the nodal stresses from the Gaussian point stresses, thus providing a good understanding of the results along the element nodes,

7. it is possible to choose either bi-linear hardening by specifying hardening parameter or the Ramberg-Osgood formulation by specifying Ramberg-Osgood parameters, depending on the type of adhesive material considered, and

8. the program can analyse a model that consists of more than two materials (normally an adherend and an adhesive) and thus provides scope for analysing hybrid joints consisting of four materials. The input subroutine has the capability to consider materials with orthotropic properties as well.

8.2.2 Validation of FE program

Numerical results obtained from the FE code are validated with analytical and experimental data for all the three case studies showing the robustness of the developed FE code. There are mainly three formulations in the program code that are to be verified: linear elastic formulation (LE), geometrical nonlinear elastic formulation (GNL) and material nonlinear elasto-plastic formulation (MNL).

Linear formulation: In the first case study on analysis of single lap joints, peel and shear stress profiles for the identical aluminium-aluminium adherends (Al-Al) and for the non-identical aluminium-composite adherends (Al-Cp) compared reasonably well with the

analytical solution formulated by Bigwood and Crocombe (1989) as seen in figures 5.6 & 5.7. There are differences in stress profiles between the numerical and the analytical solutions at the overlap ends, especially for the case of non-identical adherends. This is due to the assumptions made in analytical formulation that normal stresses do not vary through the thickness of either the adhesive or the adherends. This also highlights the advantage of using a three dimensional FE formulation that accounts for normal stress variation through the thickness.

Section 6.4.1 showed for the case of analysis of butt-strap joints, that the resultant peel and shear stress profiles obtained from the FE program agrees well with the analytical formulation of Bigwood and Crocombe (1989). However, it should be mentioned that the analytical formulation gives closer values only for smaller adhesive thickness and deviates from the numerical stress profile as the adhesive thickness is increased (figures 6.4 & 6.5).

Figure 7.2 in section 7.3.1 reveals that the linear FE results correlates well with the experimental load Vs deflection curve up to the linear region for the hybrid joint that is subjected to in-plane compressive loading. This validation is quite significant in the sense that the developed FE code can successfully analyse a complicated model like a hybrid joint that consists of more materials with contrasting properties and which has asymmetric geometry.

Geometric nonlinear formulation: One of the main objectives of this research work is to study the influence of geometrical nonlinearity on joint deformations under a varying load, for single lap joints and butt-strap joints. This is for the well-known reason of bending-twisting encountered while transferring the load through the adhesive layer, because of eccentricity in load path.

The influence of geometric nonlinearity is seen in figure 5.8 which shows axial and vertical displacement profiles along the length of the joint for identical and non-identical

adherends. It is also demonstrated that consideration of geometric nonlinearity results in a significant reduction of axial and vertical displacement from the linear displacement values, as shown in figure 5.9. Similar observation is made by Osnes and Andersen (2003) for single lap joints with dissimilar adherends, metal and composite materials. For the case of lap joint with dissimilar adherends such as aluminium and composite materials, it should be mentioned that the influence of geometrical nonlinearity decreases as the thickness of composite adherend is increased.

Material nonlinear formulation: Numerical implementation of material nonlinearity is related to three important formulations *viz.,* a flow rule to relate plastic strains to plastic stresses, characterisation of the chosen adhesive material and and a yield criterion which defines the elastic limit. Two types of adhesives: Ciba Araldite420 a rigid adhesive and Plexus MA550, classified as semi-rigid adhesive (see table 3.1) are modelled in chapter 5 & 6 respectively. While the stress-strain curve for the former adhesive is obtained by setting hardening parameter (H') as zero, to achieve elasto-perfectly-plastic condition, Ramberg-Osgood parameters are defined for the latter to obtain the stress-strain relation. Both these stress-strain curves are compared with the experimental stress-strain data.

The behaviour of bulk adhesive samples of Ciba Araldite420 under tension was experimentally characterised by Bour and Joannic (2001) and determined Young's modulus (E) as 1733MPa and the initial yield stress (σ_y) value as 32.45MPa. Bour and Joannic also obtained the ratio of compressive and tensile yield stress value as 2.086 (Raghava's equivalent, λ), that is required in the modified von Mises equation. These parameters, E, σ_y, H' and λ, are fed as input to characterise the rigid adhesive material. The obtained stress-strain curve has excellent agreement with the experimental stress-strain curve of Bour and Joannic (2001), as seen in figure 5.1. The elasto-perfectly-plastic condition obtained for the Ciba Araldite420 adhesive clearly validates the material nonlinear feature of the program. Additionally, nonlinear adhesive stresses that reflect this perfectly-plastic

phenomenon (see figure 5.11 and related discussion in section 5.4.4) in single lap joints of identical and non-identical adherends with varying thickness ratios, add credence to the material nonlinearity implemented in the FE prgoram.

In a similar approach as described above, characterisation of Plexus MA550, a semi-rigid adhesive material is attempted while analysing the butt-strap joint system in chapter 6. True stress-strain data for the Plexus MA550 is obtained from bulk adhesive tests conducted by Brede (2001). The Raghava's equivalent (λ) in this case is found to be 2.095 from the bulk adhesive experiments. The experimental stress-strain curve showed nonlinearity from low levels of stress and there was no clear definition of a yield point. As explained in section 6.3.1 it was decided to use the Ramberg-Osgood relation to obtain the stress-strain in the program. Accordingly, three parameters; initial yield stress (σ_y), characteristic stress (σ_{ch}) and r, are set for the Ramberg-Osgood equation and a stress-strain curve is obtained. Figure 6.3 shows that the Ramberg-Osgood curve agrees reasonably well with the experimental curves for the adhesive material Plexus MA550. This characterisation is appropriately reflected in peel stress plots shown in figure 6.11 particularly, for the adhesive layer thickness of 3mm which demonstrates elasto-perfectly-plastic behaviour. From the above observations, it can be said that the Ramberg-Osgood relation implemented in the FE code adequately represent the behviour of semi-rigid adhesive materials.

8.2.3 Adherend imbalances in single lap joints

A proposal for a parametric study on single lap joints with adherend imbalances with the adherends of varying thickness ratios and varying material properties is suggested in section 3.2. The tasks included observing the influence of geometric nonlinearity on joint deformation for joints with identical and non-identical adherends, nonlinear adhesive stresses and identification of three dimensional effects in the joint. Accordingly, a set of anlayses for different cases of single lap joint with varying adherend thickness ratio and

varying material properties, are outlined in section 5.2. Validation for linear and nonlinear formulation is made, as explained in the previous section.

Adhesive peel and shear stress obtained from various formulations; linear elastic (LE), geometric nonlinear (GNL), perfectly plastic (PP) and perfectly plastic condition with geometric nonlinearity (PPG) are compared and discussed in section 5.4.4. Maximum peel stress values are found to occur at the end of the overlap length for all the joint cases. However, in the case of shear stress profile for PP & PPG analyses, maximum values are seen to occur just inside the end of overlap length. This can be attributed to the spread of the plastic zone under the increasing load from either end of the overlap length. Comparison of peel and shear stress values between all the four formulations presented in tables 5.2 & 5.3 show that linear analysis predicts far higher stress values compared to the adhesive yield stress of 32.45MPa. On the other hand, the stress values obtained from PP & PPG analyses reflects the realistic state of stress in adhesive layer, thus justifying the nonlinear formulation accounted for. It is observed from the peel stress variation plots in figure 5.11 that joints with different adherend thickness ratios attain plasticity at different load magnitudes. The thicker the bottom composite adherend, the sooner the adhesive reaches a plastic state. One probable reason for this is that the adhesive layer thickness is kept constant. It has to be borne in mind therefore, that while designing a joint for practical purposes, both adherend type/thickness and adhesive thickness need to be considered in conjunction with each other. Stress profiles seen in figure 5.12 suggest that the likely mode of failure will be *'adhesive'*. The illustration shown in figure 5.14 explains the *'anticlastic'* and *'bending-twisting'* effects in a single lap joint, where the three dimensional behaviour reduces tensile adhesive peel stress.

In summary, this study brought out new understanding on the behaviour of the single lap joint with dissimilar adherends mainly on two observations from the results. First, the stiffness imbalance between the two adherends, aluminium and the composite in this case, contributed to differential elongation among them under the loading and hence showed

three dimensional effects such as *'anticlastic'* and *'bending-twisting'*. Second, the state of adhesive stresses in the joint with dissimilar material as adherends showed that though peel stress peak occurs at either end of the overlap ends, their magnitudes are not equal and that the maximum peel stress value is located at the overlap end from where the adherend of lesser stiffness extends.

8.2.4 Stress analysis of Butt-strap joints

Chapter 6 dealt with the modelling of a semi-rigid adhesive Plexus MA550 that is used to bond a butt-strap joint system which transfers load in the deck-to-superstructure connection of a 34m long Vosper Thornycroft (VT) Patrol craft. The main objective was to identify the possible failure modes in the joint, particularly for the thicker adhesive layers. Modelling of Plexus MA550, a semi-rigid type of adhesive posed challenges, given that it has a high value of Poisson's ratio (0.45) and has nonlinear stress-strain variation, even from the lower magnitude of load. As seen from the stress-strain curve (figure 6.3), it is extremely difficult to find the initial yield limit and hence the transition from elastic to plastic region. To counter this problem, it was decided to use the Ramberg-Osgood relation that could effectively model the adhesive stress-strain data obtained from the bulk adhesive traction tests. Ramberg-Osgood parameters determined by the method of least squares for the Plexus MA550 in this case, has proven to be an appropriate as seen from the figure 6.3. Four types of butt-strap joint geometry with adhesive thicknesses of 1,3,5 & 10mm respectively are analysed for the cases of linear (LE), geometrical nonlinear (GNL) and geometrical-material nonlinear (GMNL) formulation. The load-displacement relations obtained from these analyses are compared with the experimental load-displacement curves of Jarry and Shenoi (2005).

Load-displacement plots in figure 6.6 show reasonable agreement for the adhesive thicknesses of 1,3 & 5mm and deviates for 10mm thickness. Discussions related to nonlinear deformations in section 6.4.3 highlighted the influence of geometric nonlinearity on the single butt-strap joint. The performance of three dimensional analysis demonstrated the

significant existence of combined deformation in all the three directions, especially in the lateral direction as sketched in figure 6.8. Comparison of stress values given in tables 6.3 & 6.4 indicates that the linear analysis over estimates the adhesive stresses and that the prediction of nonlinear stresses are closer to the actual strength of the Plexus MA550 adhesive. Section 6.4.4 also discussed the onset of nonlinearity and further perfectly-plastic yielding, for all the joint cases; the stress variation for the adhesive thickness of 3mm in particular, proved to be similar to the stress-strain behaviour of the bulk adhesive stress-strain data. As in the case of single lap joints, the existence of a *'3D Corner'* is observed in a single butt-strap joint because of the *'anticlastic'* effect (figure 6.12). From the discussions presented in section 6.4.5, it is concluded that the failure initiates in the vicinity of the butt-gap present in the joint: it can fail in *'cohesive'* mode since rubber-like adhesive may tear apart between the extreme range of adhesive stress values and also in *'adhesive'* failure mode, because of steep shear stress gradients, as shown in figure 6.13, along the bottom interface layer.

From the above discussions it is clear that the three dimensional nonlinear analysis of a butt-strap joint system has showed large axial, vertical and lateral deformations when the bond line is thick. Particularly, the variation of lateral deformation is captured from the analysis, highlighting the behaviour of a semi-rigid adhesive, Plexus MA550 that has high Poisson's ratio of 0.47. Another key observation is regarding the state of adhesive stresses in the joint. The nonlinear stress values showed that the predicted nonlinear stress values are closer to the strength of the adhesive Plexus MA550 while linear formulation resulted in over estimation of stress values. This highlights the influence of the geometric and material nonlinearities on the butt-strap joint when bonded with a semi-rigid adhesive material and implies that the assessment of possible failure modes in a joint should be based on nonlinear state of stress instead of linear predictions while designing such joints.

8.2.5 Stress concentrations in a GRP-Steel hybrid joint

A three dimensional modelling and analyses was attempted for a GRP-Steel hybrid joint for the purpose of identifying critical stress locations that lead to failure of a joint under the three types of loading; in-plane compression, out-of-plane 4-point bending, and under the flexural loading scenario. It is observed from the literature that a three dimensional numerical modelling of a hybrid joint such as the one that is mounted on the *Lafayette* class frigates, was not addressed before. The reasons for considering a three dimensional cases are presented in section 3.2.2. Considering the complicated the joint geometry and the combination of different materials the joint is composed of, it is felt that a three dimensional analysis can result in a better understanding of the behaviour of the hybrid joint. Variation of normal stress across the width of the hybrid joint is seen when the joint is subjected to in-plane compressive loading (figure 7.4), thus highlighting the three dimensional effects present in the joint. This pheomenon of variation of stress in lateral direction is been observed for the first time, since a three dimensional analysis of hybrid joints has not been attempted before. However, such behaviour is not clearly seen for the other loading cases, in 4-point bending and in flexural loading. Regardless of the loading situation, it is found that the both the normal and axial stress components are concentrated in a *'critical zone'*, where all the three materials, steel/balsa core/GRP, join at the end of tapering. Although the steel portion in the hybrid joint can withstand high stress magnitudes, it is likely that de-bonding will occur between steel and the balsa core, thus leading to crack initiation. Delamination of GRP from steel along the bondline on the flatter side results in further propagation of the crack. It can be said that the failure pattern deduced from the analyses is similar to the damage seen in experimental specimens.

8.3 Further work

While the research works undertaken here has resulted in advancement of knowledge, it has also provided scope for further studies on adhesive bonding technologies for structural

applications in marine environment. In light of this, it is suggested here that the following issues/problems can be undertaken as the extension of the present work.

- Concerning the further development of the FE program code, it is suggested to include failure criteria like Tsai-Wu relation so that material nonlinear behaviour of composite adherends can be studied.
- Modification of input subroutine in the program code to include laminate properties and ply orientation.
- Enhancement of computational capacity of the program code to analyse the models with higher aspect ratio and with increased mesh density.
- Inclusion of other material nonlinear formulations like visco-elasticity, visco-plasticity, creep and hyper-elasticity.
- Parametric study on lap joints with non-identical adherends was considered only for aluminium-composite lap joints. Investigation on three dimensional effects can be extended to joints with laminate adherends. Effect of ply orientation on interlaminar stresses in the joint can provide further understanding on the lap joint behaviour.
- Analysis of hybrid joints has shown that the critical stresses are located around the region where all the materials, GRP-Steel-Core ends are bonded together. In order to avoid concentration of stress at one region, the hybrid joint configuration has to be modified. A more refined FE mesh should be generated to capture stress peaks at critical locations. It is therefore, suggested that a parametric study by varying the length of protrusion of steel into the balsa core can be carried out.
- Three dimensional modelling of stepped-lap and scarf joints, especially with small steps and small scarf angles that are practically used, can contribute to further understanding on their load transfer mechanisms.
- Finally, the developed program code can also be applied to study the patch repair analysis that is increasingly used as a repair method in marine industry.

Chapter 9

Conclusion

This study presented comprehensive three dimensional finite element analyses of adhesively bonded joint configurations that are employed in marine structures. A three dimensional finite element code incorporating geometric and material nonlinear equations is developed. The influence of geometrical nonlinearity on joint deformations, especially for a joint with dissimilar adherends of similar thickness is demonstrated even at very low levels of loading. For the considered case of parametric study on Aluminium-Composite single lap joint, the analyses has revealed that the thicker the composite adherend, the sooner the joint attains plasticity if the same adhesive thickness is maintained. This has highlighted the need for compromise when it comes to dimensioning of size/type of adherends and adhesive thickness for use in practical purposes. *'Anticlastic'* effect resulting in reduction of peel stresses at *3D corner* for a dissimilar lap joint is demonstrated for the first time though the earlier two-dimensional studies has just anticipated such behaviour.

Adhesive stresses in a single butt-strap joint system, particularly with thick adhesive layers are investigated in a three dimensional domain. As seen in study of a single lap joint, here also reduction of peel stresses at *3D corner* is reported. Importantly, this analyses stressed the need for accounting geometric and material nonlinearities while modelling the butt-strap joint with thicker bond lines. Novel ideas related to presence of lateral deformation in the joint and the reduced stresses identical to the actual strength of the

semi-rigid adhesive material are the main outcomes of this study.

Three dimensional modelling of a GRP-Steel hybrid joint that forms a structural component between the hull and the super-structure in a ship is attempted for the first time in the final study. Three dimensional analysis has resulted in fresh understanding that the normal stress along the interface layer is not uniform across the width of the hybrid joint. It is suggested that the more refined FE mesh model should be analysed for further understanding of the stresses that cause failure.

From practical design considerations, this work has highlighted the importance of the selection of appropriate adherend type/thickness when dissimilar materials are bonded, consideration of nonlinear stress values as limiting factors for evolution of design formulae when dimensioning a joint and re-orientation of materials in hybrid joints in order to minimize the critical stress values and also to spread out the stress concentration locations.

Appendix A

Evaluation of H_η matrix for the modified von Mises criterion

This appendix is given in connection with the section 4.5.3 as per [80].
The form of the viscoplastic strain rate matrix H_n, defined in Eq. (3.26) and required for implicit time integration, differs for each yield criterion. The H_n matrix is explicitly derived for modified von Mises criterion given in Eq. (3.20) and presented in a form suitable for numerical computation.

Substituting from Eq. (3.12) in Eq. (3.26) and dropping the superscripts, n, for convenience gives,

$$H_n = \gamma\Big(\big(\frac{d\phi}{dF}\big)aa^T + (\phi)\frac{\partial a^T}{\partial \sigma}\Big) \tag{A.1}$$

in which the flow vector, a, is derived for modified Von Mises criterion.

$$a = \frac{\partial F}{\partial \sigma} = \frac{\partial F}{\partial J_1}\frac{\partial J_1}{\partial \sigma} + \frac{\partial F}{\partial J_2'}\frac{\partial J_2'}{\partial \sigma} \tag{A.2}$$

The flow vector, a, can be expressed in the form suitable for numerical computation :

$$a = c_1 a_1 + c_2 a_2 \tag{A.3}$$

in which constants c_1 and c_2 are yield criteria dependent, and are derived for the Modified Von Mises criterion given in Eq. (3.20). The specific form of constants c_1 and c_2 and vectors a_1 and a_2 are given below.

$c_1 = \frac{\partial F}{\partial J_1}$	$c_2 = \frac{\partial F}{\partial J_2'}$

Modified Von Mises Criterion

c_v	$\frac{c_s}{2(J_2')^{\frac{1}{2}}}$

If λ=1, Von-Mises Modified Criterion.

0	$\frac{\sqrt{3}}{2(J_2')^{\frac{1}{2}}}$

$a_1 = \frac{\partial J_1}{\partial \sigma}$	$a_2 = \frac{\partial J_2'}{\partial \sigma}$

$\begin{bmatrix} 1 \\ 1 \\ 1 \\ 0 \\ 0 \\ 0 \end{bmatrix}$	$\begin{bmatrix} s_x \\ s_y \\ s_z \\ 2\tau_{yz} \\ 2\tau_{zx} \\ 2\tau_{xy} \end{bmatrix}$

where :

$$J_1 = \sigma_{ii}; \quad \text{I invariant of stress}$$

$$J_2' = \tfrac{1}{2} s_{ij} s_{ij}; \quad \text{II invariant of deviatoric stress}$$

Substituting the vector, a, in Eq. (A.1) gives

$$H_n = \gamma\Big(\frac{\partial \phi}{\partial F}\Big) M_0 + \gamma\Big(\phi\Big) \sum_{i=1}^{2} R_i M_i \tag{A.4}$$

This formulation for H_n is convenient for computational purpose since the same constants, vectors and invariants that are employed in the evaluation of the yield function and flow rule definition are again utilized. The constants R_i and the explicit forms of M_0, M_i for two dimensional cases of plane stress, plane strain and axisymmetry are given below.

R_1	R_2
$\frac{-c_s}{4(J_2')^{\frac{3}{2}}}$	$\frac{c_s}{2(J_2')^{\frac{1}{2}}}$

$$M_o = \begin{bmatrix} AA & AB & AC & AD & AE & AF \\ AB & BB & BC & BD & BE & BF \\ AC & BC & CC & CD & CE & CF \\ AD & BD & CD & DD & DE & DF \\ EA & EB & EC & ED & EE & EF \\ FA & FB & FC & FD & FE & FF \end{bmatrix}$$

where

$$\begin{aligned} A &= [c_1 + c_2 s_x] \\ B &= [c_1 + c_2 s_y] \\ C &= [c_1 + c_2 s_z] \\ D &= [2c_2 \tau_{xy}] \\ E &= [2c_2 \tau_{yz}] \\ F &= [2c_2 \tau_{zx}] \end{aligned}$$

$$M_1 = \begin{bmatrix} s_x s_x & s_x s_y & s_x s_z & 2s_x \tau_{xy} & 2s_x \tau_{yz} & 2s_x \tau_{zx} \\ s_y s_x & s_y s_y & s_y s_z & 2s_y \tau_{xy} & 2s_y \tau_{yz} & 2s_y \tau_{zx} \\ s_z s_x & s_z s_y & s_z s_z & 2s_z \tau_{xy} & 2s_z \tau_{yz} & 2s_z \tau_{zx} \\ 2\tau_{xy} s_x & 2\tau_{xy} s_y & 2\tau_{xy} s_z & 4\tau_{xy} \tau xy & 4\tau_{xy} \tau_{yz} & 4\tau_{xy} \tau_{zx} \\ 2\tau_{yz} s_x & 2\tau_{yz} s_y & 2\tau_{yz} s_z & 4\tau_{yz} \tau xy & 4\tau_{yz} \tau_{yz} & 4\tau_{yz} \tau_{zx} \\ 2\tau_{zx} s_x & 2\tau_{zx} s_y & 2\tau_{zx} s_z & 4\tau_{zx} \tau xy & 4\tau_{zx} \tau_{yz} & 4\tau_{zx} \tau_{zx} \end{bmatrix}$$

$$M_2 = \begin{bmatrix} 2/3 & -1/3 & -1/3 & 0 & 0 & 0 \\ -1/3 & 2/3 & -1/3 & 0 & 0 & 0 \\ -1/3 & -1/3 & 2/3 & 0 & 0 & 0 \\ 0 & 0 & 0 & 2 & 0 & 0 \\ 0 & 0 & 0 & 0 & 2 & 0 \\ 0 & 0 & 0 & 0 & 0 & 2 \end{bmatrix}$$

Appendix B

Determination of the Ramberg-Osgood parameters

This appendix provides information related to determination of Ramberg-Osgood parameters for an adhesive material that are required in the Ramberg-Osgood equation, described in section 6.3.1.

B.1 Ramberg-Osgood equation

The Ramberg-Osgood equation is more commonly used for representing the nonlinear behaviour of the material. This equation can represent the nonlinear behaviour of different kind of materials such as metals, alloys and polymers (Ramberg & Osgood, 1943). They had proposed an equation of the form,

$$\epsilon = \frac{\sigma}{E} + k\left[\frac{\sigma}{E}\right]^{r} \tag{B.1}$$

in which E, k & r are the material constants, termed as the Ramberg-Osgood parameters. The above equation can be written in dimensionless form as,

$$\frac{\epsilon}{\epsilon_{ch}} = \frac{\sigma}{\sigma_{ch}}\left[1 + \left[\frac{\sigma}{\sigma_{ch}}\right]^{r-1}\right] \tag{B.2}$$

where σ_{ch} is the characteristic stress,

ϵ_{ch} is the characteristic strain

and they are related as $\sigma_{ch} = E\epsilon_{ch}$.

This equation contains three parameters, of which one is Young's modulus (E) of the material under consideration that is known in most of the situations. This leaves two other parameters, σ_{ch} and r to be determined. These two unknowns can easily be deduced by a least square analysis. The above equation is simplified as,

$$\epsilon E = \sigma \left[1 + \left[\frac{\sigma}{\sigma_{ch}}\right]^{r-1}\right] \tag{B.3}$$

This is again rewritten as,

$$\epsilon E = \sigma + \sigma_{ch} \left[\frac{\sigma}{\sigma_{ch}}\right]^{r} \tag{B.4}$$

or

$$(\epsilon E - \sigma) = \sigma_{ch} \left[\frac{\sigma}{\sigma_{ch}}\right]^{r} \tag{B.5}$$

by taking logarithm on both sides,

$$log\ (\epsilon E - \sigma) = log\ \sigma_{ch} + r\ log\ \sigma - r\ log\ \sigma_{ch} \tag{B.6}$$

This particular form, Eq. (B.6), is not sufficiently useful for least square analysis as $r\ log\ \sigma_{ch}$ is a term involving both the unknowns and therefore, can not be partitioned in to matrices. Therefore, let the equation be written as,

$$log\ (\epsilon E - \sigma) = log\ \sigma_{ch} + r\ log\ \sigma - a\ log\ \sigma_{ch} \tag{B.7}$$

where $'a'$ represents a trial value of r.

Now, ϵ and σ are experimental stress-strain values and we require the difference between these and theoretical values to be minimised. Therefore,

$$s = (1 - a)\ log\ \sigma_{ch} + r\ log\ \sigma - log\ (\epsilon E - \sigma) \tag{B.8}$$

where s = difference.

For $'n'$ experimentally obtained values of stress and strain, ϵ and σ, Eq. (B.8) can be written in matrix form as,

$$\{s\} = \begin{bmatrix} (1-a) & log\ \sigma_{s1} \\ (1-a) & log\ \sigma_{s2} \\ (1-a) & log\ \sigma_{s3} \\ . & . \\ . & . \\ (1-a) & log\ \sigma_{sn} \end{bmatrix} \left\{ \begin{array}{c} log\ \sigma_{ch} \\ r \end{array} \right\} - \begin{bmatrix} log\ (\epsilon_{s1}E - \sigma_{s1}) \\ log\ (\epsilon_{s2}E - \sigma_{s2}) \\ log\ (\epsilon_{s3}E - \sigma_{s3}) \\ . \\ . \\ log\ (\epsilon_{sn}E - \sigma_{sn}) \end{bmatrix} \tag{B.9}$$

This simplifies to

$$\{s\} = [A]\{B\} - \{C\} \tag{B.10}$$

where vector $\{B\}$ contains the two unknowns. Now the square of the difference is required,

$$s = \{s\}^T \{s\} = [\ [A]\{B\} - \{C\}\ ]^T - [\ [A]\{B\} - \{C\}\ ] \tag{B.11}$$

$$s = \{B\}^T [A]^T [A]\{B\} - \{B\}^T [A]^T \{C\} - \{C\}^T [A]\{B\} + \{C\}^T \{C\} \tag{B.12}$$

For the least value of $s = \{s\}^T \{s\}$, Eq. (B.9) is differentiated with respect to the unknonws σ_{ch} and r, that is, with respect to $\{B\}^T$:

$$\frac{\partial s}{\partial B^T} = 2[A]\{B\} - 2[A]\{C\} = \{0\} \tag{B.13}$$

Eq. (B.13) then gives,

$$[\phi]\{B\} = \{w\} \tag{B.14}$$

and

$$\{B\} = [\phi]^{-1}\{w\} \tag{B.15}$$

Eq. (B.15) gives the 2x1 vector $\{B\}$ with first term $log\ \sigma_{ch}$ and second term r. Therefore,

$$\sigma_{ch} = e^{B_1} \tag{B.16}$$

$$r = B_2 \tag{B.17}$$

At this stage, r is compared with the trial value $'a'$. If $|r - a| \leq 0.01$ then r and σ_{ch} have been obtained to suitable accuracy, but if $|r - a| > 0.01$, then $'a'$ is set equal to the average of the previous $'a'$ and the computed r value, and the values are recomputed. By this approach, the values for σ_{ch} and r are found to be 9.0MPa and 12.0 respectively for the semi-rigid adhesive, Plexus MA550.

Appendix C

Bench-mark tests

Bench mark tests are performed to verify the validity of the finite element program. A 20-noded isoparametric single element is modelled for the patch test and a cantilever beam is modelled as a bench mark problem for linear analysis.

C.1 Single element test

A cubic 20 noded isoparametric element of size 10x10x10mm is modelled for the single element test as shown in the figure. C.1. The boundary conditions and load are applied in such a way that the element behaves uniaxially. (i.e) Nodal equivalent loads are applied on one face of the element and axial boundary conditions are applied in the opposite face. One corner is fixed in all three X,Y and Z directions, the second corner is fixed in x,y directions, the third corner node was fixed in x,z directions. All the interior nodes were fixed in only x direction. A 2x2x2 gauss point rule was used for the integration. Pre-processing and Post-processing for the single element model and the result is given in detail in the following appendices C & D. A load magnitude of 3000N is applied over the nodes as marked in figure C.1. The resultant stress values are given in the next appendix. It can be seen from the results that axial stress component has uniform value of 30.0MPa and all other stress component values are negligible.

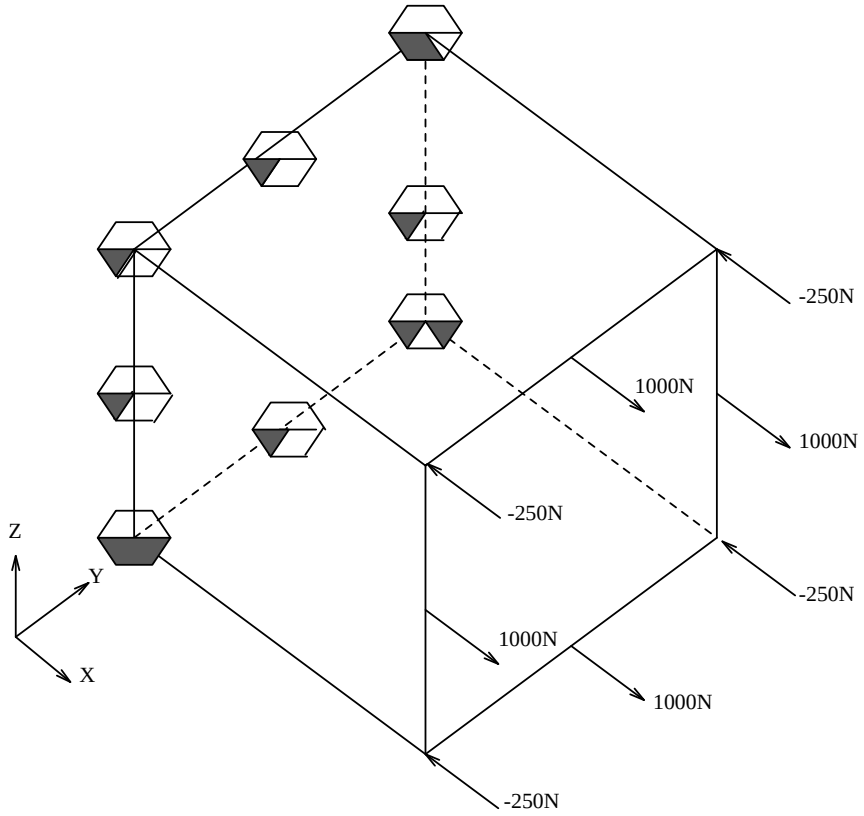

Figure C.1: Model of a Single element with boundary conditions

C.2 Bench mark test for linear analysis

In order to verify the validity of the program for linear analysis, a ten element cantilever beam of length 1000mm and a cross-section of 10x10mm was considered as shown in the fig. C.2. The beam is analysed for two linear cases viz. for axial load and vertical load at the free end of the cantilever beam. The observations were as follows:

- The axial stress obtained from the program is exactly matching with the theoretical value (Stress = Load/Area) as shown in fig. C.3.
- The plots of Load-Deflection obtained at the free end of the beam is in close agreement by 97% with the theoretical values obtained from the strength of material point of view (figure. C.3).

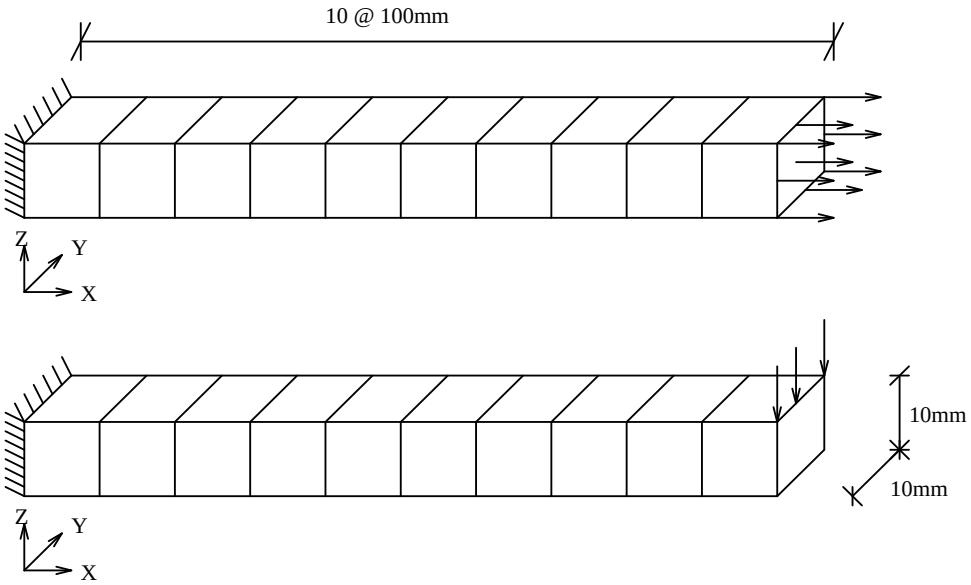

Figure C.2: Model of a cantilever beam for the linear Bench mark test

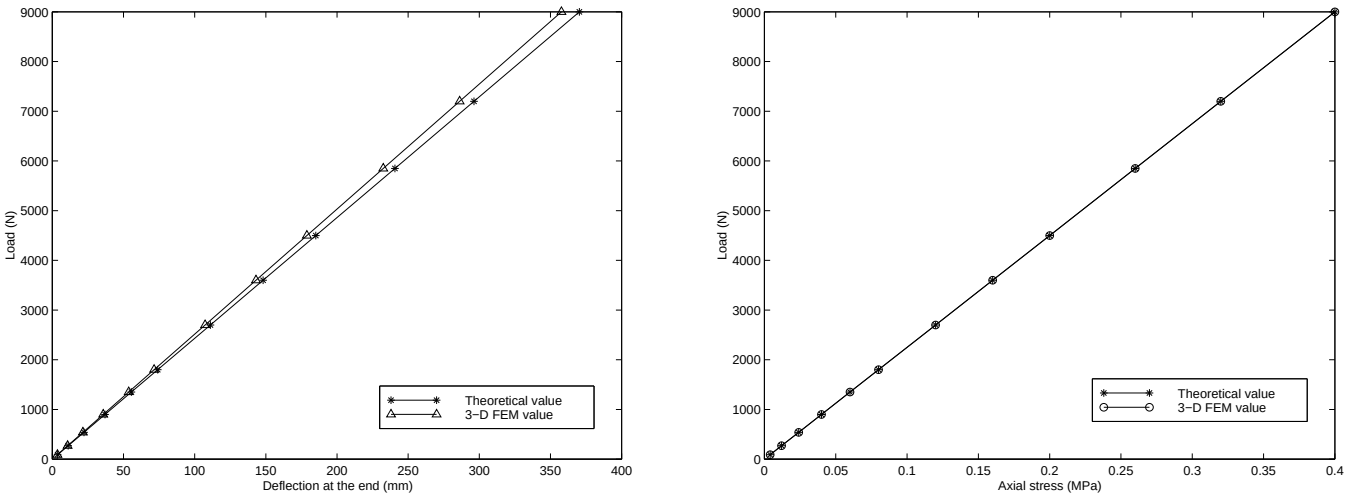

Figure C.3: Load/Displacement for bending and Stress/Strain for Axial load in cantilever beam - Bench mark test for linear analysis

Appendix D

Pre-processing

In this section, the preparation of input file and the care to be taken in its preparation are discussed. Preparation of the input file forms the major part of a user's work as any lapses in its preparation will either stop the execution of the program or give erroneous results. Finally a standard input file for a single element with a pure axial loading and boundary conditions is given and discussed.

D.1 Development of Pre-processor using NISA/ANSYS/NASTRAN : Interface module

Geometric modelling and mesh generation for the 3-D structure is cumbersome and time consuming and hence the same has been done for the 20 noded brick element with the help of one commercial package NISA/ANSYS/NASTRAN. The different steps involved in the generation of input file for the 3-D program can be summarized as follows:

- Geometric modelling and mesh generation have been done in the usual manner with the help of NISA/ANSYS/NASTRAN package. Geometric modelling of the problem was done by feeding the coordinates of the corner grid points, constructing a patch and then a hyper patch as per the thickness of the structure. The desired pattern of the mesh has been generated after feeding the required data and the boundary nodes are merged to make the structure integrated.

- The output of the file NISA/ANSYS/NASTRAN consists of extra characters like zero and commas which are not required in the input file of the viscoplastic program. Hence a systematic procedure has to be developed to convert the NISA/ANSYS/NASTRAN file to the input file of the program.

D.1.1 Generation of the input file

During the conversion of the NISA/ANSYS/NASTRAN output file to the input file two major problems have been encountered. These problems are described below in brief:

- The nodal connectivity generated by the NISA/ANSYS/NASTRAN package is different from that required by the developed program.

- The highest node number in the NISA/ANSYS/NASTRAN package is not the same as the total number of nodes due to the merger of interracial nodes at the boundary of two elements. In the developed program it is a requirement to have the highest node number equal to the total number of nodes as 'NPOIN' referring to the total number of points has been used as a parameter to terminate the 'DO' loop.

To resolve these issues inter-facial programs have been written in C-language. Three inter-facial programs have been written to convert the nodal connectivity and to make the highest node number equal to the total number of nodes.

1. At first, the NISA/ANSYS/NASTRAN output file has been split into two files as s1.dat and s2.dat. File s1.dat consists of the total number of points, its coordinates along with some extra characters associated with the NISA/ANSYS/NASTRAN output file. File s2.dat consists of elements and their nodal connectivities.

2. First interface program 01.c has been written to remove the extra character of s1.dat file. The output of this file is named as s4.dat.

3. A second interface program 02.c has been written to change the nodal connectivity of the elements as required by the new program. The output of this file is called as s3.dat.

4. By connecting these two files s4.dat and s3.dat, a new file s5.dat is made. It should be noted while concatenating the two files that the nodal connectivity should come first.

5. Now a third program in C-language 03.c is written which converts the highest node number equal to the total number of nodes. The corresponding change in the number of nodes keeping the nodal connectivities same, are also done by this program. The output of this program is termed as s6.dat. Here the input file is s5.dat and the output file is s6.dat. Another file s7.dat is created form s6.dat so that it contains only the node numbers and their coordinates.

D.1.2 Boundary conditions

Feeding the boundary conditions in a 2-D case is easy as one can visualize the structure, its restricted boundaries and the applied nodal forces. But in a 3-D case it becomes difficult. Problem becomes more difficult if symmetry of planes has been considered in solving the problem. Moreover the manual feeding of data may lead to errors besides it is a time consuming and laborious process. Two boundary conditions, i.e., the force and the displacement boundary conditions are fed into the input file with the help of two new files in C-language. The procedure is as follows:

Displacement Boundary conditions

The program has been developed on an interactive basis and one has to feed the required data asked by the computer. The concept of displacement boundary conditions is as follows:

- A three digit code is used to indicate the restricted displacement at a particular node. First digit of code indicates the X-direction displacement, second the Y-direction and third the Z-direction displacements.

- Number 0 indicates that displacement is not restricted and 1 indicates that it is restricted.

- For example, a code 111 means that the displacements have been fixed at that particular node whereas code 100 indicates that only the X-direction displacement is fixed at that particular node.

- The file s7.dat containing the nodal coordinates is fed to the fourth interface program 04.c in which one has to specify the total number of nodes, fixity code and the nodal coordinates of the nodes to be fixed. This program takes all the nodal coordinates from its input file s7.dat and fixes the prescribed nodes according to the fixity code. The node numbers and their fixity codes are given by this program as its output file d.dat. This file is concatenated to the file s6.dat created above. It has to be noted that the coordinates of the nodes to be fixed and the fixity code are to be written in the program 0m4.c by the user himself. So it is worth while for the user to have a look at these interface programs.

Material properties

- Next in the sequence the material identity number and the its properties viz. the modulus of elasticity, poisson's ratio, hardening parameter, fluidity parameter, yield stress etc should be keyed into the input file.

Force boundary conditions

This program has also been written in the interactive form and the nodal forces can be fed easily by supplying the data asked by the computer. Here also the loads, and if it is nodal loads, their corresponding node numbers have to be fed into the program like the one for displacement boundary conditions. Provisions are made for computation of the equivalent nodal forces in the load subroutine of the developed program if the value of the applied nodal forces, body forces and surface forces are fed through the input file.

- A loading code has to be fed into the input file just before writing the force boundary conditions. As stated earlier the force has been divide into 3 categories i.e., nodal force, body force and surface force.

- Code digit 1 indicates that loading exists at that particular node and code 0 indicates that it doesn't exist.The first digit is for the nodal loads, second one is for the body forces and the third one is for the surface tractions. For example a code 111 indicates that all the 3 types of forces are applied at the particular node while a code of 100 represents that only nodal loads are applied at the particular node.

- If the body force is present then one has to feed the component of intensity of body forces in x,y,z directions. If the surface force is present then one has to feed the data regarding the face on which it is acting.

- The interface program written for the above purpose is 05.c.Its input is s7.dat consisting of the node numbers and their coordinates. Its output file is f.dat giving the node numbers and the corresponding 3 components of forces with their values. Care has to taken here that the highest node in the model should not be left without applying load. If case no load is acting on that node, zero value of load has to be given there, if not this will lead to an endless loop.

- The files s6.dat, d.dat, f.dat are then concatenated to create a new file. At the top of this file some data regarding the no.of elements, nodes, materials,type of solution algorithm, total no.of fixed nodes, total no.of load increments, and whether the solution includes geometric non-linearity or not etc should be typed by the user. In between the displacement and force boundary conditions the material properties of all the materials used in the structure should be keyed in along with the material identity numbers for the different materials. After this in the next line the three-digit code for loading as described in the force boundary conditions should be keyed in. After this the force boundary conditions follow which are already present in the concatenated file. The final file with all these inclusions is the input file i1.dat.

Here a standard input file for a single element subjected to a pure axial loading and axial boundary conditions is given and explained. A portion of a sample output is also given which shows a uniaxial behaviour of the single element.

```
INPUT FILE FOR A SINGLE ELEMENT AXIAL CASE \\
%-------------------------------------------------
20 1 8 20 1 3 2 2 3 1
1 1 1 17 5 11 6 18 2 9 13 15 16 14 3 19 7 12 8 20 4 10
1  0.000000  0.000000  0.000000
2  0.000000  10.000000  0.000000
3  0.000000  0.000000  10.000000
4  0.000000  10.000000  10.000000
5  10.000000  0.000000  0.000000
6  10.000000  10.000000  0.000000
7  10.000000  0.000000  10.000000
8  10.000000  10.000000  10.000000
9  0.000000  5.000000  0.000000
10  0.000000  5.000000  10.000000
11  10.000000  5.000000  0.000000
12  10.000000  5.000000  10.000000
13  0.000000  0.000000  5.000000
14  0.000000  10.000000  5.000000
15  10.000000  0.000000  5.000000
16  10.000000  10.000000  5.000000
17  5.000000  0.000000  0.000000
18  5.000000  10.000000  0.000000
19  5.000000  0.000000  10.000000
20  5.000000  10.000000  10.000000
1   111  0.000000 0.000000 0.000000
2   101  0.000000 0.000000 0.000000
3   100  0.000000 0.000000 0.000000
4   110  0.000000 0.000000 0.000000
9   100  0.000000 0.000000 0.000000
```

```
10  100  0.000000 0.000000 0.000000
13  100  0.000000 0.000000 0.000000
14  100  0.000000 0.000000 0.000000
1  210000.0  0.3  80769.23  0.0  240.0  0.2  0.0   0.001  1.0  1
1  0  0
5   -250.0  0.0  0.0
11  1000.0  0.0  0.0
6   -250.0  0.0  0.0
16  1000.0  0.0  0.0
8   -250.0  0.0  0.0
12  1000.0  0.0  0.0
7   -250.0  0.0  0.0
15  1000.0  0.0  0.0
20     0.0  0.0  0.0
1.0   0.05  0.1  1.5
0.1   0.1   60 30 30
3.0   0.1   60 30 30
5.0   0.1   60 30 30
```

The first line in the above input file has to be typed by the user.The values to be typed in the order are

- NPOIN, the total no.of points in the structure (here 20)
- NELEM, the total no. of elements in the structure (here 1)
- NVFIX, total number of fixed points in the structure (here 8 nodes on one of the faces of the element are fixed
- NNODE, total no. of nodes per element (here 20)
- NMATS, total no. of materials used in the structure (here 1)
- NGAUS, order of the Gaussian integration used (here 3)

- NALGO, type of the algorithm parameter used (here 2 indicating the Newton-Raphson method)
- NCRIT, type of yield criteria employed (here 2 indicating the Von-Mises criteria)
- NINCS, no. of load increments to be applied (here 3)
- NLAPS, parameter for Geometric non-linearity (here 1. NLAPS=1 indicates that Geometric non-linearity is not included in the analysis. and a value of 2 indicates that Geometric non-linearity is included in the analysis.)

In the next line we have the element no.(here 1), its material identity(Here only one material is used), followed by the nodal connectivities. This part is already generated through the interface programs in file s6.dat.
Next we have the node numbers and their coordinates.
Next we give the fixed node numbers , the fixity code and the values of the prescribed displacements in x, y, z directions at the fixed points if any. Here it is assumed that the nodes are rigidly fixed and so the values of the prescribed displacements are given as zero. These are already available through the file d.dat created by the interface programs.
Next we have the material properties as follows. These have to be typed in by the user.

- MATNO, Material identification number (here 1)
- YOUNG, the Young's modulus of the material (here 21000.0)
- POISS, Poisson's ratio of the material (here 0.3)
- shear modulus (here 80769.23)
- density of the material (here 0.0)
- YIELD, the yield stress of the material (here 240.0)
- HARDS, hardening parameter H (here 0.2)
- FRICT, coefficient of friction (in the case of Mohr-Coloumb criteria here it is 0)

- GAMMA, fluidity parameter (here 0.001)
- DELTA, the value of N function used in calculation of the viscoplastic strain rate (here 1)
- AFLOW the type of function used in calculation of the viscoplastic strain rate (here 1)

Next the force fixity code is to be typed in by the user. (Here it is 1 0 0 indicating that only point loads are given).
Next we have the node numbers and the associated components of the point loads applied at each node. These are already available through the file f.dat.
After this the user has to type the highest node number (here 20) and its associated forces (here all are zero). It is a must.
In the next line the following are to be typed

- parameter TIMEX to indicate whether the scheme employed is implicit or explicit. It is 1 for the implicit and 0 for the explicit schemes. Intermediate values indicate a semi-implicit scheme (here it is 1).
- TAUFT, Time step stability factor τ (here 0.05).
- DTINT,Initial time step length (here 1)
- FTIME, time step increment parameter k for next time steps (here 1.5).

Next the user has to type for each increment the following

- Load factor (here 0.1 for the first increment).
- Convergence tolerance (here 0.1).
- Maximum no. of iterations to be performed after which the control will flow to the next increment (here 60).
- the initial and the final output parameters (here 30 and 30).

SAMPLE OUTPUT FOR THE SINGLE ELEMENT TEST

GAUSS POINT STRESSES OF THE SINGLE ELEMENT AXIAL TEST

G.P.	XX-STRESS	YY-STRESS	ZZ-STRESS	YZ-STRESS	ZX-STRESS	XY-STRESS
0	ELEMENT NO. = 1					
1	.30000E+02	.31087E-06	.31087E-06	-.31087E-06	-.26613E-14	-.31087E-06
2	.30000E+02	.31087E-06	.31087E-06	-.31087E-06	-.26613E-14	.31087E-06
3	.30000E+02	.31087E-06	.31087E-06	.31087E-06	-.26613E-14	-.31087E-06
4	.30000E+02	.31087E-06	.31087E-06	.31087E-06	-.26613E-14	.31087E-06
5	.30000E+02	-.31087E-06	-.31087E-06	-.31087E-06	.26613E-14	-.31087E-06
6	.30000E+02	-.31087E-06	-.31087E-06	-.31087E-06	.26613E-14	.31087E-06
7	.30000E+02	-.31087E-06	-.31087E-06	.31087E-06	.26613E-14	-.31087E-06
8	.30000E+02	-.31087E-06	-.31087E-06	.31087E-06	.26613E-14	.31087E-06

Appendix E

Post-Processing

E.1 Introduction

In this, we discuss the post processing part in which we plot our output data in MATLAB. To have better understanding and interprretation of results with geometry of the model, it is better to use the nodal stress values. But the program gives Gaussian point stresses. So a 3-D stress smoothing technique is employed to get the nodal stresses from the Gaussian point stresses. Stress smoothening from Gaussian results to the nodal results is given in [**?**]. The algorithm given in that paper is extended here for the 20 noded element.

E.2 Stress-Smoothing for the 20-noded element

Finite element analysis generally involves the minimization of some functional defined in terms of piecewise functions. These functions are generally required to have a certain degree of inter element continuity depending on terms in the functional. In many finite element problems, the quantities of primary engineering interest involve the function derivatives and in many instances, especially with lower order elements, these derivatives do not possess inter-element continuity. The analyst is therefore faced with the problem of interpreting quantities which have histogram type distributions. Often the subjective eye of the experienced analyst may be quite successful in interpreting such information;

equally, it may easily be prejudiced and such an interpretation may lack consistency and rationality. In many of the automatic finite element based systems for linear and non-linear analysis, design and optimization currently under development, it is crucial that some rational and consistent procedures for the implementation of discontinuous functional be adopted. The least squares smoothing procedures may be carried out over the whole of the finite element domain and this will be referred to as global smoothing. Alternatively, the smoothing process may be performed separately over each individual element and this will be called local smoothing.

In this discussion, attention will be focused on the smoothing of stresses obtained from a finite element analysis using numerically integrated three dimensional isoparametric elements. At this stage, it is appropriate to restate the general problems discussed earlier. In the displacement method, the stresses are discontinuous between elements because of the nature of the assumed displacement variation. In analysis involving numerically integrated elements such as isoparametric elements, experience has shown that the integration points are the best stress sampling points. The nodes, which are the most useful output locations for stresses appear to be the worst sampling points. Reasons for this phenomenon are immediately apparent; however, it is well known that the interpolation function tends to behave badly near the extremities of the interpolation region. It is therefore reasonable to expect that shape function derivatives sampled in the interior of the elements would be more accurate than those sample on the element periphery. To counteract such problems many analyst have taken nodal average of stresses - average of the nodal stress of all elements meeting at a common node. This economic and simple solution works very well on the whole but pays no attention to the size of the adjacent elements.

It is demonstrated that the finite element displacement method itself may be viewed as a weighted least squares error procedure where the errors are those between the exact stresses and the appropriate finite element stresses. This information helps to explain the oscillatory nature of the finite element stresses and also suggests that subsequent stress smoothing may be useful.

GLOBAL SMOOTHING

Introduction: In the conventional least squares smoothing the proposed smoothing function is defined as

$$g(x,y) = a_{00} + aa10x + a01y + a11xy + a20x^2 ...etc = \sum a_{ij}x^i x^j, i = 0,p, j = 0,q \quad \text{(E.1)}$$

where g is the pth order function of x and a qth order function of y.
If the unsmoothed data is give by function $\sigma(x,y)$ then the problem becomes one of finding the coefficients a_{ij} which minimize the functional

$$x = \int\int (\sigma - g)^2 dxdy \quad \text{(E.2)}$$

Hence for x to be a minimum

$$\frac{\partial x}{\partial a_{ij}} \quad \text{(E.3)}$$

This equation defines a set of linear simultaneous equations in a_{ij} known as the normal equations. Thus, for a smoothing function of given order, the coefficients a_{ij} may be easily obtained using standard solution procedures. In the present context, conventional least squares smoothing is not considered suitable. As an alternative method the discretization process of the finite element method is adopted. The smoothing function g(x, y) is thus represented in a piecewise fashion across the complete domain using shape functions. In this case, the unknowns are taken as the smoothed nodal stresses $\bar{\sigma}$ and the smoothed stress at any point within an element may be obtained by interpolation using the shape functions.

Finite Element formulation

If the unknowns in the least squares problem are taken as the smoothed nodal stresses, let the smoothed function $g(\xi,\eta,\zeta)$ be given at any point within an element by expression

$$g(\xi,\eta,\zeta) = \sum_{i=1,n} \bar{N}_i \bar{\sigma}_i \quad \text{(E.4)}$$

where $\bar{N}_i$ the smoothing shape function at node i is a function of the co ordinates (ξ, η, ζ) and $\bar{sigma}_i$ is the smoothed nodal stress at node i and n is the number of nodes per element in the smoothing analysis. It should be noted that the smoothing shape functions $\bar{N}_i$ may be of a different order from the shape function N_i used in the initial finite element analysis. (For example, if in the initial analysis a set of parabolic shape functions are used, then in the smoothing analysis a set of linear shape functions may be used).

The error between the smoothed and unsmoothed stresses at any point within the element is given as

$$e(\xi, \eta, \zeta) = \sigma(\xi, \eta, \zeta) - g(\xi, \eta, \zeta) \tag{E.5}$$

where the unsmoothed stresses $\sigma(\xi, \eta, \zeta)$ at any point within the element may be obtained by the usual stress-displacement relation

$$\sigma(\xi, \eta, \zeta) = [D][B]\{\delta\}^e \tag{E.6}$$

where $[D]$ is the elasticity matrix, and $[B]$ is the strain -displacement matrix, and $\{\delta\}^e$ are the nodal displacements for the element.

The problem now becomes one of finding the set of smoothed nodal stresses $\bar{\sigma}_1, \bar{\sigma}_2, ...\bar{\sigma}_p$ which minimize the functional

$$x = \sum_{j=1,ne} \int\int e(\xi, \eta, \zeta)^2 dxdydz \tag{E.7}$$

where p is the total number of nodes, ne is the total number of elements, and det J is the determinant of Jacobian matrix.

for x to be minimum

$$\frac{\partial x}{\partial \bar{\sigma}_i} = 0.0 for i = 1, p \tag{E.8}$$

Therefore, for each element the element smoothing matrix is given as

$$[S^e] = \begin{bmatrix} \int\int \bar{N}_1 \bar{N}_1 detJ d\xi d\eta d\zeta & \int\int \bar{N}_1 \bar{N}_n detJ d\xi d\eta d\zeta \\ \int\int \bar{N}_n \bar{N}_1 detJ d\xi d\eta d\zeta & \int\int \bar{N}_n \bar{N}_n detJ d\xi d\eta d\zeta \end{bmatrix} \tag{E.9}$$

and the associated right hand side force vector is given as

$$\{F\}^e = \begin{bmatrix} \int\int \bar{N}_1 \sigma det J d\xi d\eta d\zeta \\ \int\int \bar{N}_n \sigma det J d\xi d\eta d\zeta \end{bmatrix} \tag{E.10}$$

This force vector may be assembled into the overall force vector and the element smoothing matrix may be assembled into the overall smoothing matrix for the whole finite element domain and solved in the usual way for $\bar{\sigma}_1, \bar{\sigma}_2, ...\bar{\sigma}_p$. It should be noted that if the smoothing shape functions imply C^i continuity across element interfaces, then the smoothed stress will also possess C^i continuity. The smoothing matrix and right hand side of equation may be evaluated using numerical integration procedures.

References

[1] Adams R.D. and Grant L.D.R. (1993) Adhesive layer thickness as a variable in the strength of bonded joints, 16th Annual meeting of the Adhesion society, Williamsburg, USA, pp.91-94.

[2] Adams R.D. and Peppiatt N.A. (1973) Rubber model for adhesive lap joints, *Jl. of Strain Analysis*, Vol.8,No.1, pp.52-57.

[3] Adams R.D. and Peppiatt N.A. (1974) Stress analysis of adhesive bonded lap joints, *Jl. of Strain Analysis*, Vol.9,No.3, pp. 185-196.

[4] Adams R.D., Comyn J. and Wake W.C. (1997) *Structural adhesives joints in engineering*, Chapman and Hall, ISBN 0-412-70920-1.

[5] Ahn S.H. and Springer G.S. (1998a) Repair of composite laminates-I: Test results, *Jl. of Composite materials*, Vol.32, No.11 pp. 1036-1073.

[6] Ahn S.H. and Springer G.S. (1998b) Repair of composite laminates-II: Models, *Jl. of Composite materials*, Vol.32, No.11 pp. 1076-1114.

[7] Allman D.J. (1977) A theory for elastic stresses in adhesive bonded lap joints, *Jl. Mech. Appl. Math.*, Vol. XXX, No4, pp.415-436.

[8] Altus E. (1985) Three-Dimensional Singularities in Double Lap Joints, *Engg. Frac. Mechanics*, Vol.21, No.6, pp.1097-1112.

[9] Andruet R.H., Dillard D.A. and Holzer S.M. (2001)) Two- and three- dimensional

geometric nonlinear finite elements for analysis of adhesive joints, *Intl. Jl. of Adhesion and Adhesives*, Vol.21, pp.17-34.

[10] Argyris J.H. and Kleiber M. (1977) Incremental formulation in non-linear mechanics and large strain elasto-plasticity-natural approach part 1, *Comp. meth. Appl. Mech. Engg.*, Vol.11, pp.215-247.

[11] Baker A.A., Chester R.J., Hugo G.R. and Radtke T.C. (1999) Scarf repairs to highly strained graphite/epoxy structure, *Intl. Jl. of Adhesion and Adhesives*, Vol.19, pp.161-171.

[12] Bargan P.G. and Clough R.W. (1973) Large deflection analysis of plates and shells using the finite element method, *Int. J. Numr. Meth. Engg.*, Vol.5 pp.543-556.

[13] Barker R.M. and Hatt F. (1973) Analysis of bonded joints in vehicular structures, *AIAA journal*, Vol.11, No.12, pp.1650-1654.

[14] Bathe K.J., Ramm.E. and Wilson.E.L. (1975) Finite element formulations for large deformation dynamic analysis, *Int. J. Num. Meth. Engg.*, Vol.9, pp.353-386.

[15] Bathe K.J. and Ozdemir H. (1976) Elastic-plastic large deformation static and dynamic analysis, *Computers and Structures.*, Vol.6, pp.81-92.

[16] Bathe K.J. and Bolourchi S. (1979) Large displacement analysis of three dimensional beam structures, *Int. J. Num. Meth. Engg.*, Vol.14, pp.961-986.

[17] Bathe K.J. (1996) Finite element procedures, Prentice-Hall International.

[18] Belingardi G., Goglio L. and Tarditi A. (2002) Investigating the effect of spew and chamfer size on the stresses in metal/plastics adhesive joints, *Intl. Jl. of Solids and Structures*, Vol.22, pp.273-282.

[19] Bezine G., Roy A. and Vinet A. (1996) Stress in bonded adherends for single lap joints, *Jl. of Ship Production*, Vol.12, No.3, pp.166-171.

[20] Bigwood A. and Crocombe A.D. (1989) Elastic analysis and engineering design formulae for bonded joints, *Intl. Journal of Adhesion and Adhesives,* Vol. 9, No. 4, pp. 229-242.

[21] Bingham E.C (1922) Fluidity and plasticity, McGraw-Hill, Chapter VIII, pp. 215-218.

[22] Bogdanovich A. and Kizhakkethara I. (1997) Three-dimensional finite element analysis of adhesively bonded plates, *38th AIAA/ASME/ASCE/AHS/ASC Structures, Structural dynamics and Material conference and exhibit*, Part-3, pp.1984-1993.

[23] Bogy D.B. and Wang K.C. (1971) Stress singularities at interface corners in bonded dissimilar isotropic materials, *Intl. Journal of Solids and Structures,* Vol. 7, pp. 993-1005.

[24] Bour P. and Joannic R. (2001) Modelling benchmark study on rigid adhesives, GROWTH Project GRD1-1999-11012 'BONDSHIP', (http://research.dnv.com/bondship). CTA

[25] Boyd S.W., Blake J.I.R., Shenoi R.A. and Kapadia A. (2004) Integrity of hybrid steel-to-composite joints for marine application, *IMechE proceedings, Part-M:Engineering for the Marine Environment*, Vol.218, No.M4, pp. 235-246.

[26] Brede M. (2001) Final report on coupon tests for characterisation of adhesive and surface coatings, *Document No. 1-12-W-2001-05-0, GROWTH Project 'BONDSHIP' IFAM*, (http://research.dnv.com/bondship).

[27] Cao J. and Grenestedt J.L. (2003) Test of a redesigned glass-fiber reinforced vinyl ester to steel joint for use between a naval GRP superstructure and a steel hull, *Composite Structures*, Vol.60, pp.439-445.

[28] Carpenter W.C. (1991) A comparison of Numerous lap joint theories for adhesively bonded joints, *J. Adhesion*, Vol.35, pp. 55-73.

[29] Caryl L. Johnson (1989) Effect of Ply Stacking Sequence on Stress in a Scarf Joint, *AIIA Journal*, Vol.27, No.1, pp.79-86.

[30] Cheng S., Chen D. and Shi Y. (1991) Analysis of adhesive-bonded joints with non-identical adherends, *Journal Engineering mechanics,* Vol. 117, No. 3, pp. 605-623.

[31] Chiu W.K. and Jones R. (1995) Unified constitutive model for thermoset adhesive, FM73, *Intl. Jl. of Adhesion and Adhesives*, Vol.15, pp.131-136.

[32] Clifford S.M., Manger C.I.C . and Clyne T.W. (2002) Characterisation of a glass-fibre reinforced vinylester to steel joint for use between a naval GRP superstructure and a steel hull, *Composite Structures*, Vol.57, pp.59-66.

[33] Cornell R.W., Locks W. and Conn (1953) Determination of stresses in cemented lap joints, *Jl. Applied Mech.*, pp 355-364.

[34] Cossich N.H. (1998) In-plane adhesively bonded joints in sandwich structures, *MPhil Thesis*, Dept. of Ship Science, University of Southampton.

[35] Crocombe A.D. and Bigwood D.A. (1992) Development of a full elasto-plastic adhesive joint design analysis, *Jl. of Strain Analysis*, Vol.27, No.4, pp.211-218.

[36] Delale F. and Erdogan F. (1981) Viscoelastic anlysis of adhesively bonded joints, *Jl. of Applied Mechanics*, Vol.48, pp331-338.

[37] Erdogan F. and Ratwani M. (1971) Stress distribution in bonded joints, *Jl. of Composite Materials*, Vol.5, pp378-393.

[38] Frostig Y., Thomsen O.T. and Mortensen F (1999) Analysis of adhesive-bonded joints, square-end, and spew-fillet - High-Order Theory Approach, *Jl. of Engineering Mechanics*, Vol.125, No.11, pp1298-1307.

[39] Fung Y.C. (1965) Foundation of solid mechanics, Prentice hall.

[40] Gali S., Dilev G., and Ishai O. (1981) An effective stress/strain concept in the mathematical characterisation of structural adhesive bonding, *Intr. J.of Adhesion and Adhesives.*, Vol.1, pp135-140.

[41] Gadala M.S., Dokainish M.A. and Oravas.G. (1984) Formulation methods of geometric and material nonlinear problems, *Int. J. Num. Meth. Engg.*, Vol.20, pp.887-914.

[42] Guidelines for strength analyses of ship structures with the finite element method - Chapter 1, section 5, 'Rules for Classification and Construction - Analysis Techniques *Germanaicher Lloyd, Edition 2001.*

[43] Guide to the structural use of adhesives (1999) The institute of structural engineers, London-UK.

[44] Goland M. and Reissner E. (1944) The stresses in cemented joints, *J. Appl. Mech, ASME*, Vol.11,A17-22

[45] Harris J.A. and Adams R.D. (1984) Strength prediction of bonded single lap joints by nonlinear finite element methods, *Int. J. Adhesion and Adhesives*, Vol.4, No.2, pp.65-78.

[46] Hart-Smith L.J. (1973) Adhesive-bonded singla lap joints, *CR 112236*, NASA Langley research centre.

[47] Hart-Smith L.J. (1974) Analysis and design of advanced composite bonded joints, *CR 2218*, NASA Langley research centre.

[48] Hart-Smith L.J. (1981) Further developments in the design and analysis of adhesive-bonded structural joints, Joining of composite materials, *ASTM STP 749* pp. 3-31.

[49] Hart-Smith L.J. (1985) Designing to minimize peels tresses in adhesive bonded joints, In Delamination of debonding of materials, *ASTM STP 876*, (Ed. W.S. Johnson), pp. 238-266 (ASTM, Philadelphia).

[50] Hashim S.A., Winkle I.E. and Cowling M.J. (1989) A structural role for adhesive in ship building?, *Proc. of Royal Institution of Naval Architects*, Spring meetings, London, UK.

[51] Hashim S.A., Winkle I.E., Knox E.M and Cowling M.J. (1993) Advantages of adhesive bonding in offshore and marines structural applications, *5th Intl. Symposium on Integrity of Offshore Structures,* University of Glasgow, UK.

[52] Hashim S.A., Cowling M.J. and Lafferty S. (1998) The integrity of bonded joints in large composite pipes, *Intl. Jl. of Adhesion and Adhesives,* Vol.18, pp.421-429.

[53] Hashim S.A. (1999) Adhesive bonding of thick steel adherends for marine structures, *Marine Structures,* Vol.12, pp.405-423.

[54] Hildebrand M. and Hentinen M. (1998) Efficient solutions for joints between large FRP-Sandwich and metal structures, *Proc. of 19th Intl. SAMPE conf. on "progress through innovation and cost effectiveness,* pp. 417-428.

[55] Hill R. (1950) The mathematical theory of plasticity, Oxford University press, Oxford.

[56] Hofmeister L.D., Greenbaum G.A. and Evensen D.A. (1971) Large strain elastic-plastic finite element analysis, *AIAA Journal*, Vol.9, pp.1248-1255.

[57] Ikegami K., Takeshita T., Matsuo K. and Sugibayashi T. (1990) Strength of adhesively bonded scarf joints between glass fibre-reinforced plastics and metals, *Intl. Jl. of Adhesion and Adhesives*, Vol.10, No.3, pp.199-206.

[58] Jarry E. and Shenoi R.A. (2005) Performance of butt strap joints for marine applications, *Intl. Jl. of Adhesion and Adhesives*, (accepted for publication).

[59] Lam Y.C., Zhu C. and Heller M. (1995) Stress analysis of plates with bonded unbalanced laminates, *Composite Structures*, Vol.33, pp. 173-190.

[60] Li G., Lee P.S. and Thring R.W. (1999) Nonlinear finite element analysis of stress and strain distributions across thickness in composite single-lap joints, *Composite Structures*, Vol.46, pp. 395-403.

[61] Li G. and Lee P.S. (2001) Finite element and experimental studies on single-lap balanced joints in tension, *Intl. Jl. of Adhesion and Adhesives*, Vol.21, pp. 211-220.

[62] Li G., Pang S.S, Woldesenbet E., Stubblefield M.A., Mensah P.F. and Ibekwe S.I.(2001) Investigation of prepreg bonded composite single lap joint, *Composites: Part B*, Vol.32, pp.651-658.

[63] Lim.C.K. Acitelli M.A. and Hamm W.C (1974) Failure criteria of a typical amide cured epoxy adhesive, *J.Adhesion*, Vol.6, pp. 281-288.

[64] Lin C.C. and Lin Y.S. (1993) A Finite Element Model of Single-lap adhesive joints, *Intl. Jl. of Solids and Structures*, Vol.30, No.12, pp.1679-1692.

[65] Long L. and Soutis C. (2003) Recent advances in structural joints and repairs for composite materials, Kluwer Academic Publishers, Dordrecht, The Netherlands.

[66] Lubkin J.L. (1957) A theory of adhesive scarf joints, *Jl. of Applied Mechanics*, Vol.24, No.2, pp.255-260.

[67] Mattthews F.L., Kilty P.F. and Godwin E.W. (1982) A review of the strength of joints in fibre-reinforced palstics, Part-2: Adhesively bonded joints, *Composites*, pp29-37.

[68] Miao S.H., Meunier M. and Shenoi A. (2000) Report on Sikaflex360HC-Adhesively Bonded Single Lap Joint, Internal report, University of Southampton.

[69] Mitra A.K. and Ghosh B. (1995) Interfacial stresses and deformations of an adhesive bonded double strap joint under tension, *Computers & Structures*, Vol.4, pp.687-694.

[70] Mori K. and Sugibayashi T. (1992) Deformation and strength of stepped-lap joints bonded with adhesive resin, *Journal of Strain Analysis*, Vol.28, No.3, pp.171-175.

[71] Mortensen F. and Thomsen O.T. (1997) Simplified linear and non-linear analysis of stepped and scarfed adhesive-bonded lap-joints between composite laminates, *Composite Structures,* Vol.38, No.1-4, pp.281-294.

[72] Mortensen F. and Thomsen O.T. (2002a) Coupling effects in adhesive bonded joints, *Composite Structures,* Vol.56, pp.165-174.

[73] Mortensen F. and Thomsen O.T. (2002b) Analysis of adhesive bonded joints: a unified approach, *Composites Science and Technology,* Vol.62, pp.1011-1031.

[74] Mouritz A.P., Gellert E., Burchill P. and Challis K. (2001) review of advacesd composites structures for naval ships and submarines, *Composite Structures,* Vol.53, pp.21-41.

[75] Narasimhan S. (1998) Three Dimensional viscoplastic and geometrically nonlinear finite element analysis of adhesively bonded joints, *MSc. Thesis,* Indian Institute of Science, Bangalore, India.

[76] Narasimhan S., Shenoi R.A. and Jeong H.K. (2004) Three dimensional stresses in adhesively bonded lap joints with non-identical adherends, *Journal of Materials: Design & Applications, Proc. IMech (Part L),* Vol. 218, pp.283-298.

[77] Ojalvo I.U. and Eidinoff H.L. (1978) Bonded thickness effects upon stress in single lap adhesive joints, *AIAA Journal*, vol.16,pp.204-211.

[78] Olszak W. and Perzyna P. (1970) Stationary and non-stationary viscoplasticity, Inelastic Behavior of Solids, Eds. M.F.Kannien et. al., McGraw-Hill.

[79] Osnes H. and Andersend A. (2003) Computational analysis of geometric nonlinear effects in adhesively bonded single lap composite joints, *Composites: Part B,* Vol. 34, pp. 417-427.

[80] Owen D.R.J. and Hinton E. (1980) Finite elements in plasticity: Theory and practice, Pineridge press, Swansea, UK.

[81] Pandey P.C., Shakaragouda H. and Singh A.K. (1999) Nonlinear analysis of adhesively bonded lap joints considering viscoplasticity in adhesives, *Computers and Structures*, Vol.70, pp.387-413.

[82] Pandey P.C. and Narasimhan S. (2001) Three dimensional nonlinear analysis of adhesively bonded lap joints considering viscoplasticity in adhesives, *Computers and Structures*, Vol.79, pp.769-783.

[83] Perzyna P. (1963) The constitutive equations for rate sensitive plastic materials, *Quarterly Applied Mathematics*, Vol.20, pp.321-332.

[84] Perzyna P. (1966) Fundamental problems in viscoplasticity, *Recent advances in Applied Mechanics, Academic press*, Vol.9, pp.243-377, New York.

[85] Pickett A.K. and Hollaway L. (1985) The analysis of elastic adhesive stresses in bonded lap joints in FRP structures, *Composite structures*, Vol.3, pp.55-79.

[86] Raghava R., Caddell R.M. and Yeh G.S.Y (1973) The microscopic yield behavior of polymers, *J. Material Science*, Vol.8, pp.225-232.

[87] Ramamurthy T.S. and Rao A.K. (1978) Shaping of adhesives in bonded joints, Intl. Jl. of Mechanical Sciences, Vol.20.

[88] Ramberg W. and Osgood W.R. (1943) Description of stress-strain curves by three parameters, Technical notes, NACA.

[89] Renton W.J. and Vinson J.R. (1975) The efficient design of adhesive bonded joints, *Journal of Adhesion,* Vol. 7, pp. 175-193.

[90] Roy A.K., Donaldson S.L. and Schoeppner G.A. (1997) Bonded joints of unidirectional and cross-ply laminates: An experimental study, *38th AIAA/ASME/ASCE/AHS/ASC Structures, Structural dynamics and Material conference and exhibit,* Part-3, pp.1994-2003.

[91] Roy S. and Reddy J.N. (1988a) Non-linear analysis of adhesively bonded joints, *Int. J. Non-linear Mechanics,* Vol.23, No.2., pp.97-112.

[92] Roy S. and Reddy J.N. (1988b) Finite element models of viscoelasticity and diffusion in adhesively bonded joints, *Int. J. Num. Meth. Engg.*, Vol.26, pp.2531-2546.

[93] Schrefler B.A., Odorizzi S. and Wood R.D. (1983) A total Lagrangian geometrically nonlinear analysis of combined beam and cable curves, *Computers and Structures*, Vol.17, No.1, pp.115-127.

[94] Shenoi R.A. and Wellicome J.F. (1993) Composite materials in maritime strcutures: Cambridge Ocean Technology Series-5, Cambridge University Press, UK.

[95] Sheppard A., Kelly D. and Tong L. (1998) A damage zone model for the failure analysis of adehsively bonded joints, *Intl. Jl. of Adhesion and Adhesives*, Vol.18, pp.385-400.

[96] Shin K.C., Kim Y.G. and Lee D.G. (1997) Adhesively bonded lap-joints for the composite-steel shell structures of high-speed vehicles, *Composite Structures*, Vol.38, No.1-4, pp.215-227.

[97] Smith T.L. (1971) J. Poly. Science, part C, Vol.32, pp269.

[98] Soutis C. and Hu F.Z. (1997) Design and performance of bonded patch repairs of composite structures, *Proc. Instn. Mech. Engrs*, Vol.211, part G, pp.263-271.

[99] Sun C.T., Klug J. and Arendt C. (1996) Analysis of Cracked Aluminium Plates Repairs with Bonded Composite Patches, *AIIA Journal*, Vol.34, No.2 pp.369-374.

[100] Tong L., Sheppard A. and Kelly D. (1995) Relationship between surface displacement and adhesive peel stress in bonded double lap joints, *Intl. Jl. of Adhesion and Adhesives*, Vol.15, pp.43-48.

[101] Tsai M.Y. and Morton J. (1994) Three-Dimensional Deformations in a Single-Lap Joint, *J. of Strain Analysis*, Vol.29, No.1, pp.137-145.

[102] Tsai M.Y., Morton J. and Matthews F.L. (1995) Experimental and numerical studies of a laminated composite single-lap adhesive joint, *Jl. of Composite Materials*, Vol.29, No.9, pp.1254-1275.

[103] Tsai M., Oplinger D.W. and Morton J. (1998) Improved theoretical solutions for adhesive lap joints, *Int. Jl. Solids Structures*,Vol.35, No.12, pp.1163-1185.

[104] Volkersen O. (1938) Die Nietkraftverteilung in zugbeanspruchten Nietverbindungen mit konstanten Laschenquerschnitten (*Rivet strength distribution in tensile-stressed rivet joints with constant cross section*). Luftfahrtforschung, Vol. 15, pp.41-47.

[105] Wah T. (1976) Plane stress analysis of a scarf joint, *Intl. Jl. of Solids and Structures*, Vol.12, pp.491-500.

[106] Wah T. (1976) The adhesive scarf joint in pure bending, *Intl. Jl. of Mechanical Sciences*, Vol.18, pp.223-228.

[107] Wake W.C. (1986) Structural applications of adhesives, Structural adhesives in engineering, *Proceedings of Inst. of Mech. Engineers*, pp.161-169.

[108] Wang C.H. and Rose L.R.F. (1997) Determination of triaxial stresses in bonded joints, *International journal of Adhesion and Adhesives*, Vol.17, pp.17-25.

[109] Wang C.H. and Chalkey P. (2000) Plastic yeilding of a film adhesive under multiaxial stresses, *International journal of Adhesion and Adhesives*, Vol.20, pp.155-164.

[110] Wang X., Meith U. and Cappelleetti A.M. (2004) Numerical methods for design of bonded joints for ship structures, *IMechE proceedings: Part-M Engineering for the Maritime Environment*, Vol.218, No. M4, pp.247-258.

[111] Whitney J.M. (1997) Stress analysis of a composite double-lap joint using higher order plate theory, *38th AIAA/ASME/ASCE/AHS/ASC Structures, Structural dynamics and Material conference and exhibit*, Part-3, pp.2004-2009.

[112] Winkle I.E., Cowling M.J., Hashim S.A. and Smith E.M. (1991) What can adhesives offer to Shipbuilding?, *Jl. of Ship Production*, Vol.7, No.3, pp.137-152.

[113] Wood R.D. and Ziekiewicz O.C. (1977) Geometrically nonlinear finite element analysis of beams, frames, arches and axisymmetric problems, *Computers and Structures*, Vol.7, pp.725-735.

[114] Wooley G.R. and Carver D.R. (1971) Stress concentration factors for bonded lap joints, *Jl. of Aircraft*, Vol.8, pp.817-820.

[115] Wright P.N.H., Wu Y. and Gibson A.G. (2000) Fibre reinforced composite-steel connections for transverse ship bulkheads, *Plastics, Rubber and Composites*, Vol.29, No.10, pp.549-557.

[116] Wu Z.J., Romeijn A. and Wardenier J. (1997) Stress expressions of single-lap adhesive joints of dissimilar adherends, *Composite Structures*, Vol.38, No.1-4, pp. 273-280.

[117] Youzhi M.A. and Desai C.S. (1990) Alternative definition of finite strains, *J. of Engg. Mechanics*, Vol.116, No.4, pp.901-919.

[118] Yu X.X., Crocombe A.D. and Richardson G. (2001) Material modelling for rate-dependent adhesives, *Intl. Jl. of Adhesion and Adhesives*, Vol.21, pp.197-210.

[119] Zienkiewicz O.C. and Taylor R.L. (2000) The finite element method, 5th Edition, Butterworth-Heinemann, OxfordMcGraw-Hill.

[120] Zienkiewicz O.C. and Nayak.G.C (1973) General approach to problems of plasticity and large deformation using isoparametric element, *3rd Conf. Matrix Meth. Struct. Mech.*, Wright-patterson Air Force Base, ohio, pp.881-928.

[121] Zienkiewicz O.C. and Cormeau I.C. (1974) Visco-plasticity: Plasticity and creep in elastic solids-A Unified numerical solution approach, *Int. J. Num. Meth. Engg.*, Vol.8, pp.821-845.